MICROCOPY RESOLUTION TEST CHART

NATIONAL BUREAU OF STANDARDS-1963-A

AD A126417

PROCEEDINGS OF THE 1981 RADC MICROWAVE MAGNETICS TECHNOLOGY WORKSHOP, JUNE 10-11, 1981
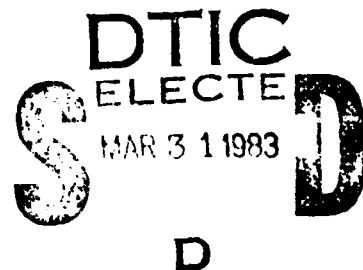
James C. Sethares

APPROVED FOR PUBLIC RELEASE; DISTRIBUTION UNLIMITED

ROME AIR DEVELOPMENT CENTER
Air Force Systems Command
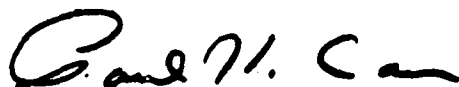**Griffiss Air Force Base, NY 13441**

DTIC
ELECTE
MAR 3 1 1983
S D

D

IIC FILE COPY

This report has been reviewed by the RADC Public Affairs Office (PA) and is releasable to the National Technical Information Service (NTIS). At NTIS it will be releasable to the general public, including foreign nations.

RADC-TR-83-15 has been reviewed and is approved for publication.

APPROVED: *[signature]*

PAUL H. CARR, Acting Chief
Antennas & RF Components Branch
Electromagnetic Sciences Division

APPROVED: *[signature]*

ALLAN C. SCHELL
Chief, Electromagnetic Sciences Division

FOR THE COMMANDER: *[signature]*

CARLO P. CROCETTI
Chief, Plans Office

If your address has changed or if you wish to be removed from the RADC mailing list, or if the addressee is no longer employed by your organization, please notify RADC (EEA), Hanscom AFB MA 01731.   This will assist us in maintaining a current mailing list.

Do not return copies of this report unless contractual obligations or notices on a specific document requires that it be returned.

COMPONENT PART NOTICE

THIS PAPER IS A COMPONENT PART OF THE FOLLOWING COMPILATION REPORT:

(TITLE): Proceedings of the 1981 RADC Microwave Magnetics Technology

Workshop, June 10-11, 1981.

(SOURCE): Rome Air Development Center, Griffiss AFB, NY.

To ORDER THE COMPLETE COMPILATION REPORT USE ___AD-A126 417___ .

THE COMPONENT PART IS PROVIDED HERE TO ALLOW USERS ACCESS TO INDIVIDUALLY AUTHORED SECTIONS OF PROCEEDINGS, ANNALS, SYMPOSIA, ETC. HOWEVER, THE COMPONENT SHOULD BE CONSIDERED WITHIN THE CONTEXT OF THE OVERALL COMPILATION REPORT AND NOT AS A STAND-ALONE TECHNICAL REPORT.

THE FOLLOWING COMPONENT PART NUMBERS COMPRISE THE COMPILATION REPORT:

DTIC
SELECTE
APR 7 1983
A

... DOCUMENTATION PAGE		READ INSTRUCTIONS BEFORE COMPLETING FORM
...NU... T...	2. GOVT ACCESSION NO. AD-A126 447	3. RECIPIENT'S CATALOG NUMBER
...nd... E... E... ... 6... ... THE 1981 RADC MICROWAVE ...HNOLOGY WORKSHOP,	5. TYPE OF REPORT & PERIOD COVERED In-House	
	6. PERFORMING ORG. REPORT NUMBER N/A	
...o)... ...es C. Sethares	8. CONTRACT OR GRANT NUMBER(s) N/A	
...I... ...TION NAME AND ADDRESS ...pment Center (EEAC) ...A 01731	10. PROGRAM ELEMENT, PROJECT, TASK AREA & WORK UNIT NUMBERS 61102F 2305J501	
...L... NAME AND ADDRESS ...pment Center (EEAC) ...MA 01731	12. REPORT DATE October 1982	
	13. NUMBER OF PAGES 359	
...14... ...Y NAME & ADDRESS*(if different from Controlling Office)*	15. SECURITY CLASS. *(of this report)* Unclassified	
	15a. DECLASSIFICATION/DOWNGRADING SCHEDULE	

...TION STATEMENT *(of the abstract entered in Block 20, if different from Report)*

...ENTARY NOTES

Project Scientist: Mr. James C. Sethares

...DS *(Continue on reverse side if necessary and identify by block number)*
...wave magnetics
...m iron garnet films
...tostatic waves
...agnetics

...CT *(Continue on reverse side if necessary and identify by block number)*
The papers which comprise these proceedings are based on presentations ...1981 Rome Air Development Center USAF sponsored workshop on ...wave Magnetics Technology held at RADC, Hanscom Air Force Base, ...chusetts on June 10-11, 1981. The workshop was hosted by the ...as and RF Components Branch of the Electromagnetics Sciences ...on, RADC.
...he objective of the workshop was to assess the state-of-the-art in micro-...magnetics with emphasis on magnetostatic wave, MSW, Technology in

epitaxial yttrium iron garnet films (EPI-YIG) on gadolinium gallium garnet substrates. It brought together individuals involved in microwave magnetics research and development with those interested in the application of this technology to microwave systems, and provided an opportunity for researchers active in the field to exchange information, ideas and experiences. Among the issues raised at the workshop were: where is the technology going from here? What should be our goals over the next two to three years? What priorities should be placed on problems such as reducing, controlling, or utilizing dispersion? What are the promising areas for R&D, and what are the important applications?

The subject matter presented at the workshop included a state-of-the-art review of MSW devices and available materials for MSW technology; the characteristics or analyses of MSW transducers, reflecting arrays, dispersion, diffraction, temperature, terminations, magnetic field profiles, wave guiding, mode structure, anisotropy, width modes and multilayer films; and requirements for phased array and adaptive antennas and for solid state transmit/receive modules. A tape recording of the panel discussion was made which has been transcribed and presented in these proceedings.

Accession For		
NTIS GRA&I	X	
DTIC TAB	☐	
Unannounced	☐	
Justification		
By		
Distribution/		
Availability Codes		
Dist	Avail and/or Special	
A		

PREFACE

The papers which comprise these proceedings are based on presentations at the 1981 Rome Air Development Center USAF sponsored workshop on Microwave Magnetics Technology held at RADC, Hanscom Air Force Base, Massachusetts on June 10-11, 1981. The workshop was hosted by the Antennas and RF Components Branch of the Electromagnetics Science Division, RADC.

The objective of the workshop was to assess the state-of-the-art in microwave magnetics with emphasis on magnetostatic wave, MSW, technology in epitaxial yttrium iron garnet films (EPI-YIG) on gadolinium gallium garnet substrates. It intended to bring together individuals involved in microwave magnetics research and development with those interested in the application of this technology to microwave systems, and to provide an opportunity for researchers active in the field to exchange information, ideas and experiences.

It is recognized that MSW is in a transition stage. On the one hand, there is basic research that remains to be done. On the other hand, specific devices are being fabricated and evaluated for their device potential and the first system application is in the planning stages. In addition, high quality thin magnetic films for MSW work (LPE-YIG) up to three inches in diameter are now available commercially for the first time - since mid 1981. Among the issues raised at the workshop were: where is the technology going from here? What should be our goals over the next two to three years? What priorities should be placed on problems such as reducing, controlling, or utilizing dispersion? What are the promising areas for R&D, and what are the important applications?

The format of the workshop consisted of papers presented in an informal atmosphere and a panel discussion. The workshop was unclassified and consisted of participants presenting papers, representatives from nonprofit organizations, interested Government personnel, representatives from industry.

The subject matter presented at the workshop included a state-of-the-art review of MSW devices and available materials for MSW technology; the characteristics or analyses of MSW transducers, reflecting arrays, dispersion, diffraction, temperature, terminations, magnetic field profiles, wave guiding, mode structure, anisotropy, width modes and multilayer films; and requirements for phased array and adaptive antennas and for solid state transmit/receive modules. A tape recording of the panel discussion was made which has been transcribed and presented in these proceedings.

The papers presented in these proceedings, excluding the tape transcriptions, have been reproduced as received, and have not been edited or reviewed. I wish to thank all of the authors for their contributions and patience. I thank the panel members, chairman, and participants for their efforts and time, and the many individuals who helped make this effort successful.

James C. Sethares

James C. Sethares
Chairman
1981 RADC MMTW

1

CONTENTS

PROGRAM FOR RADC/EEA MICROWAVE MAGNETICS TECHNOLOGY WORKSHOP

Wednesday and Thursday   June 10 - 11, 1981

WEDNESDAY MORNING

0800 - 0845 REGISTRATION

0850   OPENING REMARKS   Mr. James C. Sethares, Workshop Chairman - RADC/EEA
         Dr. Allan Schell, Division Chief, RADC/EE

         WELCOME   Colonel Donald Stukel, Commander RADC

Time	Title	Speaker	Affiliation
0915	MSFVW Devices	Dr. J. Douglas Adam	Westinghouse Research Center, PA
0945	Phased Array Antenna Requirements	Dr. Robert Mailloux	RADC/EEA Hanscom AFB, MA
1015	BREAK		
1030	Solid State T/R Module Requirements	Mr. E. Hunter Chilton	RADC/OC, Griffiss AFB, NY
1100	Adaptive Antenna Requirements	Mr. John Graniero	RADC/DCC, Griffiss AFB, NY
1130	Epitaxial Ferrites for MSW Devices	Dr. Howard Glass	Rockwell Intl., Anaheim, CA

WEDNESDAY AFTERNOON

SESSION CHAIRMAN   Prof. Charles V. Smith, Jr.   University of Texas at Arlington

Time	Title	Speaker	Affiliation
1315	MSW Reflective Filters	Prof. John Owens	Univ. of Texas at Arlington
1345	Transducers	James Sethares	RADC/EEA, Hanscom AFB, MA
1415	Nonuniform Fields	Prof. Frederic Morgenthaler	MIT, Cambridge, MA
1445	Simple MSW Delay Lines	Dr. Michael Daniel	Westinghouse Research Center, PA
1500	BREAK		
1515	Nondispersive and Linear Dispersive MSW Propagation on Multi Layer Films	Dr. Larry Adkins	Rockwell Int'l., Anaheim, CA
1545	MSW Temperature Coefficients	Dr. J. Castera	Thompson CSF, France
1600	Propagation Characterisitcs of MSW - A Review	Dr. Jay Parekh	State Univ of N.Y. at Stonybrook
1630	X-Band Delay Line Computer Study	Dr. Victor Lander	Airtron, Litton
1645	MSW Terminations	Dr. Lawrence Taylor	RADC/Post Doctoral Program (Now at Westinghouse, MD)
1700	MSW-Potential Systems Application	Dr. Pradeep Wahl	Litton, Amecon

1730-1830   SOCIAL HOUR AT OFFICERS CLUB

4

SESSION CHAIRMAN   Prof. John Owens   University of Texas at Arlington

Time	Title	Affiliation
0800	Diffraction Properties of MSW	Prof. H. Tuan	State Univ. of N.Y. at Stonybrook
0830	MSW Resonators	Dr. P. Hartemann	Thompson CSF, France
0900	Buried MSW Transducers	Prof. Jay Parekh	State Univ. of N.Y. at Stonybrook
0915	Effects of Width Modes in MSFVW	Dr. J. Douglas Adam	Westinghouse Research Center, PA
0930	MSW Propagation in YIG Double Films	Dr. Michael Daniel	Westinghouse Research Center, PA
1000	BREAK		
1015	Guiding MSSW with Nonuniform Fields	Dr. Dan Stancil	MIT, Cambridge, MA
1030	Octave Bandwidth MSW S/N Enhancer	Dr. Steven Stitzer	Westinghouse, Advanced Tech Labs, MD
1100	Microwave Pulse Compression Loops with MSW Delay Lines	Mr. K. Reed	Univ. of Texas at Arlington
1130	MSW Anisotropic Effects	Lt. Robert Floyd	RADC/EEA, Hanscom AFB, MA
1145	MSW Dispersion	Prof. I. Jacob Weinberg	University of Lowell, Lowell, MA

THURSDAY AFTERNOON

1400-1630   MSW Panel Discussion

PANEL CHAIRMAN   Dr. Richard W. Damon   President Institute of Electrical & Electronic Engineers
Sperry Research Center, Sudbury, MA

PANEL MEMBERS

Dr. J. Douglas Adam   Westinghouse Research Center, PA
Prof. Jeff H. Collins   Univ. of Edinburgh, Scotland
Dr. Howard Glass   Rockwell International, Anaheim, CA
Prof. Frederic Morgenthaler   Mass. Institute of Technology
Prof. John Owens   University of Texas at Arlington
Prof. Charles Smith   University of Texas at Arlington

OPENING REMARKS

J.C. Sethares, Workshop Chairman
RADC/EEAC

The purpose of this workshop is to assess the state-of-the-art of MSW

technology in thin magnetic films and to bring together individuals

involved in R&D with those interested in applications. We hope

to learn from one another and to address and possibly answer questions

such as:

> Where is the technology going from here?

> What should be out goals over the next 2-3 years?

> What priorities should be placed on reducing controlling or
> utilizing dispersion?

> What are the most promising areas of R&D and what are the
> important applications?

We hope this workshop can provide some overall direction to the

excellent work being done by various groups in the US and abroad.

The number of people working the area appears to be growing. At

this meeting there are representatives from the Army, Navy, Indus-

try, and Universities. This is the time and place to ask the tough

questions.

On the less serious side there is another reason for holding this

workshop. Three years ago at an International IEEE Circuits and

Systems Conference in New York City, in a special session on MSW,

Jeff Collins a prime mover of this technology, who is here today,

gave an invited paper on the state-of-the-art of this emerging

technology. He made the statement that there are only seven

people working this very interesting technology. After reflecting

upon this, I realized he left out the Air Force so that is part
of the reason we're here today. There is another reason. Damon
and Eshbach theoretically predicted MSW on a YIG slab. They
solved a boundary value problem too thoroughly and kept solutions
that most people would have thrown out as interesting mathe-
matical curiosities. John Eshbach from General Electric is here
this morning Dick Damon, now the IEEE President, will be here
tomorrow. Finally and more seriously, I hope your experience here
will be professionally rewarding and enjoyable at the same time,
and we will do our best to make it so.

ALLAN C. SCHELL
Chief
Electromagnetic Sciences Division, RADC

Our interests and concerns in the area of microwave magnetics are very strong.
We perceive this area as a next step in terms of providing components that
will be needed to provide capabilities beyond those of surface acoustic wave
devices. The work that is being done in this area, and what we hope can grow
out of this meeting, will lead to a new range of components that may have
applications not only as signal processing components such as those developed
in surface acoustic waves, but also as parts of phased arrays of the future.
I think the work that you are doing and reporting in this meeting can add a
great deal to the effort to develop components for the high performance sur-
veillance sensors and communications links needed by the Air Force. We are
delighted you're here, and are proud to host the meeting. Tomorrows' panel
session should be especially constructive; Dick Damon will be here to participate
and I think he will add a great deal to the discussion. Now, I would like to
introduce the Commander of the Rome Air Development Center, Colonel Donald
Stukel.

8

COLONEL DONALD STUKEL
Commander
Rome Air Development Center

It's my privilege today to welcome you to RADC. I'm especially pleased

that the Electromagnetic Science Division is sponsoring this workshop. As

Jim pointed out the objective of the workshop is to assess the state of tech-

nology in the MSW area. In order to do that, we've sought to bring together

those people who are involved in the basic research itself with the people

who are interested in the applications of the technology. I think that we all

appreciate that MSW is in a transition phase, where on the one hand there's an

awful lot of basic research to be done while at the same time devices are

being fabricated and evaluated for potential systems use. From my viewpoint

and the viewpoint of the United States Air Force and I suspect from the view-

point of everyone in this audience, to expedite that transition of technology

is very important. I know if I look at it from the larger perspective of Rome

Air Development Center where I'm responsible for the command, control, com-

munications and intelligence technology that feeds the United States Air Force

it's important that we get these devices introduced into systems. At RADC we

have about 1400 people, about 800 scientists and engineers, some of them located

here on Hanscom. As a matter of fact there are two divisions here, primarily

technology oriented, and over at Griffiss AFB, Rome, NY we have five separate

divisions. Most all of them are applications oriented. There's an intelligence

reconnaissance division, a command and control division, communications division,

surveillance division, and then a division that addresses the reliability/com-

patibility area. So from my perspective we're very interested in this technology.

Our budget is approximately 1/3 of a billion dollars a year. At any given time

we have ongoing contracts valued at about a billion dollars. So, to cross that

spectrum that we call C^3I we've got a deep and inviting interest in the transition of technology. We have and will continue to support substantial amounts of research and development in MSW and at the same time we will be pushing very hard to transition that technology that's ready to be transitioned into systems. So it's with a great deal of pleasure that I join you here this morning and wish you well in this very important endeavor.

MAGNETOSTATIC FORWARD VOLUME WAVE DEVICES*

J. D. Adam, Michael R. Daniel and T. W. O'Keeffe
Westinghouse Electric Corporation, Research & Development Center
Pittsburgh, PA   15235

Summary

The design, construction and performance of four magnetostatic wave devices operating at X-band is described. They comprise a dispersive delay line with a 1 GHz bandwidth and a differential delay of $\sim$ 200 nS, a programmable tapped delay line capable of generating and correlating 4-bit Barker codes, a delay stabilized oscillator with output frequency stable to within $\pm$1 MHz over the 0 to +65°C range and a 10-channel filter bank.

Introduction

Magnetostatic wave (MSW) devices, based on epitaxial YIG are potentially useful for signal processing at microwave signal frequencies or at a broadband microwave i.f. MSW are attractive because of their low propagation losses of less than 30 dB/µS at microwave frequencies and their planar geometry and bandwidths of the order of 1 GHz are compatible with presently available semiconductor amplifiers or signal sources. The objective here is to describe four types of devices developed and delivered on a U.S. Air Force Avionics Lab. program.[1] The devices were a dispersive delay line, a delay stabilized oscillator, a programmable tapped delay line and a 10-channel filter bank, all operating in X-band. These devices were all packaged with permanent bias magnets with the aim of allowing potential users to evaluate and gain experience with MSW devices and provide feedback on areas requiring further development. The device types were selected since these functions are currently performed by SAW devices operating at i.f. frequencies below 1 GHz.

The forward volume mode of propagation was used in all of the devices. This mode was chosen since the dispersive delay line required a bandwidth of 1 GHz at X-band which would be impossible to achieve with a simple surface wave device. In addition, although forward volume wave

require a larger bias field than either surface or backward volume waves,
the field is applied normal to the YIG film, thus minimizing the magnet
gap. Device design and fabrication relied where possible on simple
transducer structures and the use of adjacent ground planes to achieve
the desired delay characteristics. Equations describing FVW propagation
and transduction in structures consisting of a YIG film spaced from a
ground plane have been described elsewhere[2,3] and will not be discussed
in detail at this time.

Dispersive Delay Line

The desired delay versus frequency characteristics of the
dispersive delay line were obtained by taking advantage of the strong
influence of an adjacent conducting plane on the wave dispersion.
Studies[4] showed that an approximately linear variation of group delay
with frequency was obtained when the ground plane was spaced from the YIG
film by a distance approximately equal to the YIG film thickness. A nominally
20μm YIG thickness was selected as giving a reasonable time bandwidth product
of ∿ 200 at a bandwidth of 1GHz with a deviation from linear delay with
frequency of less than ± 5nS.
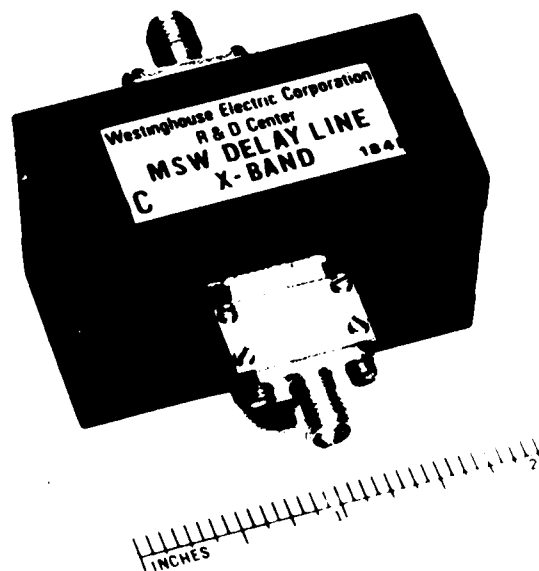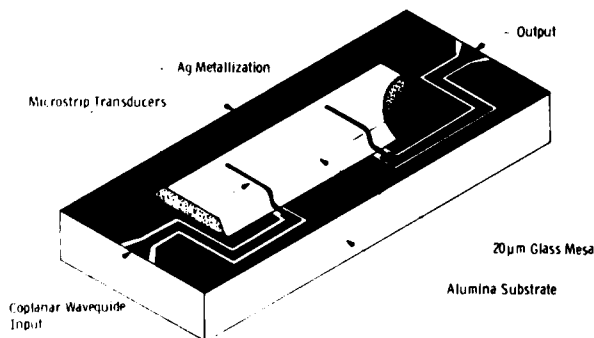
Figure 1. Transducer and dielectric
spacer configuration for the linearly
dispersive delay line.

Figure 2. Linearly dispersive delay
line.

The construction of the device is shown in figure 1, where
the YIG film of dimensions 5mm x 25mm x 20μm would be placed face down
on the glass mesa so as to contact the microstrip transducers. The
glass mesa was deposited on the gold ground plane by sputtering. The

gold microstrip transducers were 5mm long, 50μm wide and 5μm thick
and were open circuited at one end with the opposite end connected to
co-planar waveguide of 50Ω characteristic impedance. The packaged device
is shown in figure 2 complete with the SmCo permanent magnets and soft
iron yoke required to supply the 4.8 kOe bias field.

Figure 3. Measured group delay vs.
frequency for the linearly dispersive
delay line.
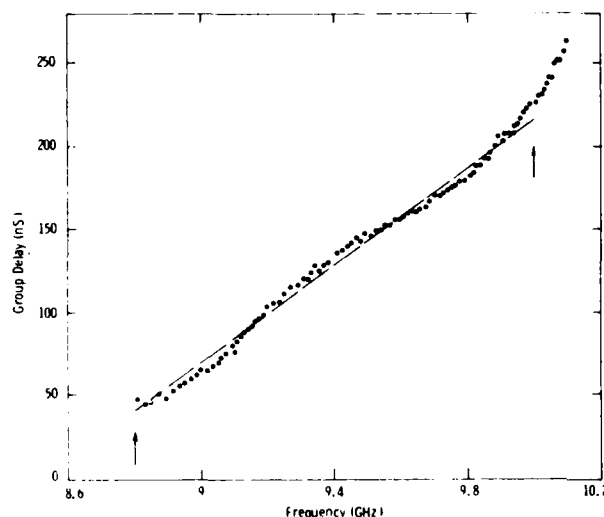
The variation in group delay
with frequency is shown in figure 3.
The dots are measured points and the
broken line is a best fit straight line.
Arrows denote the 1.2 GHz bandwidth
over which the delay is linear with
frequency to within ±5nS and the
differential delay is 190nS. Phase
deviation from quadratic phase
with frequency is a more sensitive
parameter than deviation from linear
delay with frequency. The
maximum phase deviation for the
device shown is approximately 240°
which will require to be reduced by
at least an order of magnitude to
satisfy most applications.

The measured insertion loss is
shown in figure 4, together
with calculated curves which include the effects of the finite resistivity
of the conducting plane on the propagation loss. Two cases were calculated,[1]
the first assumed a silver conducting layer with a skin depth of 0.6μm
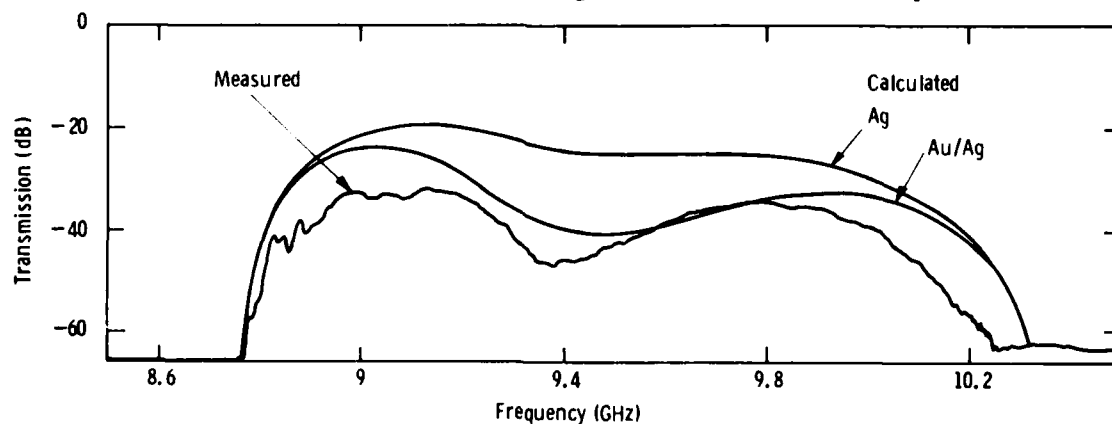
Figure 4. Transmission loss vs. frequency for the linearly dispersive
delay line.

at 9 GHz and the second a gold/silver alloy with a skin depth of 2μm.
The measurements are in good agreement with the latter case since
in this device a thin gold film was used to passivate a thick silver
layer resulting in a gold/silver alloy by diffusion.

13

Providing the phase error of the dispersive delay lines can be reduced they will find important applications in compressive receivers and in variable delay lines for phased array antennas.[5] This progress is likely owing to the number of more sophisticated techniques such as double YIG film[6] and reflective array devices which have not yet been fully developed.

Programmable Tapped Delay Line

The device discussed in this section is a programmable tapped delay line[7] which can be used to generate and correlate a phase coded pulse sequence. The 4-tap device is shown in Figure 5. The YIG film is the dark strip towards the bottom of the photograph and is 7.1μm thick, 2cm long and 1mm wide. The input transducer is at the bottom center and the four output taps are arranged two on either side of the input so that there is a 1mm path length increment between the input transducer and successive output taps. The taps are connected via 50Ω microstrip to PIN diode, 0 or π, phase shifters and then combined together. The microstrip circuit was fabricated on a 10 mil thick alumina substrate, 1" square. Switching and bias inputs for the PIN switches can be seen on both sides of the box. When completely assembled, the field produced by the permanent bias magnets was normal to the film. The insertion loss from the input to any output was typically 22dB.
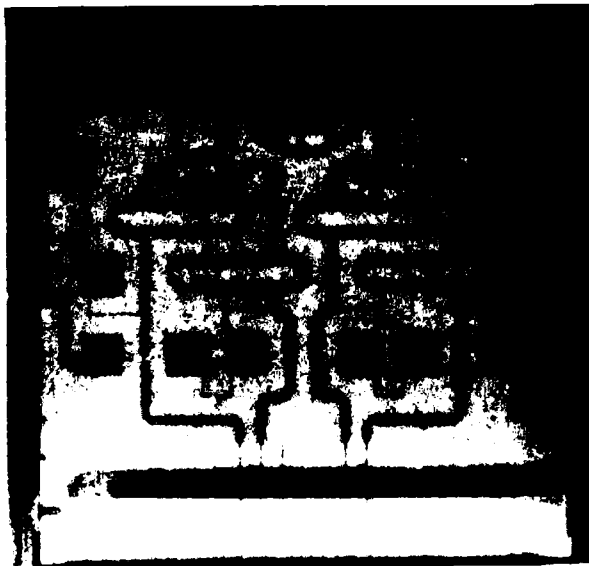
Figure 5. Programmable 4-tap delay line.
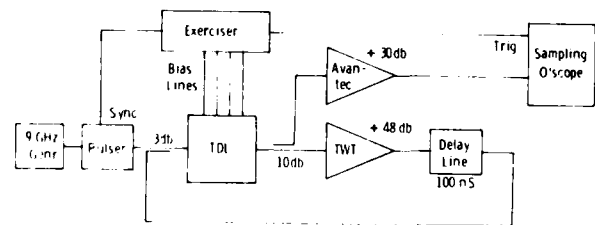
Figure 6. Tapped delay line test arrangement.

The tapped delay line was tested by using the same device to generate and then correlate a 4-bit Barker code, Figure 6. A 9 GHz pulse of length 20nsec was applied to the input transducer resulting in a phase coded train of four pulses from the output of the tapped

14

delay line. The phase coded pulses were delayed for 100nsec in a constant MSW delay line and during this time the phase of the four taps was changed by an exerciser so as to represent a time reversed version of the generated pulse train. The pulse train was then amplified and reintroduced to the input of the tapped delay line via a directional coupler. The tapped delay line acted as a matched filter and performed a correlation on the four coded pulses. The sequence of pulses observed at the output to the tapped delay line is shown in Figure 7. Feedthrough from the input pulse is seen on the extreme left followed by the four generated pulses which are coded with the π, π, o, π Barker code. The correlation peak is seen towards the right of the photo. For this 4-bit Barker code the correlation is a 7 pulse sequence with normalized amplitudes 1, 0, 1, 4, 1, 0, 1. The experimental results are in good agreement with this although some extra undesired pulses are evident which are due to reflections and higher order width modes.

100mV   <50nS
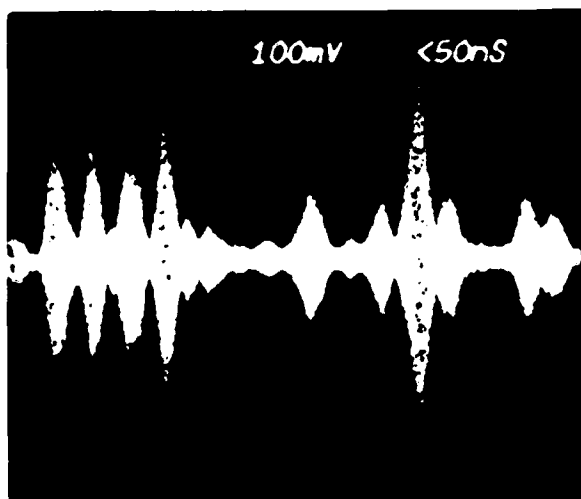
Figure 7. 4-bit Barker code genera-
tion and correlation.

Generation and correlation using two separate devices was less successful due to difficulty in matching the characteristics of the devices with sufficient accuracy. The main problem lay in achieving sufficient bias field uniformity since an 0.5 Oe change in bias field was sufficient to produce an $10°$ phase change between taps. This problem will be minimized with improved magnet design. The techniques described are capable of extension to the generation and correlation of 13-bit Barker codes as well as other sequences for use in radar and communications systems.

Delay Stabilized Oscillator

An important goal in the design of this oscillator was that the variation in output frequency as a function of temperature be at least as good as commercially available YIG sphere oscillators which is typically less than 10MHz over $0°C$ to $+60°C$.[8] The frequency stability achieved with the MSW devices was $\pm$ 1MHz over the same temperature range with no internal heater. In epitaxial YIG devices the center frequency depends upon the temperature variation of both the $4\pi M$ and the anisotropy field (H_A). Techniques which were previously described and achieved temperature stable operation relied either on a special $Y_{3-x}La_xFe_{5-y}Ga_yO_{12}$ film composition[9] or used a separate temperature stabilizing component in the permanent magnet assembly. In the device described here, the frequency drift was minimized by designing the permanent bias magnet to compensate for the variation of the YIG film parameters, $4\pi M$ and H_A, with temperature.

15

Both periodic transducers and reflective arrays[10] have been used in MSW oscillators. However, the present device was designed as a MSW analogue to a SAW delay stabilized oscillator. Figure 8a is a diagram of a delay stabilized oscillator consisting of an amplifier and an attenuator to provide controlled loop gain, a directional coupler to extract the signal from the oscillator and the delay line. If the delay line and other components in the loop are broadband, then oscillation will occur at any frequency where the total phase change around the loop is $2n\pi$ radians. The possible "comb" of frequencies is shown in Figure 8b. If the delay line is made narrow band, through the use of IDTs for example, then one frequency can be selected from the "comb" as shown by the broken line in Figure 8b. The situation shown here is ideal since the desired frequency is positioned at the maximum of the delay line amplitude response while other "comb" frequencies are positioned at zeros. This was achieved, as shown in Figure 9, by using a long IDT[11] (10 fingers) and a short IDT (4 fingers).

(a)

(b)
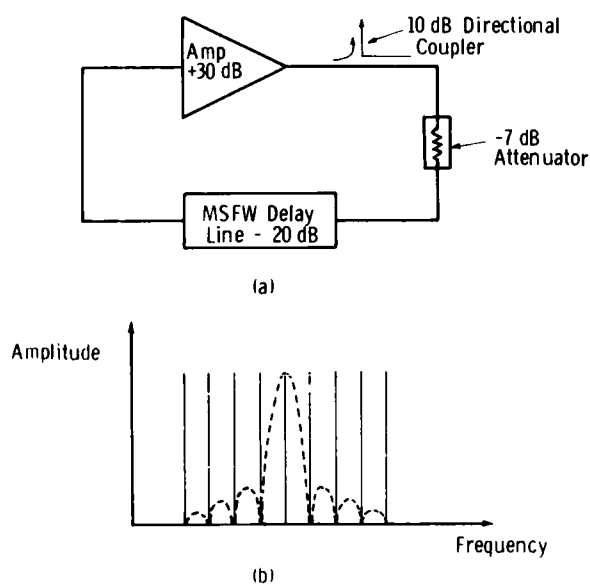
Figure 8. Magnetostatic wave delay stabilized oscillator: a) oscillator loop; b) selection of one oscillation mode by IDT response.
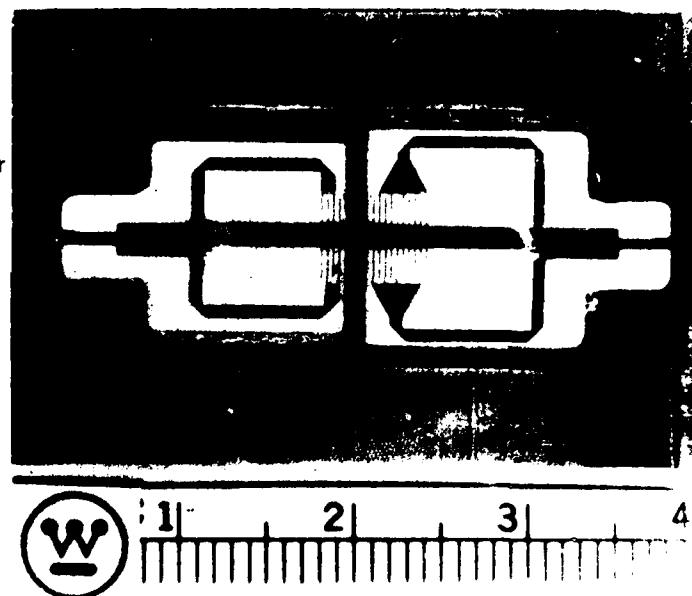
Figure 9. Magnetostatic forward volume wave delay line with IDTs for oscillator.

Ideally the center to center spacing of the transducers should equal the length of the longer transducer which was 3mm. The actual separation between the transducers was 4mm and was necessary to reduce e.m. feedthrough between input and output to less than 50dB. The additional separation did not seriously affect the rejection of other "comb" frequencies which were found to be attenuated by at least 14dB relative to the desired frequency where the minimum insertion loss was 19dB. Both transducers had fingers which were 5mm long and 50μm wide separated by 300μm. The YIG film was 7μm thick and, in order to reduce the coupling

to the transducer was made 1mm wide and spaced 75μm from it. The ends of the film were bevelled at $\sim 1/2°$ to prevent relections. The bias field was applied normal to the film so that MSFW were launched.

Measurements of the temperature dependence of the center frequency of the delay line, in a constant bias field, showed the frequency increased by +9MHz/°C. This frequency change corresponds to a variation in internal field of +3.2 Oe/°C. In order to achieve zero frequency change with temperature, this variation in internal field was compensated by an equal but opposite change in the bias field. For a device operating at 9GHz the required bias field change is approximately 0.065%/°C. The two materials considered in the construction of the bias magnets were SmCo and RARENET-B[12] with temperature coefficients of remanence of -0.04%/°C and -0.09%°C respectively. A combination of these two materials were used to achieve the required behavior. Bias field uniformity over the length of the delay line is critical when IDTs are used and soft iron pole pieces were added to give a field uniform to less than 1 Oe over the active device area.
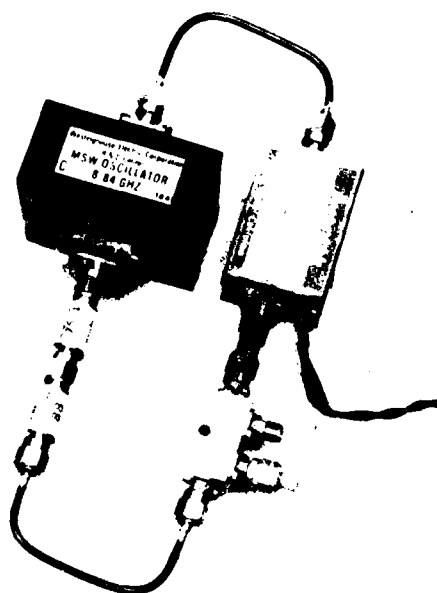
Figure 10. Delay line stabilized oscillator.
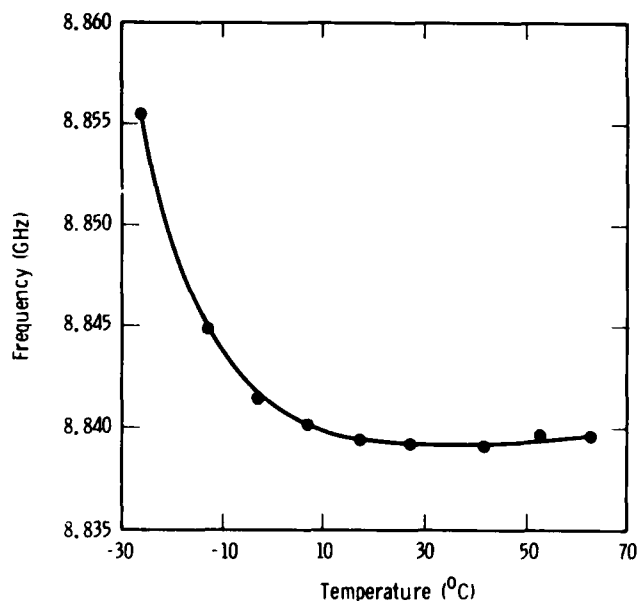
Figure 11. Variation in frequency of the delay stabilized oscillator as a function of temperature.

The assembled oscillator is shown in Figure 10. An amplifier having nominally 30dB gain over the range 7-12GHz was used. The open loop transmission amplitude and phase response was measured and the length of the semi-rigid coax and the attenuator values adjusted to give a net loop gain of +3dB with a phase change of 2nπ at 8.84GHz which was the center frequency of the delay line. The variation in center frequency of

oscillator with temperature is shown in Figure 11 over the range -30°C to +70°C. The frequency is stable to within ± 1MHz over the range +0°C to +65°C. At lower temperatures the frequency increases more rapidly with decreasing temperature. A similar increase in frequency with temperature is expected above the range shown here. This occurs because the variation of $4\pi m$ and anisotropy field are not linear functions of temperature.

Output power from the oscillator increased from +7.6dBm at +60°C to +9.8dBm at -20°C. Noise measurements were not performed but the effective Q, determined from the delay time (τ) by $Q_e = 2\pi f\tau$ was 5000. This Q_e value will be degraded by amplifier noise contributions. Although tuning using a coil wound on the bias magnet was not attempted, the low variation in oscillator frequency with temperature should be maintained. However the phase change with frequency which occurs in the loop external to the delay line would limit the tuning frequency range.[10]

10 - Channel Filter

The aim of the work described here was to design, fabricate and test a 10-channel multiplexed filter bank having minimum dispersion with 50MHz bandwidth channels continguous at their 3dB points. The performance goals for the filter bank were:

Center frequency	9.0GHz
Number of Channels	10
Channel 3dB bandwidth	50MHz
Out of band rejection	55dB
50dB bandwidth	100MHz
Multiplexed insertion loss	20dB
Bandpass ripple	1dB

The filter bank was designed as 10 narrow band delay lines, each fed from a common input transducer but with separate output transducers, as show in Figure 12. A bias field gradient was applied along the device so that each delay line experienced a different bias field and hence had a different center frequency. The transducers were formed from 50Ω impedance microstrip line on 0.635mm thick alumina and were open circuited at the end. The position of the delay lines along the input transducer was such that each was close to (N-$\frac{1}{2}$) electromagnetic half wave lengths from the open circuited end at its center frequency.

Narrow band pass characteristics were obtained by use of wide transducers (0.635mm) spaced 160μm from the YIG surface. The measured
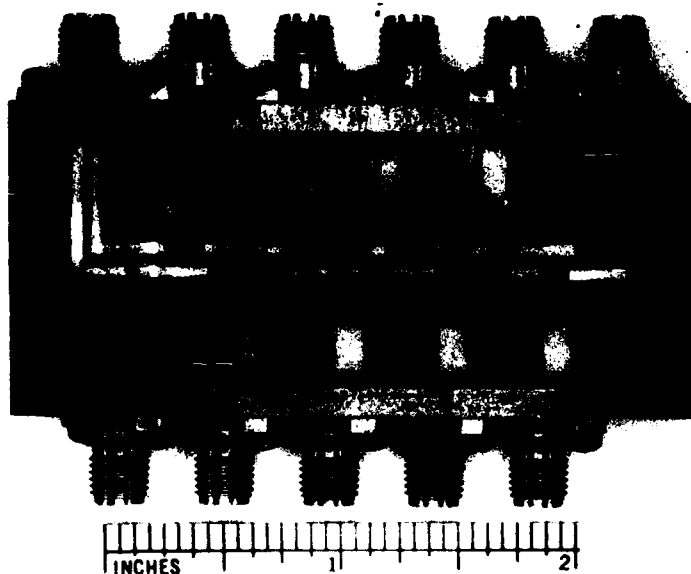
Figure 12. Interior of 10-channel filter bank.

Figure 13. Measured transmission loss as a function of frequency for an 18.6 μm thick YIG film, 1 mm wide, spaced 160 μm from 5 mm long by 0.635 mm wide transducers.

transmission loss as a function of frequency for an 18.6μm thick YIG film of width 1mm is shown in figure 13. In this test, both transducers were 5mm long, and 0.635mm wide on 0.635mm thick alumina. The YIG film was spaced from the transducer by 160μm and the applied bias field was 4880 Oe. In common with the other devices, the ends of the YIG were bevelled at a $\frac{1}{2}°$ angle to prevent reflections. Three seperate peaks labelled m = 1, 3, and 5 are clearly resolved. These correspond to width modes with transverse wave number $k = \frac{\pi}{w}, \frac{3\pi}{w}$ and $\frac{5\pi}{w}$, respectively. The behavior of width modes is discussed in more detail in a separate paper[13] and will not be dwelt on here. Note that the m = 1 mode shows characteristics which approximate the bandwidth goals for this device.

Techniques to suppress the effects of the higher order width modes were investigated[13] and it was found that the most effective approach in this configuration was an array of thin aluminum strips evaporated onto the surface of the YIG with the strips normal to the propagation direction. Eighteen strips of 300A° thick aluminum each 0.14mm wide and separated by 0.13mm resulted in attenuation of the m = 3 mode by 30dB. The aluminum strips also produced a small but undesirable, ∿ 2dB, attenuation on the m = 1 mode. In order to compensate for the increased attenuation and also to improve the symmetry of the passband, the ends of the YIG were cut parallel to the transducers. The distance from the end of the YIG to the transducer was adjusted to give constructive interference of the waves at mid-band. Figure 14 shows the transmission loss, over a 1 cm path length, as a function of frequency measured on an 18.5μm thick YIG film. This YIG film had 18 evaporated aluminum strips 364A° thick, to attenuate higher order width modes, and reflecting ends. The spacing from the ends of the film to the edge of the transducer was
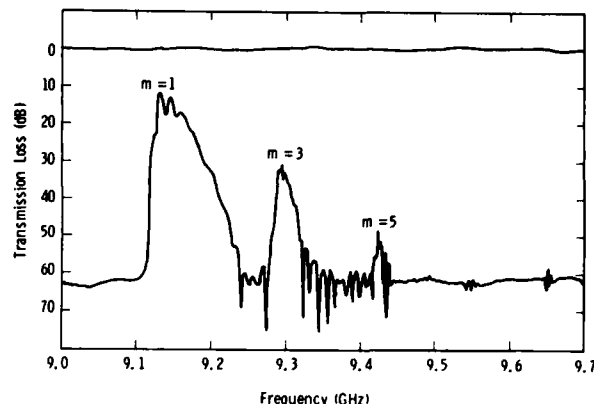
19
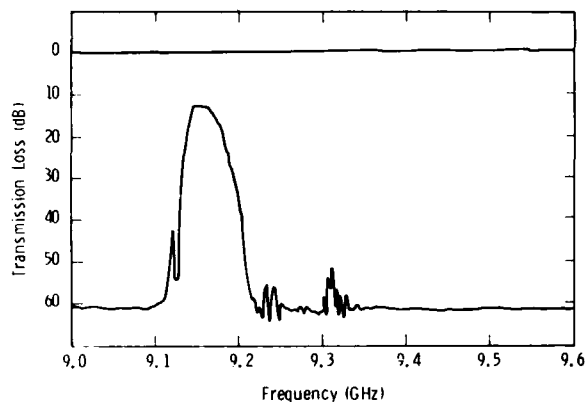
Figure 14. Measured transmission loss as a function of frequency for same parameters as Figure 13 except ends of YIG were reflecting and 0.31 mm from the transducers and 18 aluminum strips 364Å thick evaporated onto the YIG surface.

Figure 15. 10-channel filter.

0.31mm. Now the m = 3 mode is approximately 40dB down on the m = 1 mode which is reasonably symmetrical in passband shape.
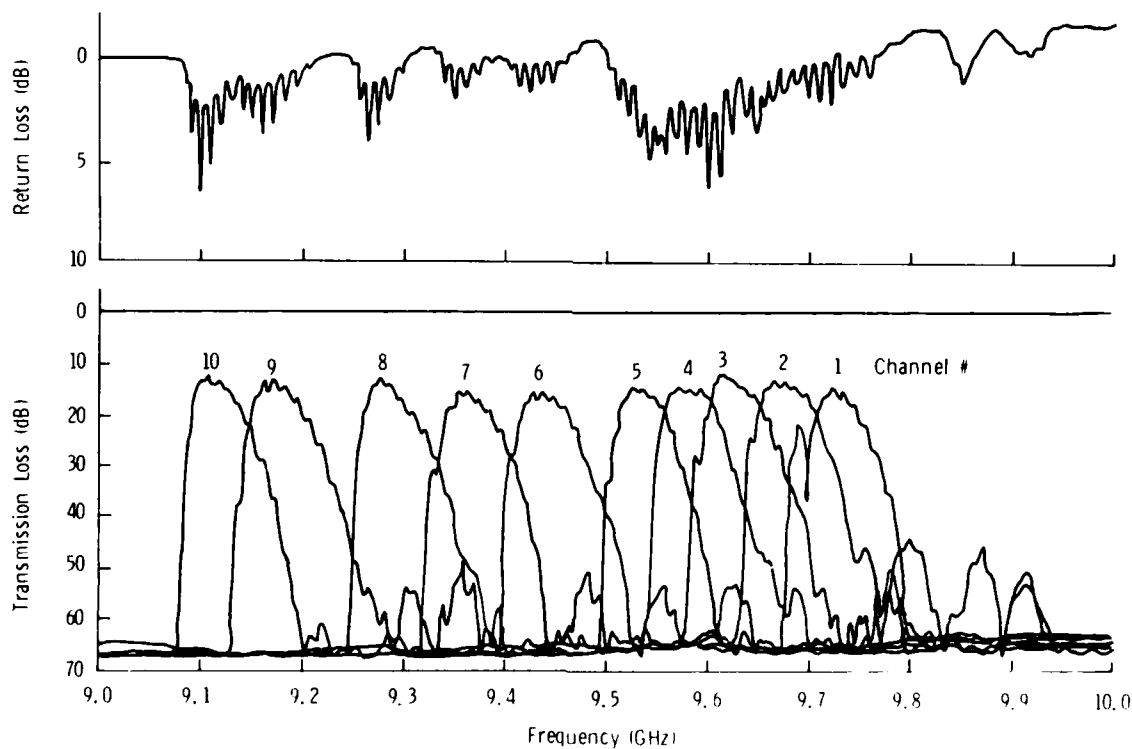
Figure 16. Measured transmission loss and return loss from input for 10-channel filter.

10 YIG strips each 23µm thick, 1mm wide and 6.65mm long were positioned as shown in figure 12. The spacing from the end of the YIG strip to the transducer was 0.31mm and the path length ∿ 5.4mm. The YIG strips were spaced from the transducer by glass slides 160µm thick. The assembled device, complete with bias magnet, is shown in figure 15 and the measured transmission and return loss for all 10 channels as a function of frequency is shown in figure 16. In these results the out of band m = 3 responses are higher than desired probably due to a reduction in the number of thin aluminum strips to 15 without any compensating change in thickness. The non-uniform spacing of the pass band center frequencies is due to the non-linear variation in bias field along the device length. In addition, variations in the spacing of the ends of the YIG from the transducers resulted in changes in the pass band shapes. In spite of these short comings, which are all potentially correctable, a general technique for obtaining multichannel filter operation has been demonstrated. In addition it has been shown that a degree of control of the pass-band shape can be obtained with simple single element microstrip transducers. Further control may be possible with relatively simple multi-element transducers.

Conclusions

The successful operation of these 4 devices demonstrates that MSW can indeed perform functions at X-band equivalent to those performed by SAW at VHF. Further development is required on all the devices before their performance is sufficient for systems use but they show sufficient promise that they warrant consideration for future radar and ecm systems applications.

REFERENCES

1. "Magnetic Surface Wave Device Technology" J. D. Adam, M. R. Daniel, T. W. O'Keeffe and P. R. Emtage. Final report on Contract Number F33615-77-C-1068; AFSC Aeronautical Systems Division, Wright Patterson AFB, OH 45433.

2. Z. M. Bardai, et. al. AIP Conference Proc. No. 34, 268, (1977).

3. P. R. Emtage, Journal of Applied Physics, 49, 4475, (1980).

4. Michael R. Daniel et al, IEEE Ultrasonics Symposium Proc. 806 (1979) IEEE Cat. No. CH1472-9/79/0000-806.

5. J. C. Sethares, et al, Electronics Letter, 16, 825, (1980).

6. "Magnetostatic Wave Propagation in YIG double films", Michael R. Daniel and P. R. Emtage, 1981 Microwave Magnetics Technology Workshop Proceedings.

7. T. W. O'Keeffe et al, IEEE Ultrasonics Symposium Proceedings, 522 (1980), IEEE Cat. No. 0090-5607/80/0000-0522.

8. YIG Device Catalogue, Watkins Johnson Co., (1978).

9. H. L. Glass et al, Materials Research Bulletin, 12, 735, (1977).

10. J. P. Castera, IEEE Trans., MAG-14, 826, (1978).

11. J. D. Adam et al, Journal of Applied Physics, 49, 1797 (1978).

12. Manufactured by Brown Boveri-Recoma Inc.

13. "The Effects of Width Modes in Magnetostatic Forward Volume Wave Propagation", J. D. Adam, 1981 Microwave Magnetics Technology Workshop Proceedings.

PHASED ARRAY REQUIREMENTS
FOR TIME DELAY DEVICES

Robert J. Mailloux

Rome Air Development Center

Electromagnetic Sciences Division

Phased Array Requirements for Time Delay Devices

Needs for wideband phased array technology have generally become more restrictive with applications demanding wide bandwidth and very low sidelobes. It is this sidelobe requirement that heightens the need for true time-delay divices while at the same time presents a challenge to researchers in the microwave magnetics area who would compete with conventional array technology.

The essence of this challenge is to produce highly accurate time-delay devices, comparable with phase shifters and switched line delays with accuracies on the order of a few degrees of phase shift, high power, fast switching times and temperature stable performance. Indeed phased array technology has long past an era where laboratory curiosities could compete merely on the basis of uniqueness. Magnetic devices must provide accurate control and in addition must be highly reliable and cost effective.

This paper describes the use of phase shifters and time delay devices at array and subarray levels of wideband scanning arrays, and presents data defining delay line specifications for low sidelobe phased array applications. In addition to random delay errors it is pointed out that the effects of correlated errors, like multiple transit effects and some dispersive effects, can give rise to high level peak sidelobes.

Figures 1 and 2 show why time delay devices are required for wideband phased array applications. Figure 1 shows the radiation pattern for an idealized linear array scanned to an angle θo by means of phase shifters using the phase increment

$$\Delta\phi = 2\pi\frac{d}{\lambda_o}\sin\theta o$$

between each element spaced "d" from adjacent elements. The figure shows that for scan to θo the wavefront should be delayed the normalized distance

$$\frac{D}{\lambda} = \frac{d}{\lambda}\sin\theta o$$

24

ARRAY SQUINT

$$F(\theta) = f_n(\theta) \sum_n |1n| e^{\frac{j2\pi}{\lambda_0}\left(\frac{\lambda_0}{\lambda}\sin\theta - \sin\theta_0\right)nd}$$
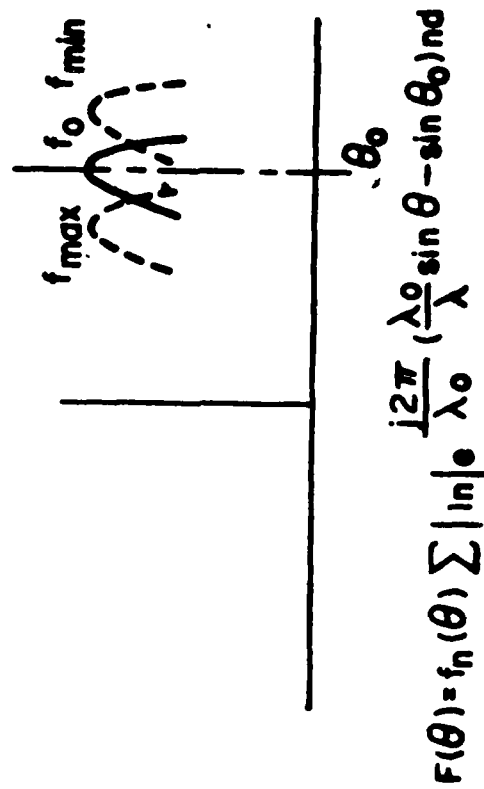
$$\frac{\Delta f}{f_0} = \frac{\theta_3}{\sin\theta_0} \sim \frac{\lambda}{L\sin\theta_0}$$

ARRAY SIZE L
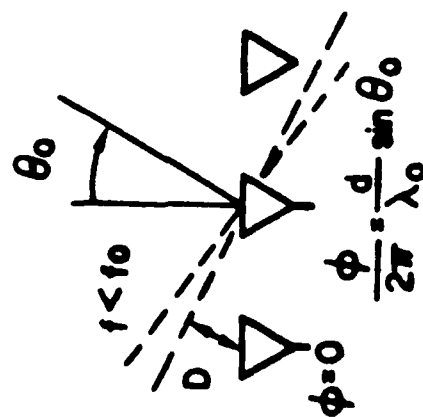
$$\frac{\phi}{2\pi} = \frac{d}{\lambda_0}\sin\theta_0$$

$$\frac{\Delta\phi}{2\pi} = \frac{d}{\lambda_0}\sin\theta_0$$

$$\frac{D}{\lambda} = \frac{d}{\lambda}\sin\theta_0$$

FIGURE 1.   PHASED ARRAY SQUINT

FIGURE 2. PHASED ARRAY BANDWIDTH

26

between elements and this corresponds to a time delayed phase front with phase $2\pi\frac{D}{\lambda}$. Thus an array with phase control can produce this correct delay only at the design frequency ($\lambda = \lambda_0$). At other frequencies the beam squints, and this change in beam position defines a three dB bandwidth of an array or subarray of size L as given in the figure.
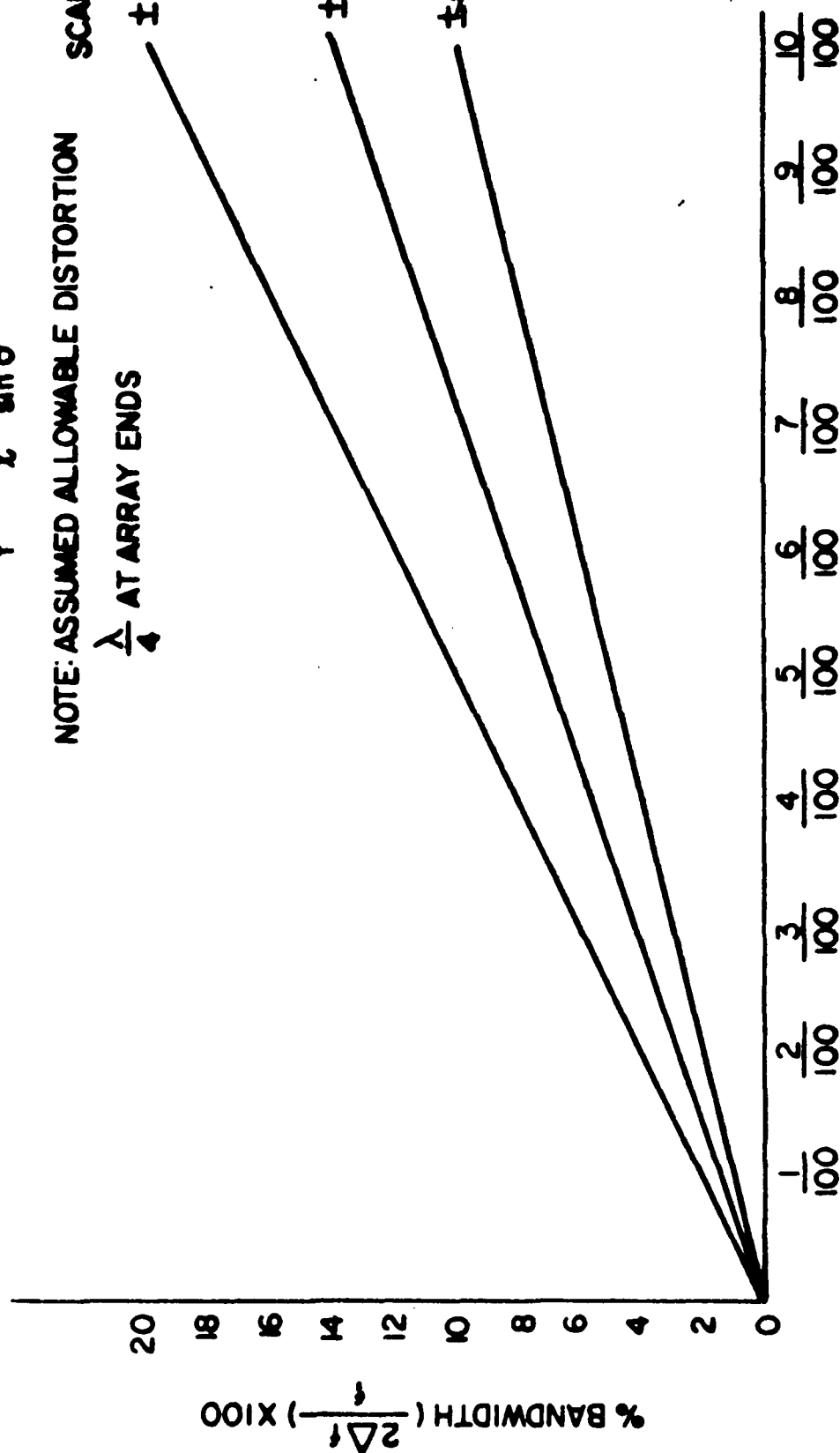
Figure 2 shows the computed bandwidth vs normalized inverse length ($\frac{\lambda}{L}$) for a typical array. Here it is assumed that the beamwidth θ_3 is approximately equal to λ/L.

Figure 3 gives the required ideal phase shift between elements and indicates the required frequency linearity of the phase shift, which of course is eqivalent to true time delay behavior.

Figure 4 indicates that if one chooses the array or subarray length L such that the band edges are defined by the equation

$$\frac{\Delta f}{fo} = \frac{\theta_3}{\sin\theta_0}$$

then the array time-bandwidth product is approximately unity. This relationship is used to determine approximate maximum delays required across the array.

Time delays are often conveniently used at the subarray level. Figure 5 shows the bandwidth of a square array divided into delayed subarrays with phase control within each subarray. The figure indicates the bandwidth reduction for increased gain, and points out the need to divide the array into many subarrays to achieve wideband high-gain operation. In this case the bandwidth criterion is 1.5dB loss and so bandwidth is halved relative to earlier figures.

The proper excitation of subarrays is one of the more difficult problems facing modern array technology. Figure 6 indicates the formation of substantial grating lobes when subarrays are contiguous. These lobes can be avoided by exciting near-random subarray sizes, on by synthesizing sophisticated overlapped feed distributions to produce flat-topped subarray patterns as shown in Figure 7.

TIME DELAY PER-ELEMENT

PHASE $\phi = \dfrac{2\pi}{\lambda}\, nd \sin\theta_0$

$= \dfrac{2\pi}{C}\, nd \sin\theta_0\, f$

LINEAR WITH FREQUENCY

DELAY: $\tau_n = \dfrac{nd}{C} \sin\theta_0$

FIGURE 3.   TIME DELAY REQUIRED AT EACH ELEMENT

28

TIME x BANDWIDTH

ARRAY BANDWIDTH

$$\frac{\Delta f}{f_0} = \frac{\theta_3}{\sin\theta_0} \sim \frac{\lambda}{L}$$

REQUIRED DELAY

$$\tau = \frac{L}{c}\sin\theta_0$$

$$\tau = \frac{L}{c} = \frac{\lambda}{\frac{\Delta f}{f_0}} \cdot \frac{1}{c} = \frac{1}{\Delta f}$$

$$\boxed{\tau \Delta f \sim 1}$$

L = ARRAY OR SUBARRAY SIZE

100 MHz ~ $10^{-9} \times 10$ sec

1 GHz ~ 10^{-9} sec

10 GHz ~ $10^{-9} \times 0.1$ sec

FIGURE 4. DELAY-BANDWIDTH PRODUCT AT SQUINT LIMIT

BANDWIDTH VS. GAIN
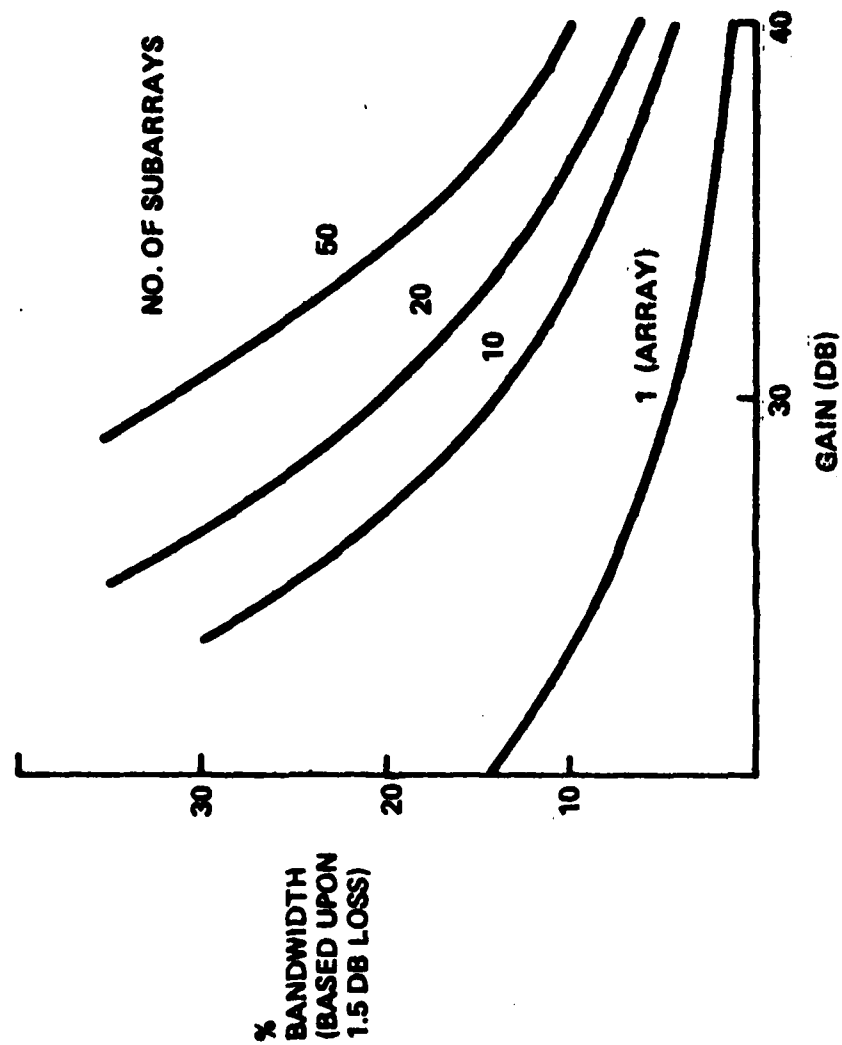
FIGURE 5. ARRAY BANDWIDTH VS GAIN FOR SUBARRAYED ARRAY

29a
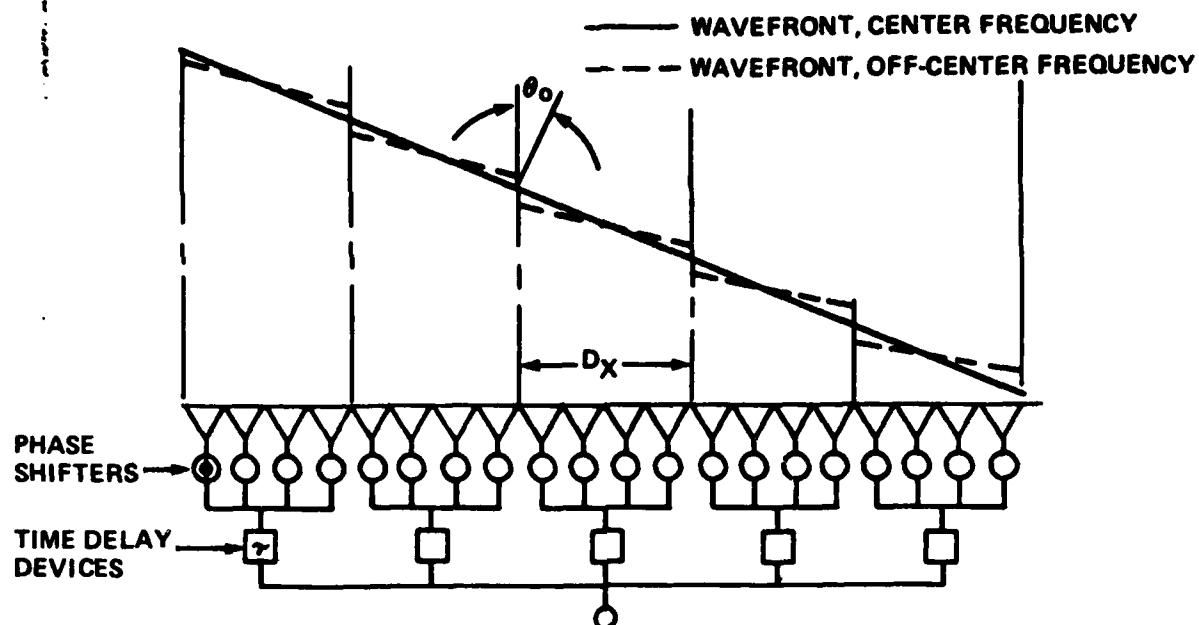
FIGURE 6. GRATING LOBE FORMATION
WITH CONTIGUOUS SUBARRAYS

30
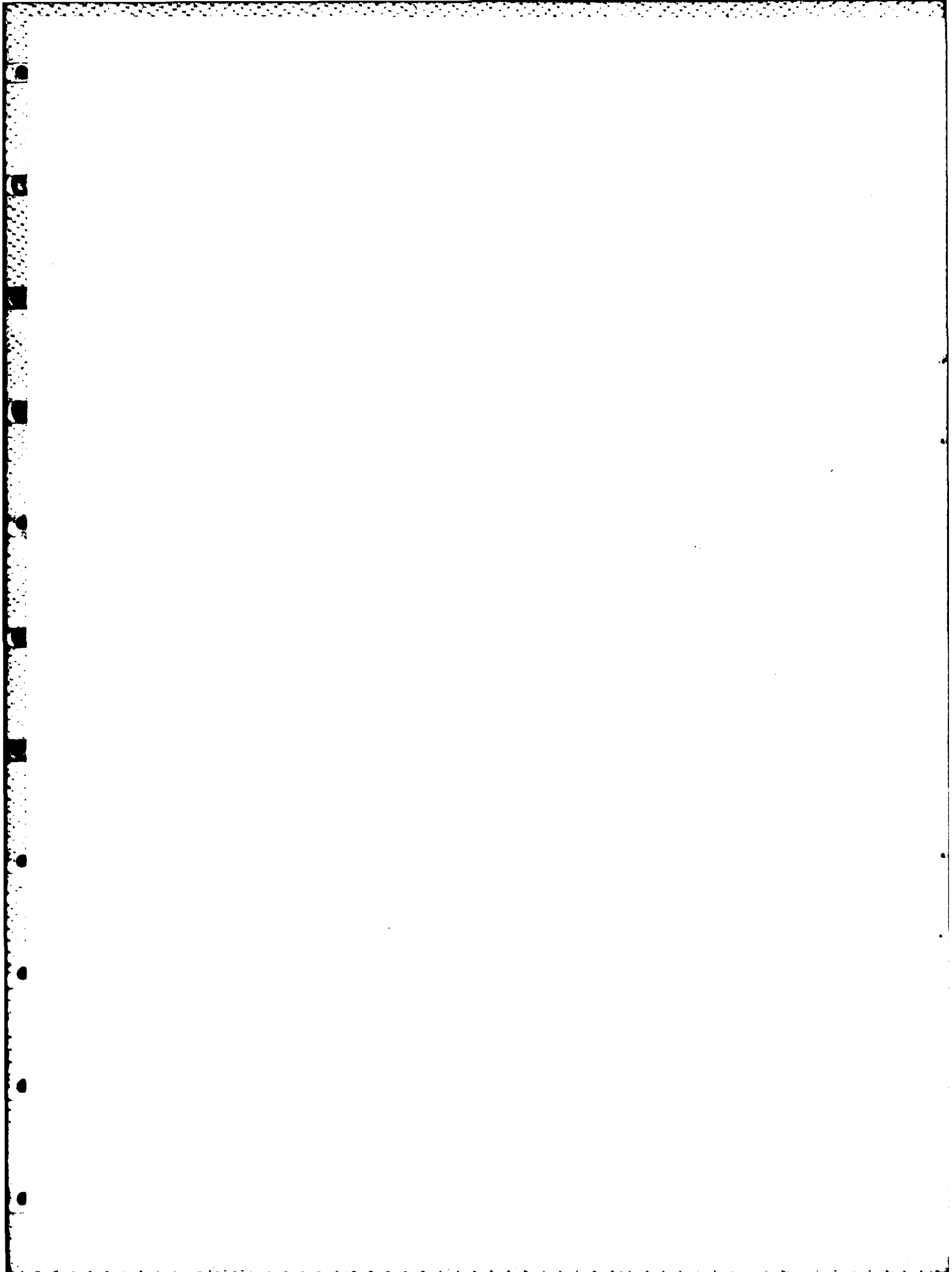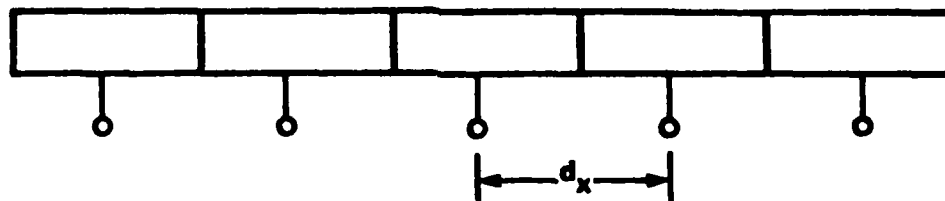
A. OVERSIZE ELEMENTS OR SUBARRAYS

$$-\frac{d_x \sin \theta_m}{\lambda} \qquad \frac{d_x \sin \theta_m}{\lambda} = 0.5 \qquad \frac{d_x \sin \theta}{\lambda}$$
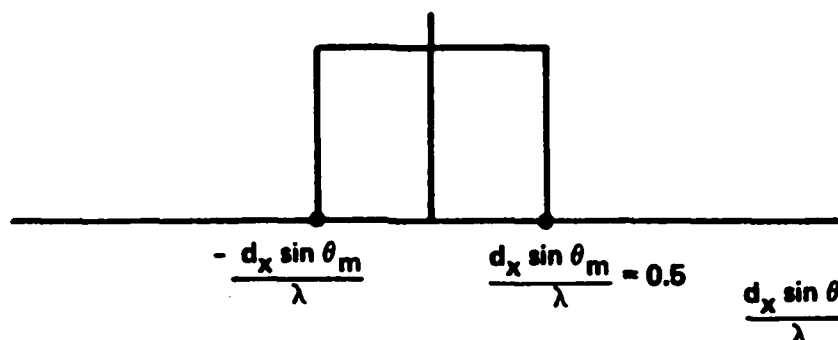
B. "IDEAL" ELEMENT PATTERN
(cos θ SUPPRESSED)
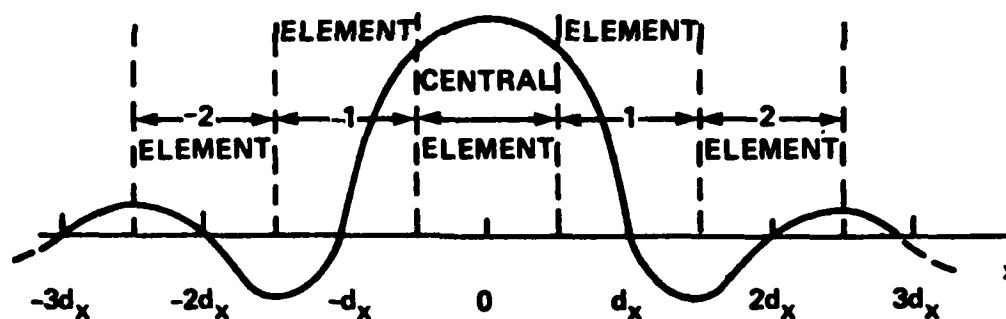
C. SUBARRY DISTRIBUTION FOR SCAN

TO $\frac{d_x}{\lambda}$ $\sin \theta_m$ = 0.5
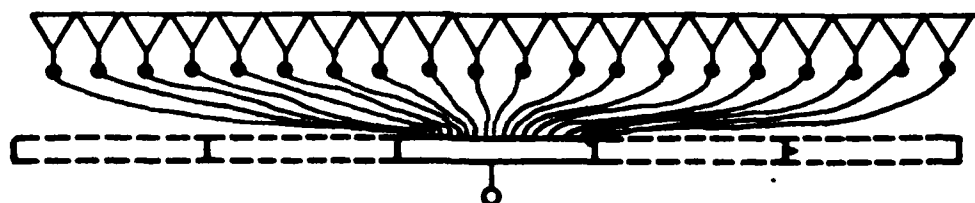
D. OVERLAPPED DISTRIBUTION NETWORK

FIGURE 7.   OVERLAPPED SUBARRAY FOR GRATING
            LOBE REDUCTION

31

Figure 8 shows one example of a feed network that produces a properly

flat topped subarray pattern. This network, called a completly overlapped feed,

uses a Butler Matrix or a focussing (Rotman)lens to form a Fourier Transform

of the focussed energy at the center of a cylindrical lens. The operation of such

a feed is too complex to describe in this paper, but it does represent one of the

possible ways of suppressing grating lobes in wide band subarray scanning arrays.

In addition to meeting the required subarray size criterion and choosing the

true-bandwidth product subject to the gain criterion or some other selected

criterion, one must develop highly accurate delay devices in order to avoid

forming high sidelobes. Figure 9 gives approximate equations for peak and average

(far) sidelobes of an array with random (Gaussian) errors. Figure 10 shows the peak

sidelobes vs gain for an array of columns (dashed) in the plane perpendicular

in the columns and a fully agile array in the scan plane. The figure includes the

assumption of three dB system loss, and shows that highly precise phase or time

delay controls are required to achieve the very low sidelobe (-40 to -50 dB) levels

often proposed for future tactical radars, and that much more precise settings are

required for the array of columns than for the full two dimensional array.

In any situations the time delay device competes directly with phase shifters.

Although it offers wider band array performance, it must still have characteristics

as good as the competing phase shifter. To discuss these requirements more lucidly,

let us look at specifications which, if taken all together, would represent a very

difficult phase shifter development:

Frequency: x-band

Loss: 1 dB (easy with ferrites, harder with diodes)

Speed: 2 µ -sec (easy with diodes, harder but possible with ferrites. There's

also a market for much slower, highly accurate controls)

Accuracy: 0.5° to 5° (lower number is about the state-of-the-art for best

ferrites and diodes)
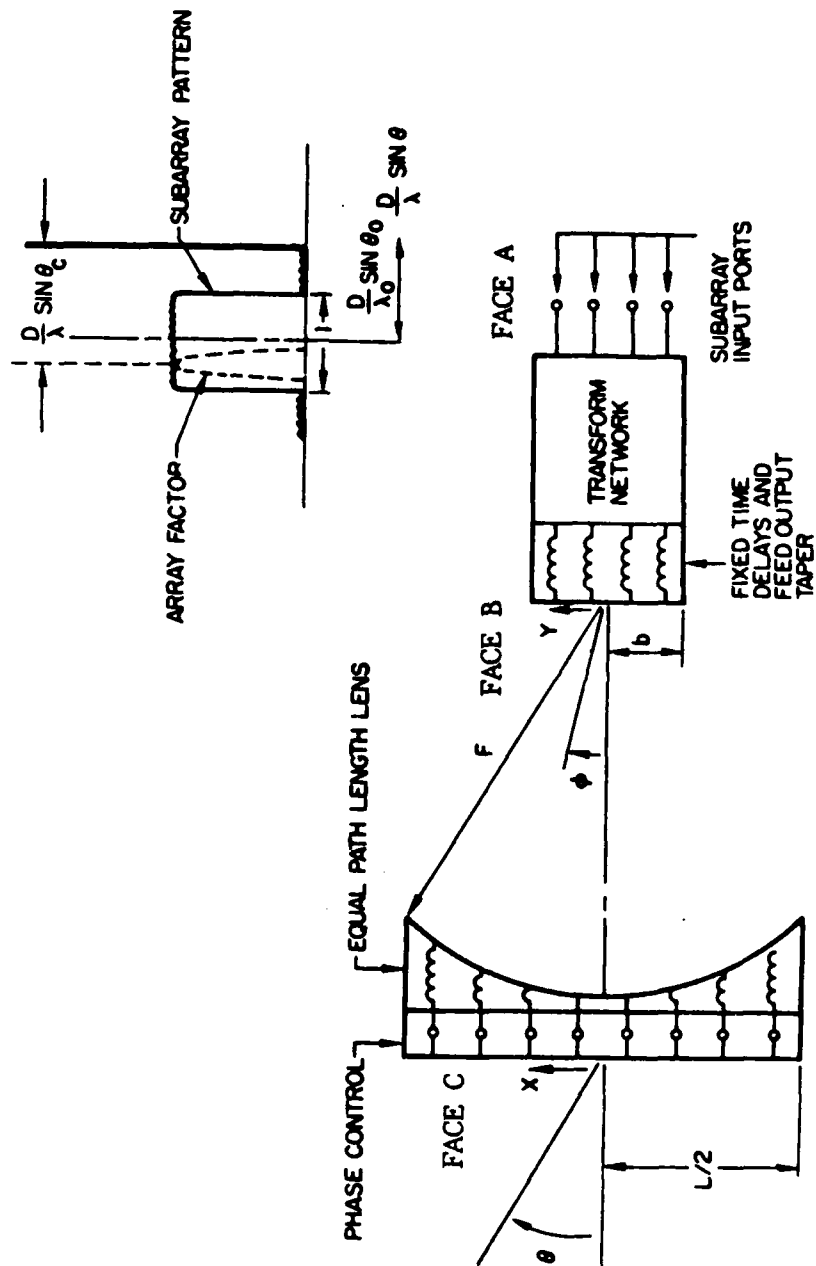
FIGURE 8. COMPLETELY OVERLAPPED
SUBARRAY SYSTEM

33

ERROR SIDELOBES:

FAR SIDELOBES

$$\sigma^2 \sim \frac{\delta^2 + \Delta^2}{N\eta}$$

PEAK SIDELOBES

$$\delta^2 \leq \frac{1}{10\pi}\frac{G}{R}$$

Δ^2 = AMP. VARIANCE

δ^2 = PHASE VARIANCE

N = NO. ELEMENTS

η = EFFICIENCY

σ^2 = AVG. SIDELOBE LEVEL

G = ARRAY GAIN

R = NUMERICAL SIDE LOBE RATIO

FIGURE 9. PHASE AND AMPLITUDE CONTROL ACCURACY

PEAK SIDELOBES VS. GAIN FOR COLUMN ARRAY AND TWO DIMENSIONAL ARRAY
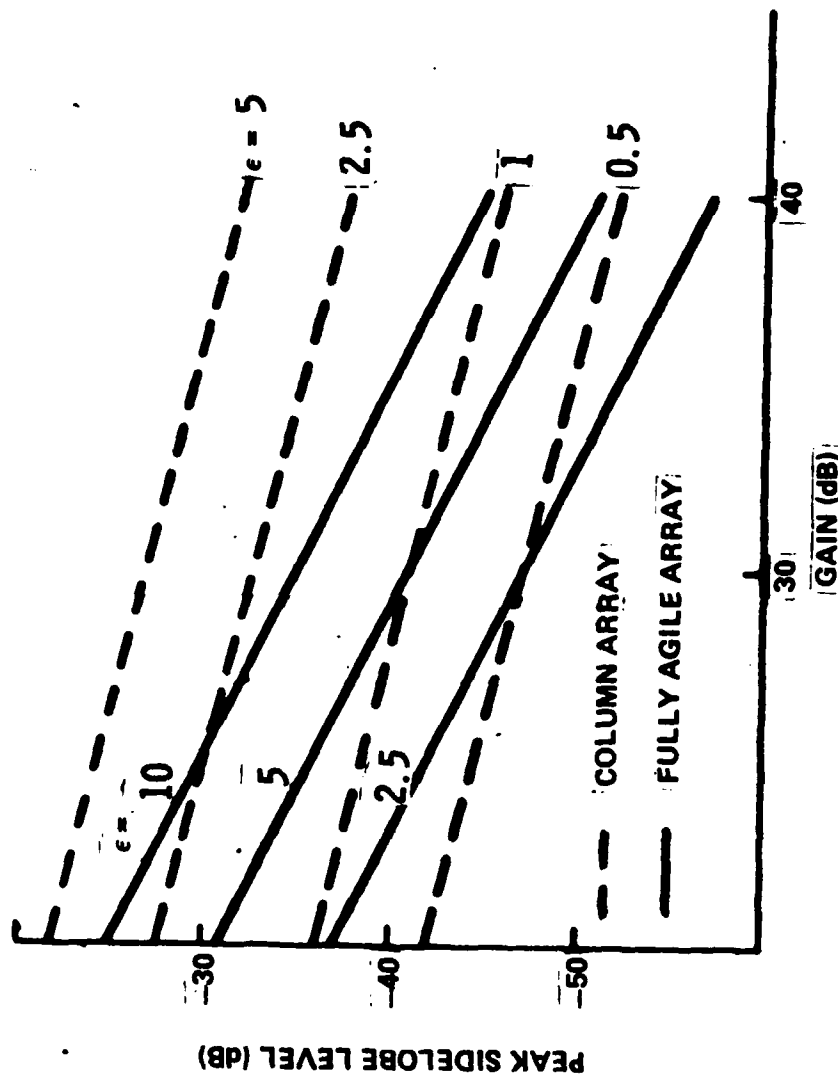
FIGURE 10. PEAK SIDELOBES VS GAIN

35

Power: 10 to 100 watts

Cost: $50 to $100 (I doubt that $50 has been achieved when phase shifter and driver are considered)

The phase shifter accuracy requirements are based upon the assumption of random error across the array. When the error is correlated there may be much larger peak sidelobes. One such case is illustrated when quantized phases are used to scan an array. Figure 11 shows the phase error across an array excited with N-bit phase shifters and Figure 12 shows the peak sidelobes resulting from such quantization. This data, due to Miller shows the dramatic effects of relatively small errors correlated across the entire array.

Correlated errors are likely to occur in time delay steered arrays because identical devices are used everywhere in the array but subject to different applied fields. An example[2] is seen in the early data of Sethares, Owens and Smith in Figure 13 for the case of dispersion compensated magnetostatic-wave time delay elements. If one assumes that elements across the array are excited by identical elements with varied magnetic bias fields, then a vertical line through the curves samples the element time delay. Since the curves are not parallel, any field selections that would give ideal steering control at one frequency would necessarily be incorrect at another. These errors are not random but are progressive with long correlation lengths as indicated in the lower figure, and corresponding to compression or expansion in the group of τ vs frequency curves. Depending on the amplitude and correlation length of the error this could result in deterioration of the main beam or discrete sidelobes.

One final example of errors with long correlation lengths is a result of internal reflections within a time delay device. Depending upon the reciprocal properties of the medium, several types of multiple transit effects can occur. As indicated in Figure 14 triple transit occurs when a component of the signal is delayed by three times the required delay for proper scanning. The resulting inter-element phase shift is also three times the required shift ϕ, and one can evaluate-

PHASE ERROR DUE TO QUANTIZATION
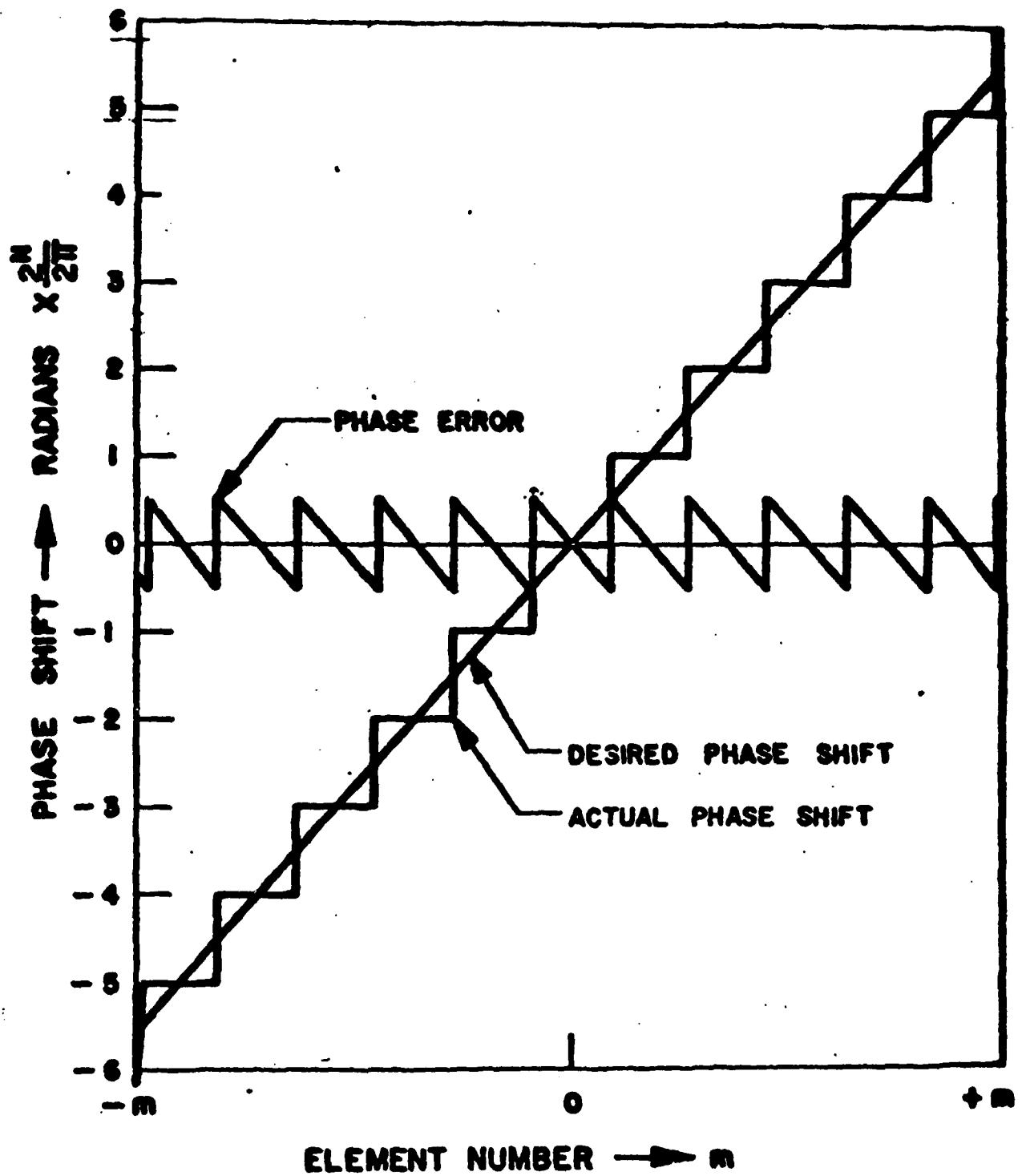
FIGURE 11. PHASE QUANTIZATION ERROR (REF 1)

37

PEAK SIDE LOBES DUE TO QUANTIZATION
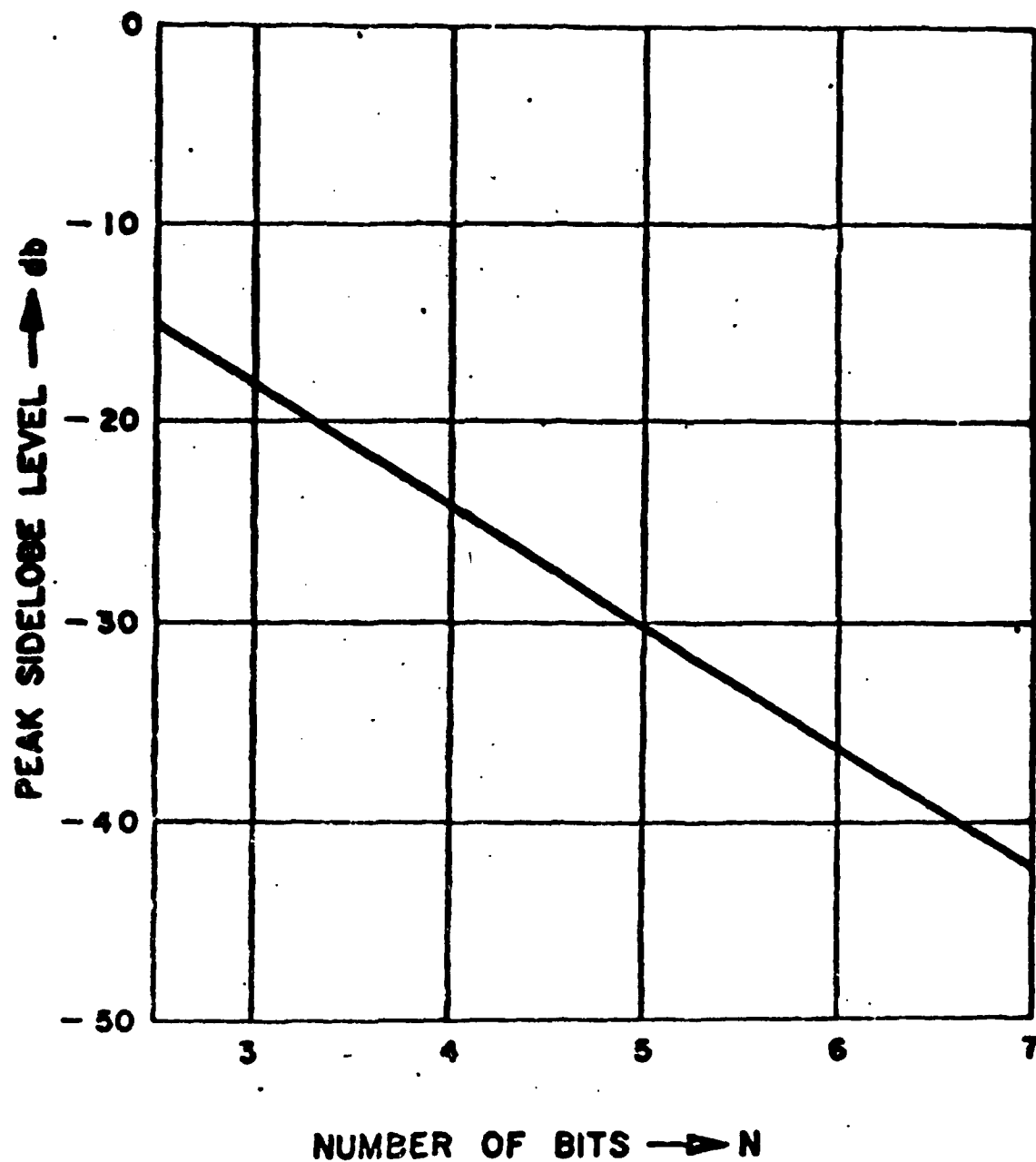
FIGURE 12.   PEAK SIDELOBES DUE TO
             QUANTIZATION (REF 1)
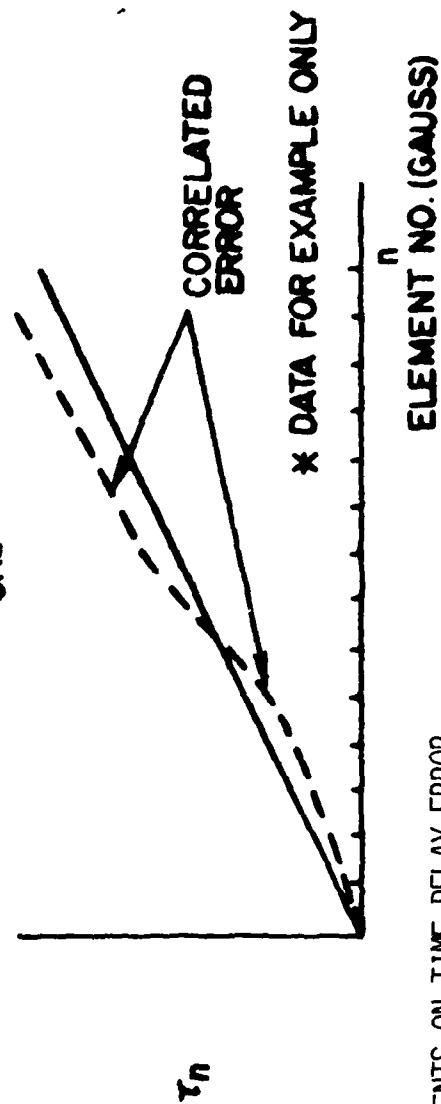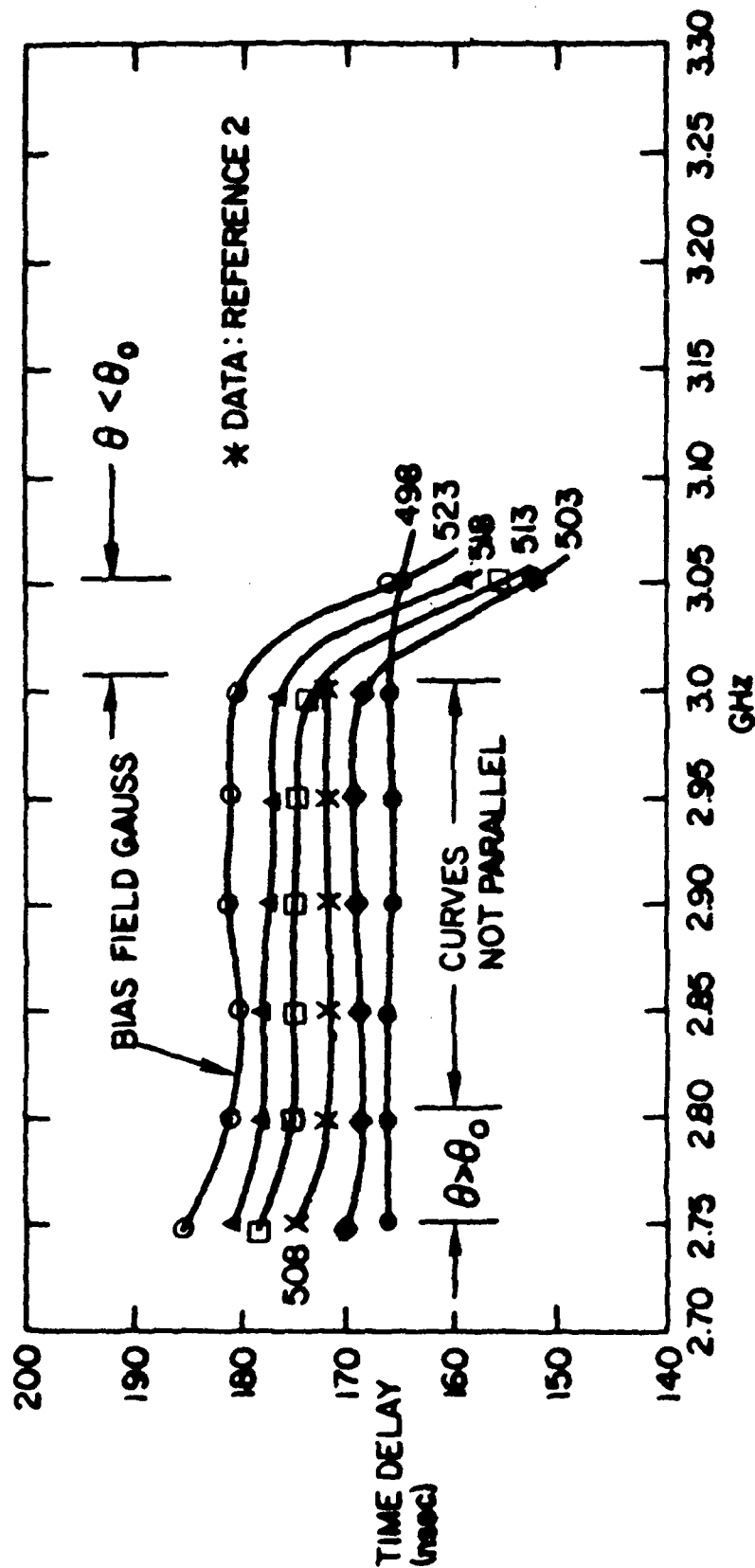
FIGURE 13. COMMENTS ON TIME DELAY ERROR

39

several angles θ_{3T} corresponding to the primary angle (q=o) and several grating
lobe angles (q=1,2) that represent real radiation of this triple transit wave.
Figure 15 shows angles for triple and five-times transit corresponding to a main
beam angle θ_0 and reasonable inter-element spacings d=-0.55 λ . The amplitude of
the radiated wave at each of these angles is the product of the element pattern and
the triple or multiple transit transmission amplitude coefficient.

These are some of the phenomena governing array performance for time delay
steering. Taken together they comprise an imposing assortment of challenges
for the designers of microwave time delay devices for array antennas. The challenges
are severe because of the need to compete with very advanced phase shifter technology
that supports exceedingly low sidelobe array performance, while in addition the possibility
of systematic errors makes requirements for time delay devices much more stringent
than for phase shifters. These errors have long correlation lengths and are
recognizable as non linear (dispersive) phase shift with frequency and multiple
transit phenomena. Despite these difficulties, there is so great a need for
accurate wide band time delay devices for array steering, that this application
should provide a major and continuing stimulus to magnetics research.
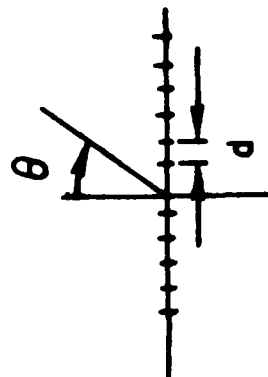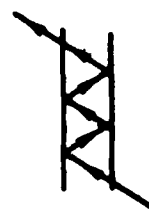
FIGURE 14. RADIATION LOBE ANGLES ASSOCIATED WITH MULTIPLE TRANSIT EFFECTS

41
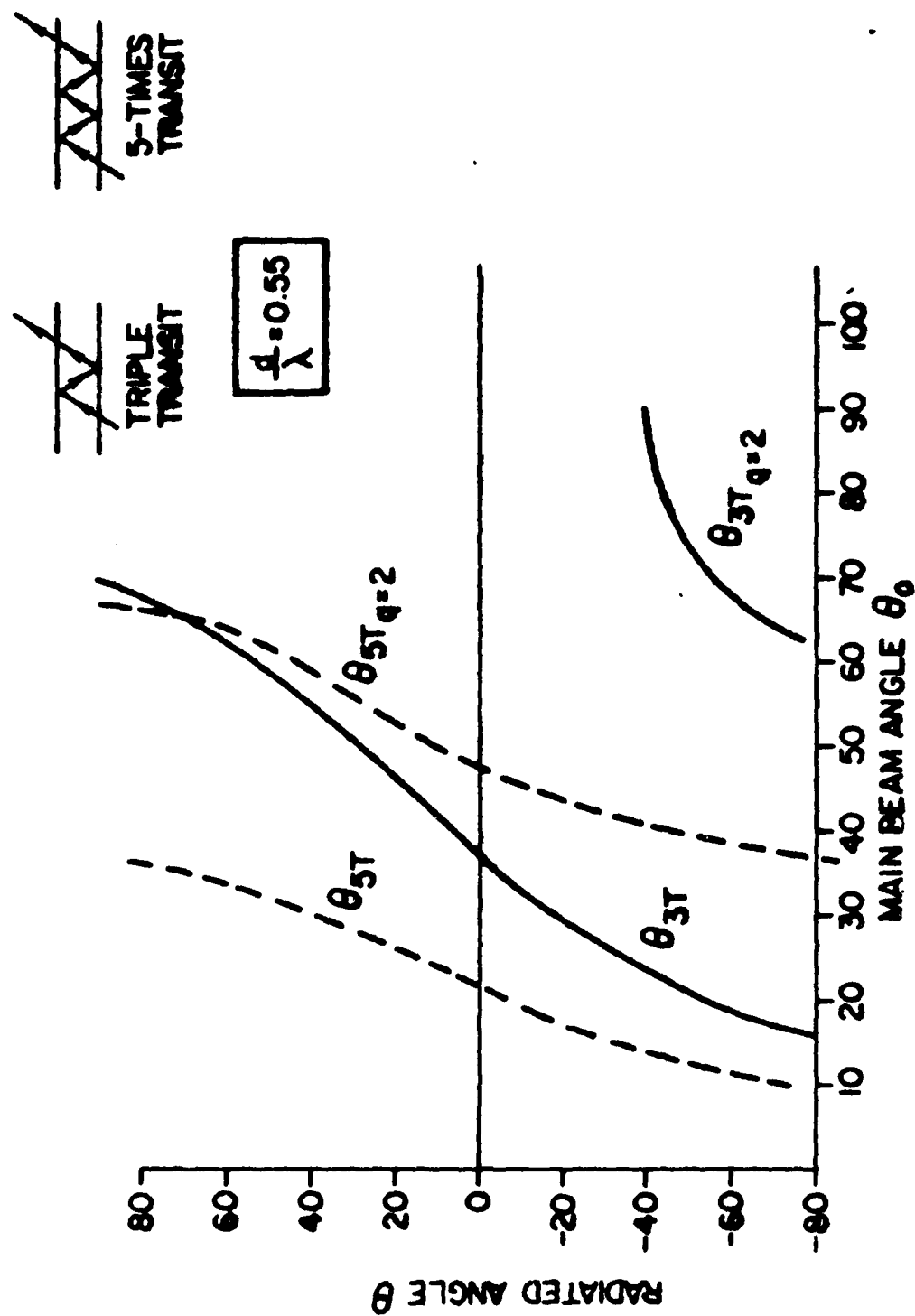
FIGURE 15.   MULTIPLE TRANSIT RADIATION LOBE
ANGLES

42

REFERENCES

1. C.J. Miller, "Minimizing the Effects of Phase Quantization Errors in an Electronically Scanned Array, Proc. 1964 Symp. on Electronically Scanned Array Techniques and Applications, RADC-TDR-64-225, Vol 1, pp 17-38.   RADC, Griffiss AFB, NY.

2. J. C. Sethares, J.M. Owens and C.V. Smith, "M.S.W. Nondispersive, Electronically Tunable Time Delay Elements" Electronics Letters, 23 Oct 1980, Vol 16, No. 22, pp. 825-826.

SOLID STATE T/R MODULE REQUIREMENTS

E. Hunter Chilton

RADC/OC, Griffiss AFB, New York

(Transcription of a tape recording made at the
Workshop)

I'd like to thank Bob Mailloux and one of the questioners following his

talk. It makes pretty much a total and natural introduction to my remarks.

What I'm going to be talking about are some fairly major programs we

have, to develop transmit receive modules for phased array radars\ We're

doing this in conjunction with developing monolithic microwave integrated

technology in two media, silicon on sapphire, and gallium arsenide, to

cover the frequency range 1-10 GHz. To set the stage a little bit more

as to what we're emphasizing, I'll call your attention to various parts

of this Fig., especially to the RF portion. We have a TR module that

would be used in each radiating element of a phased array. This shows a

space feed. This could also be a corporate feed array. We have a phase

shifter before any stages of amplification. A signal passes through a

TR switch and amplifier chain, out through a TR switch. It is radiated,

and comes back through a low noise amplifier and back through the channel.

Phasing information is contained on the feed signal and is decoded by a

micro processor, co-located with the module to set the phase shifters. I

want to come back to the TR switch especially, in a few minutes, because

it's an area where, perhaps, some of you and some of your technology

could be of help to us. The monolithic technology we're talking about

is different from the microwave integrated circuits we've used in the past.

I have some pictures of those. We're doing everything via process control.

All of the active and passive components are placed on a single substrate.

It is totally process controlled. For the most part the human is out of the

loop. And by doing that and by going to lumped elements as opposed to distributed

circuit elements we obtain at least 10-1 reduction in size and weight and cost.

However, when we do that, the circuit complexity increases.

45

While the area of a monolithic microwave circuit is large, the complexity
and the density of it is considerably less than that of a VHSIC type
circuit, although we are borrowing in many cases from the digital technology.
When I talk about monolithic, I don't want to get hung up on semantics, I
mean that it will eventually be nice to complete the blocked diagram that
I just showed totally on one chip. That may not be feasible either
technically or economically. To do that you go to rather large areas,
that is maybe an inch or so square, and, as the area goes up (bear in mind
again it is totally process controlled) for instance if your processing
something like 3" wafers the yield will go down. So eventually, in
production it may be more economical to fabricate various submodule
components totally and monolithically, and then join them together-
integrate them into a package. Cost is one area that I'd like to emphasize
a little more. Bob touched on it. He touched on what the projected cost
of phase shifters ought to be, in the neighborhood of $50-100. We're
shooting for a complete transmit receive module, to be produced and tested
in large quantities at a cost in the $100 neighborhood. That's the phase
shifter, power amplifier, low noise amplifier, TR switches, etc., everything
for $100, and if you stop and think about the cost, for just a moment,
you can see at least the economic necessity of it. The technical
realization of it is not easy. But, take a tactical radar system, one
that is not unrealistic, a tactical radar system of 20,000 elements. If
the Air Force were to buy 50 of these systems, which again is a reasonable
number, you are up to a million modules per radar system. At $100 an
element, this amounts to $100,000,000. At $1000 per element, or so, as
in other projected costs of hybrid modules, one begins to see the problem.

This is a hybrid module developed a number of years ago. It is not
a totally direct comparison with this one right here, this mock-up right

here, but, it is a reasonable one. For example, this area back here

is a 4-bit phase shifter. One quarter of this is an equivalent 4 bit

phase shifter. This does have higher power capability than the one right

here. This one employs a circulator. This one doesn't. We don't know

how to make a monolithic circulator. It's an area I'd like to ecourage

some of you in this group to consider with magnetic materials and so

forth, maybe it is feasible to make something like a circulator. It's

going to be a problem for us doing it with a TR switch. Expecially as we

increase the power handling capabilities, as we do that, insertion losses

go up the complexity goes up and reliability probably comes down.

Why the two technologies? Why the two different media for the

technology we're developing? Gallium arsenide seems to be a preferred

material that has a much higher electron mobility therefore a higher

operating frequency capability, or conversely probably better performance

at lower frequency. Probably the biggest thing lies in this area here.

Gallium arsenide has been under development for a number of years. Its

been primarily funded by the military. There has not been, and there

probably won't be, as large a commercial market, (even though there is

one emerging) as there has been in the case of silicon. The silicon

material, the processing, the handling, everything, is benefiting us. We

are benefiting totally from the commerical market. Eventually, the cost

(if the people that are growing gallium arsenide can do it

reproducibly and in quantities for production) may be reduced by as much

as 3 times, (although that is not necessarily a major factor) at the rate

gallium arsenide is produced at the moment. I use this just as an example.

It varies somewhat when we're talking about silicon. It doesn't really

matter that much. We're starting out in either case with some media, silicon on sapphire or gallium arsenide. The thing is totally photographically metalized or insulated and so forth. Ion implantation is used for the active devices, etc., Things like air bridges are fabricated for something like junmping from one part of the circuit to the other. Consider the hybrid microwave integrated circuit with the bipolar transistors in it. Each one of those were packed in a separate package, and, when you take the package off of that you see a whole bunch of individual wire bonds in it. That not only adds cost to the production of it, they add a reliability problem. Anytime there's a wire bond or a human in the loop the reliability, we know, goes down. They also, because they are not exact and not process controlled, they have variable conductances which requires more specific and individual circuit matching for the device. So by going to a total process control we are gaining in many areas. I put this up just as a sort of typical set of numbers that we're shooting for. It could be anywhere from L-X band. I don't have numbers on here like Bob alluded to earlier of the phase shift RMS error and so forth, but the 5 degree numbers that he mentioned are typical. Again, the necessity to keep the production cost way down is important.

Here is another example of how the work is going: This happens to be at L band, and its silicon on sapphire. This is a 3 stage low noise amplifier that was built a few years ago. We've used the same basic technology, in hybrid form today. There are three bipolar transistors in it. This is the circuit right here, up in the corner of it, in monolithic form again a 3 stage low noise amplifier. At this stage of our development the noise figure is not quite as good as this, however, the power consumption of this is roughly 1/2 of the hybrid circuit. The size is

1/40 of the hybrid circuit. And, some of the cost numbers I'll show

you a little later come out to imply that the cost can be 1/10 of that

of the hybrid circuit. It doesn't matter much how I orient this. This is a 4

bit phase shifter in monolithic form. This is again silicon on sapphire.

I've picked some phase shifters here around the edges, but again notice

the lumped inductors and capacitors that are in this as opposed to the

distributed elements. The physical size here is in the neighborhood of

3/10 of an inch, from one side to the other, or, looking down at the technology

a little more, I just show this as a more detailed view of one of the

circuits, an air bridge going over on top of another circuit element.

We have in the first picture I used of the hybrid module and the mock-up

monolithic module, We have a scale in it other people use coins and so

forth to set the scale. This is an artificial unit put in here as a

scaler. It is one red blood cell. We have some of the units that have

been developed so far. This is a 3-stage amplifier putting out in the

neighborhood of 3/10 of a watt or so in monolithic form. And this is the

test fixture for it. This was developed by Raytheon, we're testing it at

RADC. They obviously don't trust us not to burn out the device and

they've taken care of that. To date we haven't burned any out, and they

have performed very nicely. The phase shifters here use (I shouldn't say

approximately 0, I should say) micro watts of DC power, a little clearer

there. Phase shifters now, instead of using diodes we're using active

devices, field effect transistors and the holding power is miniscule as

opposed to the power used by pin diodes. Noise figures that we're getting

today are not as good as we'd like, obviously we'd like lower than 5 db.

That's pretty much as low as possible. Power and efficiency are coming

on nicely. Some of the applications we're considering, like for space,

radiation hardening is a concern. This is a fairly low power module like that mock up I showed. I won't pass it around because this is the only one I've got, but you can see it later. We're projecting something like this, a complete module, to weigh on the order of 2 grams, and to be something like this, a 1X1 inch mock-up. It was on the earlier viewgraph, it may even be less than that. This is the 3 stage hybrid amplifier I showed. And I have a 3 inch silicon on sapphire wafer here, which you probably can't see that well, but, you can

imagine the number of circuits that you can begin to produce all on a single wafer. And typically in the integrated circuit business, they process 25 wafers at a time. The other part of the program using GaAs for the higher frequency, a 4 stage amplifier; the dimensions are not on this figure, the dimensions are somewhere between 6-8 mm and it is putting out about 8/10 of a watt of power. I have various viewgraphs from various contractors. Altogether we have four contractors working on this, the viewgraphs I've picked are coincidence rather than a reflection on the work. All four are doing excellent work. The previous 4 stage amplifier I showed, happened to be done by T.I. These are some results from Raytheon. Again, very nice performance over a fairly broad band, and overall efficiency of around 17%. However things are not necessarily totally great. This is a predicted performance based on the variation in capacitance of a 2-stage amplifier with a "+" or "-" variation in the capacitance value of an amplifier. The performance would be predicted to vary by this amount as opposed to the actual design performance so that it obviously points out the need for very good process control.

Again somewhat of a summary of the GaAs type of work. The noise figure is down in the neighborhood of 5 dB or so for a 2 or 3 stage

amplifier. Insertion loss of the TR switch is very good. As we go to
these modules and we start talking about large quantities it's necessary
to go to automated testing, and that's what we're equipped to do. Most
of the contractors are also equipped to do it, to test all the RF parameters
of modules under dynamic loads, under varying thermal loads. Many of
the immediate applications we envision, that the Air Force envisions,
are for phased arrays in space.
They'd be sitting in full exposure to the sun, or fully eclipsed by the
earth so they would be exposed to very wide thermal fluctuations. They
would be in a tactical environment operating anywhere in the world.
So we're instrumenting to thoroughly test these. Their performance has
been very similar to that obtained by the contractors.

Let me go back to the cost again because in many respects it is
probably one of the most critical drivers we have. Now, I've sort of
broken it out this way. This is based on a single function, say a 3 stage amplifier
or a 4-bit phase shiter, (something in the neighborhood of this size)
one of the major sub module components. By the time you've taken into
account the cost of the material, the processing, projected yields and so
forth, we see a 2:1 difference in the cost of a circuit. However, when we
begin to factor in the cost of packaging and testing, (this is ten here
instead of twenty although 20 may be a more realistic and still conservative
number) and all, the bottom line is that the total cost delta is not nearly as
much as it appears here. But the testing and assembly is a major portion
of the cost of a module. These modules as I indicated are exposed to a
wide thermal environment, they don't have good circulators in them so mis-
matches coming from scanning of the array, mutual coupling of other elements, etc.,

51

can have an impact on the modules. We're looking at various schemes to
sense and adaptively control so we can (regardless of what's causing the
fluctuations or deviation) maintain whatever the phase and amplitude
at the radiating element is, that the systems designer requires.

We begin to look at the hybrid technology for equivalent modules. They are
always projected to cost about $1000 maybe even more, but, by going to
monolithic technology we see at least a 10:1 reduction in both the size
and the weight and the cost. Once you do that, it opens up new ways
of looking at total systems, and you can begin to consider possibly
increasing the number of functions you perform on a single chip or a single
module, if for some reason the systems person would want to do that.
Obviously the cost would go up. This scale does not directly correspond
to this. This shows basically trends you can begin to look, at various
future possibilities for modules. It is possible to have digital signals
coming in and out, or all of the receive functions being performed on the
modules, as well as the normal functions I've been talking about here.
The monolithic integrated circuit work that's been going on here has
been underway for about 2 years. We've made tremendous progress. I
think we've established the fundamental feasibility of the technology, however
before we can put this into a system, a tremendous amount of work has to
be done. R.F. performance is coming along nicely but in many areas it
needs continual development. Preliminary results on radiation hardness
with silicon on sapphire, MES FETS and GaAs look good but there's much
more work to be done. There is a potential question of reliability, due to
the effective electromagnetic fields from whatever source. Theoretically,
reliability should be very good for the modules. We're taking the

52

human error out of the loop and not putting in wire bonds and so forth, however, until we do that reliability remains an open question as will questions like reproducibility. Yes, we can process a wafer under laboratory conditions and get good results, but, its not until we produce large numbers of them and test them and find statistical spreads that we will really know about the reproducibility. Thermal considerations I've already discussed. There are many open questions that will be in many cases depend on the particular system configuration of the module antenna interface that we're operating, the type of radiating element and so forth, as well as the physical connections between them.

In conclusion the technology we're developing we feel will make phased array radars if not affordable, much more affordable than they have been in the past. And they are also allowing systems people much greater flexibility. As I emphasized before - cost is a very critical factor. There are areas that I won't go into here, Bob has already discussed delay lines and so forth, time delays, but other areas that possibly your technology could be beneficial, especially in replacing the TR switch with something like a circulator.

Questions and Comments

Q. (Paul Carr) Can you comment on replacing a phasor by a time delay unit?

A. Assuming you can control them and you can make them for $25 in production quantities, make and test them, and they're compatible with easy integration into the rest of it then that would be desirable. It comes down to the technical economic considerations for a particular system.

Q. (John Owens) On the circulator problem. If your speaking of MSW technology

53

then you're forced back into using a hybrid approach on microwave integrated circuit modules. The question is, in order to achieve that circulator function would you be willing to give up say 2-3 square millimeters of substrate area to achieve that function; because there are some possible viable alternatives to circulators based on MSW technology that requires that you in some manner stuff a piece of EPI YIG or its equivalent directly on top of the substrate and give up 2-3 square millimeters.

A. I don't see that as being a limiting factor. The sizes are coming out, particularly at the lower frequencies say around S band for the mock-up module that I showed, about one inch square. It's a viable alternative.

Q. A related question. How much loss can you tolerate in that circulator?

A. That is very much of a systems question. We've got in the neighborhood of a db of loss. It's sitting right on the front end so it's a two way loss. It translates back into power generation, prime power requirements and so forth. So, anything over a db or so is a lot.

Q. Who does the SOS work, and when do you see these solid state modules finding their way into a system?

A. SOS work is being done by GE and Raytheon. When will they find their way into systems? Based on the technology as its evolving, and most of the contractor have been turned on considerably by the success we've had to date, I think that in the next 2-3 years we'll begin to see various subparts of the monolithic technology, sub modules, put into application. One of my biggest fears personally is that, based on our success to date, someone will come along and want to configur a total system based on this-that is still somewhat premature - we've got a long way to go before we validate this; that we can make 1000, or 10,000 elements that are reproducible and that will totally operate in an array environment, although we have high confidence in it.

Q. This TR switch approach to modules. Normally TR switches don't have passive protection of the receiver amplifier from an adjacent radar. Since the TR switch is not synched to an adjacent radar the receiver amplifier can be damaged. What are your feelings about that?

A. It worries me. It may very well be an Achilles heel in the whole system.

Q. Is there a way of getting around that by monolithically printing protection diodes, etc.?

A. Yes. As the monolithic technology comes along, you can begin to envision all sorts of extra functions that would be nice to have, obviously there is a price to them.

Q. Could you allow 2 db loss on the circulator to help protect you from that?

A. I don't know. Two db (or three total) gets to be pretty expensive.

Q. (John Eshbach) I wonder if you or someone else could comment on the magnetic field requirements.

A. Small sammarium cobalt magnets would be used.

(THIS ARTICLE IS UNCLASSIFIED)

THE ROLE AND NATURE OF ADAPTIVE
ANTENNAS IN ECCM

John A. Graniero

Rome Air Development Center

Griffiss Air Force Base, New York

ABSTRACT

This introductory article will set the stage for the technical articles that follow by providing background on why we need adaptive antennas, a brief introduction to the general theory of adaptive antennas and discussions of key issues addressed by the technical articles.

INTRODUCTION

Adaptive array antenna systems are currently the subject of intense interest and investigation/development to provide interference protection to communications and radar systems. The reason is their ability to reject interference through adaptive spatial filtering, i.e., automatically forming antenna pattern nulls in the direction of sources of interference, thereby reducing output noise and enhancing the detection of desired signals. The adaptive array provides the flexibility of performing both spatial and temporal filtering to enhance desired signal reception. When combined (in some optimum configuration) with other Electronic Counter Countermeasure (ECCM) technologies, i.e., spread spectrum waveform processing, coding, higher radiated power and/or low sidelobe antennas, significant combined anti-jam capability is achieved that can cope with the present and projected ECM threats. By combining ECCM technologies in an optimal fashion, very high levels of jam-resistance can be achieved without stressing each individual technology beyond its favorable cost vs. performance characteristic.

In addition to automatic nulling in the spatial domain, adaptive arrays also are able to null in the frequency domain and in polarization. The more traditional adaptive array capabilities of self-focusing on receive and the conjugate function of retrodirective transmit can also be incorporated. Also, important side benefits are possible, such as compensation for antenna and/or scatter distortion effects. The adaptive array has potential benefits in forcing a more expensive and complex ECM threat. Single large jammers are usually easily handled by the adaptive array. This feature will force distribution of jamming assets with associated increase in personnel and cost. Jamming waveforms also must

58

be more complex to attempt to attack the adaptive feature of the array in order to reduce the amount of nulling.

This special issue presents a collection of papers describing analyses, hardware developments and test programs that establish the feasibility of adaptive antennas for communication and radar ECCM.

BACKGROUND

Adaptive antennas have their roots in a number of different fields, including retrodirective and self-phasing RF antenna arrays, sidelobe cancellers, adaptive filers, acoustic or sonar arrays and seismic arrays. Work in the early 1960's by Applebaum (1), Howells (2), and Widrow (3), on the key capabilities for achieving adaptive interference nulling, has produced a progressively expanding field of research. An excellent introduction to adaptive arrays is presented by Gabriel in (4). A workshop on Adaptive Antenna Systems was held at the Naval Research Laboratory in 1974 (5) and a special issue of the IEEE in 1976 (6) was devoted to this subject. Since the mid-1970's the interest in the adaptive antenna field has expanded rapidly. The military incentive in developing ECCM was seriously jogged by the Yom Kippur War in which the intent to use countermeasures against vital communications and radar links was demonstrated. And, they were effective. Today, the U.S. has a perceived weakness of its electronic systems in an EW environment. The magnitude and sophistication of the Soviet threat is leading to increased emphasis on ECCM techniques for U.S. electronics systems. Adaptive Antennas and Spread Spectrum are the two major ECCM techniques for countering the threat.

In July, 1980, a Symposium on Adaptive Antennas was held at the U.S. Air Force Academy (7). Sixty-one papers were presented that included: analyses/examples of each of the current major classes of adaptive

algorithms; sensitivity analyses of adaptive arrays to a variety of jammer waveforms, array geometry and antenna polarization; the use of adaptive arrays for precision direction finding; and applications to virtually every communications and radar mode. It was evident from the Symposium that adaptive antennas are rapidly becoming a mature technology that will add to our arsenal of ECCM techniques.

BASIC ADAPTIVE ARRAY THEORY

General Adaptive Array Antenna System

A general adaptive array antenna system is shown in Figure 1. The signals from the antenna array are combined to produce a single signal at the array output which corresponds as closely as possible to a desired received signal(s). As shown, this is achieved by an adaptive spatial filter which places antenna pattern nulls on directional interferences (x) and gain on the desired signal(s). The filter parameters are controlled by an algorithm which seeks to optimize performance in the signal and jamming environment at hand. The algorithm operates on information obtained from the sampled antenna signals and a priori knowledge of the signal and jammer field to optimize performance in accordance with a specified performance measure. Some a priori knowledge is required as a means for the algorithm to distinguish between desired signal and interference. Characteristics of signal and interference that are potentially useful include:

Interference (Jammer or RFI Characteristics)

1. Dominant jammer power (always greater than the signal).
2. Separable jammer power, either by spectrum (often wider than the signal's), or by time waveform.
3. Polarization.

60

Signal Characteristics

1. Known time waveform or spectrum (e.g., spread spectrum code, frequency-hopping pattern or known frequency channel).

2. Known direction-of-arrival of the signal.

3. Known expected received signal power.

The spatial filter can be interpreted as a prewhitening operation (typical of the solution methods used for colored noise filtering problems where the coloring here is due to the spatial distribution of the noise sources), prior to the use of the standard Wiener filter for a minimum mean square error (MMSE) estimate. The filter architecture for narrowband nulling consists of a complex weight, W_i (amplitude and phase control or quadrature weighting) in each channel as is shown in Figure 2. For wideband nulling a tapped delay line filter architecture (Fig. 3) is used in each channel. The exact number of taps and size of the time delays must be chosen for the particular application.

Performance Measures and the Optimal Solutions.

To define an optimal solution, a performance criterion must be selected. Of the performance measures used, mean square error, signal-to-noise ratio and the likelihood function are the most common. It has been shown (8) that the optimal solution for each of these performance measures differ only by a scalar factor, which leads to the result that they all produce identical signal-to-noise ratios at their outputs. The optimal solutions are of the form

$$W_{opt} = M^{-1}P$$

where W_{opt} = weight values at the optimal solution

M = the input signal covariance matrix and is defined as

61

$$M = \begin{bmatrix} x_{1j}x_{1j} & x_{1j}x_{2j} \cdots & x_{1j}x_{nj} \\ x_{2j}x_{1j} & & \vdots \\ \vdots & & \vdots \\ x_{nj}x_{1j} & & x_{nj}x_{nj} \end{bmatrix}$$

where
$$\begin{bmatrix} x_{1j}, & x_{2j} \cdots \cdots x_{nj} & = X_j \end{bmatrix}$$

are the jth set of input signals received by the n array elements.

and P is a cross-correlation vector between X_j and the desired response, R_j

$$P = X_j R_j$$

Adaptive Algorithms

Various adaptive algorithms have been developed to solve for the optimal weights either by cirect solution (if M is known), or by iterative methods. Of concern in many applications is the speed at which a given algorithm reaches the optimal solution. Also, the implementation aspects of the various algorithms can produce a wide range of hardware complexities. A brief summary of the major classes of algorithms is given below.

Direct Matrix Inverse

If the signal, clutter and interference situation were know a priori, then the covariance matrix could be evaluated and the optimal solution for the adaptive weights computed dir_tly by inverting the matrix and post-multiplying by P.

In practice, the signal, clutter and interference situation are generally unknown beforehand, and the interference environment frequently changes so the adaptive processor must continually update the weight vector solution to meet new requirements imposed by changing conditions. The need for

determining the external environment leads to the expedience of obtaining statistical estimates of M and P based on K samples of input data and employing these estimates to obtain the desired weight vector via direct matrix inversion, using any convenient method. It has been shown in (9) that effective convergence is achieved when the sample size K is on the order of twice the number of adaptive elements.

Gradient Algorithms

Gradient algorithms avoid the necessity for inverting the covariance matrix. They are based on the fact that the performance function to be maximized or minimized (output power, S/N, mean square error), is a quadratic function of the weights, possessing a unique stationary point (maximum or minimum). Hill climbing or steepest descent/ascent methods can be employed in an iterative fashion to converge to the optimum weight vector. The method of steepest descent uses gradients of the performance surface in seeking its minimum. The gradient of any point on the performance surface may be obtained by differentiating the performance function with respect to the weight vector. The method of steepest descent makes each change in the weight vector proportional to the gradient vector. The method of steepest descent can thus be described by the following relation:

$$W(i + 1) = W(i) + k_s \ F$$

Where F is the gradient of the performance function and k_s is a scalar which controls the iteration step size. Fixed step size gradient algorithms can suffer from long convergence times due to the fact that the step size must be small at the optimum for good performance. Variations of the gradient algorithms have been proposed which vary the step size and direction as a function of the performance measure to improve convergence time.

63

<u>Random Search</u>

Although potentially inefficient, any kind of vector random search can be effective in determining optimum array weights as long as an intelligent interpretation is made of changes in the performance function. The three basic types of random search algorithms include linear random search, accelerated random search and guided accelerated random search. Random search algorithms are particularly useful in situations where it is expected that the performance surface has many local optima. Another significant practical feature is that individual array element signals are not processed to yield the desired weight vector (i.e., the multipliers and integrators of the gradient type algorithms are not required). Weighting can also be performed at RF to eliminate down converters required for IF weighting. This feature has a significant economic impact on adaptive systems.

ISSUES ADDRESSED IN TECHNICAL ARTICLES

In addition to addressing the application of adaptive arrays to a broad spectrum of radar and communications systems, the articles treat the following critical issues:

Application to Aircraft

Aircraft are recognized as severe problems for adaptive antenna systems because of on-aircraft multipath, aircraft dynamics and antenna systems. Successful flight testing of adaptive antennas are described in "Global Positioning System (GPS) Null Steering Antenna Tests Results", by Mikenas et al; "Adaptive Controlled Phased Array Antenna For Protection of ASW Data Links", by Cerino et al; and "HF Adaptive Antenna Flight Test", by Cerino et al. The HF paper also addresses the use of electrically small active antennas to solve the difficult HF aircraft antenna problem. Aircraft limitations on

achievable null depth are addressed in "Performance of UHF Adaptive Antenna Systems on Aircraft", by Luvera, et al. Mineo, et al in "Integrated Adaptive Array and Spread Spectrum Modem ECCM Test Program" address the integrated performance of a spread spectrum modem and an adaptive array on an aircraft.

Vulnerability to Smart Jammers

A key issue has been the question of the vulnerability of adaptive antennas to jammer waveforms designed to attempt to keep the adaptive antenna in a continual transient state, thus either reducing or totally eliminating nulling performance. In the article "Adaptive Array Considerations for TDMA SATCOM Uplinks", by Gleich, et al, pulsed and blinking jammer effects are analyzed and shown to present few problems to the adaptive array.

Matrix Inversion Processors

This processor is of interest because its convergence is essentially independent of the environment. The A/D converters, high speed digital processor for computing M^{-1} and high computational accuracies have caused many designers to select gradient processors instead. The future prospects, however, are very encouraging considering projected VLSI advances. Adams, et al in "Application of Spread Spectrum and Main Beam Antenna Nulling to Wideband Data Reception" describe measured data on a processor which demonstrates the feasibility of the Sample Matrix Inversion Algorithm. Finn, et al, in "Digital Sidelobe Canceller--An Analysis of Field Test Results", present measured results of a matrix inversion processor for a radar application. Also, various strategies are analyzed for operation in an environment with smart jammers.

Gradient Adaptive Processors

By far, gradient processors are the best understood and most used processors. A good general analysis and test results of the gradient correlation loop type processor is presented in "Performance Evaluation of a

65

Breadboard UHF Adaptive Nulling Processor", by Mayhan, et al. An excellent

design procedure for the design of analog gradient processors is presented

in "Analysis and Measurement of a Multiple Sidelobe Canceller for MICNS",

by Tarmy. The use of the design criteria for the MICNS system is also

presented.

Random Search Processor

The random search processor is of interest because of its potential

low implementation cost. "Adaptive Arrays Using Random Search Optimization",

by Rassweiler describes the results of studies, computer simulations and

experiments of adaptive arrays that use random search optimization. Sim-

plicity and lower cost than conventional techniques are possible because down

converter receivers and correlators are eliminated or simplified. Flight

test results of a random search processor are described in "Global Pos-

itioning System (GPS) Null Steering Antenna (NSA) Flight Test Results",

by Mikenas, et al.

Performance with Spread Spectrum Modems

The combined operation of adaptive antennas with spread spectrum

modems provides high jam-resistance, but presents some interesting design

challenges. Adams, et al, address the "Application of Spread Spectrum and

Main Beam Antenna Nulling to Wideband Data Reception". The high anti-jam

capability of wide bandspreading and main beam nulling techniques are

shown for the difficult problem of protecting imagery reception within

a critical range of a protected target.

The overall requirements and design of an adaptive array to increase

the jam-resistance of the frequency-hopping JTIDS communications equipment

is discussed by Mineo, et al, in "Design and Performance of JTIDS Adaptive

Array Antenna System for F-15 Aircraft".

Retrofit to Existing Radios

Protection of existing communications radios without requiring new spread spectrum modems is of major interest particularly when considering the current equipment investment and retrofit costs. Adaptive arrays offer this potential for some applications. "Adaptive Antenna Systems for Army Tactical Radio Communications", by Meincke and Buehrle, describes the SNAP-I, an adaptive antenna for VHF-FM tactical radios (VRC-12s) in the 30-76 MHz band, and an improved version emphasizing broadband nulling and transmit using the null pattern as the framework for the development of a SNAP-II for SINCGARS-V. "AJ Antenna Techniques for LOS Communications Links", by Masak and Lackey, describes an adaptive antenna system for microwave line-of-sight communications links employing dish-type antennas. Computer simulations of the proposed technique shows substantial jam-resistance over a wide range of jammer scenarios. Application to HF communications is discussed by Cerino in "HF Adaptive Antenna Flight Test".

Radar Sidelobe Cancellers

Geometrical anomalies causing slow convergence, time delay mismatch and mainbeam multipath, limit performance for sidelobe cancellers. Kowalski, et al, in "Recent Developments in Radar Sidelobe Cancellers" describe techniques developed to overcome these problems.

SUMMARY

Adaptive antennas offer substantial jam-resistance for communications and radar systems. This special issue addresses numerous applications of adaptive antennas and critical issues on performance and implementation aspects. The future prospects for adaptive antennas is very encouraging. Projected advances in VLSI will allow complex digital processing with small, low power hardware.

Analog integrated circuit technology advances will enable wideband high frequency devices for analog weights and processors in chip packages. Surface Acoustic Wave Devices (SAW) and Charge Coupled Devices (CCD) as tapped delay lines with electrically programmable tap weights will allow their widescale application as low cost wideband adaptive processors. These advances and others will enhance performance to counter advances in ECM providing protection against an escalating jamming threat.

REFERENCES

1. Applebaum, S.P., "Adaptive Arrays", Syracuse University Research Corp. Report SPL TR 66-1, Aug 1966.

2. Howells, P.W., "Intermediate Frequency Sidelobe Canceller", U.S. Patent 3 202 990, Aug 24, 1965 (file May 4, 1959).

3. Widrow, B., "Adaptive Filters I: Fundamentals", Stanford University Electronics Lab., System Theory Lab., Tech Report 6764-6, Dec 1966.

4. Gabriel, W.F., "Adaptive Arrays - An Introduction", Proceedings of the IEEE, Vol. 64, No. 2, Feb 1976 pp 239-272.

5. Gabriel, W.F., Chairman, Proceeding Adaptive Antenna Systems Workshop, Sept 30, 1974, NRL Report 7804.

6. Special Issue on Adaptive Antennas, IEEE Transactions on Antennas and Propagation, Vol. AP-24, No. 5, Sept 1976.

7. Graniero, J.A., Willis, J.W., Co-Chairmen, Proceedings of the 1980 Adaptive Antenna Symposium, Dec 1980, RADC-TR-80-378.

8. Baird, Jr., C.A., Rassweiler, G.G., Zahm, C.L., Martin, G.P., "Adaptive Processing for Antenna Arrays", Radiation Inc., RADC-TR-72-174, July 1972.

9. Reed, I.S., Mallett, J.D., Brennan, L.E., "Rapid Convergence Rate in Adaptive Arrays", IEEE Transactions on Aerospace and Elect. Systems, Vol. AES-10, pp 853-863, Nov 1974.
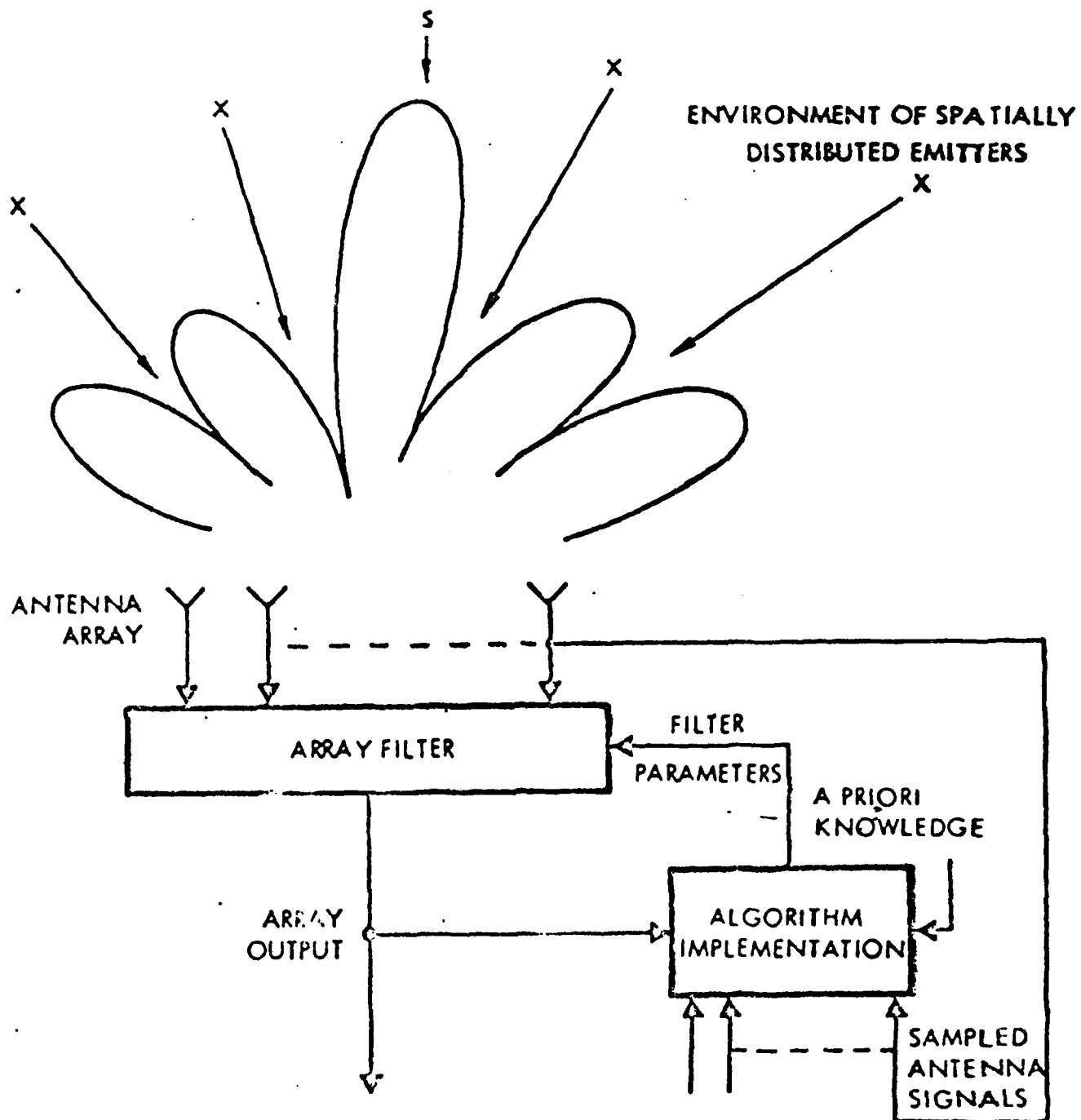
Figure 1. General Adaptive Array Antenna System

70
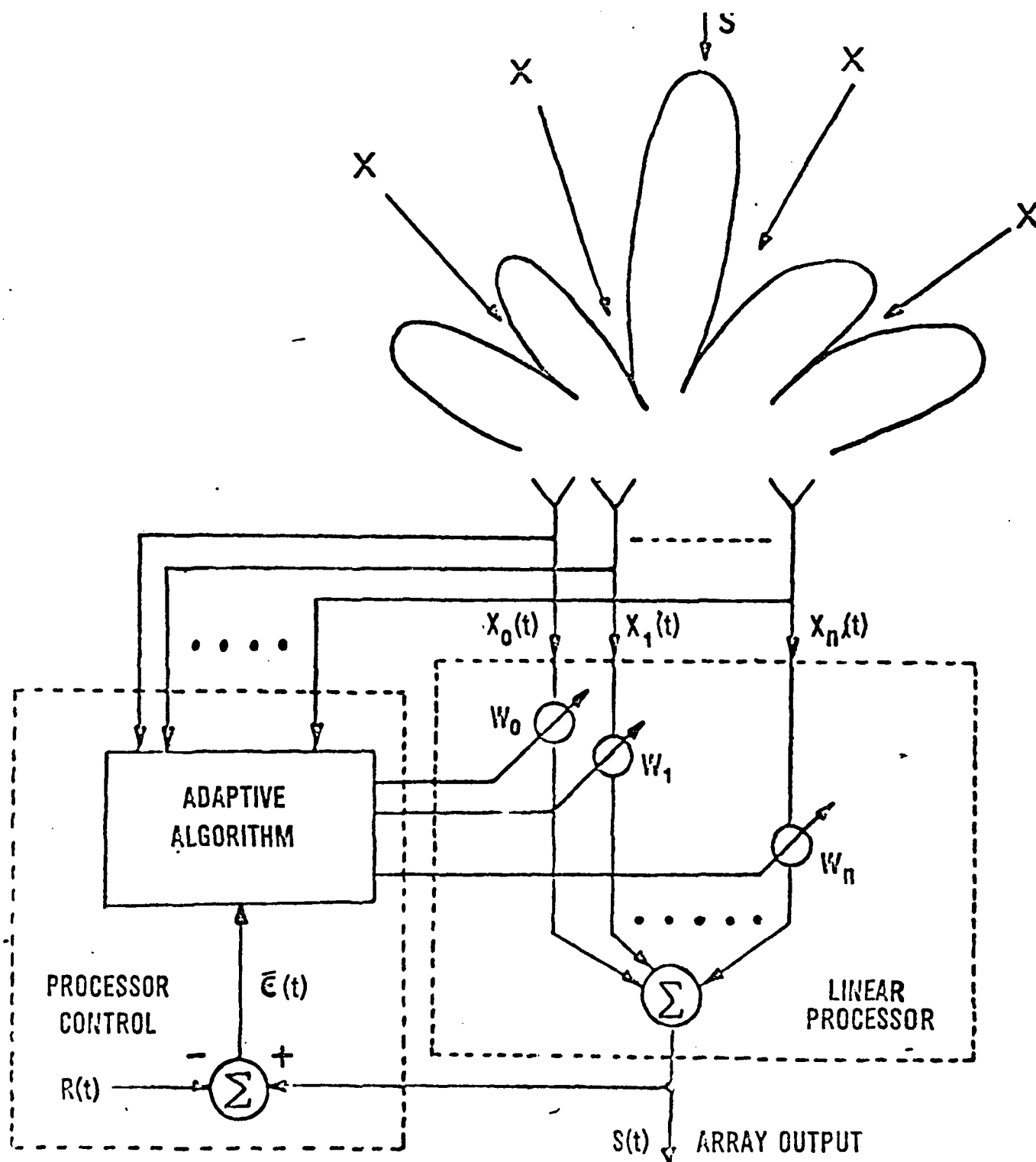
Figure 2.   Narrow-band Adaptive Array Antenna
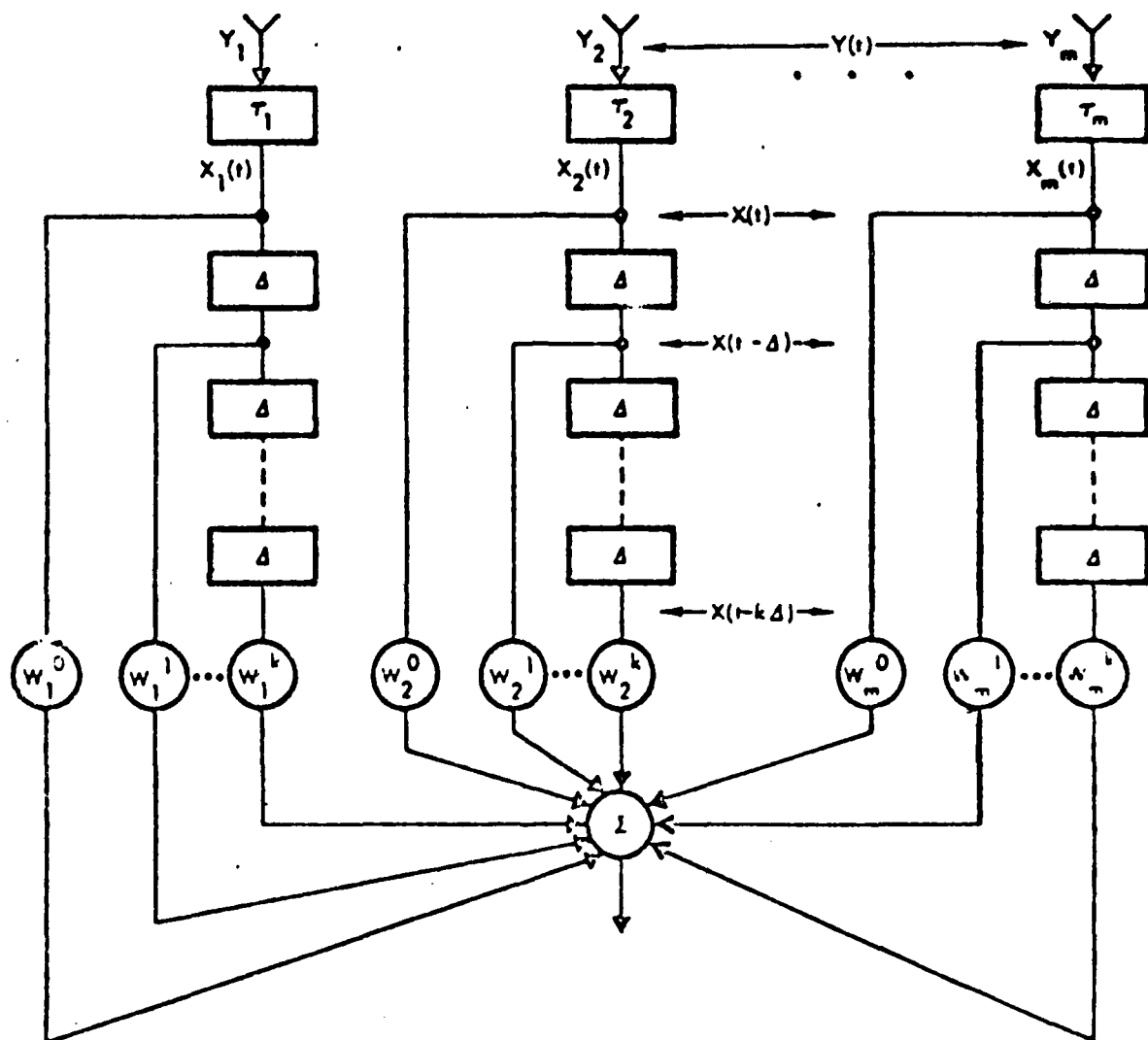
Figure 3. Multichannel Tapped Delay Line Filter for Wide-band Nulling

AD P000924

ADAPTIVE ANTENNA REQUIREMENTS *for the design*

of ... filters.

John Graniero

RADC/DCC, Griffiss AFB

Rome, New York

1981 RADC/EEA Microwave Magnetics Technology Workshop

(Transcription of a tape recording made
at the Workshop)

Hopefully I'll touch on some of the requirements that might be of interest to the group. I am not familiar with microwave magnetics sciences, so to translate what the requirements would be that your interested in to adaptive antenna technology would be a little bit difficult so if you see an area that is a little bit interesting just interupt me and maybe we can explore it a little bit further. Basically what we are trying to do in adaptive antenna technology is to design an adaptive spacial filter. We have an environment with desired signals, one or more, and a number of jammers or interferring sources that we are trying to eliminate. What we are going to do is form a spacial filter by using an array of antenna elements, weighting the outputs of the antenna elements to form an array filter and ajusting the weight parameters according to algorithms. The algorithm works on samples of the antenna signals and some apriori knowledge that we may know about the signal or jammer environment. The objective is a gain in the signal direction and very little gain in the interferring source direction. There are many different ways of controlling an adaptive array, there are different parts to the problem, and in designing the spacial filter the RF frequency that your operating with could range depending on the system application from VLF into the millimeter wave frequency bands. Weighting the output signals again could be almost anywhere depending on the implementation, and the various algorithms shown here could be used. There are four classes of algorithms to develop the weight control voltages I'll touch on some of these. They could be either closed loop algorithms such as gradiant type or sample matrix inversion, they are essential digital algorithms, random search or cascade processors. The reason I am putting this

74

up here is that the algorithms generally control or influence the

type of weights that you can use at the output of the antenna array.

If you have a closed loop algorithm such as gradiant algorithm it

allows you more flexibility in the type of weight you might have. It

has reduced absolute accuracy requirements as to what you would

need to provide to the algorithms in terms of the absolute value of

the weight that you are applying to the output of each individual an-

tenna element. Open loop algorithms on the other hand need very

precise weights and you have to know exactly what the weights are

that your applying to the output of the antenna elements. You al-

so need to know something about the desired signal or the jammer that

allows the algorithm to discriminate between signal and jammer. These

are some of the discriminates that you can use to obtain some of the decrements

such as the weight form, spectrum or estimates of the direction of

arrival. You can use signal processing technology, matching

filters that match expectant codes etc., which again could get

you into magnetostatic wave, possibly matched filters, for that

portion. This breaks down where adaptive array is, a little further,

using one particular implementation called the Least Means Square Error

Algorithm. We have a number of antenna elements, generally each an-

tenna element output is put into inphase and quadrature components.

I-and-Q outputs are then weighted and amplitude. This could also be

a complex weight and amplitude phase. Generally the way it is done

now is, you need to develop a weight that will adjust the output of the

antenna in phase over 360° and amplitude over probably a 40 or 50 dB

range. Generally that is done by I-and-Q and amplitude weighting.

The algorithm to develop the weight voltage in this case is a least

means square error algorithm. The objective is to minimize the error between the desired and actual response, which is the desired signal weight form in the output of the array. The estimate of the desired signal is obtained from the modem, I have an example of how that is done. Subtract the signal estimate from the array output and try to drive that to zero. That is done by correlating the error with the output of each antenna element, so that a correlator integrating that output produces the weight voltage. So to implement an adaptive array, you need one of these per antenna element at least for narrow band solution and that involves a weight correlator and integrator, and there is some gain in the loop also. In this portion of the loop, the implementation could be either at the same frequency that the weighting is done or could be done digitally or at another frequency. To get an estimate of the desired signal for example the desired signal may have a spread spectrum code on it, and what we need to do is estimate the code and the information that is imparted on the desired signal. Here is one way suggested for doing this, this is the adaptive array that weights the summer, the array output. The coded L.O. would essentially remove the spread spectrum code on the signal, go through a data band filter and a limiter and at this point we essentially have an estimate of the information that was on the signal that was transmitted. Take the information remodulate the spread spectrum code and you essentially have a duplicate of the desired signal that was transmitted. There are other ways of getting this reference which could be a matched filter matched to the particular code, which might be a canidate for a magnetostatic wave device. There are other ways of developing

the weight, you could do it instead by a feedback control loop,
you could do it all digitally by an algorithm which is essentially
called a random search. Here you have the antenna elements that are
weighted in amplitude and phase, summed, and then you adjust the
weights using trial and error weight changes and monitoring perform-
ance in the output in the antenna system. What you are doing is
essentially selecting weight vectors and then testing to see whether
it was a good vector or not, and if it was a good vector, the
things you could monitor could be total output power, an estimate of
the interference power, an estimate of the signal power and adjust
the weights to get to an exceptable performance measure. The nice
things about weights search control is that you can use weights
that are at the rf frequency. There is no requirement for correlating
the output with the signal received at each antenna element. So
this could be an rf weight and a digital controller to develop the
weight control voltages. There are several advantages to doing it
at rf that I'll touch on a little bit later. Some of the processes
for developing the control voltages for the weight are complex. Again
we have antenna element in-phase and quadrature, the weights, and you
want to develop the control voltages, summer. And this is an imple-
mentation of a maxi-minprocessor. What we want to do is maximize
the desired signal while we're minimizing the interference. What
it involves is getting estimates of the desired signal, total signal
power, signal power received at each antenna element and an estimate
of the noise power and interference power, the totals and the noise
and interference power received at each antenna element. And this

77

shows using the maxi-min with a fast frequency type system where the outputs of the elements are frequency hopped. You have band pass filters to estimate the desired response in the filter and band reject filters to look at the interferring signals. And by having estimates of signal and interference you can then go into an algorithm which would develop weight values based on the estimates you have on signal to jammer. Some of the implementations I showed you previously essentially had the adaptive array the output of the antenna elements and then you would follow that with some signal processing quota. There are also implementations where you can do the de-spreading and then the adaptive null steering second, and this essentially would be the received signal that is spread with a pseudorandom sequence. It would first despread it, remove the code that gives you the antenna elements and you compress the bandwidth of the desired signal and then you do the null steering function. To do this you need to know time so that you can apply the code at the right time. Other implementations that are being looked at right now would be to have a tapped delay line device here which would give you outputs in time sequence of the correlation of the spread spectrum code and receive signal and then go through a complex on how to maximize the signal interference ratio. The reason for doing it that way is that <u>adaptive arrays are essentially narrow band devices,</u> they like to work at bandwidths that are <u>1% or less</u> and by compressing the signal bandwidth before you do the null steering we hope to get increased jam resistance over what we would get or over a conventional approach where you do the null steering first over the full bandwidth of the received signals.

There are two basic limitations to the depths of null you can achieve with an adaptive antenna. One is caused by dispersion in the antenna aperture itself. This shows an example of a sidelobe cancellor being used to cancel a jamming signal received in the side-lobes of an antenna array, and, by example you can see that, suppose the jamming pulse were received off boresight of the antenna array, it would be essentially filtered by the aperture. It comes out at a different time. It's being received at a different time by each of the array elements so the pulse is smeared. The single sidelobe cancellor element is not distorted at all, so now you're trying to cancel a distorted jammer signal with a nice clean replica. The amount of distortion you get is a function of the bandwidth of the jamming signal. So that's one limitation. The larger the antenna aperture the narrower bandwidth signal that you can null over. The second limitation is in the circuits that you can produce. Generally, the antenna elements and the weighting are done at different frequencies. You could have a satellite system which might be operating at 30 GHz. It would be very difficult to develop weights at 30 GHz, so generally you go through an RF-IF conversion and then into your weighting circuits. And this shows an I&Q weight with an LMS algorithm. The problem is that you need to accurately match the devices RF-IF. One of the problems that we have right now is that, say at 30 GHz you wanted to buy match down converters at 30 GHz, you'd have a very difficult time buying matched down converters. The people developing millimeter wave devices are right now trying to measure something like 6° phase accuracy over a bandwidth, and requirements for a null steering are much more stringent

than that. The next slide which would show the matching require-
ments. This is the basic problem. This is channel to channel or
weighting device to weighting device, RF amplifier, IF amplifier etc.
You want to achieve 20 dB nulls. Then, you have to match the channels,
this is rms errors in amplitude, to 1/10th of a dB and in phase
by about 6°. This is a kind of design that you have for a conven-
tional antenna, or for beam forming. However, a lot of the interference
problems are more like 30, 40, or 50 dB problems. These are the kinds of
cancellation that we would like to achieve on interferring signals,
and that puts you into channel tracking accuracies like .02 dB of
a dB in amplitude and .20 of a degree in phase. This gets
into a very expensive device. At lower frequencies with some care
you can probably achieve that, if you're talking systems where
technology is well in hand for building filters and down converters
and mixers. At higher frequencies, right now, there're trying to
make the basic devices themselves; and getting that kind of accuracy
let alone measuring it from device to device is a very expensive
process. The way around that is to put in back of each antenna
element a transversal filter or equalizer. Essentially instead of
having a single weight per antenna element you go through a time
delay and additional weights depending on the kind of equalization
that is required. So now our single amplitude and phase control for
each antenna element is multiplied by the number of taps in a trans-
versal filter. By employing a tapped delay line structure they will
allow you to be much more relaxed in the requirements that you
would put on the rf amplifiers, down converters, etc. in your rf pad,

80

because you could equalize the channels now adaptively with an equalizer. It also will give you some flexibility in null depths because it can happen say for dispersion across the antenna aperature and can get rid of near field multipath. The path spacings that you would require would be in the order of 3 nanoseconds up to 50 or 100 nanoseconds depending on the operating bandwidth that you'd be interested in. This is generally what an adaptive loop looks like right now with the hybrid microwave integrated circuit technology, and weighting circuits using pin diodes, attentuator and correlators. For some applications its fine, for others it gets to be a problem. One primary area we are interested in is satellite communications. We want to put adaptive arrays on satellites. The satellites would be operating at 30 GHz or above. The weighting frequencies, they are not operated at 30 GHz, you'd like the weighting to be done somewhere around 2-10 GHz, bandwidth around 200 MHz would be interesting with 30 to 35 dB nulls, weights and size, 6 cu inches and 1/4 lb. These are critical parameters for a space package. This is again the requirements we developed for a single weight per adaptive array element. If we could develop a weight that had a tapped delay line in it, a transversal equalizer essentially, it would really increase the performance we'd be able to achieve, and it would really ease some of the requirements that we have to put on the designers of the down converters and other elements in the satellite system.

ANSWERS

No it really varies over very very slow speeds. If you have a ground application where you have ground based signals and jammers you essentially have a static environment and might have response times which could be in milliseconds or longer. But if your on a high performance aircraft thats rolling at 400° a second, and you've got some other requirements, there's really a range of requirements that you can get involved in with that prospect.

That's right the absolute is not the thing, you need the tracking from device to device and even that can be relaxed if you have a tapped delay line structure. But the absolute accuracy can be compensated for and will be compensated by the feedback controller, providing you're using a closed loop algorithm. If you happen to be using an open looped algorithm, where essentially sampling element signals and developing and applying the weights and that's your output, then the accuracy requirements are very stringent, and they get to what I showed depending on the null depths you want, that through the whole system from rf through the weighting network. So if you do have a closed loop algorithm then you do have the algorithm which will compensate for some errors, absolute errors, and might result in a slightly longer conversion time. But the feedback will take out the absolute errors.

No, no that's just center of frequency. We don't know where to put it, what we would select right now. We need about a 200 MHz bandwidth, we like an IF somewhere in the 2 to 10 GHz region, that whatever it

would be, would depend on the technology you choose to implement the weights.

Probably six would be nice. Each path has a corresponding device to develop the weight required for that tap, also, if tap structure and correlators can be put on one device that would make a super package. A self contained package that does all the computing and weighting required for that individual antenna element; then you could use as many taps as you could put on the device.

Generally correlators right now. You'd build them at lower IF frequencies. Here for the satellite time requirements we proabaly do the correlateion somewhere around the same frequency, 2 GHz or so.

Well, intertap spacing somewhere around 3 nanosecond would be on the low end, and then up to 20 nanoseconds, something like that, and then the number of paths would get you to probably 200 nanoseconds total. For a 10 MHz system, we're building one now for a microwave system with 50 nanoseconds spacing for a system that equalizes over about a 10 MHz bandwidth. So the bandwidth increases the interpath spacing or decreases it.

Yes, there are many ways you can implement the weights. The total delay? Actually if you had a tapped delay line then the inter-tap spacing would be somewhere from 3 nanosecond to 20 nanoseconds, in that region. Over the frequency? You would probably have 3 nanoseconds at center band, something like that, whatever that

83

variation would be.

The intertap spacing is not that critical. The variation from tap to tap is not really a critical parameter. The adaptive features of the loops can do a lot for selecting the proper kind of spacing. One of the problems is to pack them in to get something like a 3 nanosecond delay but whether it's 3, 3.1, 3.5, is not as critical as getting them packed in initially.

If your getting dispersion which is different from device to device. If it's the same from device to device then thats not a problem. It's the difference from device to device that you have to worry about, because if you weight one sample different from the other and you try to subtract and you get zero, you're out of luck.

ADAPTIVE ARRAY ANTENNA SYSTEM
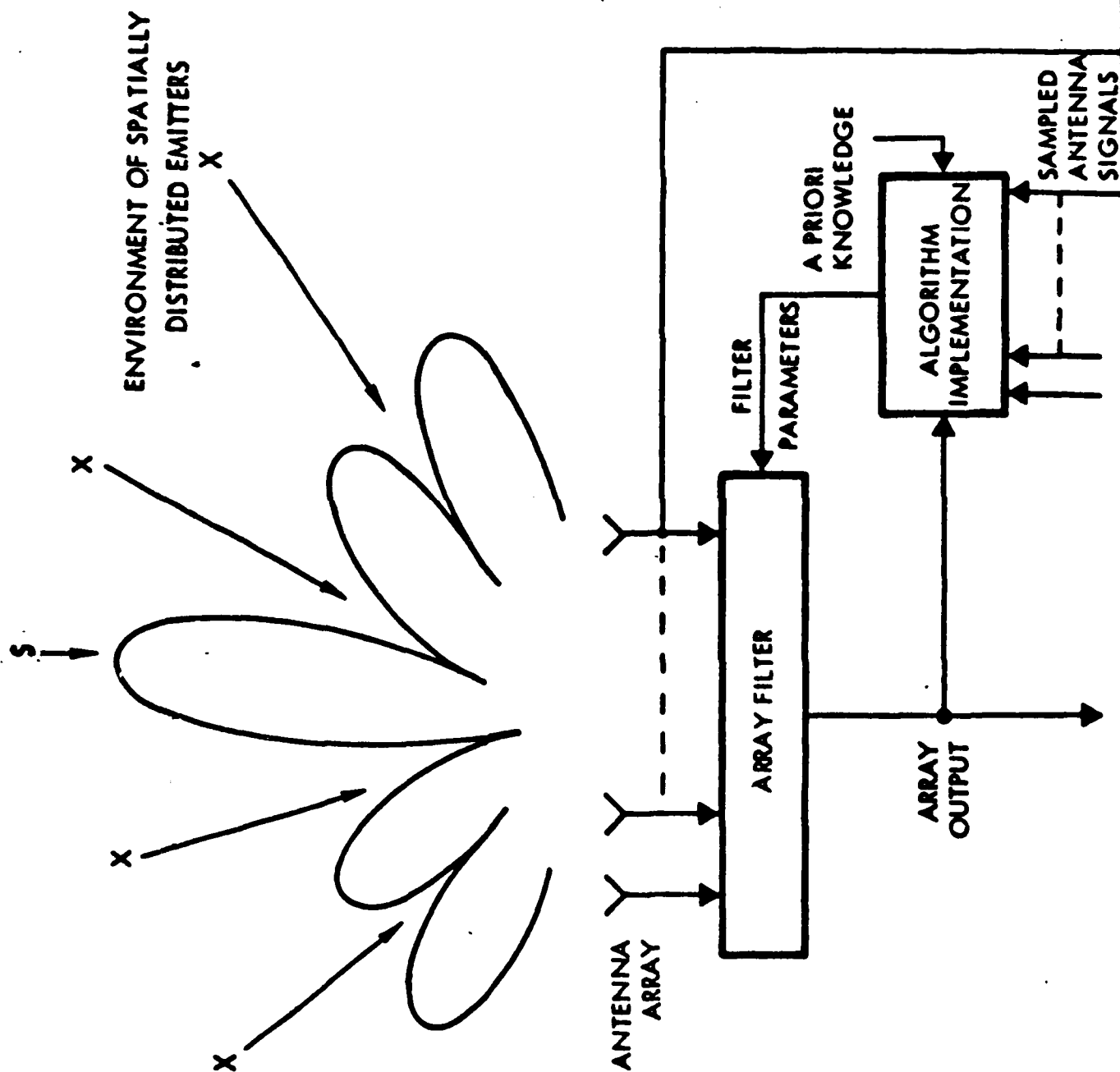
TYPES OF ADAPTIVE ALGORITHMS

- GRADIENT ALGORITHMS

- DIRECT SAMPLE MATRIX INVERSION

- RANDOM SEARCH

- CASCADE PROCESSORS

DESIRED SIGNAL IDENTIFICATION/DISCRIMINATION TECHNIQUES

KNOWN:

DIRECTION OF ARRIVAL

SPECTRUM

WAVEFORM

RECEIVED POWER

87

BASIC TYPES OF ADAPTIVE OPTIMIZATION
CORRELATION CONTROL
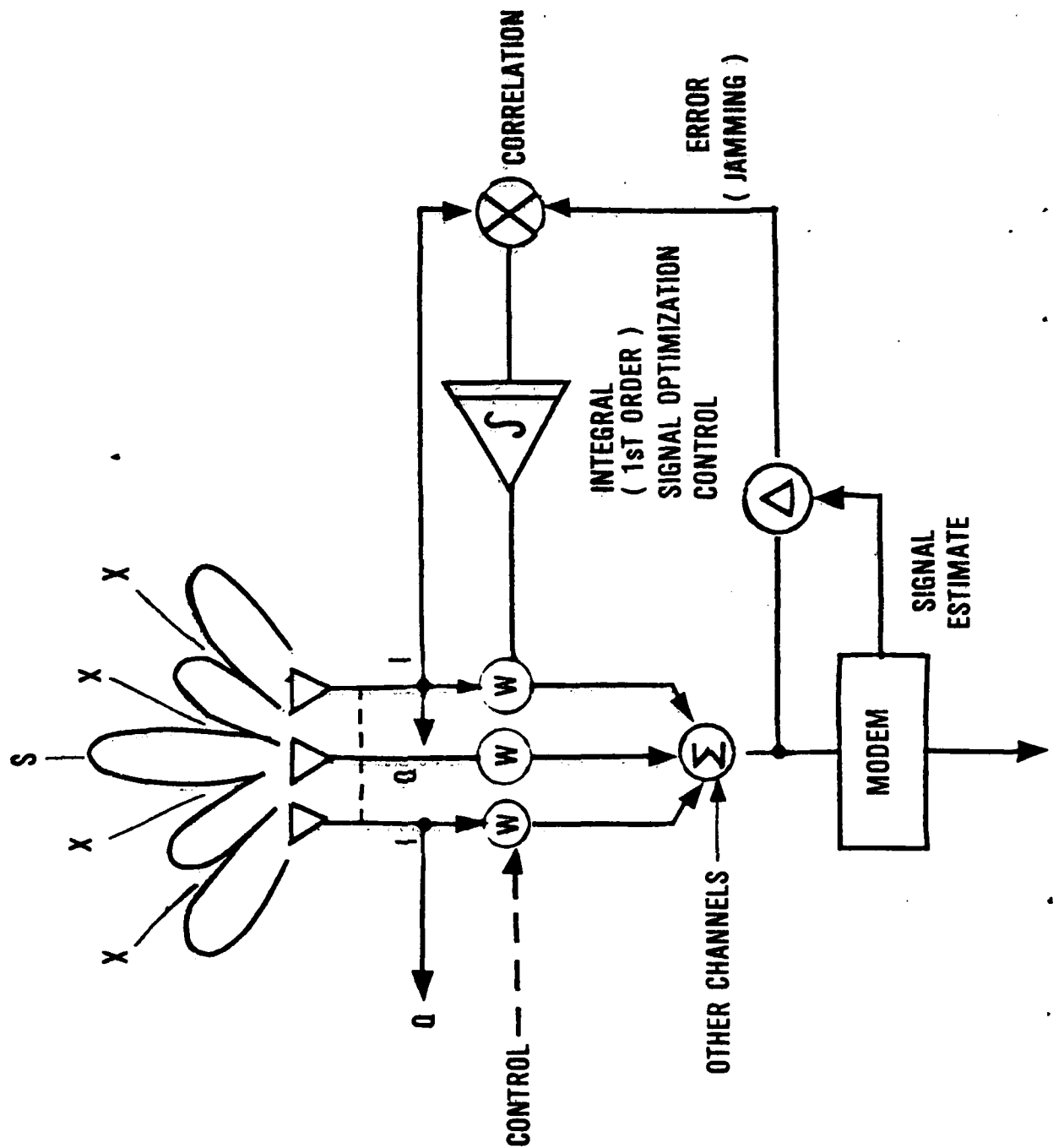
ADAPTIVE ARRAY — WAVEFORM PROCESSOR
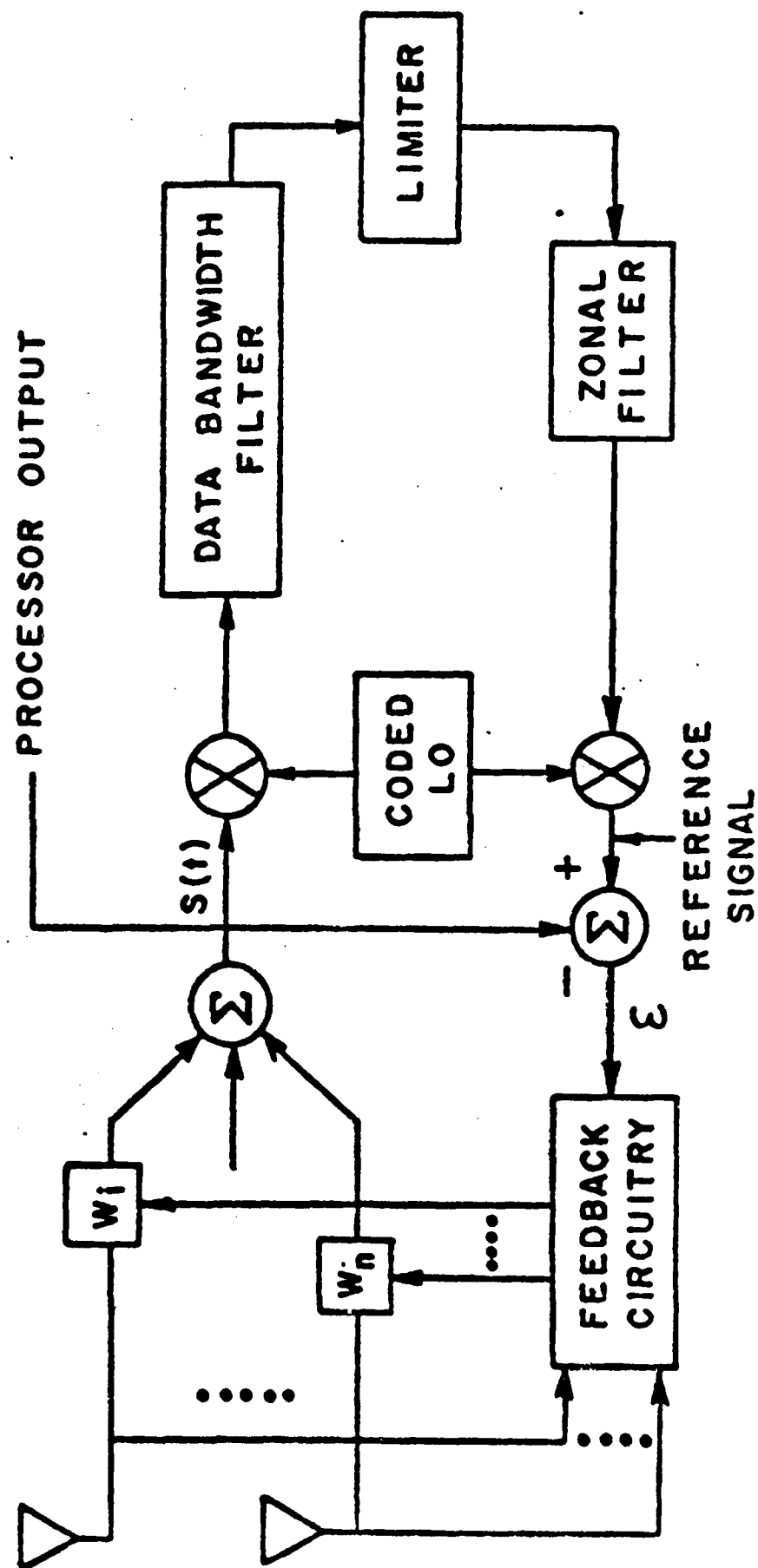
89
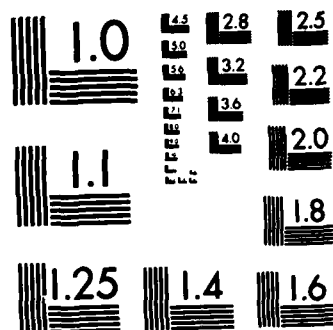
MICROCOPY RESOLUTION TEST CHART

NATIONAL BUREAU OF STANDARDS-1963-A

ADAPTIVE ARRAY — WAVEFORM PROCESSOR
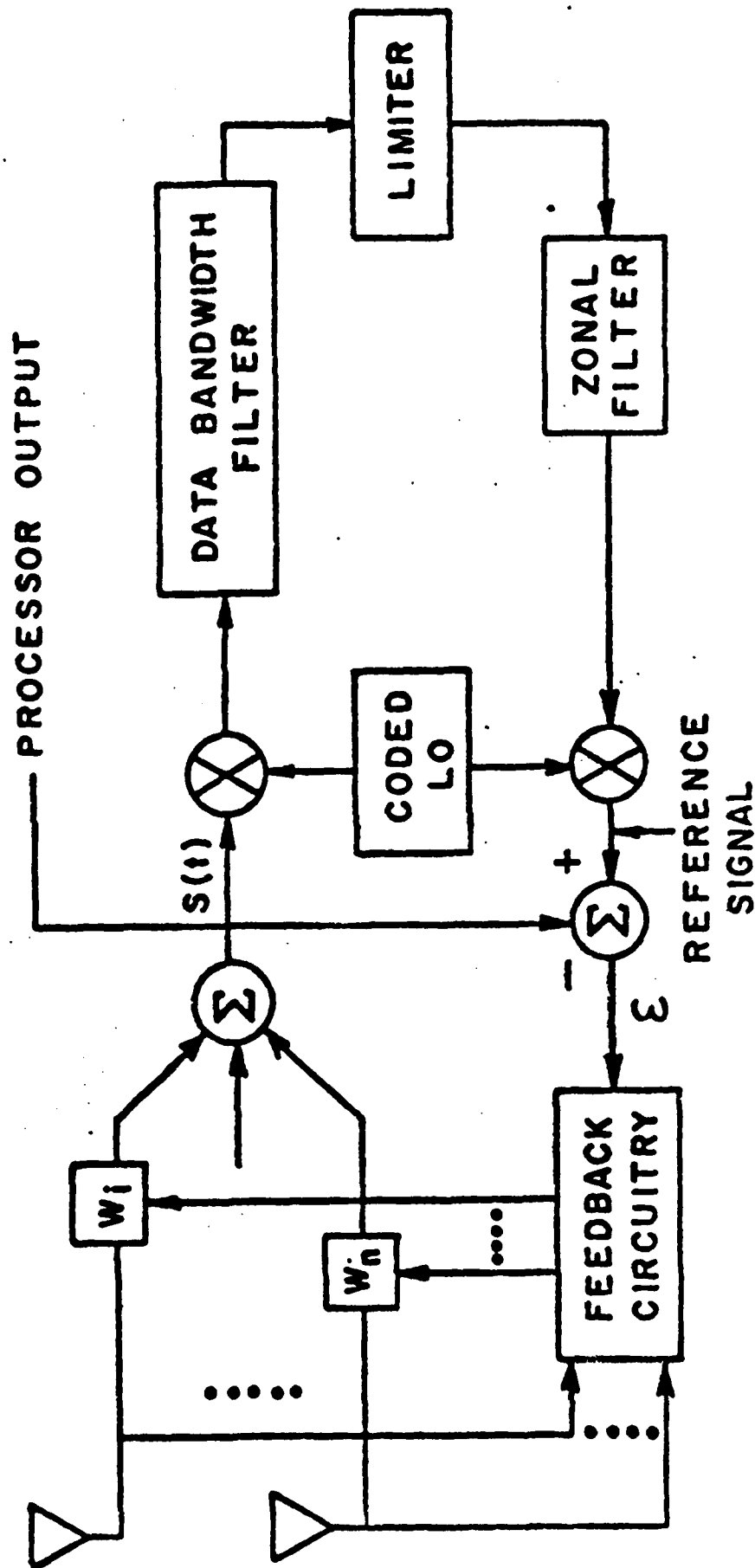
BASIC TYPES OF ADAPTIVE OPTIMIZATION

WEIGHT SEARCH CONTROL
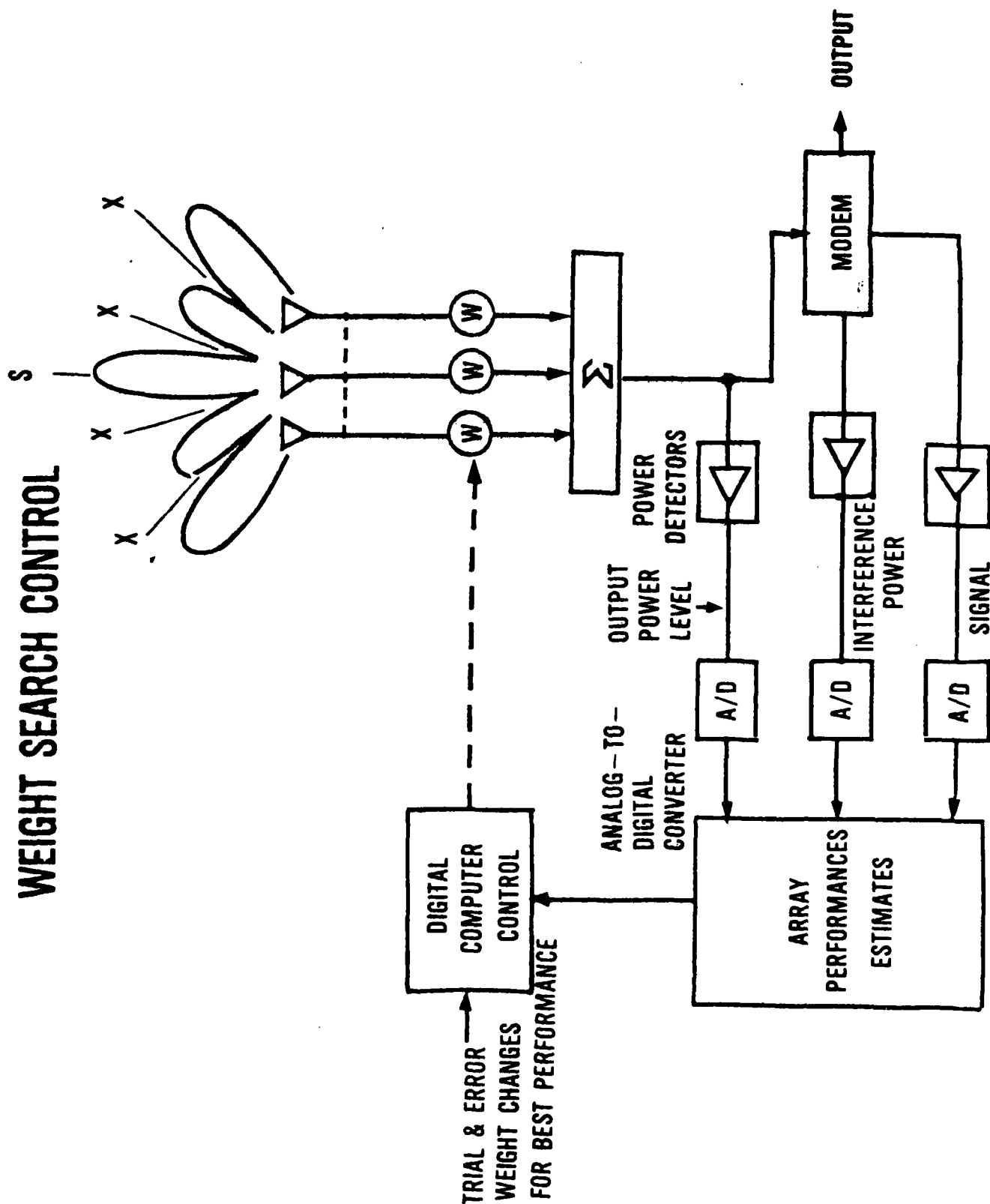
MAXIMIN PROCESSOR

91
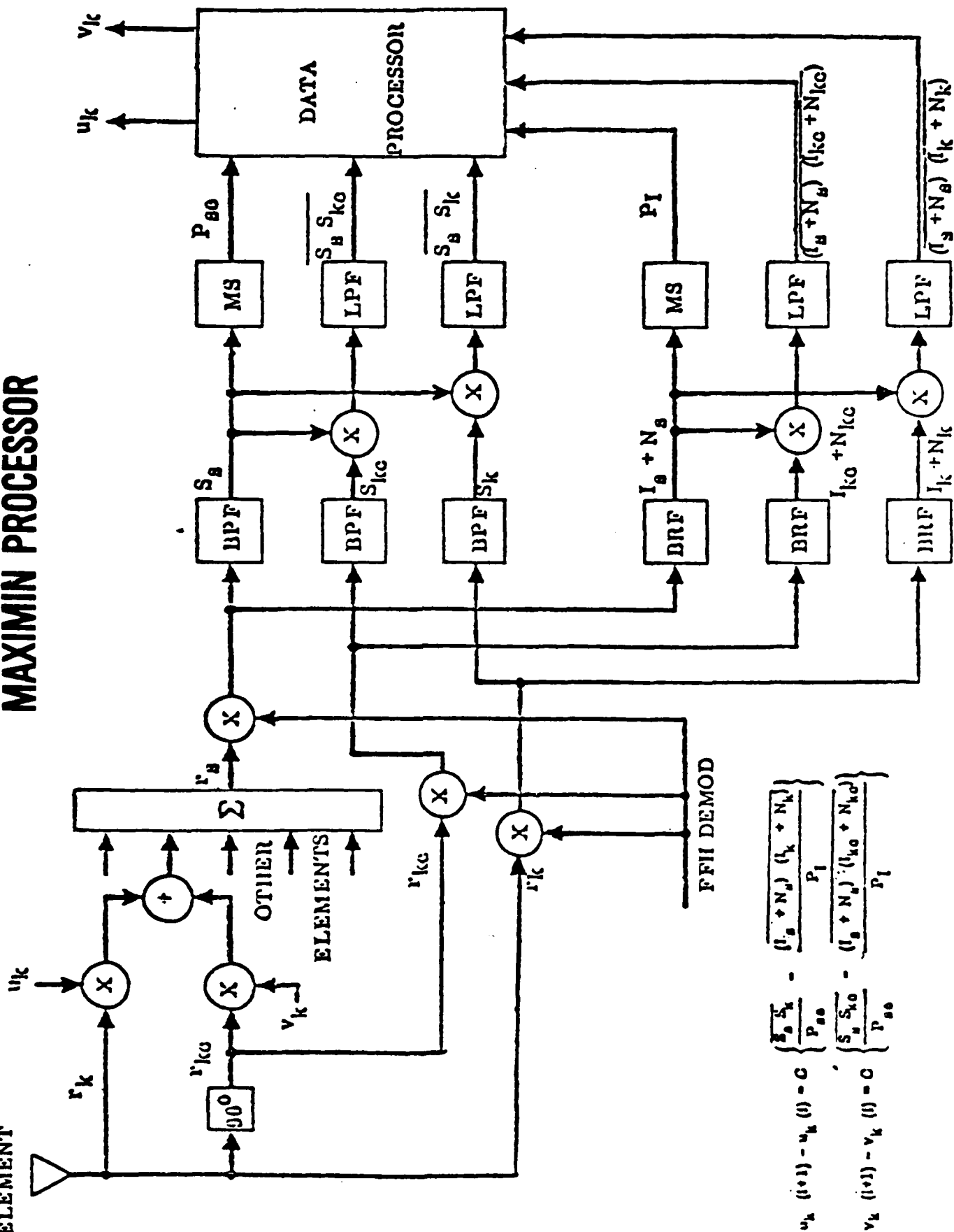
LIMITATION OF JAMMING NULL DEPTH DUE TO BANDWIDTH (TIME-OF-FLIGHT); SIDE LOBE CANCELLER

JAMMER

JAMMING IMPULSE

SIGNAL

MAIN ARRAY

Σ

SIDE LOBE CANCELLER ELEMENT

NONDISPERSED JAMMING

ADAPTIVE WEIGHT

W

CONTROL

DISPERSED IMPULSE CANNOT BE COMPLETELY CANCELLED BY NONDISPERSED SIDE LOBE CANCELLING CHANNEL

CANCELLATION NODE

Δ

OUTPUT

87441-10

92
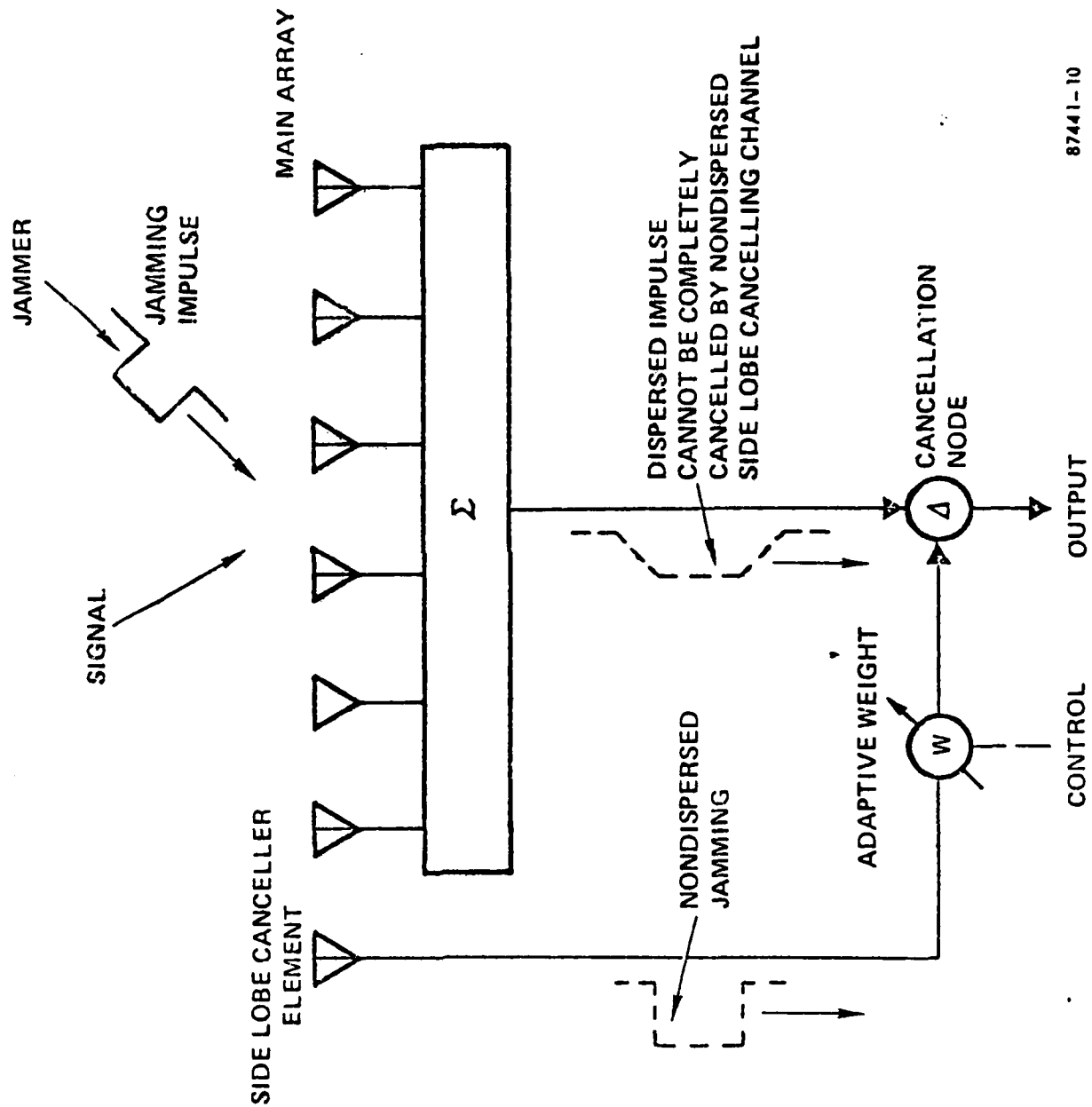
ELEMENT CODE STRIPPING TECHNIQUE
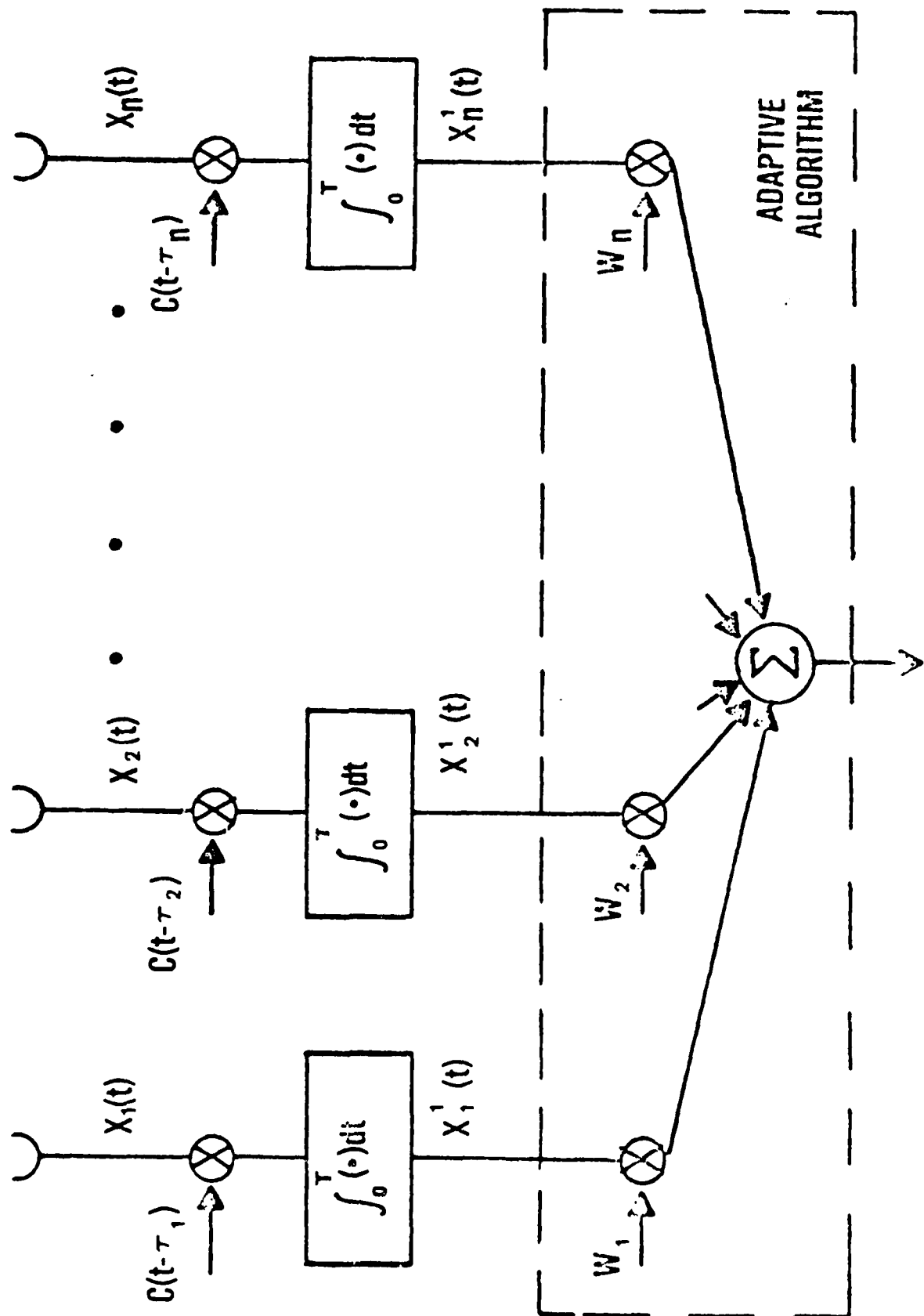
CODE STRIPPING VS CONVENTIONAL ARRAY/MODEM PERFORMANCE

94
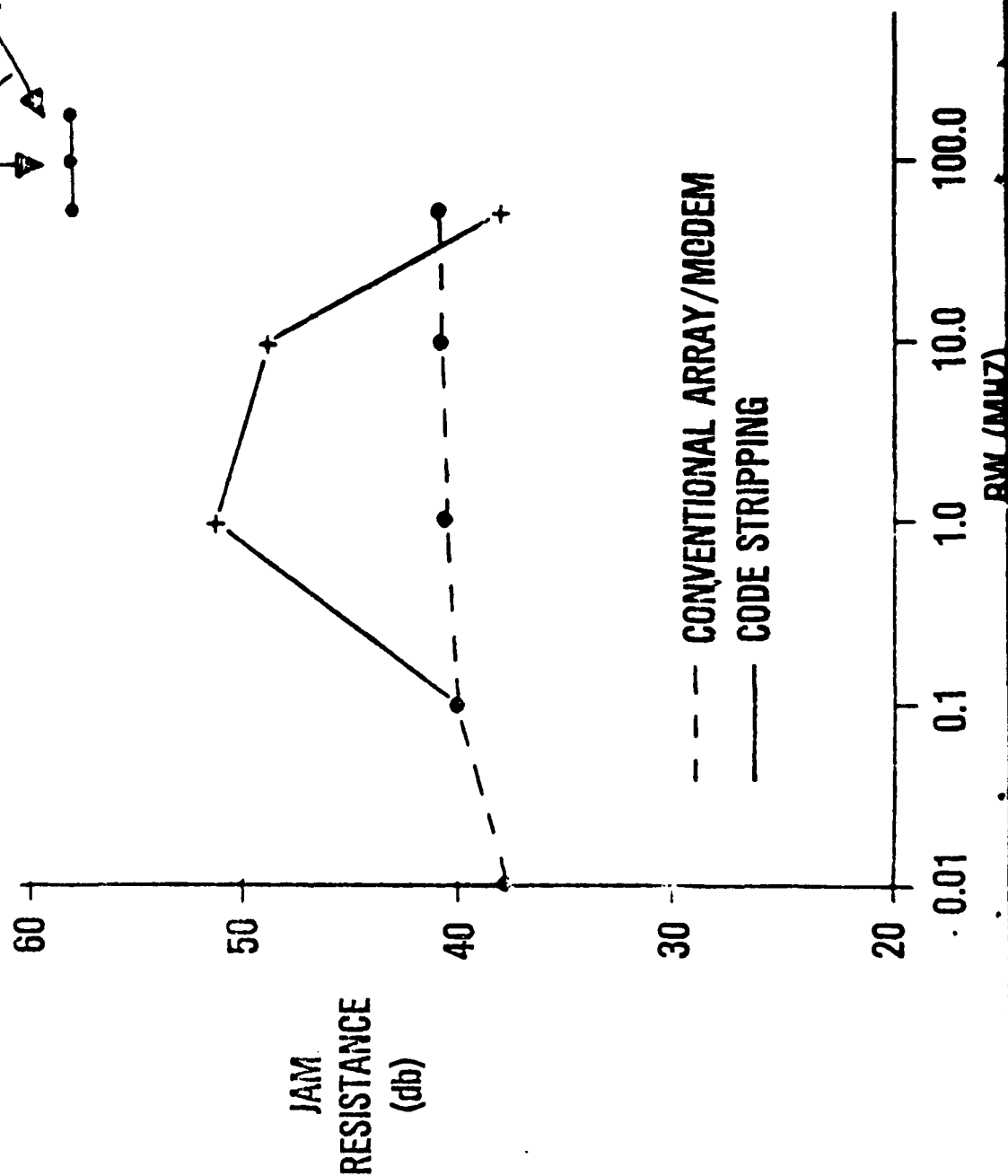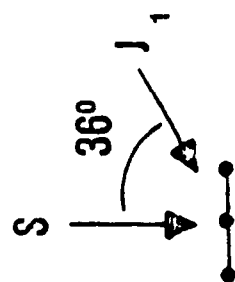
CHANNEL MATCHING REQUIREMENTS

DESIRED NULL DEPTH (dB)	CHANNEL MATCHING ACCURACY	
	AMPLITUDE (dB)	PHASE (DEGREES)
20	.83	5.7
30	.27	1.8
40	.086	.57
50	.027	.18
60	.0087	.057

MULTICHANNEL TAPPED DELAY LINE FILTER
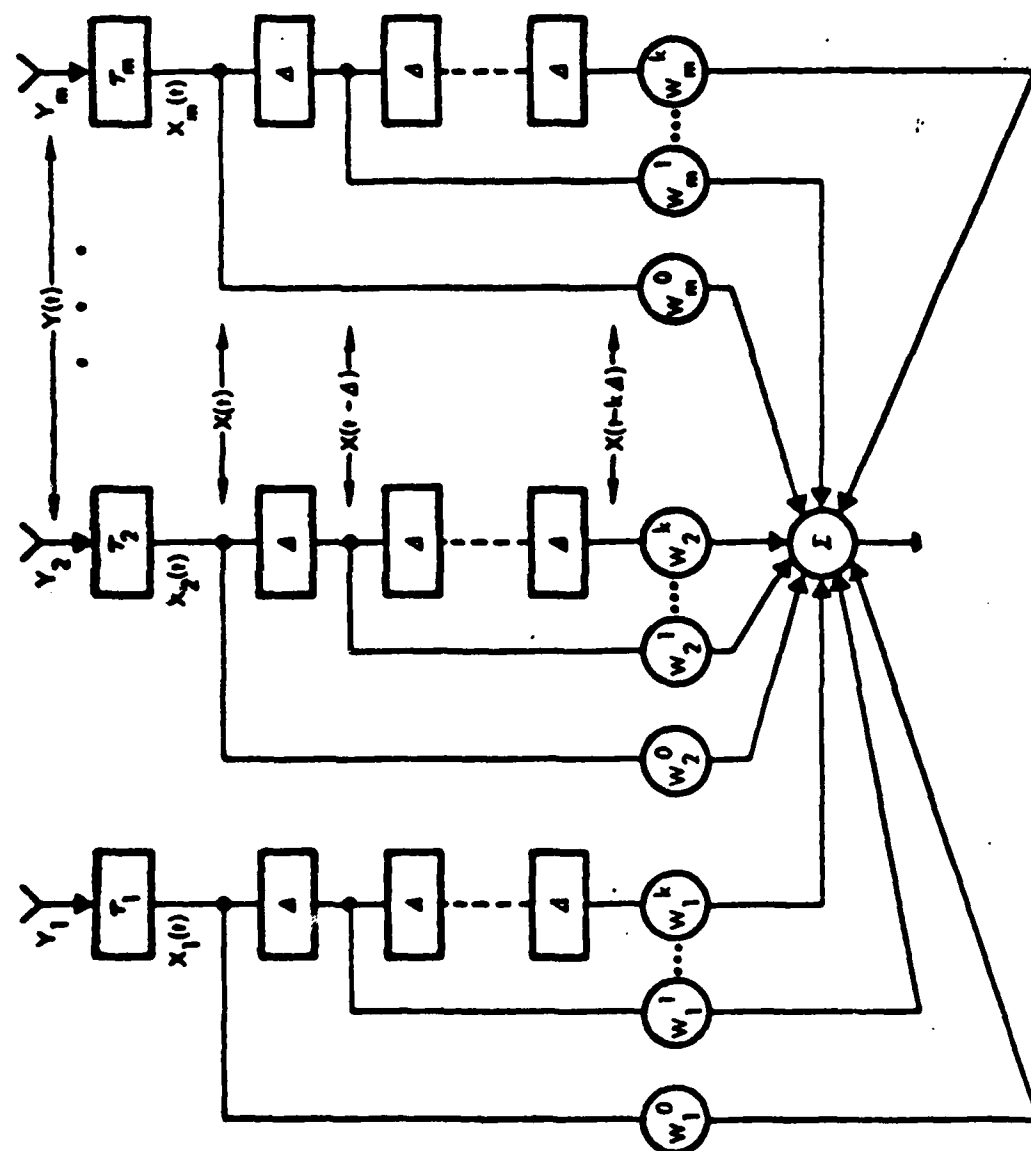
LIGHTWEIGHT ADAPTIVE WEIGHT CHANNEL MODULE

97

EPITAXIAL FERRITES FOR MAGNETOSTATIC WAVE DEVICES
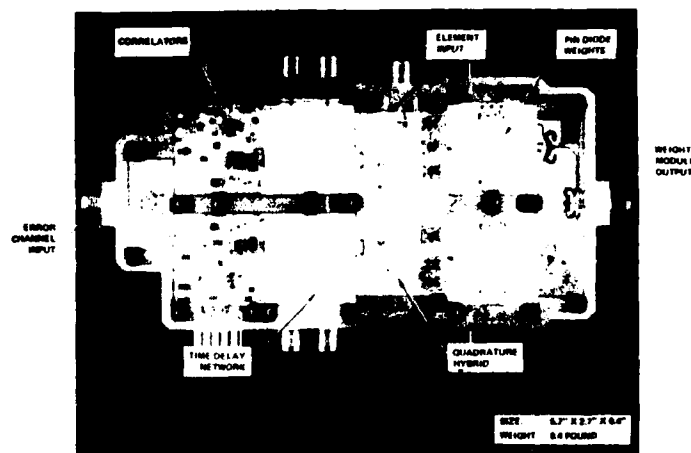
H. L. Glass

Rockwell International, Microelectronics Research & Development Center
P. O. Box 4761, Anaheim, California 92803

Summary

The liquid phase epitaxy (LPE) method for the growth of single crystal ferrite thin films is reviewed with an emphasis on yttrium iron garnet (YIG) materials suitable for microwave device applications.

1. Introduction

The earliest experiments on propagation of magnetostatic waves were carried out on rods and slabs fabricated from bulk crystals of YIG (yttrium iron garnet, $Y_3Fe_5O_{12}$). Although these experiments were successful, there are some serious limitations to the use of bulk crystals. For one thing, it is difficult to grow large, homogeneous, defect-free crystals of YIG by the commonly used flux method. Even if these difficulties can be overcome by new methods such as the traveling solvent float zone technique[1,2], another set of problems remains; namely, the undesirable effects associated with the nonuniform internal fields in nonellipsoidal magnetic bodies[3].

A thin film approximates an infinite disc and has a nearly uniform internal field. It is generally easier to grow a homogeneous, large-area thin film than to grow a homogeneous, large-volume bulk crystal. Also, thin films are compatible with planar device and circuit designs. If the thin film is single crystal YIG, then it will be a suitable medium for the propagation of magnetostatic waves. Moreover, if the film is thin, the waves will be accessible at the film surface. Additionally, there is the potential for preparing multilayered structures which may provide improved dispersion characteristics for magnetostatic wave propagation.

Single crystal thin films are usually prepared by epitaxy, crystallographically oriented growth onto a substrate. The first epitaxial YIG films were grown by CVD (chemical vapor deposition). Even in this early work[4,5], applications to microwave devices including delay lines were envisioned. However, attention swiftly shifted to magnetic bubble memory applications which required more complex magnetic garnet compositions. CVD could handle the two component $(Y_2O_3\text{-}Fe_2O_3)$ YIG system, but it was difficult to maintain homogeneity for bubble garnets which required a minimum of four components.

Fortunately, the LPE (liquid phase epitaxy) method was developed at just the right time[6].

2. The LPE Method

LPE, as applied to magnetic garnets, is an isothermal dipping technique. It can be thought of as a variation of the flux method that is used to grow bulk crystals of YIG. Growth is carried out from a fluxed melt which consists of the garnet constituents, Y_2O_3 and Fe_2O_3 in the case of YIG, dissolved in a flux or solvent. The most commonly used flux is a mixture of PbO and B_2O_3. The melt composition is chosen so that garnet will be the primary crystallizing phase[7].

As an example, we have used the following formulation for LPE growth of YIG: PbO 1278.8g, B_2O_3 23.74g, Fe_2O_3 84.71g, Y_2O_3 5.99g. These quanti ties are appropriate for a platinum crucible having a nominal volume of 250 ml. The starting materials are in the form of powders which have a volume much greater than that of the crucible. Therefore, the crucible is loaded in several steps. That is, part of the oxide mixture is placed in the crucible which is then heated until the oxides melt, then more oxides are added and melted, etc.

Although the noun "melt" is commonly employed, the LPE melt is really a solution of garnet in the flux or solvent. For the composition given above, the saturation temperature is about 910°C. At temperatures above this value, the solution is unsaturated. The normal procedure is to prepare the melt at a temperature much higher than saturation, perhaps 1050 or 1100°C, in order to make certain that all the solids are dissolved. After this the temperature is reduced to about 25 or 50 degrees above saturation. The melt can be maintained in this unsaturated state for extended periods. To grow a YIG film, the temperature is lowered to a value below saturation and the system is allowed to reach thermal equilibrium. In this undercooled or supersaturated state, crystallization of YIG can occur. A remarkable feature of these LPE melts, however, is that it is difficult for crystallization to occur spontaneously. For example, if the temperature is 20 or 30 degrees below saturation, many hours (perhaps even a few days) will pass before there is evidence of crystallization. Even if the undercooling exceeds 100 degrees, a few hours may elapse before spontaneous nucleation occurs.

99

The relative stability of these melts is exploited in the LPE method. During the period after thermal equilibrium has been attained but before spontaneous crystallization has begun, a suitable substrate is immersed in the melt. This substrate, which is allowed to warm up to the furnace temperature before immersion, acts as a seed on which crystallization occurs. After an appropriate period of time has elapsed, the substrate is removed from the melt and withdrawn from the furnace. For the commonly used substrates, the melt will have drained almost completely and a clean, epitaxial film will have grown (at a typical rate of several tenths of a micrometer per minute). Melt residues are removed by washing the sample in hot, dilute acetic and nitric acids. Normally, the crystallization is confined to growth on the substrate; no crystallization occurs on the melt surface, within the volume of the melt, or on the walls of the crucible. Therefore, the process can be repeated immediately by immersing another substrate.

If a film several micrometers thick is grown on a one inch diameter substrate using the 250 ml melt, the mass of garnet in the film will be insignificant compared to the mass of garnet in the melt. Thus, the composition of the melt is virtually constant throughout the growth period and, in fact, hardly changes over the course of several growth runs. Eventually, after many films are grown, the melt will become depleted. Also, there will be some loss of PbO through evaporation. (Since PbO is a toxic substance, provision must be made for handling the vapors and condensate.) Replenishment of the melt by addition of the appropriate oxides is straightforward.

In practice, the substrate is not simply immersed in the melt. Rather, the substrate wafer is held in a nearly horizontal position and is rotated during the growth period. Typical rotation rates are in the range of 60 to 100 rpm. This rotation quickly establishes a reproducible, steady state flow pattern which helps to provide uniform growth conditions over most of the substrate surface. The flow also stirs the melt. The rotation may be unidirectional or may be reversed periodically. Reversal is particularly useful when the substrates are large or when growth is carried out on several substrates simultaneously[8].

The three features just mentioned, that growth is carried out at a constant temperature from a melt of constant composition under reproducible

steady state flow conditions, are crucial to the success of LPE. However, these are features of the melt. Epitaxial growth cannot be successful without appropriate substrates. Fortunately, in the case of YIG and other magnetic garnets, rare earth gallium garnets make good substrates. In particular, GGG (gadolinium gallium garnet, $Gd_3Ga_5O_{12}$) is available in the form of single crystal wafers which, for most purposes, behave as though they are free of bulk defects and surface damage. Wafers up to three inches in diameter are available from several commercial sources.

GGG has the same crystal structure and nearly the same lattice constant as YIG. Along with the absence of defects and surface damage, these seem to be conditions which will lead to good epitaxial growth. However, there is no clear understanding of all of the conditions which must be satisfied for a substrate to function successfully. The commonly used (111) orientation of GGG behaves ideally. Other orientations do not. For example, when (100) orientations are used, a thin layer of melt remains on the film and may prevent attainment of high quality surfaces. To some extent, therefore, we must acknowledge that we are lucky that GGG works so well. The difficulty in finding a suitable substrate is the major factor which limits extension of the LPE method to the growth of other ferrites such as lithium ferrite and hexagonal ferrites.

3. Device Requirements

For magnetostatic wave device applications YIG films must meet certain requirements. The films must be uniform in thickness and in magnetic properties over the area of the device. The required film thickness depends upon the specific device, but is generally 20µm or more. Magnetostatic wave propagation losses must be low. These requirements can be met by LPE YIG films. Other requirements, for example films which offer improved temperature stability for the devices or multilayer films which offer improved bandwidth or more favorable dispersion for the devices, entail modifications of the YIG composition and are more difficult to meet.

Film thickness uniformity is determined mainly by the substrate rotation. The optimum rotation scheme must be found empirically since it depends upon such factors as the size and shape of the crucible, the diameter of the substrate, and the design of the substrate holder. It is not difficult to grow films which are uniform in thickness to within about

1% except for a narrow band around the periphery. Film thickness uniformity can be checked by observing the thin film optical interference fringes when the sample is illuminated by an extended source of monochromatic light.

If the film is uniform in thickness, it follows that the growth rate was uniform over the same area. Since the temperature and melt composition are also uniform during growth, the composition and magnetic properties will also be uniform. Although this uniformity has not been subjected to detailed investigation for microwave materials, it has been verified for bubble materials[8].

Film thickness is generally measured by optical interference. It is convenient to make this measurement in the near infrared, at a wavelength of about 2μm, where dispersion is negligible. A conventional spectrophotometer having reflection geometry can be used. The film thickness is the product of the average film growth rate and the LPE deposition time. Growth rate is a function of melt composition, undercooling, and rotation rate[7,9]. These parameters are chosen to meet various conditions. For example, the rotation rate may be chosen to obtain the desired thickness uniformity. Thus, the desired film thickness is achieved by determining the average growth rate and then, keeping the growth parameters fixed, selecting the appropriate deposition time. This can be done successfully because the growth parameters, melt composition, undercooling and rotation rate are reproducible.

The principal concern in meeting the film thickness requirement is that the film may crack. Pure YIG has a lattice constant which is about 0.06% smaller than that of commercial GGG. This produces a tensile misfit stress in the film and this stress is sufficient to cause cracking before a film thickness of 20μm is attained. Fortunately, LPE YIG films contain a small amount of Pb as an impurity which is picked up from the PbO in the flux. The Pb increases the lattice constant of the YIG and reduces the tensile misfit. By appropriate choice of melt composition and growth temperature, the Pb content can be made large enough to reduce the misfit to zero or even to introduce a compressive stress[10]. When the misfit is reduced by this means, it is possible to grow good quality YIG films more than 100μm thick[11].

At one time it was believed that incorporation of Pb would increase microwave losses by inducing formation of tetravalent Fe and, thus, opening up the valence exchange loss mechanism. It has been shown, however, that incorporation of a small amount of Pb actually reduces losses to values close to the theoretical value for pure YIG[12]. This result seems to be a compensation effect. Pb tends to enter YIG as a divalent ion substituting for Y, which is trivalent. The Pb can compensate tetravalent impurities. The tetravalent impurities of significance are Pt, which comes from a slight attack of the crucible, and Si, which is a common contaminant. Divalent Pb can also compensate oxygen vacancies which will be present. If Pb were not present, tetravalent impurities and oxygen vacancies would be compensated by divalent (ferrous) Fe and the valence exchange mechanism would be activated[13].

The requirement for low magnetostatic wave propagation losses can be met by growing films at temperatures at which an appropriate concentration of Pb is incorporated. Since the total impurity content is not really controllable, the optimum growth temperature (Pb content) must be found empirically for each melt. Of course, valence exchange is only one potential loss mechanism. To obtain low losses it is also necessary to avoid magnetic impurities which can provide direct relaxation mechanisms. Also, it is important to use good quality substrates and to maintain a reasonably clean environment to avoid physical defects. Microwave losses can be determined by a simple magnetostatic wave propagation measurement or by ferromagnetic resonance. The latter is more useful in determining which loss mechanisms are operating.

4. Doped or Substituted YIG

Nearly all of the magnetostatic wave devices which have been demonstrated up to now have used nominally pure YIG. Other garnet compositions, which can be described as doped or substituted YIG, offer certain advantages. In general, substitution changes magnetic properties. Even the incorporation of the relatively small amounts of Pb found in nominally pure YIG produces measurable changes in magnetic anisotropy, Curie temperature, and magnetization[10,14]. Larger changes can be produced without serious increases in losses if Ga is substituted for some of the Fe. At the levels of substitution normally used, the magnetization and the Curie

temperature will decrease monotonically with increasing Ga content. It is, in fact, possible to reduce the magnetization to zero. This corresponds to magnetic compensation of the two magnetic sublattices. However, microwave losses tend to become very large as this condition is approached.

Substitution of Ga also reduces the lattice constant of the YIG and increases the tensile misfit stress when the film is grown on GGG. As previously described, this stress can result in cracking of the film. Also, the misfit affects the magnetic anisotropy through the so-called stress-induced term. The stress-induced anisotropy field can be well over 100 Oe[15], so it is far from negligible. In order to adjust the misfit and to control both stress-induced anisotropy and cracking, La is substituted for Y simultaneously with the Ga substitution for Fe. La increases the lattice constant of the YIG.

Ga,La substitution has been used to modify the dependence of ferromagnetic resonance frequency on temperature and thus to improve the temperature stability of microwave devices[16]. This same sort of substitution is being used to form multilayer films for magnetostatic wave delay lines. In the case of magnetostatic surface waves, a structure containing two YIG layers of different composition resulted in improved flatness of the nondispersive delay passband[17]. Triple layers offer advantages for linearly dispersive delay lines using magnetostatic forward volume waves[18]. In this application it was shown that a low magnetization Ga,La:YIG film can function as a nonmagnetic dielectric layer.

Physically, Ga,La substitution is accomplished by adding Ga_2O_3 and La_2O_3 to the melt. These additions greatly complicate the LPE process. The incorporation of La and Ga into the growing film differ from their relative concentrations in the melt. Moreover, the incorporation varies with growth rate and, to some extent, with growth temperature. The result is that small fluctuations in growth conditions can lead to significant fluctuations in film composition and magnetic properties. The problems are not insurmountable; in fact, they have been solved for bubble materials. Nevertheless, unavoidable small fluctuations in growth conditions, especially growth temperature, may limit the attainable uniformity.

Acknowledgments

References

1. S. Kimura and I. Shindo, J. Crystal Growth 41 (1977) 192-198.

2. S. Kimura, I. Shindo, K. Kitamura, Y. Mori and H. Takamizawa, J. Crystal Growth 44 (1978) 621-624.

3. J. D. Adam and J. H. Collins, Proc. IEEE 64 (1976) 794-800.

4. J. E. Mee, J. L. Archer, R. H. Meade and T. N. Hamilton, Appl. Phys. Letters 10 (1967) 289-291.

5. J. E. Mee, IEEE Trans. Mag. MAG-3 (1967) 190-194.

6. H. J. Levenstein, S. Licht, R. W. Landorf and S. L. Blank, Appl. Phys. Letters 19 (1971) 486-488.

7. S. L. Blank and J. W. Nielsen, J. Crystal Growth 17 (1972) 302-311.

8. R. G. Warren, J. E. Mee, F. S. Stearns and E. C. Whitcomb, AIP Conf. Proc. 18 (1974) 63-67.

9. E. A. Giess, J. D. Kuptsis and E. A. D. White, J. Crystal Growth 16 (1972) 36-42.

10. H. L. Glass and M. T. Elliott, J. Crystal Growth 27 (1974) 253-260.

11. H. L. Glass, J. Crystal Growth 33 (1976) 183-184.

12. H. L. Glass and M. T. Elliott, J. Crystal Growth 34 (1976) 285-288.

13. M. T. Elliott, AIP Conf. Proc. 29 (1976) 676-677.

14. M. T. Elliott and H. L. Glass, AIP Conf. Proc. 29 (1976) 115-116.

15. P. J. Besser, J. E. Mee, P. E. Elkins and D. M. Heinz, Mat. Res. Bull. 6 (1971) 1111-1124.

16. H. L. Glass, J. H. W. Liaw and M. T. Elliott, Mat. Res. Bull. 12 (1977) 735-740.

17. L. R. Adkins and H. L. Glass, IEEE 1980 Ultrasonics Symposium Proc. 526-531.

18. L. R. Adkins and H. L. Glass, this conference.

AD P000926

MSW REFLECTING ARRAY FILTERS

J. M. Owens, C. V. Smith Jr. &. R. L. Carter
The University of Texas at Arlington

ABSTRACT

Surface Acoustic Wave (SAW) Reflective array filters (RAF's) which operate very effectively in the VHF/UHF range experience significant technical difficulties[1] as the operating frequency is increased above 1 GHz and bandwidths greater than 300 MHz are required. In particular, operation above 3 GHz requires submicron device dimensions and corresponding propagation loss is high. Recently, it has been proposed[2] and demonstrated that quasi-isotropic magnetostatic forward volume waves (MSFVW) propagating in liquid phase epitaxially grown. YIG films can be obiquely reflected by arrays similar to those used in SAW RAF's to provide bias field tunable, compact, nonrecursive transversal filter at microwave frequencies (1-20 GHz).

• This paper will describe the background and status of this new RAF technology based on MSFVW propagation in low linewidth ($\Delta H < 0.5$ Oe) thin film YIG. The propagation of MSFVW is nominally isotropic in the plane of the film, with a lowest order mode bandwidth of greater than 2 GHz with center frequency bias field tunable.◄

As in the SAW case, a magnetostatic wave RAF consists of an input and output transducer pair which performs limited bandpass shaping and one or more reflective arrays which perform the majority of the transversal filtering. Reflecting arrays utilized thus far have consisted of either metal bars or dots or regions of strain induced by ion implantation[3]. Etched groove arrays, used so successfully in SAW, have proved unusuable due to mode conversion to transverse standing spinwave resonances occurring at the etched steps[4].

The paper will present theory for single and double reflector arrays based on impedance discontinuities induced by the reflectors. Experimental results will be presented for simple uniform arrays, weighted arrays, a 400 MHz bandwidth linear phase nondispersive delay line with a 30 dB insertion loss and a quadratic phase "up chirp" filter with a 200 MHz bandwidth product greater than 60 and 3 GHz center frequency. Finally, the future of these devices will be discussed as well as their systems implications.

INTRODUCTION

This paper reviews the status of this new reflective array filter technology, based on oblique reflection of magnetostatic forward volume waves (MSFVW) by periodic propagation impedance discontinuities created in the EPI YIG propagation media by metal stripe and dot arrays and by ion implantation induced regions of strain.

The propagation behavior of these MSFVW is nominally isotropic in the plane of the film. As in the SAW case, wave anisotropy exists as a result of crystalline anisotropy associated with the growth process[5]. This effect must be taken into account in detailed response calculations. The MSFVW is characterized by magnetic energy which is distributed transversely across the volume of the film with multiple modes resembling those seen in EM wave propagation between parallel metal plates. The lowest order mode has a single half-sinusoid variation across the film with an exponential decay into the dielectric on either side of the film; the external part of the field permits spatial tapping and transversal filter applications. The lowest order mode dominates MSFVW propagation since it is the mode which is most strongly couplers used[6].

As in the SAW case, an MSW reflecting array filter (RAF) consists of an input and output transducer pair which performs limited bandpass shaping and one or more reflective arrays which performs the majority of the transversal filtering. Fig. 1 shows a simple single refletion oblique incidence filter schematically. Reflecting array utilized thus far consist of either metal bars or dots, or ion implanted regions. Etched groove arrays are highly limited due to mode conversion to transverse standing spinwave resonances occuring at the etched steps.

The single reflection was used initially since it is simpler to construct and simplifies analysis. The transducers have in general been single wires or loops with periodicity chosen to maximize transmission at the filter center frequency and minimize generation at long wavelengths (k=0). The filters retain the desirable features of tunability and microwave frequency operation, associated with previous YIG technology. However, since in principle any wavelength can be achieved at any frequency, submicron wave lengths are not required and broad bandwidths are possible.
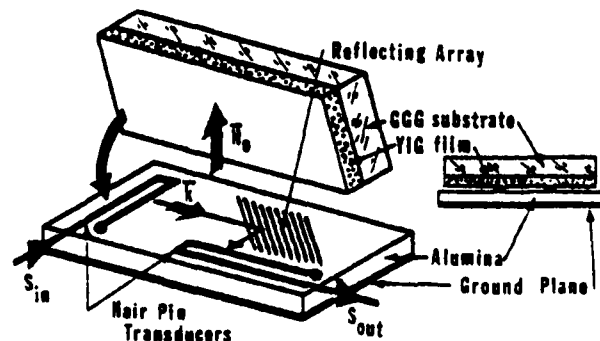
Fig. 1 Schematic of oblique incidence reflective array filter.

MODELING AND THEORY

Arrays of shallow grooves acting as right angle reflective grating for Surface Acoustic Waves has been proposed and first analyzed by Melngailis[7] utilizing transmission line analogs. The principal contribution to the reflection coefficient is due to the impedance mismatch at the two edges of the grating element. Analogous to the transmission line theory, the ratio of electric field to magnetic field is the wave impedance. The wave impedance[8] for an MSW is

$$Z = (j\omega\mu_o)/k \tag{1}$$

where ω is the wave angular frequency and k is the wave number in the wave propagation direction and it is assumed two adjacent step discontinuity do not interact each other. MSFVW spin wave mode conversion by etched groove gratings in epitaxial YIG film have been observed[4]. It is believed that the grooves cause a mode conversion between the MSFVW propagating in the film plane and a standing wave resonance normal to the film plane. Power absorption due to mode conversion limits the use of etched groove grating for normal or oblique incidence MSFVW microwave signal processing devices. Melngailis' method for the Acoustic wave can be applied directly to the corresponding calculation for the metal stripe array, dots or ion implanted regions. Linear arrays of metal dots with d (the dot diameter) $\ll \lambda$ (the interaction wavelength) can be modeled in the same way as a metal stripe arrays with an equivalent width cd where c is a weighting factor proportional to the metal dot density along a transverse line. Ion implantation produces a localized strain in the epitaxial YIG proportional to the implantation flux. This strain results in a change in the local magnetization (calculated from the uniaxial anisotropy constants) and thus a resulting wave impedance change[3]. Looking at a metal stripe grating as an example (the structure is shown in Fig. 2) a front or an incident wave up edge followed
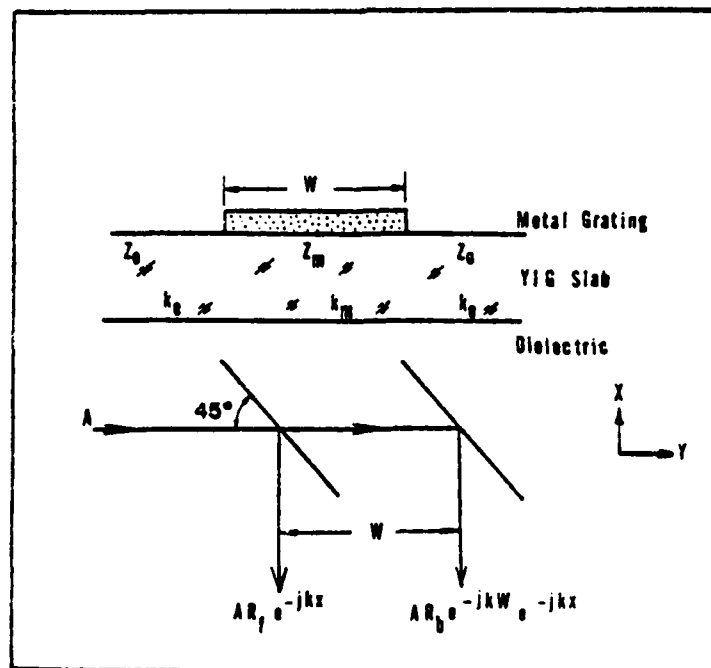
Fig. 2 A schematic representation of incident signal reflection at the two edges of the metal strip neglecting propagation attenuation under the strip.

by a metallized region and a back or a transmitted wave down edge. From transmission line theory[9] the reflection coefficients, R_f and R_b for front and back edges are respectively

$$R_f = -R_b$$

$$= C\frac{Z_m-Z_o}{Z_m+Z_o} \tag{2}$$

where Z_m and Z_o are the wave impedance in the metallized and unmetallized region respectively, k_m and k_o are the wave number in the metallized and unmetallized regions, C is a coefficient to be determined by experiment. From Fig. 2 the single metal grating reflection coefficent obtained by coherent superposition of front and back edge reflection is given by

$$\rho = C\frac{Z_m-Z_o}{Z_m+Z_o} \sin\left(\frac{kW}{2}\right) \tag{3}$$

For weak reflection we assume that the amplitude of back edge wave is the same as the front edge wave.

For device applications, the interest is in getting the maximum power from input transducer to output transducer. Losses in the grating pattern should be minimized. Experimental evidence indicates that ion implantation provides the lowest loss, with dot arrays next. For initial design, the grating pattern is assumed lossless. For such assumptions the reflection coefficient is given by equation 2. Also for this lossless system the transmission and reflection coefficients are related by

$$1 = |\rho|^2 + |\tau|^2 \tag{3}$$

where τ is the single metal grating transmission coefficient.

The grating transfer function was developed by Martin[10]. For application to a reflection mode dispersive delay line using the reflection of an acoustic shear mode from symmetrical arrays of oblique grooves in the surface of a steel strip delay line. An idealized theory for the transfer function of oblique incidence reflective array is

$$H(\omega) = \sum_{n=1}^{N} \rho\tau^{n-1} \exp\{-jk(X_i + 2(n-1) W + X_o)\} \tag{4}$$

where W is the reflector width measured along the signal direction, ρ and τ denote respectively the grating elements reflection and transmission coefficient, X_i is the distance from the first grating, X_o is the distance from the lower end to the output transducer, N is the number of elements, and k denotes the wavenumber at angular frequency

109

ω. Equation 5 represents the sum of signals reflected from individual grating elements. The overall path length for each grating line as $X_i + 2(n-1) W + X_o$ as shown in Fig. 3. This transfer function is simply the summation of the reflection from each individual element and is only applicable for small reflection coefficients, ρ. This requirement is particularly hard to meet using metal bars, since $Z_{metalized}/Z_{unmetalized}$ is equal to 2 and to achieve low ρ, W must be very small.

A closed form of the transfer function for the uniform grating filter can be written as

$$H(\omega) = C \sin \left(\frac{kW}{2}\right) \left(\frac{\sin NkW}{\sin kW}\right) \exp \{-jk(X_i + (N-1) W + X_o)\} \quad (6)$$

The overall frequency response of a reflective array device can be given by

$$H_o(\omega) = T_1(\omega) H(\omega) T_2(\omega) \quad (7)$$

where $H(\omega)$ is the transfer function of reflective array, $T_1(\omega)$ and $T_2(\omega)$ are the frequency response of the input and output transducer. The loop transducer design provides good pass band response near the center frequency, as shown in Fig. 4b. The insertion loss is defined as $-20 \log |H_o(\omega)|$ (dB). Theoretical results of combining equations 2, 4, 5 with the appropriate MSFVW dispersion relation is shown in Fig. 5a with N=10, and W=150 μm for the frequency range from 2.5 to
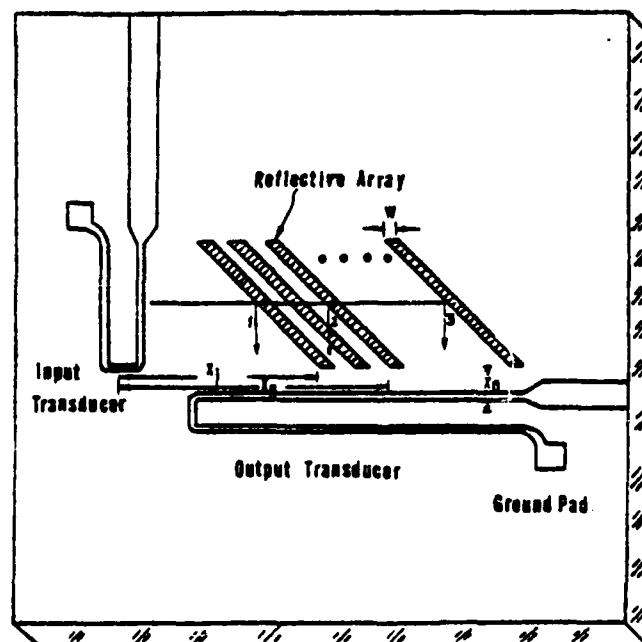
Fig. 3 Schematic diagram of oblique incidence reflective array. Input transducer sends a MSFVW in the film plane. The reflector selectively reflects part of the signal and is picked up by the output transducer.

110
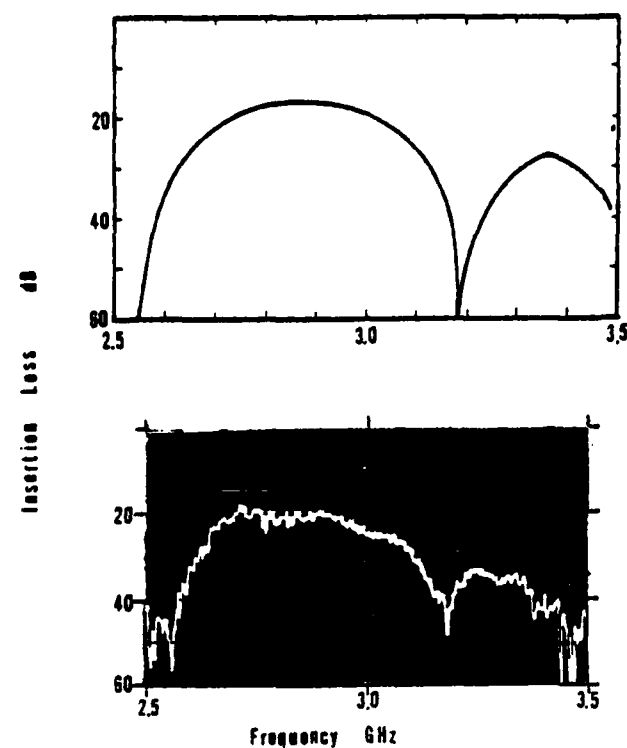
Fig. 4 (a) Calculated insertion loss versus frequency of a loop
transducer without grating, microstrip 50 um wide, transducer
center-to-center spacing 1 cm, YIG film 20 um thick.
(b) Experimental results of loop transducer, using reflection
from an edge of YIG film placed at 45° relative to the
incident wave path.
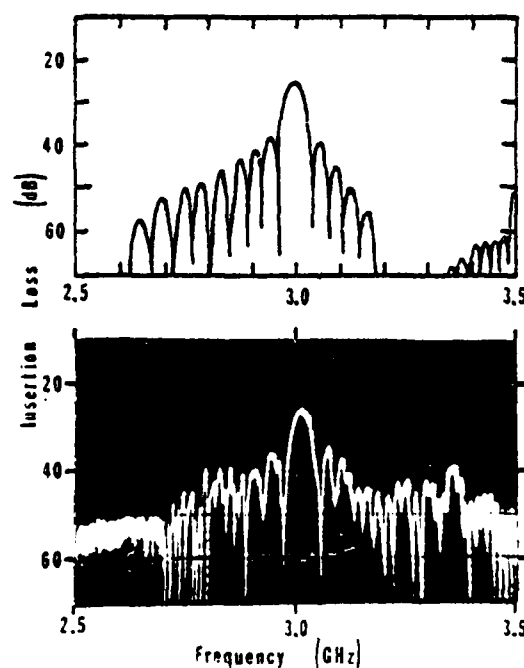
Fig. 5 Comparison of theory and experiment for insertion loss of uniform
grating structure with N = 10 and W = 150 um.

3.5 GHz. Note that the peak response occurs at the incidence wavelengths of 2W, (2/3)W and (2/5)W and that the first sidelobe is approximately 12 dB down. The spatial harmonic response seen which results from the dispersive nature of MSFVW represents a significant problem in designing broad band devices.

EXPERIMENTAL RESULTS

Swept CW insertion loss measurements were performed between 2.5 and 3.5 GHz on a 20 μm thick epitaxial YIG film, grown on a gadolinium gallium garnet (GGG) substrate, with a normal magnetic bias field. The loop transducers were spatially orthogonal and fabricated with 50 μm wide conductors. The input transducer was 3 mm long and output transducer was 6 mm long. Fig. 6 illustrates a typical pictorial view of the test unit. The uniform grating consisted of 10 periods of 150 μm open circuited stripes, each one separated by 150 μm. The 20 μm thick YIG sample which was placed in direct contact with transducer pair and reflecting array had MSW terminations formed along various edges by abrasion. Further, two of the sample edges were aligned parallel and perpendicular to the incident wave propagation path. Fig. 5 shows the measured insertion loss which occurs with the peak at center frequency 3.0 GHz (λ = 300 μm). The input and output transducer both have bandwidths of greater than 600 MHz, Fig. 4. Therefore all the filtering occurs at the reflector elements. The theory shows a bandwidth of approximately 70 MHz and the adjacent sidelobes are 12 dB down, while the experiment shows about 75 MHz and the first sidelobe about 11 dB down.

An effective technique for amplitude weighting has been theoretically evaluated and tested experimentally. The technique utilized is width weighting of the metallic reflecting stripes. Variations in dot density and variation of implantation density or width should have the same effect. This technique overcomes the problems associated with
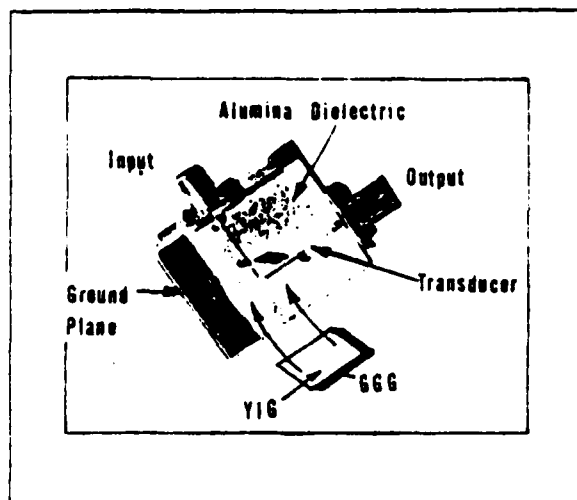
Fig. 6 Test jig for oblique incidence reflective array.

112

apodization when element length weighting is used. Fig. 7 shows the theoretical and experimental response characteristics of an 11 element triangular weighted reflective array. Element widths were varied from zero to λ and back to zero across the 11 period array; the significant reduction in the sidelobe level can be seen.

A 20 period oblique incidence reflective dot array has been fabricated and experimentally evaluated. The dots were ∿100μm in diameter and were randomly placed along oblique angle lines spaced by 300 μm. There were typically 20 dots/line. Input and output was accomplished by orthogonal loop transducers. Insertion loss was 32 dB with a bandwidth of 40 MHz. Sidelobes were 14 dB down from the main peak. Simple theory based on the ratio of the dot array to an equivalent metal line gives a bandwidth in good agreement with theory. This technique offers a simple weighting system applicable to shaped band-pass filters.

The majority of SAW reflective array devices rely on a double reflectors. A ten element double reflecting array device is shown in Fig. 8, as well as the response of this device with a 16 μm thick YIG
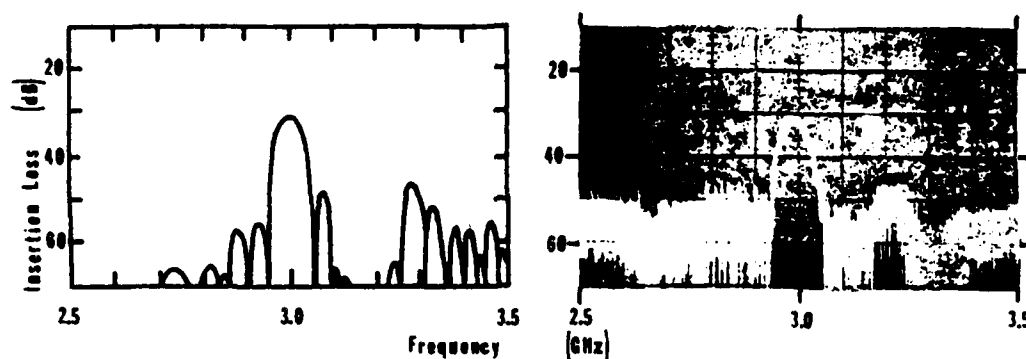
Fig. 7 Theoretical and experimental insertion loss (dB) versus frequency
(GHz) for 11-element triangle weighted oblique incidence
reflective array filter. Transducer effects are included.
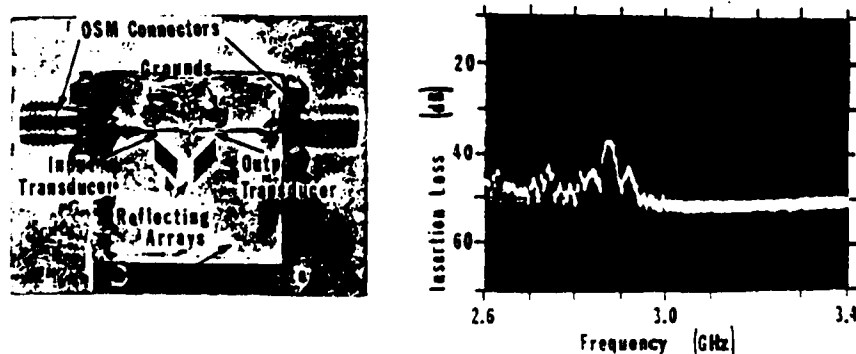
Fig. 8 Double reflective array device (YIG film removed) and insertion
loss (dB) versus frequency (GHz) for a 16 um film.

113

film. The response of this device is in good agreement with a simple double reflection theory which predicts a 50 MHz main lobe bandwidth and insertion loss of 35 dB.

As a next step, a simple reflecting array has been designed to remove the dispersion from an MSFVW delay line over a limited bandwidth (350 MHz). This array consisted of 14 periods of 4 μm thick aluminum reflectors λ wide. Spacing was graded from 600 μm to 200 μm to remove MSFVW dispersion so producing a linear phase characteristic. There was no amplitude weighting (uniform 3 mm aperture reflectors). The experiment configuration is as shown in Fig. 1. The theoretical and experimental insertion loss versus frequency characteristics and the theoretical and experimental group delay compared with that of a conventional 1 cm path MSFVW delay line, are shown in Fig. 9. It can be seen that the insertion loss and group delay characteristics are in
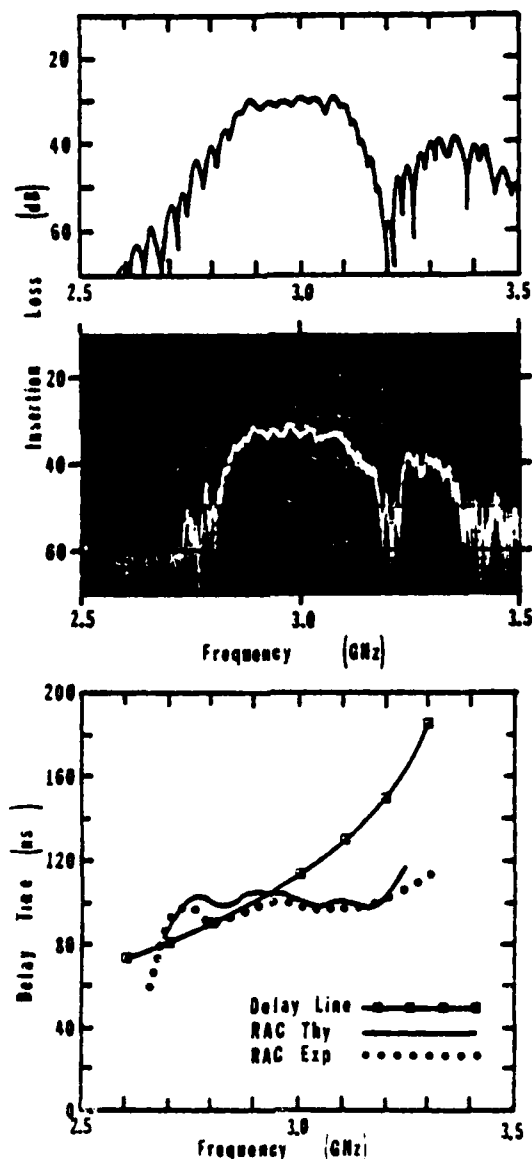
Fig. 9 Theoretical and experimental insertion loss(dB) versus frequency (GHz) of a graded periodicity reflective array, and theoretical and experimental group delay (usec) versus frequency (GHz) of the graded array compared with that of a 1 cm long MSFVW delay line.

114

good agreement with theory considering the terminations were far from perfect. The phase error from linear was + 30°. Fig. 10 shows a quadratic phase double reflective array filter. The device has a 250 MHz bandwidth and a time-bandwidth product of 70, and a linearity of better than + 2 nsec.
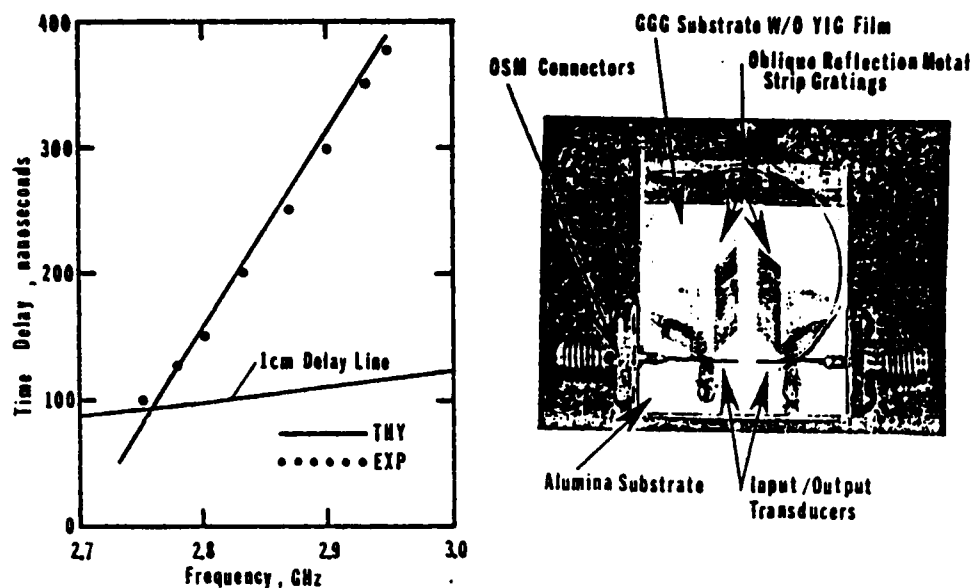
Fig. 10 Quadratic phase, double reflective-array filter.

SUMMARY AND CONCLUSIONS

Table 1 shows the present status of MSW RAF's and future projections.

TABLE I MSW REFLECTIVE ARRAY PERFORMANCE		
Parameter	Reflective Array	
	Current	Future
Center Frequency (GHz) Tunable	1-20	1-40
Bandwidth (MHz)	30-500	10-1800
Time Dispersion/Delay	.5 µsec	5 µsec
Time x Bandwidth	100	>1000
Am Ripple dB	4	<1
Phase Error DEG (RMS)	30	5
Temperature Stability	NA	NA
Insertion (dB) Loss	30	20

With SAW RAF's devices have been under intensive study for the past 12 years, MSW devices have only been under limited active study for about 8 years. Thus, only the basic proof of principles have been reported. Also various technical problems, including higher frequency of operation and dispersion to name a few, makes MSW more complex than SAW in general. Still progress has been significant and the promise is great.

ACKNOWLEDGEMENT

REFERENCES

1. J. D. Manes, E.G.S. Paige Proc. IEEE 64, 639-652, 1976.

2. J. M. Owens and C. V. Smith, Jr. 1978 Ultrasonics Symposium Proc., IEEE Cat. #78CH.

3. G. Volluet, to be published IEEE-Trans Mag Nov., 1981, presented at 1981 Intermag Conference.

4. R. L. Carter, C. V. Smith, Jr., J. M. Owens, IEEE Trans. Mag. 16 #5, pp 1159-1162, 1980.

5. C. V. Smith, Jr., J. M. Owens, R. L. Carter, and N. D. Parikh to be published IEEE Trans. Mag., Nov. 1981 presented 1981 Inter-Mag Conf.

6. H. J. Wu, C. W. Smith, Jr., J. M. Owens, J. Appl. Phys 50(3), pp 2455-2457, 1977.

7. J. M. Melongailis and R. C. M. Li, 1975 Ultrasonics Symposium Proc., IEEE, pp 426-429.

8. E. Sawado J. Appl Phys. 41, 6 May (1970).

9. S. Ramo, J. R. Whinnery and T. V. Duzer, Field and Wave in Communication Electronics, John Wiley and Son, Inc., 1965.

10. T. A. Martin, IEEE MTT-22, 1973, pp 186-195.

MAGNETOSTATIC WAVE TRANSDUCERS

James C. Sethares

June 1982

117

MAGNETOSTATIC WAVE TRANSDUCERS

ABSTRACT

This paper investigates the coupling of
magnetostatic wave energy into and out of fer-
rimagnetic films using flat current carrying
conducting strips. An electrical equivalent
circuit model is developed, from which inser-
tion loss is derived for a magnetostatic wave
delay line, made up of two multi-element trans-
ducers and a YIG film. Experimental/theoretical
comparisons are made and the range of validity
of present MS transducer models is discussed.

118

1. INTRODUCTION

This paper investigates the coupling of magnetostatic wave (MSW) energy into and out of ferrimagnetic films, such as yttrium iron garnet (YIG), using flat current carrying conducting strips. For many years, from the late sixties to early seventies, when basic MSW phenomena were under investigation fine wire couplers were often used for generating and detecting MSW. There was no theory then for predicting insertion loss as a function of frequency and transducer parameters so the phenomena was unattractive from a device point of view – both because of the practical problems associated with fine wire structures and the lack of a suitable theory. Then in 1975 Ganguly and Webb[1] derived an expression for radiation sresistance of an MSW transducer made up of a length of microstrip line. This work provided a basis for extending the theory to more complicated transducers and developing more sophisticated transducer models. Several extensions of the theory have been made.[2-9] They rely, to a large degree, on concepts and ideas generated in surface acoustic wave (SAW) transducer theory; SAW and MSW transducer models being to some extent analogs of one another. This has been both a help and a hindrance. It has been helpful because SAW transducer theory with its MSW analog works well for predicting fundamental and space harmonic transducer responses. It has been a hindrance because theoretical problems peculiar to MSW transssducer theory have been somewhat put aside, partially because of the success of SAW analog theories in providing a first order theory adequate for many MSW investigations. These problems include non-reciprocity of MSW and the presence of long wavelengths in the MSW pass band. The presence of long wavelengths is particularly trouble-some, and crucial, as will be evident in the theoretical/experimental comparisons presented here.

A transducer theory for magnetostatic surface waves (MSSW) can be developed from a pure TE (transverse electric) mode analysis. The other two principal MSW propagating modes, magnetostatic forward volume, (MSFVW) and backward volume (MSBVW) waves are not pure TE modes. However a first order transducer theory for all three principal MSW modes can be handled in a unified way. This is done here. We point out the range of validity of present transducer models and, where work remains to be done.

2. DEVELOPMENT OF MSW TRANSDUCER MODEL

A fundamental approach which may be used to develop expressions for radiation resistance and reactance for multi-element transducers for all three principal magnetostatic modes of propagation, is presented here. With reference to the coordinate system and geometry shown in Fig. 1, the basic approach is to solve an electromagnetic boundary value problem subject to the following assumptions and restrictions.

a. Nonuniform electromagnetic plane waves propagate in the x direction. The waves may be bounded by two ground planes, wave amplitude varies in the y direction, and the waves are uniform in the z direction.

b. Non propagating modes are neglected.

c. The magnetostatic approximation is employed.

d. The gyromagnetic equation is linearized to first order terms in small signal variables.

119

e. The RF magnetic field $\vec{h} = \nabla\psi$ where ψ has the form $Af(y)e^{i(\omega t - kx)}$

f. When the two ground planes are moved respectively to $\pm\infty$ in the y direction, the time varying fields decay exponentially with distance from the YIG surfaces.

g. Ground planes and YIG are infinite in the xz plane, the conducting strip array is finite in the x direction, infinite in the z direction, and it supports current sheets of zero thickness in the y direction. Current flows in the z direction.
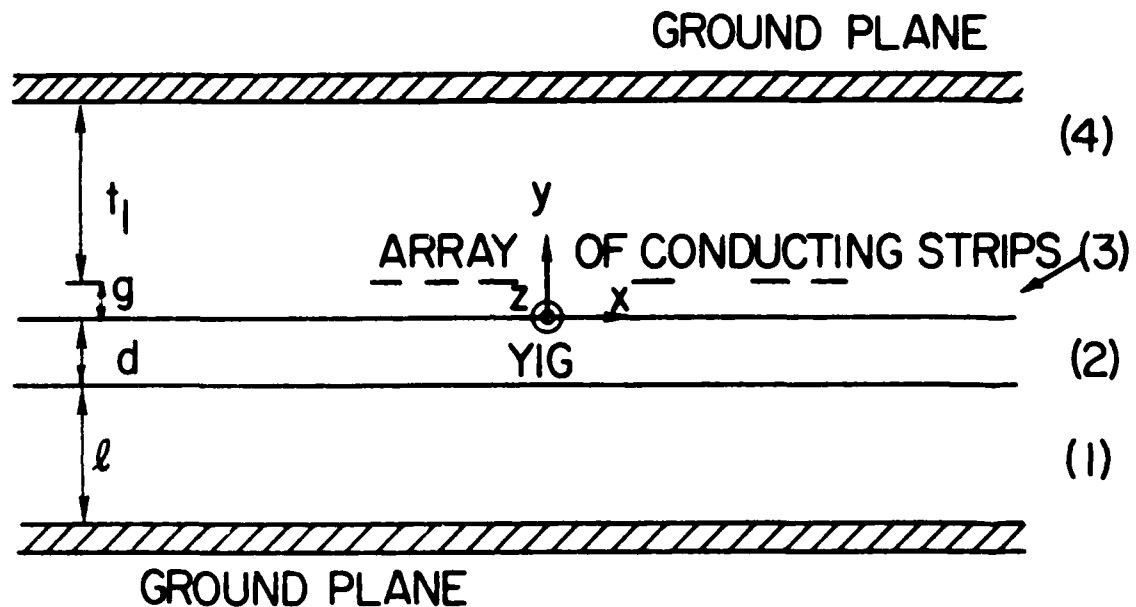
GROUND PLANE

Fig. 1. Geometry for the boundary value problem comprising YIG film, conducting strip array, and ground planes.

The assumptions of uniformity in the z direction, $\frac{\partial}{\partial z} \rightarrow 0$, and the magnetostatic approximation, $\nabla \times \vec{h} = 0$, (which implies $\vec{h} = \nabla\psi$) forces $h_z = 0$ for all magnetostatic wave modes. This simplifies the analysis considerably and makes the power flow proportional to $E_z H_y^*$ for all three principal MSW modes.

In solving the boundary value problem, electromagnetic field components can be separated into stationary, sinusoidal in time, near fields and radiating far

fields. Near fields decay rapidly with distance in the x direction away from the array or transducer. A poynting vector is formed from the far fields giving the power flow per unit width. From this, a radiation resistance per unit width is determined. Then assuming causality, a Hilbert transform of radiation resistance provides the radiation reactance. The reactance is a significant portion of the radiation impedance and should not be neglected.

Figure 2 shows some practical transducers for launching and detecting MSW. Using RF current sheets, which can vary with x, as reasonable approximations to the actual current distribution in the transducer strips yields a good first order theory. One can analyze the coupling between MSW and microstrip, coplanar, slot lines, meander and grating structures. In particular, expressions for insertion loss for a delay line configuration can be derived.
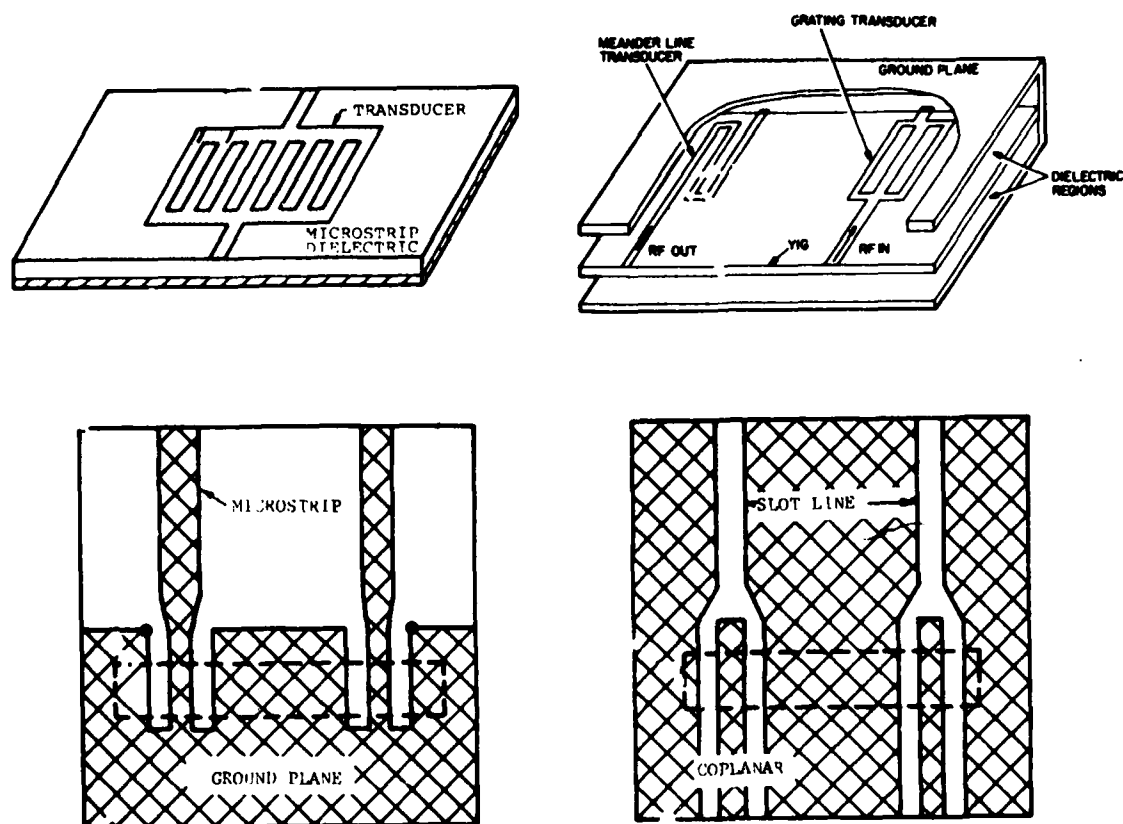
Fig. 2. Various transducers for launching and receiving magnetostatic waves.

We initially follow a procedure used earlier[8] to obtain expressions for surface wave radiation resistance. Using the above assumptions and restrictions only, Maxwell's equations reduce to the following:

121

$$\frac{\partial h_y}{\partial x} - \frac{\partial h_x}{\partial y} = 0 \ , \qquad \frac{\partial e_z}{\partial y} = -i\omega b_x \qquad\qquad (1), \ (2)$$

$$\frac{\partial e_y}{\partial x} - \frac{\partial e_x}{\partial y} = -i\ \omega b_z, \qquad \frac{\partial e_z}{\partial x} = i\ \omega\ b_y \qquad (3), \ (4)$$

where e, h and b are small signal field components and

$$\vec{b} = \overset{\leftrightarrow}{\mu}\vec{h} \qquad\qquad (5)$$

The components of $\overset{\leftrightarrow}{\mu}$ are defined[10] elsewhere in these proceedings. Solutions for magnetic potential ψ, having the following form, are assumed for each region.

$$\psi_n = \int_{-\infty}^{\infty} f_n(y)e^{i(\omega t - kx)}\ dk \qquad\qquad (6)$$

$f_n(y)$ is constructed, in general, of two exponentials with the form

$$f_n(y) = A_{n1}e^{a_{n1}y} + A_{n2}e^{-a_{n2}y}$$

All constants a_{n1} and a_{n2} are determined from Maxwell equations, and all A_{n1} and A_{n2} are determined in terms of one arbitrary constant by using the boundary conditions continuity of tangential h and normal b at both YIG surfaces, and vanishing normal b at both ground planes. Then, the remaining constant is determined from the remaining boundary condition at the conducting strips.

The boundary condition at the conducting strips, y = g, is

$$h_x^{(4)} - h_x^{(3)} = J(x) \text{ amps/meter,} \qquad\qquad (7)$$

with superscripts indicating regions. The final constant is found to be proportional to the spatial Fourier transform, J(k), of the transducer current distribution* defined by

$$\tilde{J}(k) = \int_{-\infty}^{\infty} J(x)e^{ikx}dx \qquad\qquad (8)$$

All field components are thus known in terms of $\tilde{J}(k)$ which in this model is independent of YIG parameters. The magnetic field h is known in terms of ψ, b follows from Eq. 5, and e is found from Equations (2)-(4). The next step, in developing the model, is to obtain field expressions in closed form by performing the integration over k. This is done individually for all field components. We note that all integrals have the same form, as follows:

$$\begin{bmatrix} \text{complex} \\ \text{field amplitudes} \end{bmatrix} \alpha \int_{-\infty}^{\infty} \frac{\tilde{J}(k)\ Q(k,\omega)}{F(k,\omega)}\ dk \qquad (9)$$

*This is worked out in detail in Ref. 3 on Page 12.

where $Q(k,\omega)$ only is different for each field component. $\tilde{J}(k)$ is the only term in the field expressions involving transducer geometry. It allows a variety of transducer structures, such as the ones shown in Fig. 2, to be handled by the same analysis. For instance, when $J(x)$ represents a uniform current sheet in a single strip of width a, that is $J(x) = I_0/a$ for $a/2 < |x|$; then

$$\tilde{J}(k) = \frac{I_0 \sin (ak/2)}{(ak/2)} \qquad \text{from Equation 8.}$$

The integral Eq. 9 splits naturally into two parts:

$$\frac{1}{F(k,\omega)} = \frac{1-F(k,\omega)/F(\infty,\omega)}{F(k,\omega)} + \frac{1}{F(\infty,\omega)}$$

Integration of the first part by contour integration yields the radiated fields. These are guided waves which are attenuated only by the material, magnetic line width, loss in the YIG and by beam spreading. Integrating the second part directly, or numerically as is generally necessary, yields stationary fields which are concentrated near the transducer. The near fields give rise to an energy storage reactance associated with the transducer structure. As a first approximation this reactance may be neglected because it is small in comparison with radiation reactance. Inclusion of near field effects will give an improved but very complex model.

MSW power density is given by the Poyntings vector in the x direction,

$$p^{(s)} = 1/2 \, e_z^{(s)} \, h_y^{*(s)} \text{watts/m}^2, \tag{10}$$

where s denotes propagation in the $\pm$ x direction. Total MSW power, for width ℓ_1 in the z direction is given by

$$P_{TOT}^{(s)} = \frac{\ell_1}{2} \int_{-(\ell+d)}^{(g+t_1)} e^{(s)}_z \, h_y^{*(s)} dy \text{ watts}, \tag{11}$$

This expression can be integrated analytically. The real part of Eq. 11 gives the real average power and it can be put into the following form

$$P_{TOT}^{(s)} = (1/2)R_1^{(s)} \left\{ \ell_1 |\tilde{J}(k)|^2 \right\} \tag{12}$$

where the bracketed term depends only on transducer dimensions, and $R_1^{(s)}$ on YIG parameters and ground plane spacing only. $J(k)$ includes a factor I_0, the current in a transducer strip.

Radiation resistance for the total transducer is

$$R_m(s) = 2 P_{TOT}(s)/|I_T|^2 \qquad (13)$$

where: for identical parallel strips $I_T = NI_O$, for a meander line $I_T = I_O$, and for identical parallel "π" transducers $I_T = (N/2)I_O$.

Here N is the number of strips. Upon substitution of Eq. (12) into (13) the I_O cancels leaving an expression for total radiation resistance of the entire transducer in terms of $R_1(s)$, normalized $\tilde{J}(k)$ and the number of conducting strips.

Finally, radiation reactance, X_m, is obtained from the Hilbert transform of total radiation resistance[5,11] as, $X_m = (1/\pi) \int_{-\infty}^{\infty} \frac{R(\omega')\, d\omega'}{\omega' - \omega}$.

$$X_m \text{ IS HILBERT TRANSFORM OF } (R_m^+ + R_m^-)$$
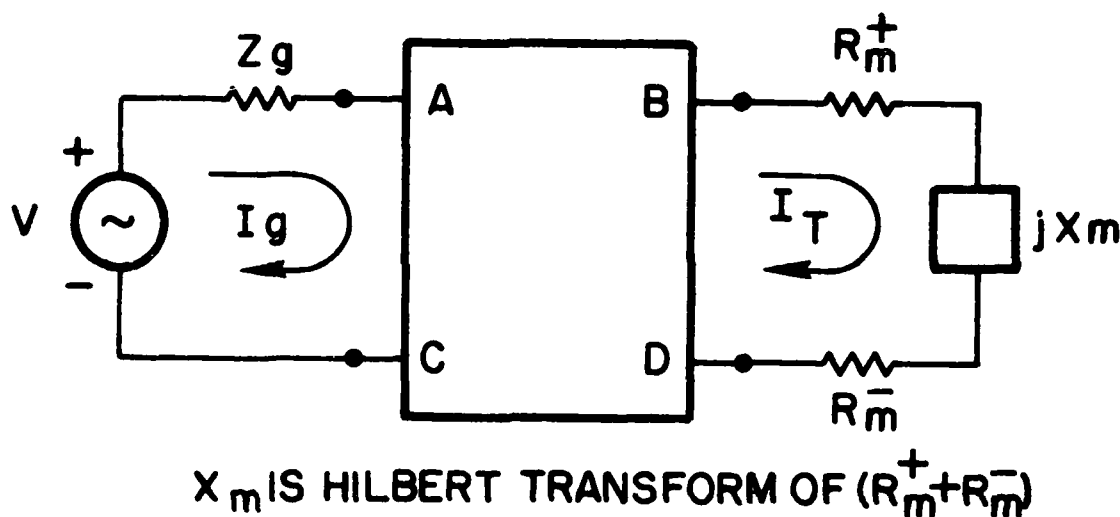
Fig. 3. Equivalent Circuit of MSW Transducer with Matching Network ABCD and Voltage Source with Internal Impedance Zg.

An equivalent circuit for a delay line, made up of an input and output transducer, and its insertion loss can now be obtained. With reference to Fig. 3, B and D are the transducer terminals. A and C are the output terminals of a microwave generator. All matching networks and connecting wire reactances are included in network ABCD. Consider the case of no matching and short connecting leads. Then A and B are connected and so are C and D. Insertion loss of a single transducer is defined as

$$I.L. = -10 \log TE \qquad (15)$$

124

where TE is the transmission efficiency given by Eq. 16

$$TE = \frac{\text{Power delivered to load}}{\text{Maximum power available}} \tag{16}$$

Power delivered to the load, in this case, is the total power carried by an MSW, say the positive wave, $(1/2)R_m^{(+)}|I_T|^2$ where, from the circuit,

$$I_T = \frac{V}{R_m^{(+)} + R_m^{(-)} + R_g + jX_m}$$

Maximum power available from the source V occurs when everything to the right of terminals A and C is replaced by a resistance $R_g = Z_g$. The maximum available power is $(1/2)R_g|I|^2$ where $I = V/2R_g$.

When these expressions are substituted into Eq. 15 and 16, I.L. for one transducer is obtained. Assuming reciprocal coupling efficiency between the electromagnetic system and MSW, the total I.L. for a pair of identical transducers is twice that given by Eq. 15. We find, for a transducer pair,

$$\text{I.L.}^{(\pm)} = 20 \log \left[\frac{(R_g + R_m)^2 + X_m^2}{4R_g R_m^{(\pm)}} \right] \tag{17}$$

This insertion loss is identical with S_{21} in dB, the transmission loss measured by commercial network analyzers. Propagation loss can be included by adding a term $76.4\, T_g\, \Delta H$ to Eq. (17) where T_g = group delay and ΔH the full magnetic line width.

3. DISCUSSION OF THE MODEL

In this section we discuss some aspects of single and multiple element transducers, compare MSW transducer models with experiment, and discuss the range of validity of the models.

3.1 Multiple Strip Transducers

First, we give some analytical and graphical results for an MSW grating transducer. Consider a grating transducer made up of N parallel conducting strips each of width a, length ℓ_1, center-to-center spacing p, and carrying a spatially uniform current I_0. The spatial transform, $J(k)$, of this current distribution as defined by Eq. (8) is

$$\tilde{J}(k) = I_0 \left[\frac{\sin(k_s a/2)}{(k_s a/2)} \right] \left\{ \frac{1 - e^{1k_s pN}}{1 - e^{ik_s p}} \right\} \tag{18}$$

When Eq. (18) is substituted into Eq. (12), which in turn is substituted into Eq. 13, the result is,
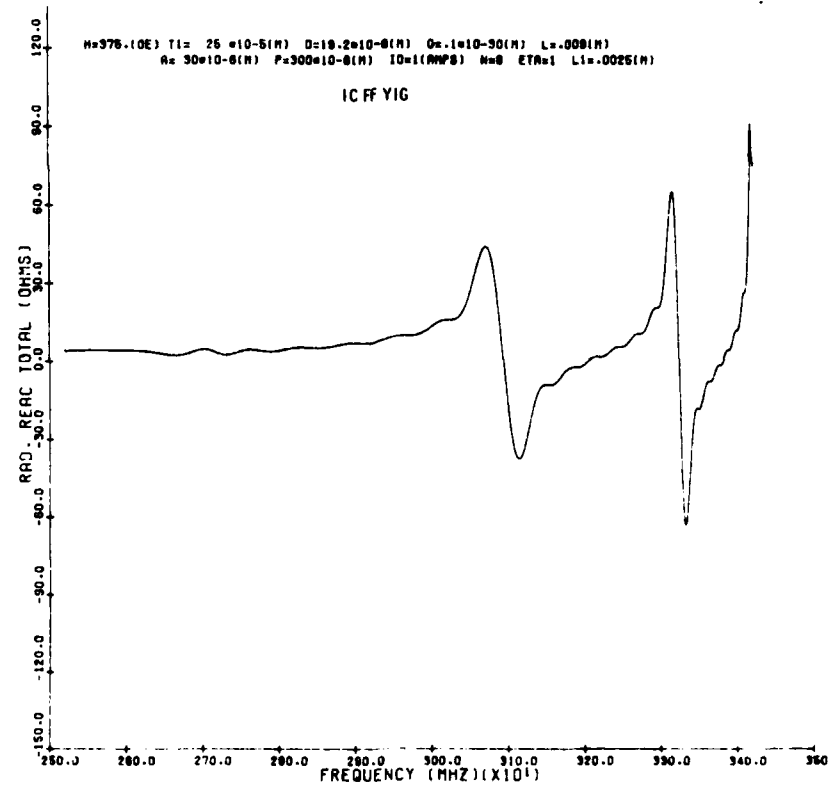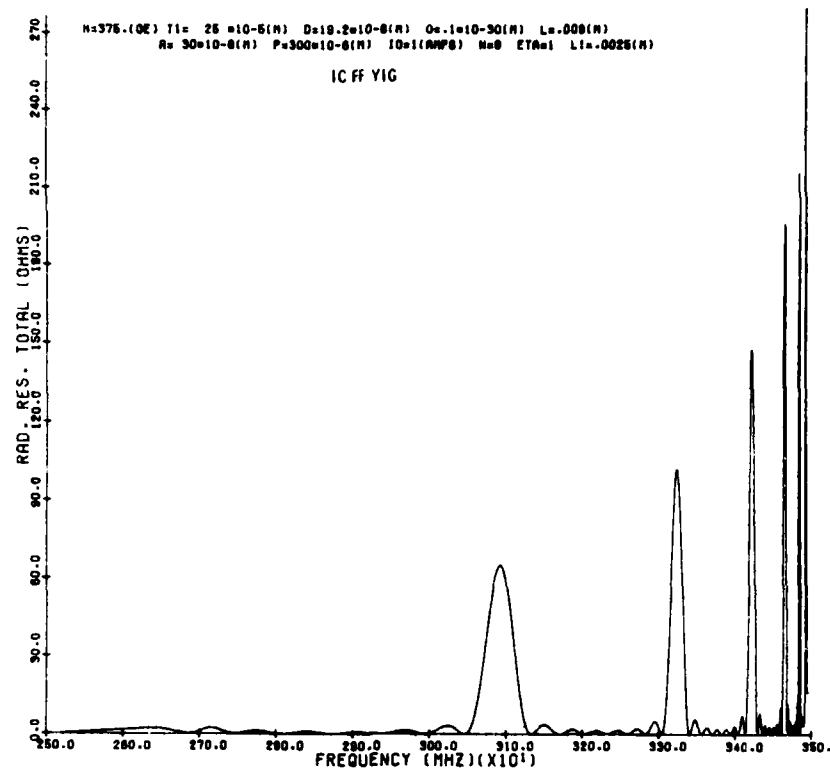
Fig. 4. Radiation Resistance using Eq. 19, and Radiation Reactance
using the Hilbert Transform method.

126

$$R_m^{(s)} = \frac{R_1^{(s)} \, \ell_1}{N^2} \left[\frac{\sin(k_s a/2)}{(k_s a/2)} \right]^2 \left\{ \frac{\sin (k_s pN/2)}{\sin (k_s p/2)} \right\}^2 \qquad (19)$$

This expression and the Hilbert transform of $R_m^{(+)} + R_m^{(-)}$ are plotted in Fig. 4, for MSSW values for $R_1^{(s)}$. The frequency at the peak radiation resistance near 3100 MHz corresponds to an MSW wavelength equal to the transducer periodicity, p = 300 µm; the second peak corresponds to the second spatial harmonic, and so forth. In this figure TI and L are ground plane spacings, D the YIG thickness, G the liftoff, and LI = ℓ_1, the strip length which is the same as the transducer aperture.

IND COND UNIFORM
H=375 oe, TI=25*10-5 m, L=.009 m, D=19.2*10-6 m, A=30*10-6 m, P=300*10-6m
N=8 ,ETA =1, LI=.0025 m, Delta H=0, Dist= .01 m

G=150 MICRONS
G=10 MICRONS
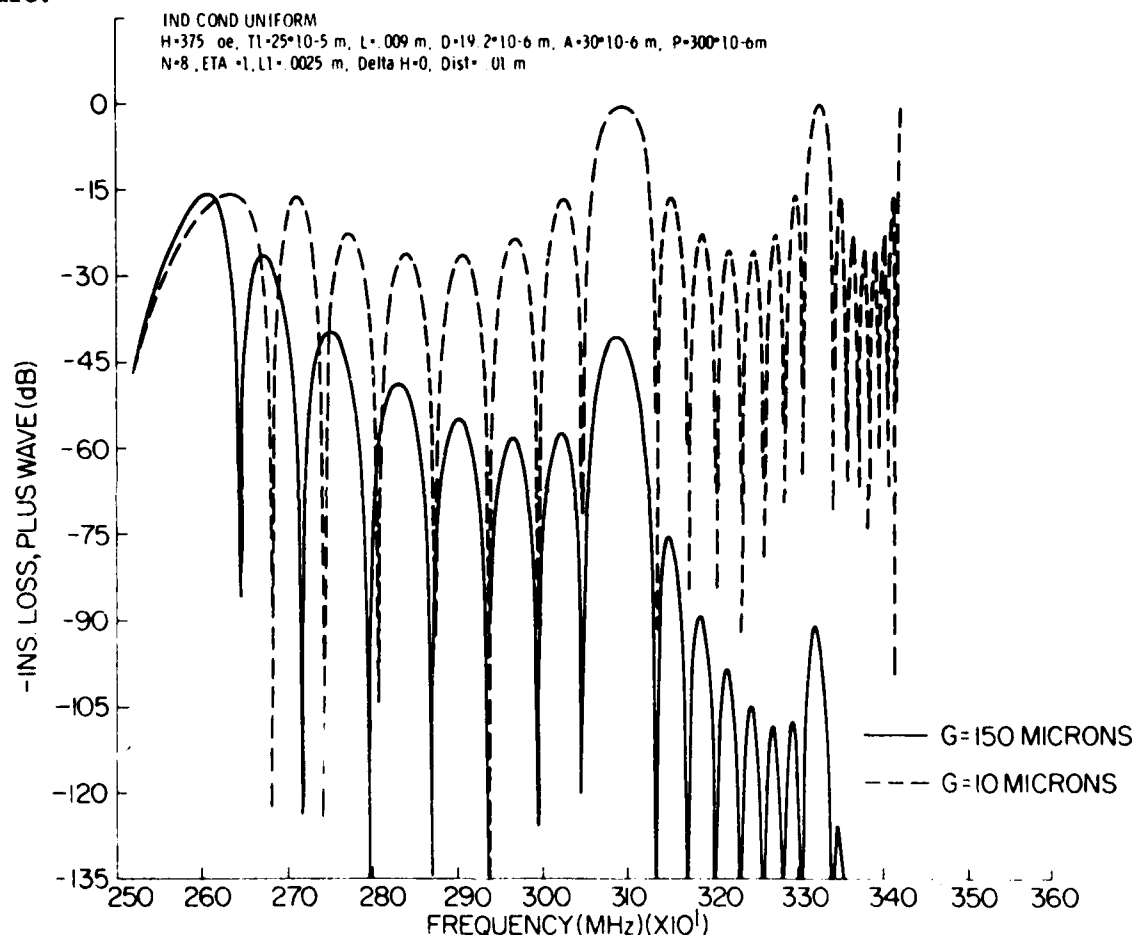
Fig. 5.   Insertion Loss for two Values of Liftoff Parameter G for an
Eight Element Grating Transducer Pair.

Insertion loss for the (+) wave, the one most strongly excited, is shown in Fig. 5 for two values of lift-off G. Results such as these are in reasonably good agreement with experiment. Parameters for Figs. 4 and 5 are identical. Minimum insertion loss for the G = 10 µm curve occur at the fundamental frequency of the transducer and a subsequent peak, or minimum insertion loss,

127

occurs at the next spatial harmonic. Both peaks occur within the MSW pass band which extends from 2500-3400 MHz. Within this band a wide range of wavelengths are present. This is in marked contrast to acoustic wave transducers where spatial harmonics are widely separated in frequency. Moreover, in the MSW case very long wavelengths are present at one end of the passband. As shown in the decoupled case, G = 150 µm, in Fig. 5, the long wavelength limit response dominates the passband. It is this long wavelength limit where surface acoustic wave concepts fail.

3.2 Comparison of Three Models

Figure 6 compares the insertion loss of three models for single strip transducer pair delay lines. Two of the curves use the theory presented here, with different current distributions. The third is derived from a microstrip
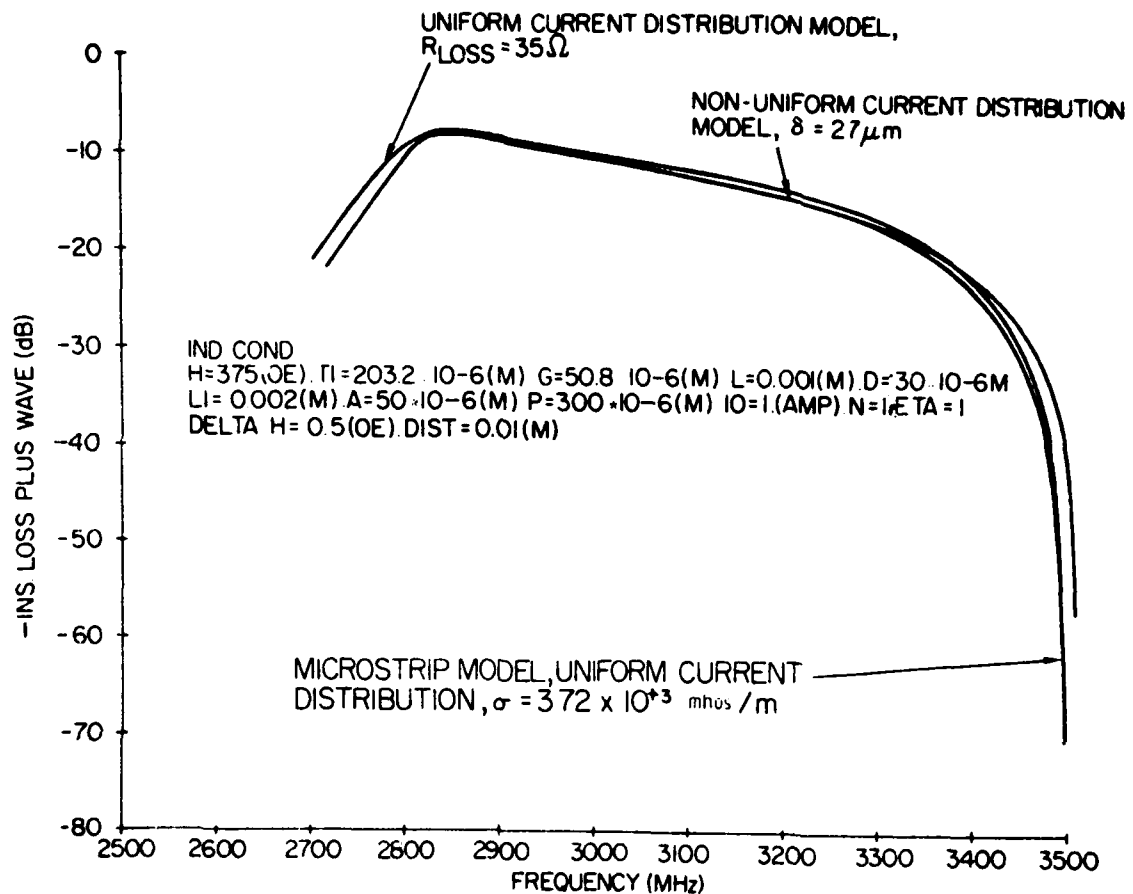
Fig. 6.   Comparison of Insertion Loss for Single Strip Transducers as Predicted by Microstrip and Two-Port Model.

model.[2] Agreement between the models is seen to be quite good. The different current distributions were obtained from

$$J(x) = \left(\frac{I_0}{a}\right) \frac{\cosh\ (x/\delta)}{\left[\dfrac{\sinh\ (a/2\delta)}{(a/2\delta)}\right]} \qquad \text{amps/meters} \qquad (20)$$

127a

with $-a/2 < x < a/2$, $x = 0$ is located at the conducting strip center, and $\tilde{\delta} = \delta/(1 + i)$ with δ the strip skin depth defined by $\delta = (\pi f \mu \sigma)^{-1/2}$. Equation (20) represents a normalized current distribution where magnitude is minimum at the strip center and maximum at the strip edges at $x = \pm a/2$. In addition,

$$\int_{-a/2}^{a/2} J(x)\, dx = I_o, \text{ for all } a \text{ and } \delta.$$

The two limiting cases of zero and infinite conductivity σ produce, respectively, a flat current distribution and a double impulse current distribution model. The flat current distribution is the one most commonly used.

The curves in Fig. 6 were obtained in the following way. For the curve labelled "uniform current distribution model $R_{LOSS} = 35\ \Omega$," $\delta \to \infty$ in Eq. (20).

$$J(x) = I_o/a. \text{ For } N = 1, \tilde{J}(k) = I_o \frac{\sin(ka/2)}{(ka/2)}$$

from Eq. (18) and $R_m{}^{(s)} = R_1{}^{(s)} \ell_1 \left[\frac{\sin(ka/2)}{(ka/2)} \right]^2$

from Eq. (19). R_{LOSS} was added to Eq. (17) by replacing $(R_g + R_m)$ with $(R_g + R_m + R_{LOSS})$. For the curve labelled "non-uniform current distribution model, $\delta = 27\ \mu m$" ($\sigma = 1.2 \times 10^5$ mhos/m at 3 GHz) Eq. (20) is substituted into Eq. (8). This is integrated directly and substituted into Eq's. 12 and 13, which in turn, is substituted into Eq. 17. For the microstrip model the theory given in reference 2 is used with conductivity $\sigma = 3.72 \times 10^{+3}$ mhos/m ($\delta = 0.15 \times 10^{-3}$ meters at 3 GHz). Differences between the three models as reflected in the curves of Fig. 6 are not considered significant. Similar results pertain to multi-element transducers provided individual elements are narrow compared to center-to-center spacing and the number of strips is not too large, < 8. Theoretical curves for this case are shown in Fig. 7.
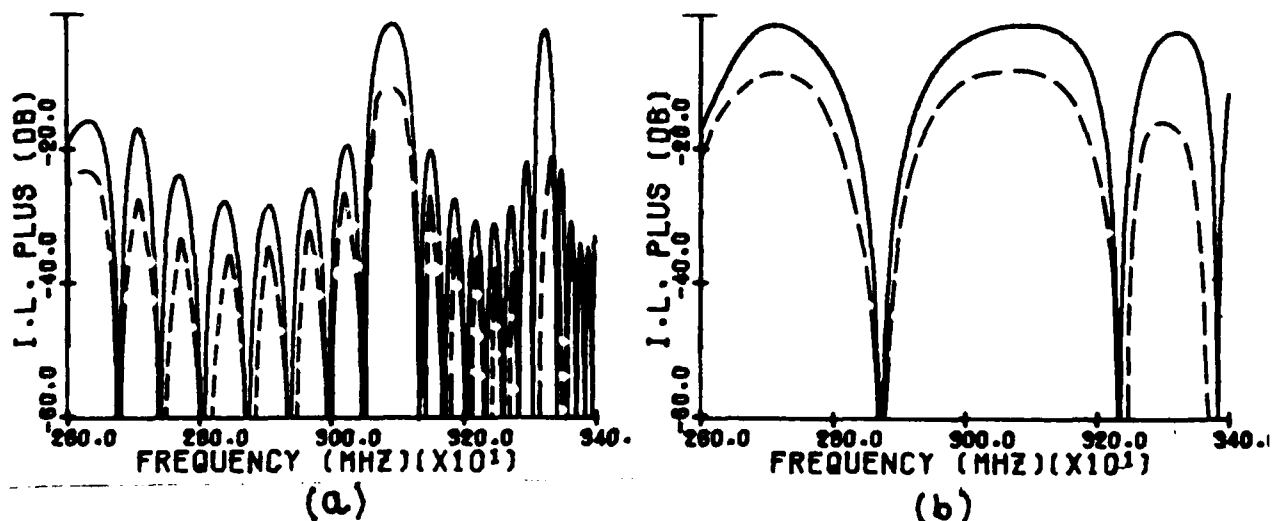

Fig. 7. Comparison of Insertion Loss for Multistrip Transducers as Predicted by Microstrip (Dashed Line) and Two-Port (Solid Line) Model. Loss is not Included in the Two Port Model Here. (a) Eight Element Grating. (b) Two Element Grating.

are obtained using the theory presented here, with no loss, and with a flat current distribution. Dashed curves are taken from reference 2, Wu et al. Figure 7a is for an eight element grating transducer and Fig. 7b for a two bar grating transducer. These results are also in reasonably good agreement with experiment (2) as is the agreement between models.

3.3 Range of Validity of Models

In this section we consider some aspects of the assumptions and restrictions made in   developing the transducer models.   In the magnetostatic limit, MSW wavelengths are much smaller than electromagnetic wavelengths in the propagation media; that is $\lambda_{MSW} \ll \lambda_{EM}^\varepsilon$, where ε is the relative dielectric constant. This is equivalent to

$$k_s \gg \sqrt{\varepsilon}(\omega/c) = k_{EM}^\varepsilon \qquad (21)$$

For $\omega = 2\pi \times 3 \times 10^9 \text{ sec}^{-1}$, $c = 3 \times 10^8$ m/sec, and $\varepsilon = 10$, we get $k_{EM}^\varepsilon \approx 2 \text{ cm}^{-1}$ or $\lambda_{EM}^\varepsilon \approx \pi$ cm. This means MSW wavelengths up to a few thousand microns satisfy inequality Eq. 21 very well. Practical MSW wavelengths are on the order of hundreds of microns and so Eq. 21 is well satisfied in practice. However, even though MSW wavelengths may be small in comparison with EM wavelengths, they may be too large in comparison with sample or transducer aperture. This would cause the theory to break down at wavelengths even shorter than that specified by (21).

The next two illustrations, Figs. 8 and 9 compare theory and experiment. They show how well the theory predicts some experimental features and, where it breaks down. Here again, the plots are of insertion loss versus frequency for a delay line configuration. The theory used for Fig. 8 is the non-uniform current distribution model with the same parameters as used in Fig. 6; and, since we have already seen the good agreement between various models for these parameters, the theoretical/experimental comparison is a fair one. The high frequency roll off between 3000 and 3400 MHz in Fig. 8 is accurately predicted by the theory. Most of the pass band ripple can be eliminated by tapering the YIG film along its edges, or by other techniques such as the use of non uniform biasing fields or absorbers. Consequently, in comparing theory and experiment here the ripple above 3000 MHz is neglected. The low frequency end of the pass band, which corresponds to the long wavelength region in the case of MSSW, is not in agreement with experiment. Moreover, the experimental bandwidth is wider than the theoretical one. This suggests other modes are being excited within the passband. Wavelengths in the region between about 2700 and 2800 MHz are approaching physical dimensions of the propagation media and overall dimensions of the transducer. It is therefore not surprising, in view of the assumptions made, that the theory breaks down in the long wavelength limit. The above interpretation is strengthened by the results depicted in Fig. 9 for a multi-element transducer. A pair of 15 element aluminum grating transducers on a 254 µm thick microstrip dielectric were used as input and output transducers. Center-to-center strip spacing was 356 µm, strip width and interstrip spacing were both 178 µm for the uniform transducer Fig. 9a, strip length one centimeter and the transducers were spaced one centimeter center-to-center. A rectangular YIG film was placed on top of the transducers. The fundamental frequency response of the transducers near 3 GHz is in fair agreement with the theoretical response, which did not include losses. The largest transducer response occurs near 2.5 GHz where the theory predicts no response. Again this is the long wavelength limit.

INSERTION LOSS(dB)   H=375 oe

```
  0 ┤
    │                    THEORY
 12 ┤
    │                              EXPERIMENT
 24 ┤
    │
 36 ┤    IND COND
    │    H=375(OE)  TI=203.2 *IO-6(M) G=50.8*IO-6(M) D=30*IO-6(M)
 48 ┤    LI=0.002(M) A=50*IO-6(M) P=300*IO-6(M) IO=I(AMP) N=I ETA=I
    │    DELTA H =0.5 (OE) DIST=0.0I (M)            DELTA =25*IO-6
    │                          3000 MHz
 60 ┤
  2500MHz              100 000 MHz/DIV                        3500
```
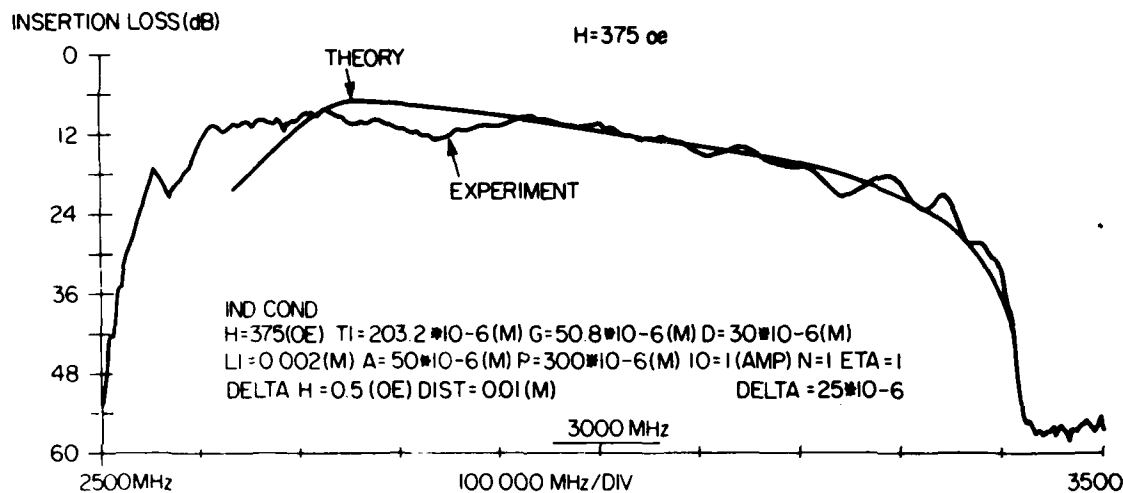
Fig 8. Theoretical/experimental comparison of insertion loss for
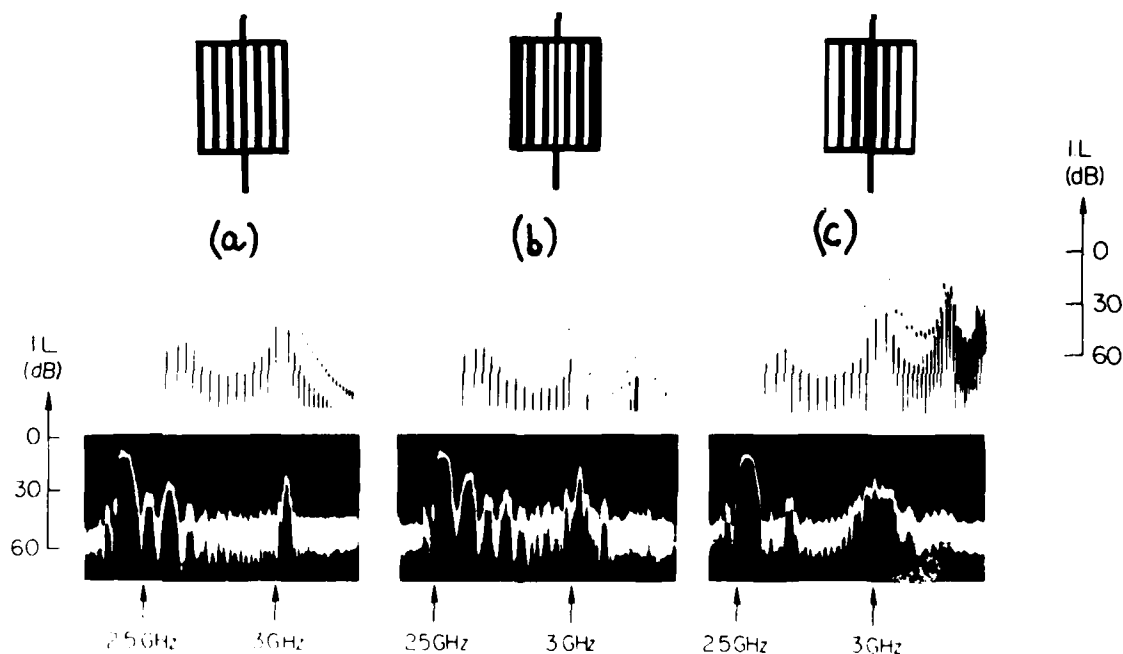   single element transducer pair delay line.

Fig. 9. Theoretical/experimental comparison of insertion loss for
        fifteen element transducer pair delay line.

130

Two important implications of these results are as follows. First, in the case of time delay units utilizing single strip wide band transducers, mode suppression techniques will be needed to control the long wavelength region of the passband. Second, there are two alternative approaches to filter design. In one approach the long wavelength response is suppressed and the fundamental response apodized. Apodization of the fundamental response, near synchronism, using surface acoustic wave design techniques to produce desired filter characteristics can be used. The other approach is to develop techniques for apodizing transducers in the long wavelength region. This is attractive because of the lower insertion loss at the longer wavelengths.

The 15 element transducers were apodized, width weighted, and checked against theory with the results shown in Figures 9b and 9c.

Equation (22), an expression for an apodized grating line transducer[7] based on surface acoustic wave concepts[12], was used for the theory.

$$R_m(s) = \frac{R_1(s)}{N^2} \left| \sum_{n=1}^{N} \ell_{1n}^{1/2} e^{-iknp_n} \frac{\sin(a_n k/2)}{(a_n k/2)} \right|^2, \qquad (22)$$

where ℓ_{1n} and a_n are the length and width of the nth element, respectively, and p_n the center-to-center spacing of adjacent elements. Equation (22) reduces to Eq. (19) when all elements are identical. One can see qualitative agreement near synchronism, ~ 3 GHz, between SAW apodization theory and experiment, and, again the complete breakdown of the theory at long wavelengths, near 2.5 GHz. One can also see apodization in the long wavelength region where the insertion loss is low. In addition, Fig. 9 shows a fairly decent filter response in the long wavelength region. The development of a practical theory valid in the long wavelength limit might be very useful.

4. SUMMARY AND CONCLUSION

An analysis has been presented for developing a first order transducer theory for the three principal MSW modes of propagation. From expressions for radiation resistance and reactance an equivalent circuit is defined from which the insertion loss, or transmission loss as measured by commercial network analyzers, is derived. A comparison is made between several models, and between theory and experiment for single multi-element, and apodized transducer. It is concluded that present MSW transducer theory, based on SAW concepts, provides a reasonably good first order theory, but, that it fails in the long wavelength limit, and further improvements are crucial before the theory is useful for high precision.

Other theoretical problems requiring investigation are the inclusion of mutual coupling between transducer elements - similar to mutual coupling in multi-element antenna theory, the inclusion of near fields, the development of a three port transducer scattering matrix, to account for non reciprocity, and the removal of the uniformity assumption in the z direction. Solution of these problems will lead to a useful second generation magnetostatic wave transducer model.

REFERENCES

1. A.K. Ganguly and D.C. Webb, "Microstrip excitation of magnetostatic surface waves: theory and experiment" IEEE Trans Microwave Theory and Techniques, vol MTT-23, pp 998-1006, Dec 1975.

2. H.J. Wu, C.V. Smith, J.H. Collins, and J.M. Owens, "Bandpass filtering with multibar magnetostatic surface wave microstrip transducers", Electronics Letters, vol 13, No. 20, pp 610-611, Sep 1977.

3. J.C. Sethares, T. Tsai, and I, Koltunov, "Periodic magnetostatic surface wave transducers," RADC Technical Report TR-78-78, (available from NTIS or DTIC, No. ADA 057214), April 1978.

4. P.R. Emtage, "Interaction of magnetostatic waves with a current", J Appl Phys, vol 49, pp 4475-4484, Aug 1978.

5. A.K. Ganguly, D.C. Webb, and C. Banks, "Complex radiation impedance of microstrip - excited magnetostatic surface waves," IEEE Trans MTT (1978) pp 444-447.

6. J.P. Parekh, "Theory of magnetostatic forward volume wave excitation," J Appl Phys $\underline{50}$ (3), pp 2452-2454, March 1979.

7. J.C. Sethares and I.J. Weinberg, "Apodization of variable coupling MSSW transducers," J Appl Physics $\underline{50}$ (3), pp 2458, 2460, March 1979.

8. J.C. Sethares, "Magnetostatic surface wave transducers," IEEE Trans on Microwave Theory and Techniques, vol MTT-27, No 11, pp 902-911, Nov 1979.

9. H.J. Wu, C.V. Smith, Jr., and J.M. Owens, "Bandpass filtering and input impedance characterization for driven multielement transducer pair-delay line magnetostatic wave devices," J. Appl. Physics $\underline{50}$ (3), pp. 2455-2457 ,

10. I.J. Weinberg, "Magnetostatic wave dispersion relations," Proc. of the 81 RADC Microwave Magnetics Technology Workshop, 1981.

11. I.J. Weinberg, "Hilbert transform by numerical integration, "RADC-TR-79-3, Jan 1979.

12. T.L. Szabo, "Advanced SAW electromagnetic transducer design," 1976 IEEE Ultrasonics Symp Proc, (IEEE Cat. 76 CH1120-5SU).

FIELD GRADIENT CONTROL OF MAGNETOSTATIC WAVES
FOR MICROWAVE SIGNAL PROCESSING APPLICATIONS

F. R. Morgenthaler

Department of Electrical Engineering
and Computer Science
Massachusetts Institute of Technolgy
Cambridge, MA 02139

Abstract

Although magnetostatic wave devices normally employ spatially uniform
magnetic bias, control of important features of the modes is afforded through
judicious use of dc field gradients. Such control can be the basis for new
forms of microwave signal processors.

We discuss the manner in which gradients in either the field magnitude,
direction or both can be employed to synthesize wave dispersion characteristics
or mode spectra. This is done to control prespecified characteristics such as
frequency rf energy distribution, impedance, velocity of energy propagation and
the threshold governing the onset of nonlinear effects due to parametrically-
unstable spin waves. The way in which the normal boundary conditions, controlled
by the sample geometry, interact with those imposed by the field gradient is
also described.

For certain of the modes, the gradient induced volume divergence of the rf
magnetization becomes very large at special radii. These previously discussed
"virtual-surface" modes, are represented pictorially in terms of the rf magnetic
field, magnetization, and induction vectors.

Before we utilize magnetostatic surface wave propagation in nonuniform bias
fields, we must fully understand the uniform bias case. To this end, we have
previously developed a coupled integral equation approach to the general boundary
value problem governing three-dimensional magnetostatic modes or waves in a thin
film with rectangular geometry that applies when the dc magnetization M is entire-
ly in the plane of the film, and the bias field and/or material parameters of the
ferrite vary along $\overline{M}$.

The boundary conditions required at the film surfaces are built directly into
these equations which have now been solved numerically for a single uniform ferrite
strip. We here present pictorial representations of the mode patterns

FIELD GRADIENT CONTROL OF MAGNETOSTATIC WAVES
FOR MICROWAVE SIGNAL PROCESSING APPLICATIONS

F. R. Morgenthaler

Department of Electrical Engineering and Computer Science
and the Research Laboratory of Electronics
Massachusetts Institute of Technology
Cambridge, Massachusetts 02139

Introduction

Our interest in controlling magnetostatic waves and modes by means of dc field gradients dates from the experimental observation of localized high-Q resonance in single crystal yttrium iron garnet (YIG) reported by Zeskind and Morgenthaler.[1]

Our interpretation of these resonances is that localized magnetic mode patterns are formed in which the resonant energies are guided or confined by regions of high dc field gradient within the crystal. By appropriately designing internal magnetic field profiles, one can create apparent "surfaces" or "tracks" of magnetic field discontinuity. Magnetic waves bound or guided by such gradients can be made to follow appropriate propagation paths with controlled group velocity. If the mode amplitudes are very small at the edges and corners of the sample, the surface scattering (which one would expect to be enormous) is largely prevented. Consequently, the Q of the resonance governed primarily by the intrinsic linewidth of the bulk crystal together with normal circuit loading considerations.

In the first experiments such gradients arose naturally from the nonuniform shape demagnetizing fields; in subsequent work by Cooley[2] and Horowitz[3], we have created pre-specified gradients with shaped pole pieces designed by field synthesis techniques. A similar approach has recently been followed by Tsutsumi at al.[4]

We have recently reviewed[5] those early experiments as well as our theoretical treatment[6] of quasi-two-dimensional magnetostatic modes of single domain thin

ferrite circular disks or annular rings, when the dc magnetic field is normal to the plane and varies radially. The methods of analysis employed can also be used to synthesize modes with pre-specified characteristics, such as velocity, of energy circulation and rf energy distribution.[7,8]

The analysis and synthesis of magnetostatic plane waves (MSW) bound to a dc field gradient[8,9] is closely related to the modes in disks or annular rings with radial bias gradients and we make such a connection.

We also consider the guiding and control of magnetostatic surface waves (MSSW) on films with a bias fields that may vary in magnitude and/or direction with respect to those coordinates transverse to the propagation direction.[10] Finally, we provide numerical solutions for the important case of a rectangular ferrite strip with uniform in-plane bias.

Magnetostatic Resonances in a Nonuniformly Biased Thin Disk

Formulation of the Basic Two-dimensional Equations

We consider a ferrimagnetic film disk magnetized to saturation in the z-direction by a dc field H; radial components are assumed negligible throughout the disk. Since we are interested in magnetic modes of frequency ω that have negligible electric field energy, the magnetostatic approximation is suitable and the rf magnetic field may be expressed as $h = -\nabla\psi$. Because the ferrite is assumed to be saturated by a cylindrically, symmetric field $H_z(r)$ and modes without z-variation are sought, we take the complex magnetostatic potential (with suppressed exp $[j\omega t]$ variation) to be of the form

$$\psi = \exp(|m|\int \frac{q(r)dr}{r} - jm\phi) \tag{1}$$

where m is a positive or negative integer and $q(r)$ determines the radial variation of the mode. The latter also describes the polarization of the rf $\bar{h}$-field

$$h_r/h_\phi = j \frac{|m|}{m} q(r) \tag{2}$$

The other field quantities follow from the Polder susceptibility tensor and the Maxwell Equation governing the curl of the electric $\bar{e}$-field.

They are

$$m_r = -\frac{|m|}{r}\left(xq - \kappa\frac{m}{|m|}\right)\psi \tag{3a}$$

$$m_\phi = j\frac{m}{r}\left(x-\kappa\frac{m}{|m|}q\right)\psi \tag{3b}$$

and

$$e_z = \omega\mu_0|m|q^0(r)\psi r \tag{4a}$$

where

$$q^0 = (1+x)\,q - \kappa\frac{m}{|m|} \tag{4b}$$

Here $x = Z/(Z^2-\Omega^2)$, $\kappa = -\Omega/(Z^2-\Omega^2)$ with $Z(r) = H_z(r)/M$ and $\Omega = \omega/\omega_M$. The latter are, respectively, field and frequency normalized to the saturation magentization M; $\omega_M = -\gamma\mu_0 M$ where γ (negative) is the gyromagnetic ratio. It is also convenient to take $\Omega>0$ and define $\sigma = \Omega m/|m|$.

The polarization factors of the rf magnetization and rf flux have been found to be very helpful in clarifying mode characteristics. We therefore define

$$m_r/m_\phi = j\frac{m}{|m|}\,p(r) \quad\text{and}\quad b_r/b_\phi = j\frac{m}{|m|}\,p^0(r) \tag{5a\,),(5b)}$$

where from Eqs. (3a,3b) and (4)

$$p = \frac{Zq+\sigma}{Z+\sigma q} = \frac{Zq^0+\sigma}{Z+1+\sigma q^0} \quad\text{and}\quad p^0 = \frac{(Z+1)p-\sigma}{Z+1-\sigma p} \tag{6a),(6b}$$

The magnetostatic equations $(\nabla\times\bar{h}=0,\ \nabla\cdot\bar{h}=-\nabla\cdot\bar{m})$ require that

$$\frac{dq^0}{dr} = \frac{|m|}{r}(1+x(r))(1-q^2) \tag{7}$$

The wave impedances are defined by

$$\eta_r = \frac{e_z}{h_\phi} = j\ \frac{m}{|m|}\ \omega\mu_o rq^0(r) \tag{8a}$$

$$\eta_\phi = \frac{e_z}{h_r} = \frac{m}{|m|}\ \omega\mu_o\ r\ \frac{q^0(r)}{q(r)} \tag{8b}$$

The former quantity must be a continuous function of r .

As a concrete example, consider a thin ferrite disk of thickness d and radius R placed between perfectly conducting circular plates that extend to the radius R_o . As shown in Fig. 1, the cylindrical surface $r=R_o$ is assumed either conducting for $|z| < d/2$, (a) or for $|z| > d/2$, (b) .

For (a), $\eta_r=0$ at the radius $r=R_o$ and from Eq. (7a), $q^0(R_o)=0$.

For (b) a reasonable approximation[8] valid when $d/R_o \ll 1$ is

$$[q^0(m,R_o)]^{-1} \simeq -\frac{|m|d}{\pi R_o}\ \ell n \left(\frac{\frac{2\pi R_o}{d} + 1 + 2\sqrt{\left(\frac{\pi R_o}{d}\right)^2 + \frac{\pi R_o}{d} + m^2}}{2|m|+1}\right) \tag{9}$$

Sketches of possible rf magnetic field contours are given in Fig. 2.

For weak gradients, $BR^{2n} \ll 1$ and non-"virtual-surface" modes exist for $m > 0$ when

$$\Omega_m \simeq A + \frac{m}{n+m}\ BR^{2n} + \frac{1}{2}\left[1 + \frac{1+q^0(R_o)}{1-q^0(R_o)}\ \left(\frac{R}{R_o}\right)^{2m}\right] \tag{10}$$

In the absence of a radial gradient, all of the modes of a solid disk have circularly-polarized rf h-fields with zero volume-divergence. These modes are strongly influenced by the magnetic pole distribution on the edge of the disk and the rf energy becomes progressively concentrated near the rim as the mode index increases.

When the field gradient is modest, the modes retain these general charac-
teristics but develop non-zero values of $\nabla \cdot \bar{h}$ throughout the volume which
change both the state of polarization either in the central portion or near
the edge of the disk. In addition, both the mode frequency and the velocity
with which the mode energy circulates are found to be altered.

For increased gradient strength, the volume divergence of certain modes
can change so dramatically that selective localization or expulsion of the
energy occurs. The sense of polarization can also actually reverse. In cer-
tain cases[6], the volume divergence of the rf magnetization can become infinite
(in the lossless exchangeless approximation) at a certain interior radius, r_x .
The magnetic pole distribution at this "virtual-surface" thus resemble that of
a true surface and can serve to guide and localize the mode.

The properties of an m=1 virtual-surface" mode are illustrated with the
profile $Z = .3+1.095(r/R)^4$ for which, if y(m=1,R) = -1, such a mode occurs
when $\Omega = .655$. The associated $\bar{m}$-field, $\bar{h}$-field and $\bar{b}$-field loci are plotted,
respectively, in Figure(3a,b,c) with the "virtual-surface" radius ($r_x = .385R$)
shown by the dotted circle. Notice the reversed direction of $\bar{m}$ leading to
"surface" magnetic poles near $r-r_x$. Notice too, that p(r/R = .59) = 0 .
Along with changes in Ω , larger values of BR^4 will cause r_x to shrink;
smaller values to expand. It should be noted that quantum-mechanical exchange
effects (Refs. 8, 11) are ignored in these plots.

Synthesized Magnetostatic Resonances in a Nonuniformly Biased Thin Disk Without Conducting Boundaries

If the conducting plates bounding the ferrite are either separated or removed
entirely, the rf field inside the disk will fringe. Then field variations with
respect to z may be important even for the quasi-two-dimensional modes, as the
outer and inner fields interact along the entire disk surface.

When the bias field gradients are weak to moderate, the disk is thin and the modes in question do not have "virtual-surfaces", alternative analysis[7,8] is possible.

For mathematical convenience, we choose to model the thin disk as a very oblate spheriod with semi-axes a and b. The thickness of the "disk" at its center is 2b and the radius is a where b<<a.
The normalized dc bias is generalized to

$$H_z/M = Z(r) = A + \sum_{n=1}^{N} B_n r^{2n} \tag{11}$$

The complex magnetostatic potential __within__ the ferrite is approximately given by $\psi = R(r)e^{-jm\phi}$ where r and ϕ are cylindrical coordinates and m is a positive mode integer.

The normal frequency spectrum is found to be

$$\Omega_m = A + N(m) + \frac{1}{1+\frac{3/2}{m}} \left(B_1 a^2 + \frac{1}{1+\frac{3/2}{m+1}} \left(B_2 a^4 + \frac{1}{1+\frac{3/2}{m+2}} \left(B_3 a^6 + \ldots\right)\right)\ldots\right) \tag{12}$$

where

$$N(m) = \frac{b}{a} \frac{\left(\frac{a}{c}\right)^{m+1} F_m^{(m)} \left(\frac{a}{c}\right)}{(m-1)!2^m} \tag{13}$$

and

$$F_m^{(m)}(\xi) = (2m-1)!!\,\xi^m \sin^{-1}\left(\frac{1}{\xi}\right) - \frac{\sqrt{\xi^2-1}}{m}\left[(2m-2)!! + (2m-1)(2m-4)!!\,\xi^2\right.$$

$$\left. + (2m-1)(2m-3)(2m-6)!!\,\xi^4 +\ldots+ (2m-1)!!\,\xi^{2m-2}\right] \tag{14}$$

when $n!! = n(n-2)(n-4)\ldots$

When all $B_k = 0$, this spectrum reduces to the corresponding set of Walker modes.[11]

Electromagnetic corrections to Eq. (12) are given in Reference 7.

Synthesized Dispersion Relations

If it is desired to create a spectrum with the resonance frequencies separated by pre-specified amounts or if one wishes to control the velocity of energy circulation v_ϕ^E of individual modes, the independent constants B_n can be adjusted and the required field $H_z(r)$ synthesized. In the former case Eq. (12) is used alone whereas in the latter, the relation $v_\phi^E(m) = r\partial\omega(m)/\partial m$ (analogous to the group velocity for a plane wave) is also employed.

If is useful to realize that v_ϕ^E can be forced to be independent of m over some range of m. This also suggest that magnetostatic plane wave propagation can be made precisely nondispersive over a predetermined bandwidth.

We review a single example in which N(9m) is negligible.

We require that B_1, B_2 and B_3 force $\partial\Omega/\partial m = .01$ for m=1,2,3

The required values are

$$B_1 a^2 = .1699 \quad B_2 a^4 = -.6543 \quad \text{and} \quad B_3 a^6 = .6453$$

In Figures (4a,b) the values of $\Omega(m)$ and $\partial\Omega/\partial m$ are plotted vs. m for the two cases; in Figures (4c) the required field profiles of Z-A is plotted vs. r/a. Other examples are contained in References 5 and 7. The synthesis of the required dc field patterns has been treated in Reference 13.

Synthesis of Magnetostatic Plane Waves in Rectangular Geometries

The analysis and synthesis of magnetostatic plane waves bound to a dc field gradient[9] is closely connected to the discussion of the preceding section because modes in disks or annular rings dependent upon $\exp(-jm\phi) = \exp[-j(\frac{m}{r})(r\phi)]$ represent wave propagation around a curved path of distance $S = r\phi$ with propagation constant $\beta(r) = \frac{m}{r}$. If the mode energy is strongly concentrated near some special radius (such as the disk radius), the value of "β" is essentially constant

and if the effective radius of curvature is large the wave propagation can be analyzed in terms of local cartesian coordinates $d\hat{x}=dr$, $d\hat{y}=rd\phi$ and $d\hat{z} = dz$.

It therefore follows that $H_z(x)$ can control the wave dispersion $\omega(\beta)$ in a manner analogous to that by which $H_z(r)$ controls $\omega(m)$ through Eq. (12).

The prospect of guiding magnetostatic waves is of considerable interest because of possible deivice applications.[14] Such guided waves might be used to increase the delay time realizable on a given size samplw by meandering the path, or to make a resonator by guiding the waves along a closed loop. In addition, controlling the coupling between adjacent waveguides is important for signal routing devices such as directional couplers.

For these reasons, the analysis and synthesis of magnetostatic surface and volume waves (MSSW and MSVW) when the dc bias is either uniform or nonuniform takes on special significance. For example, guiding an MSSW around a bend is complicated due to mode conversion to backward volume waves.

It should be possible to overcome this difficulty by employing gradients that arise from a change in the direction of the bias field.

The in-plane fields permit magnetostatic surface wave propagation whereas the normal fields do not. Such an approach has been described by Stancil and Morgenthaler,[15] and is based upon considerations found in the work of Damon and Eshbach,[16] Morgenthaler[17,18] and Jao[19].

Magnetostatic Surface Modes in Nonuniform Thin Films With In-plane Bias Fields

In most of the analyses of nonuniform magnetostatic modes in thin ferrite films, the bias field was assumed to be directed normal to the plane of the film and the modes considered were quasi-two-dimensional in that thickness variations of the rf magnetization were ignored. Subsequently, we have developed a general theory,[19] based upon coupled integral equations, that can deal with surface like modes in thin film disks rectangular and strips when the bias and any material nonuniformities (such as variations of the saturation magnetization) are purely transverse. Variations of the bias field and material parameters over the film

141

thickness are not included in the model but because surface wave character is expected, such variations of the rf fields are permitted.

Recently, the basic analysis was extended [21] to include the effects of perfectly conducting ground planes spaced distances D_+ above and D_- below the ferrite film of width w and thickness d; The geometry is shown in Fig. 5.

If MSSW modes are to be used in exacting signal processing applications, it is essential that the entire mode spectrum associated with a single rectangular ferrite strip of finite width and thickness be well understood for the case of uniform in-plane dc bias; this is a prerequisite for dealing with cases of nonuniform bias.

O'Keefe and Patterson[22] have made substantial progress in detailing the manner in which volume wave character is added to the surface modes by the finite width of the strip. However, their theoretical treatment assumes that the rf-magnetization is always pinned at the film edges. Unless such boundary conditions on $\bar{m}$ are consistent with continuity of both tangential $\bar{h}$ and normal $\bar{b}$, it is essential that exchange effects be included. Therefore if spin pinning does occur because of exchange branch wave solutions of high wave number will be required.

Our formulation attacks the problem by also neglecting exchange effects but insisting that the Maxwellian boundary conditions be satisfied.exactly.

Using the methods detailed in Reference 19 we expand the magnetostatic potential in the region $|z| < d/2$ as

$$\psi = e^{-j\beta y} \int [C_1(\alpha)e^{\alpha z} + C_2(\alpha) e^{-\alpha z}] X_\beta(\alpha, x) d\alpha \qquad (15)$$

where for suppressed exp (jωt) variation,

$$\frac{d^2 X_\beta}{dx^2} + (1+\chi) (\alpha^2 - \beta^2) X_\beta = 0 \qquad (16)$$

When χ (the diagonal Polder susceptibility) is piecewise constant, it follows that for X_β is either an even or odd function of x.

The pair of coupled integral equations that determine $C_1(\alpha)$ and $C_2(\alpha)$ are

$$\int_{x=0}^{L}\int_{\alpha=|\beta|}^{\infty} \begin{matrix} \cos \\ \sin \end{matrix} (\hat{\alpha}x) \, X_\beta \, (\alpha,x) \, \left\{ \left[\pm\sqrt{\hat{\alpha}^2+\beta^2} \, \tanh(\sqrt{\hat{\alpha}^2+\beta^2} \, D_+) \right. \right.$$

$$\left. + (1+\chi)\alpha + \kappa\beta \right] e^{\pm\frac{\alpha d}{2}} C_1(\alpha) + \left[\pm\sqrt{\hat{\alpha}^2+\beta^2} \, \tanh (\sqrt{\hat{\alpha}^2+\beta^2} \, D_\pm) - (1+\chi)\alpha \right.$$

$$\left. \left. + \kappa\beta \right] e^{\pm\frac{\alpha d}{2}} C_2(\alpha) \right\} d\alpha \, dx = 0 \qquad (17)$$

where $\cos\hat{\alpha}x$ is used for even and $\sin\alpha x$ for odd modes. Although the upper limit of the integration is actually $L=\infty$, the contributions due to the fringing field are generally negligible for values of $2L/W$ on the order of 2 or less. Because we approximate the integration over α by a finite sum, that approximation is more accurate in the range of small x when L is moderate.

For the general case, no simple analytical approximations are possible and recourse to numerical methods is required.

The case: $D_+ = D_- = \infty$, and $H/M = 1$ has been studied in some detail.

The dispersion curves for even and odd modes are plotted in Fig. 6 for $d/w=.1$. The associated magnetostatic potentials for several even and odd modes are plotted in Figs. 7 and 8.

We are presently implementing a computer program capable of solving these integral equations for a wide variety of cases that may be given to the case of parallel or concentric tracks, separated by air gaps and coupled via the fringing fields of the magnetostatic waves. Such geometries are potentially useful for filters, directional couplers, circulators or diplexes.

Acknowledgement

The author would like to thank present and past members of the Microwave and Quantum Magnetics Group for many helpful discussions.

144

References

1. D. A. Zeskind and F. R. Morgenthaler, "Localized High-Q Ferromagnetic Resonance in Nonuniform Magnetic Fields," IEEE Trans. on Mag. Vol. MAG-13, No. 5, September (1977).

2. J. J. Cooley, "Magnetostatic Modes Bound by DC H-Field Gradients," S.M. Thesis, Dept. of Electrical Engineering and Computer Science, M.I.T., September (1977).

3. P. N. Horowitz, "Variable Speed Magnetostatic Modes in Uniform or Nonuniform DC H-Fields," S.M. Thesis, Dept. of Electrical Engineering and Computer Science, M.I.T, February (1979).

4. M. Tsutsumi, et al, "The Effect of an Inhomogeneous Bias Field on the Delay Characteristics of Magnetostatic Forward Volume Waves," Applied Physics Letters, Vol. 35, July (1979), p. 204.

5. F. R. Morgenthaler, "Novel Devices Based Upon Field Gradient Control of Magnetostatic Modes and Waves", 3rd International Conference on Ferrites, Kyoto, Japan, Sept. 29-Oct 2 (1980).

6. F. R. Morgenthaler, "Bound Magnetostatic Waves Controlled by Field Gradients in YIG Single Crystals and Epitaxial Films," IEEE Trans. on Mag., Vol. MAG-14, September (1979), pp. 806-810.

7. F. R. Morgenthaler, "Synthesized Magnetostatic Resonances in a Nonuniformly Biased Thin Disk Without Conducting Boundaries," IEEE Trans. on Mag. Conference Proceedings, MAG-16, No. 5, p.1150, September (1980).

8. F. R. Morgenthaler, "Synthesis of Magnetostatic Waves and Modes Using Nonuniform Bias Fields" 1980 Ultrasonics Symposium, October 1980.

9. F. R. Morgenthaler, "Magnetostatic Waves Bound to a Field Gradient," IEEE Trans on Magnetics, Vol. MAG-13, NO. 5, September (1977), p. 1252-1254.

10. D. D. Stancil and F. R. Morgenthaler, "Magnetostatic Surface Modes in a Thin Film with Nonuniform In-plane Fields," IEEE Trans. in Mag. Conference Proceedings, September (1980).

11. D. D. Stancil, "Magnetostatic Waves in Nonuniform Bias Fields Including Exchange Effects," IEEE Trans.on Magnetics, Vol. MAG-16, No. 5, September (1980). p. 1153-1155.

12. L. R. Walker, "Resonant Modes of Ferromagnetic Spheroids," J. Applied Physics, Vol. 29, p. 318, (1958).

13. F. R. Morgenthaler and A. Platzker, "Magnetic Field Synthesis Procedures for Magnetostatic and Magnetoeleastic Devices," Proc. of the 1978 International Symposium on Circuits and Systems, N.Y.C., May 17-19, (1978).

14. J. D. Adam and H. H. Collins, "Microwave Magnetostatic Delay Devices Based on Epitaxial Yttrium Iron Garnet," Proc. IEEE, Vol. 64, No. 5, May (1976).

15. D. D. Stancil and F. R. Morgenthaler, "Guiding Magnetostatic Surface Waves with Nonuniform In-plane Fields," presented at the RADC/EEA Microwave Magnetics Technology Workshop, Hanscom Field, MA June 10-11 (1981).

16. R. W. Damon and J. Eshbach, "Magnetostatic Modes of a Ferromagnetic Slab," J. Phys. Chem. Solids, Vol. 19, p. 308 (1961).

17. F. R. Morgenthaler, "Nonreciprocal Magnetostatic Surface Waves with Independently Controllable Propagation and Decay Constants," J. Appl. Phys. 41, No. 3, p. 1014, March (1970).

18. F. R. Morgenthaler, "Magnetic Control of Exchange Torques and the Penetration Depth of Magnetostatic Surface Spin Waves," J. de Physique, C1-1159 (1970).

19. J. K. Jao, "Propagation of Magnetostatic Surface Spin Waves in YIG Slabs," MIT Department of Electrical Engineering and Computer Science, S.M. Thesis, February 1975. Available as Microwave and Quantum Magnetics Group Technical Report #35.

20. F. R. Morgenthaler, "Magnetostatic Surface Modes in Nonuniform Thin Films with In-Plane Bias Fields," 26th Annual Conference on Magnetism and Magnetic Materials, Dallas, Texas, Nov. 11-14 (1980).

21. F. R. Morgenthaler, Unpublished study performed for the U.S. Army under Battelle STAS Study No. 1671

22. T. W. O'Keefe and R. W. Patterson, "Magnetostatic Surface-Wave Propagation in Finite Samples," J. Appl. Phys. 49 (9), p. 4886-4895, September (1978).

146

Figure Captions

Figure 1   Physical boundary conditions for the two-dimensional magnetostatic modes under consideration. A normally magnetized thin ferrite disk of radius R and thickness d is placed between perfectly conducting plates having either a short circuit condition (a) or an open circuit condition (b) at the outer plate radius, R_o.

Figure 2   Sketches of the rf magnetic field contours, in the plane of a thin ferrite disk, that are associated with m=+1 modes for five different combinations of boundary conditions and normalized parabolic field profile. In (a), the dc field gradient is zero, q-+1, and the Kittel uniform precession results; in (b) q(R)<1, and the mode energy is reduced near the disk rim; in (c) the reduction is great enough to cause q(R)<0. In (d) q(R)>1 with increased mode energy near the rim. In (e) q is singular and a "virtual-surface" exists at $r=r_x$ (shown dotted).

Figure 3   Locus of field lines for the "virtual-surface" mode $\Omega(m=1) = .655$ when $Z = .3+1.095 \, (r/R)^4$. The rf $\overline{m}$-field is shown in (a) the $\overline{h}$-field in (b) and the b-field in (c). All patterns rotate at the normalized frequency Ω. The "virtual-surface" (shown dotted) occurs at $r_x/R = .385$.

Figure 4   The normalized mode frequency (a) and pre-specified energy frequency (b) both plotted vs. mode number together with the required field profile (c) plotted vs. radius.

Figure 5   Cross-sectional view of thin ferrite strip between perfectly conducting ground planes. The direction of the uniform in-plane bias field is shown.

Figure 6   MSSW Dispersion in a Rectangular Strip when $H_z/M = 1$ and $D_+ = D_- = \infty$ for $d/w = .1$.

Figure 7   MSSW potentials for even modes.

Figure 8   MSSW potentials for odd modes.

Figure 1

148

Figure 2

149
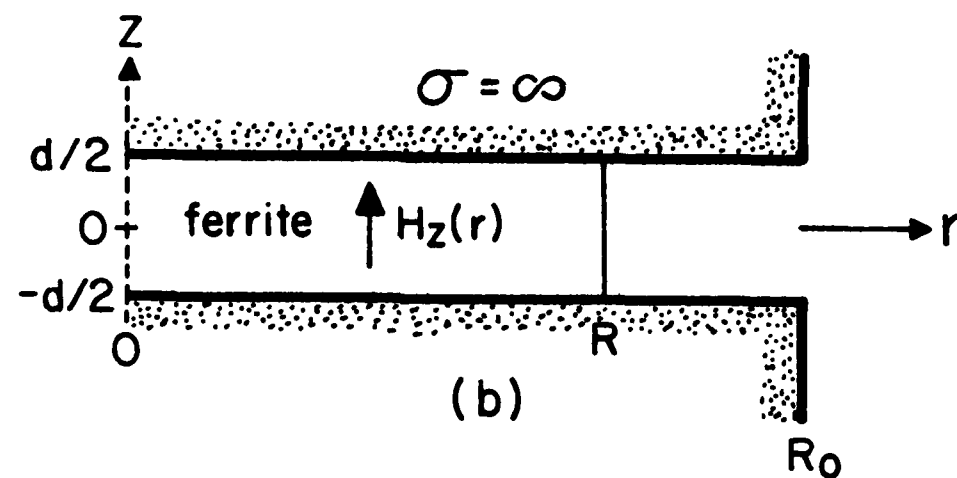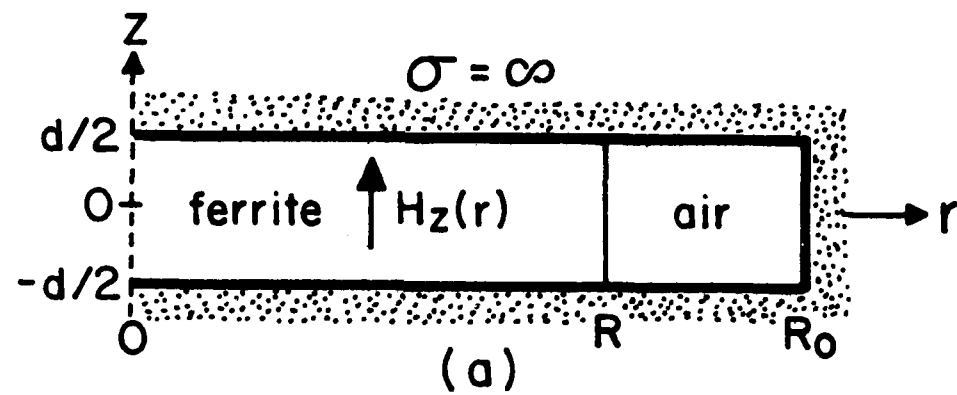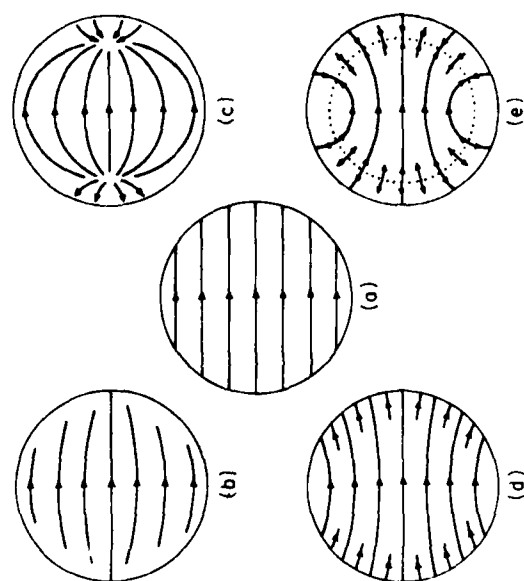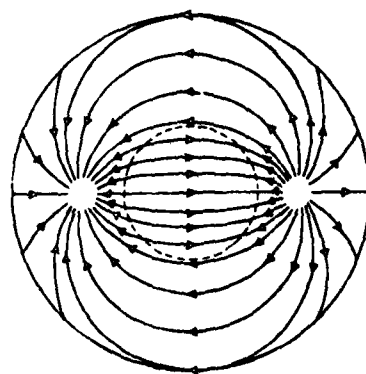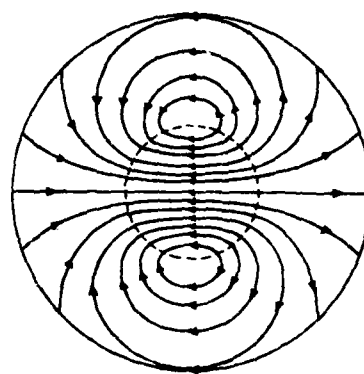
(a) $\overline{m}$-field locus

(b) $\overline{h}$-field locus
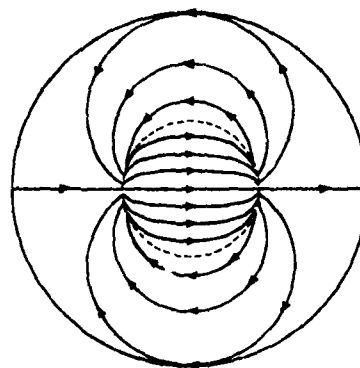
(c) $\overline{b}$-field locus

Figure 3
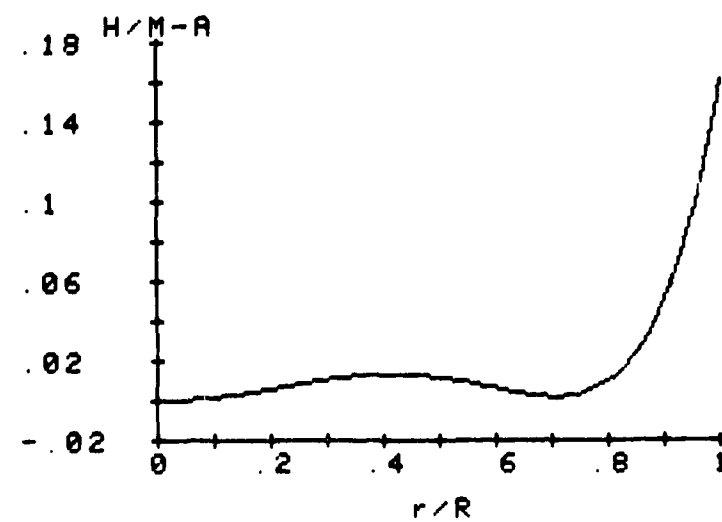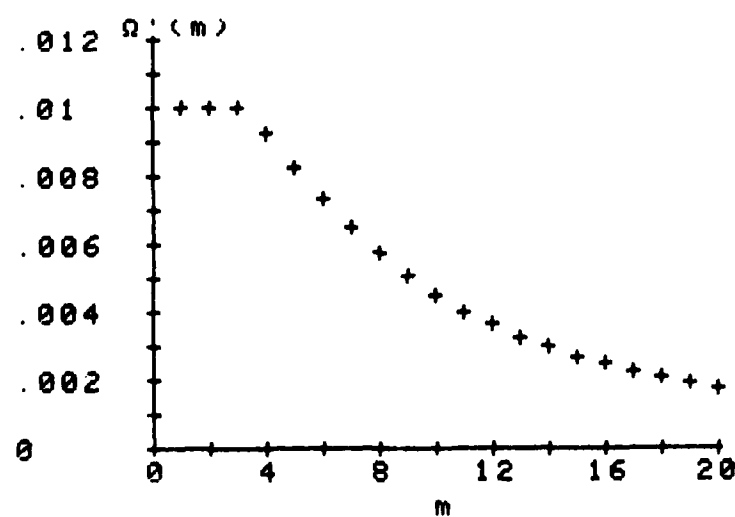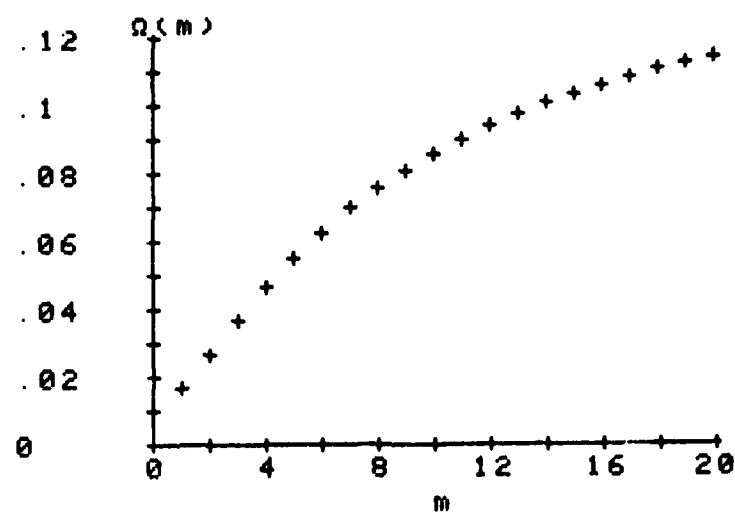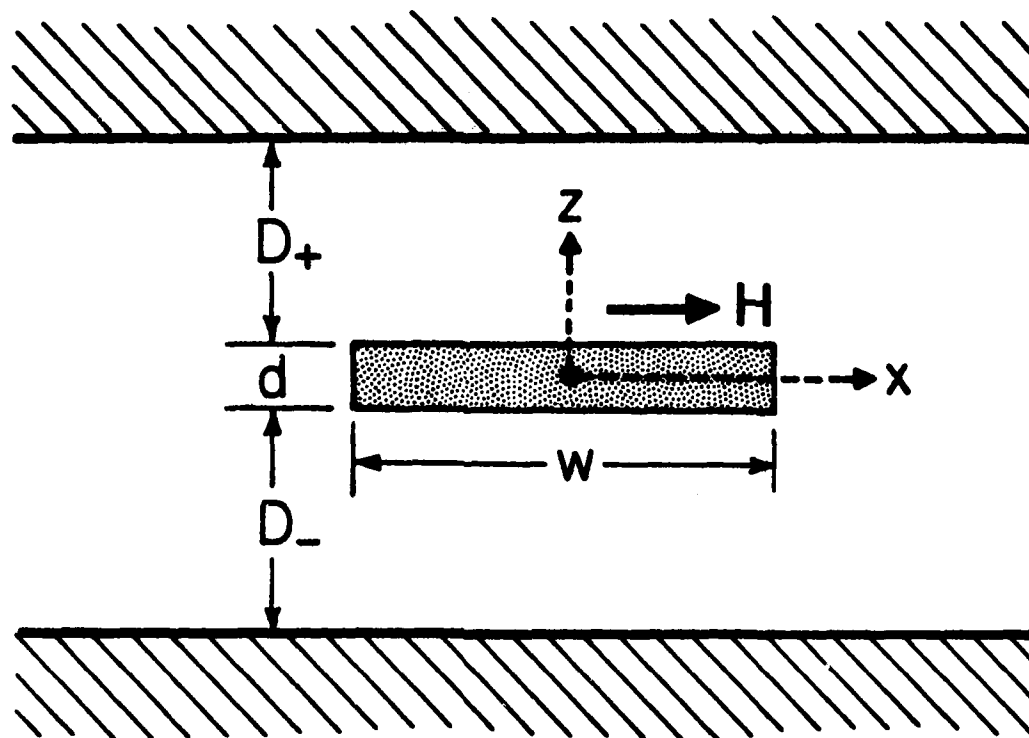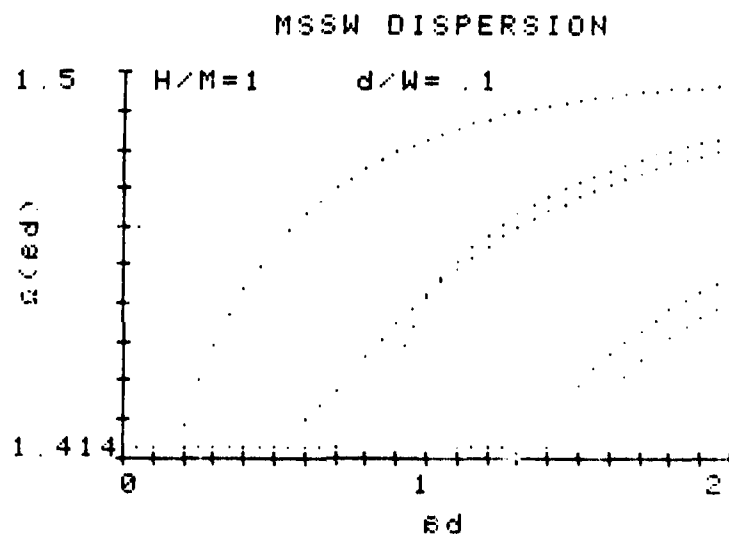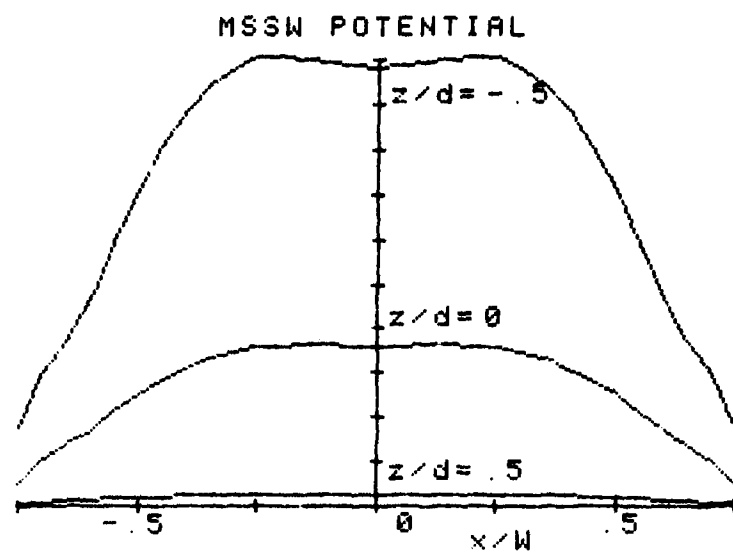
150

Figure 4

151

Figure 5

152

MSSW DISPERSION

Figure 6

MSSW POTENTIAL

Figure 7a

MSSW POTENTIAL

Figure 7b

154

Figure 7c

Figure 7d

155

MSSW POTENTIAL

Figure 8a

MSSW POTENTIAL

Figure 8b

156
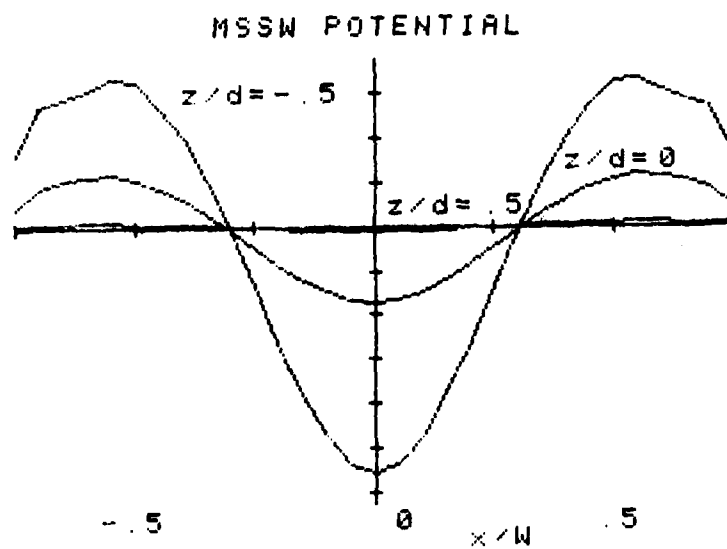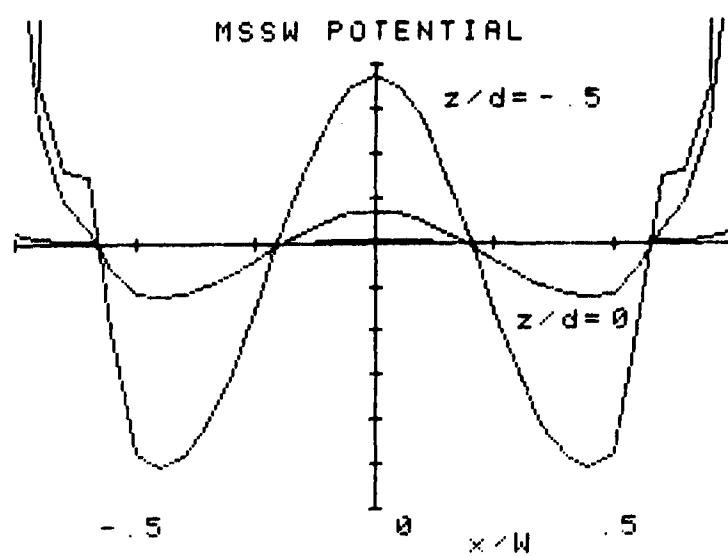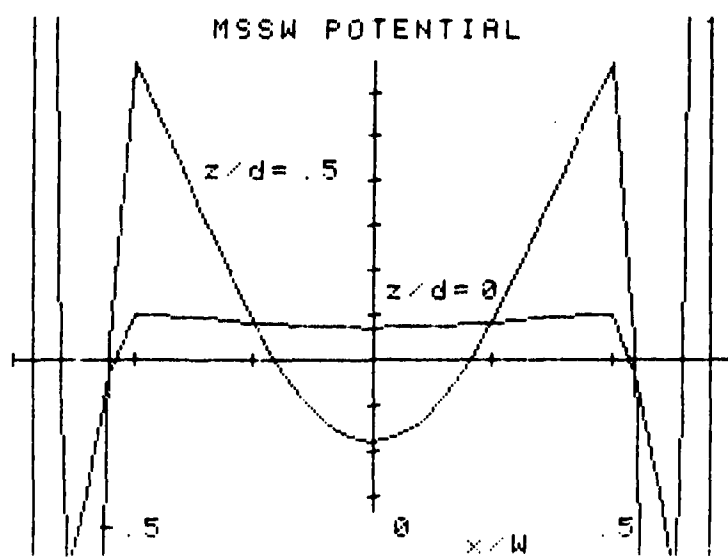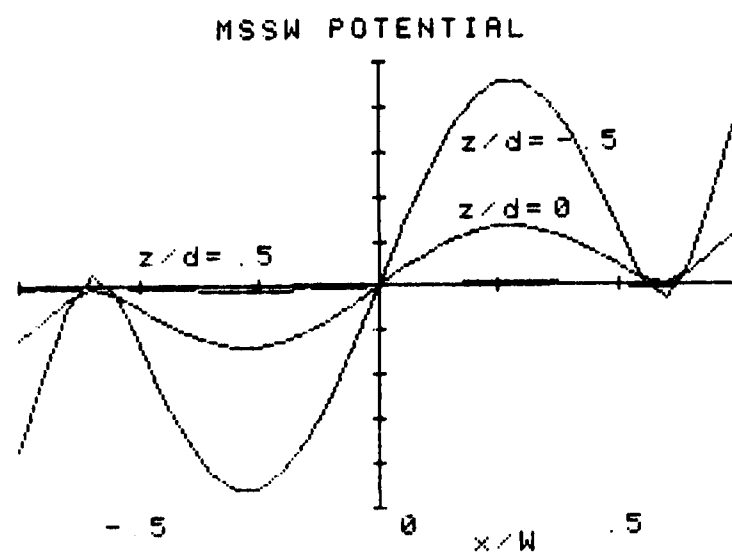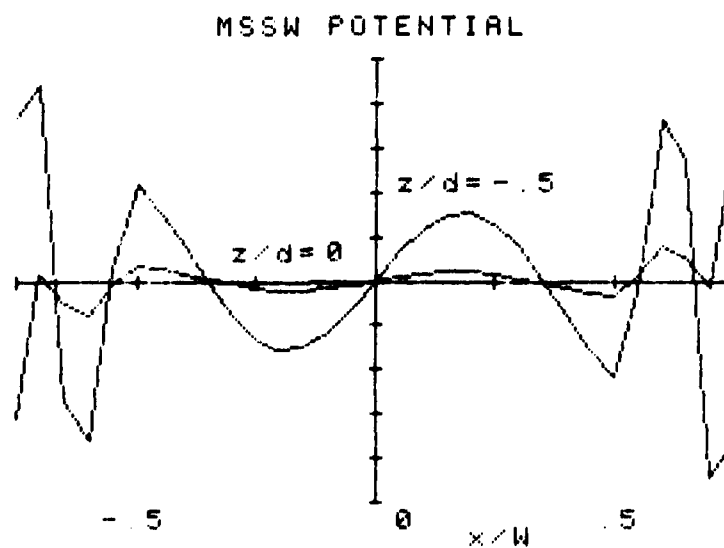
SIMPLE MAGNETOSTATIC DELAY LINES[*]

Michael R. Daniel and J. D. Adam
Westinghouse Electric Corporation
Research & Development Center
Pittsburgh, PA   15235

ABSTRACT

We describe, through calculation and experiment, how simple,
single finger, microstrip transducers may be used to demonstrate
both linearly dispersive and constant delay type magnetostatic delay
lines. The desired delay behavior is achieved over some useful measure
of bandwidth through the influence of a close proximity ground plane to
the yttrium iron garnet film. The two limitations of this technique
are pointed out and one possible remedy to one of them is shown.

1. INTRODUCTION

The promise of magnetostatic waves as delay line elements
at microwave frequencies rests on their strong electromagnetic coupling
to transducers and their low propagation losses in films of yttrium
iron garnet (YIG). However, the implementation of either a constant
delay or a linearly dispersive delay versus frequency characteristic is
governed by the need to modify the inherently non-linear dispersion
which magnetostatic waves show in general. The very successful
exploitation of the interdigital transducer and the reflective array

for surface acoustic wave (SAW) devices rests on the weak coupling which these waves have. Thus, the strong coupling magnetostatic waves have not, so far, been able to take advantage of these tools for delay line design except with a very limited number of finger pairs. But photolithographic limitations and transducer losses limit SAW devices to an upper frequency of around 1 GHz whereas magnetostatic devices have relaxed photolithographic requirements and, in YIG films, an upper frequency limit of around 20 GHz. There was, thus, a strong motivation for, temporarily at least, bypassing the high coupling problems and examining the possible exploitation of simple single finger transducers on single YIG films. The problem of controlling the dispersion was addressed by recognizing the strong influence of a close proximity ground plane on the magnetostatic wave delay time.

2. EXPERIMENTAL RESULTS AND CALCULATIONS

Figure 1 shows the geometry of the simple delay line together with the static bias field orientations required to launch each of the three magnetostatic wave types. The single finger transducers are typically 2 mils (50 μm) wide defined photolithographically in 5 μm thick gold. The ground plane spacing can be controlled by the alumina substrate thickness. Examples of the delay performance which can be obtained using forward volume waves (FVW's) are shown in Figure 2. In the upper, dispersive delay curve, a 20 μm thick YIG film was placed 20 μm from a ground plane resulting in delay versus frequency response linear to within ± 5 nS over 1.2 GHz of bandwidth. This particular delay line has already been referred to in the first paper of this session. It is presently being evaluated by Westinghouse in both the

Bias Field Direction	Magnetostatic Wave
x	Surface
y	Backward Volume
z	Forward Volume
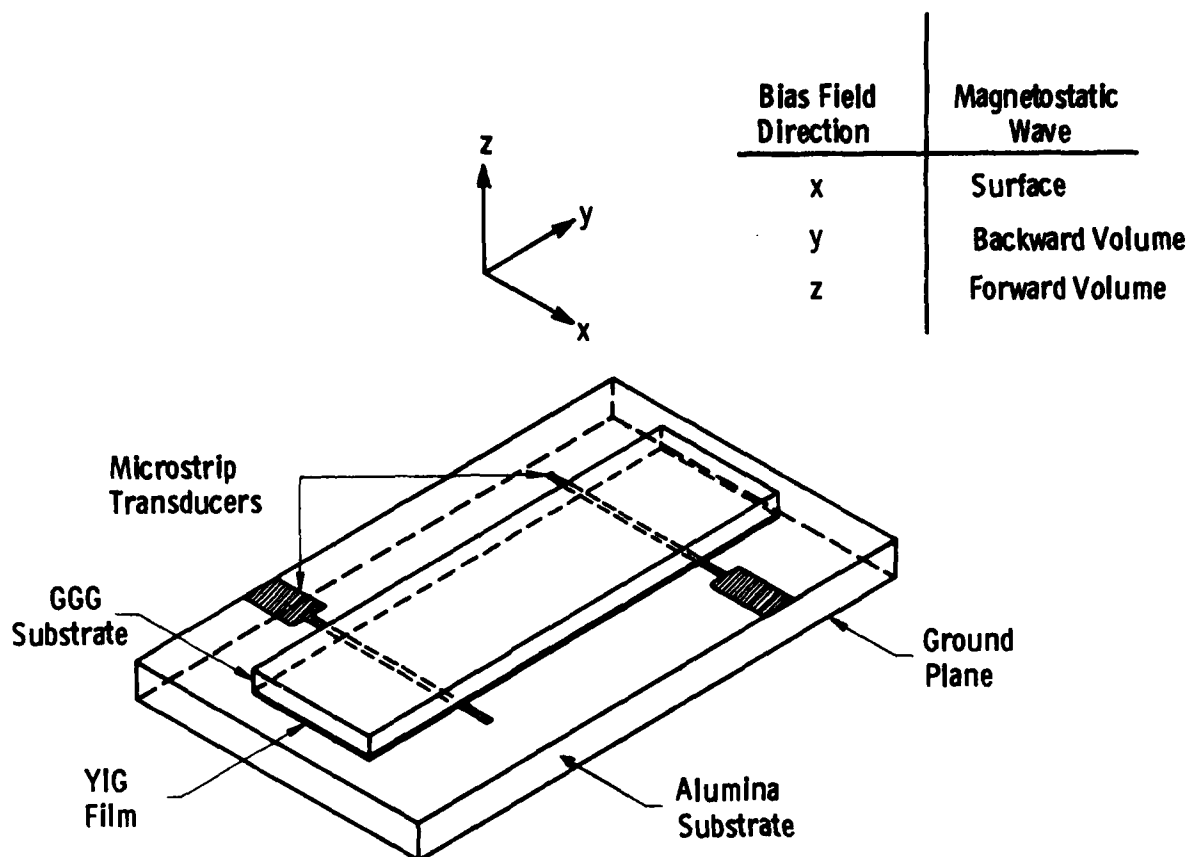
Figure 1. Magnetostatic delay line configuration with the inset at top right showing the magnetic bias field directions required to launch each of the three magnetostatic wave types.

X-band and S-band versions as the dispersive delay element in a microscan receiver. The unmatched insertion loss was in the range 35 to 40 dB over the active bandwidth. This relatively high value for magnetostatic waves was also commented on in the first paper and represents the price to be paid for simplicity of design using the close ground plane technqiue. Depending on the closeness of this plane to the YIG surface some measure of increased insertion loss will always be experienced due to finite conductivity damping of the magnetostatic wave by the ground plane. The lower curve of Figure 2 shows a delay response constant to within a ± 5 nS tolerance. Achieving

a constant delay with a ground plane was first recognized by Bongianni[1] and later by Bardai, et al.[2] and Miller.[3] Figure 2 shows how, using two ground planes—one above and one below the YIG film, an increased operating bandwith results. A delay of about 95 ± 5 nS over a 400 MHz bandwidth was obtained for this device with an insertion loss of 20 dB.

Backward volume waves (BVW's) have shown linearly dispersive and constant delays as shown in Figure 3. In the upper curve a 15 μm YIG film was placed 150 μm from a ground plane to give a "down-chirp" dispersion linear to about ± 5 nS over an 800 MHz bandwidth. This delay line had a 20 dB insertion loss. The lower curve of Figure 3 was measured with a 20 μm film spaced about 10 μm or less from a ground plane. This configuration was achieved by placing the YIG film on a coplanar waveguide transducer. The close proximity of the ground plane to the YIG undoubtedly contributed to the higher insertion loss of 30 dB. As with the FVW delay line this BVW device gave a delay constant to within ± 5 nS over a 400 MHz bandwidth.

Finally, in Figure 4 are shown delay results for surface waves (SW's). Since SW's are unidirectional we differentiate between the +k and -k modes. Also SW's give smaller operating bandwidths than their volume wave counterparts even at S-band. In Figure 4 a 20 μm thick film was placed 250 μm from a ground plane using a 10 mil dielectric alumina wafer. For the -k waves we get a small but significant linear dispersion over a 350 MHz bandwidth. The insertion loss was 30 dB and resulted primarily because this -k wave was launched and received on the YIG film surface opposite to that of the transducers. The lower curve, for +k waves, shows a 200 MHz bandwidth of constant delay with an insertion loss of only 8 dB. This 8 dB figure was by no means a

160
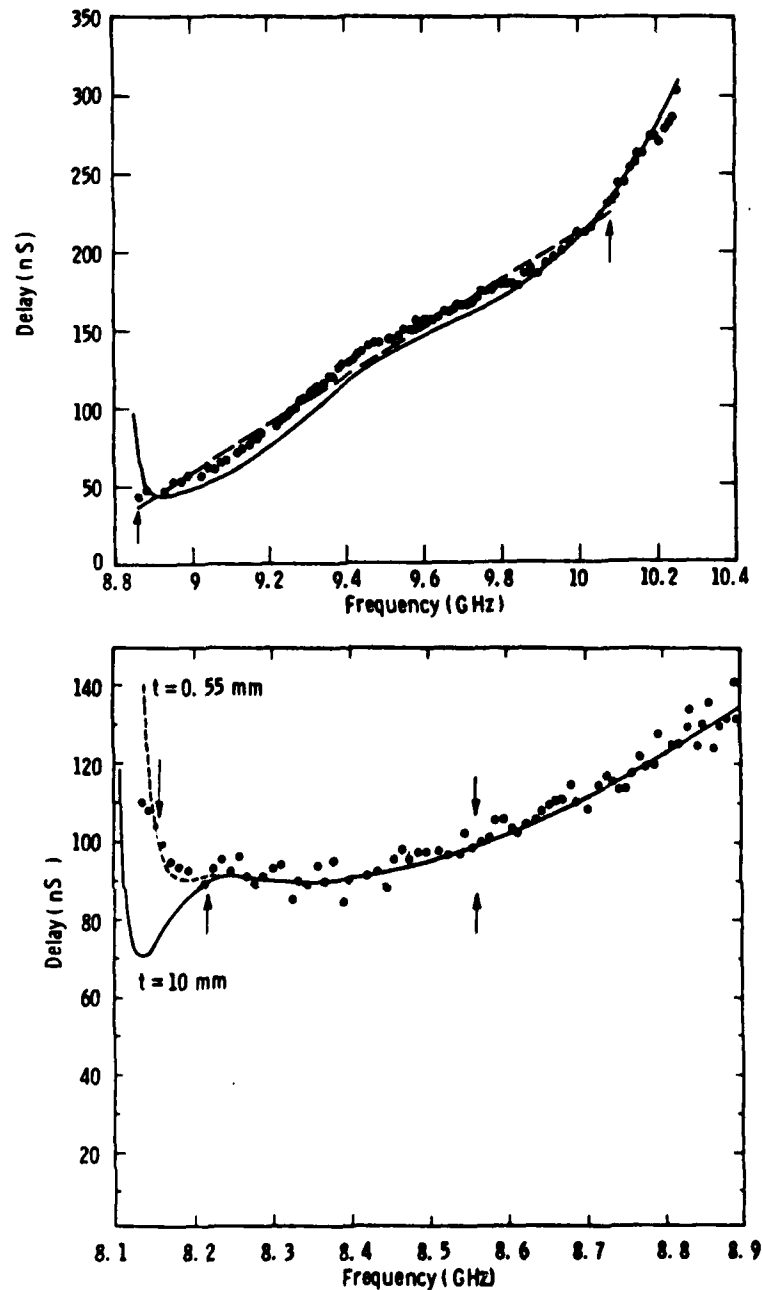
Figure 2.   Upper: Delay versus frequency for a 20 μm thick film spaced
            20 μm from a ground pland supporting forward volume waves.
            Lower: Delay versus frequency for a 20 μm thick film spaced
            150 μm from an upper ground plane and (a) 10 mm (solid curve),
            (b) 0.55 mm (broken curve) from a lower ground plane. Dots
            are the experimentally measured values.
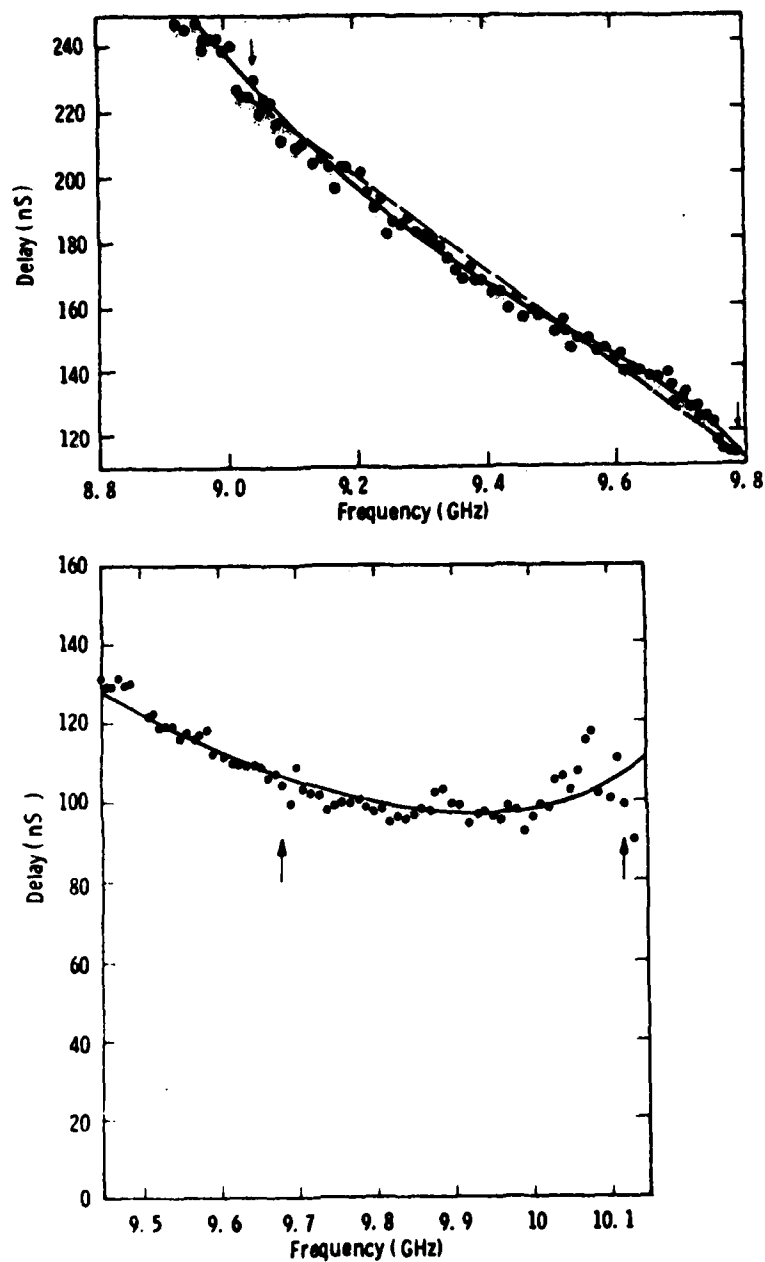
Figure 3. Upper: Delay versus frequency for a 15 μm thick film spaced 150 μm from a ground plane supporting backward volume waves. Lower: Delay versus frequency for 20 μm thick film spaced about 10 μm from a ground plane. Dots are the experimentally measured values.

162
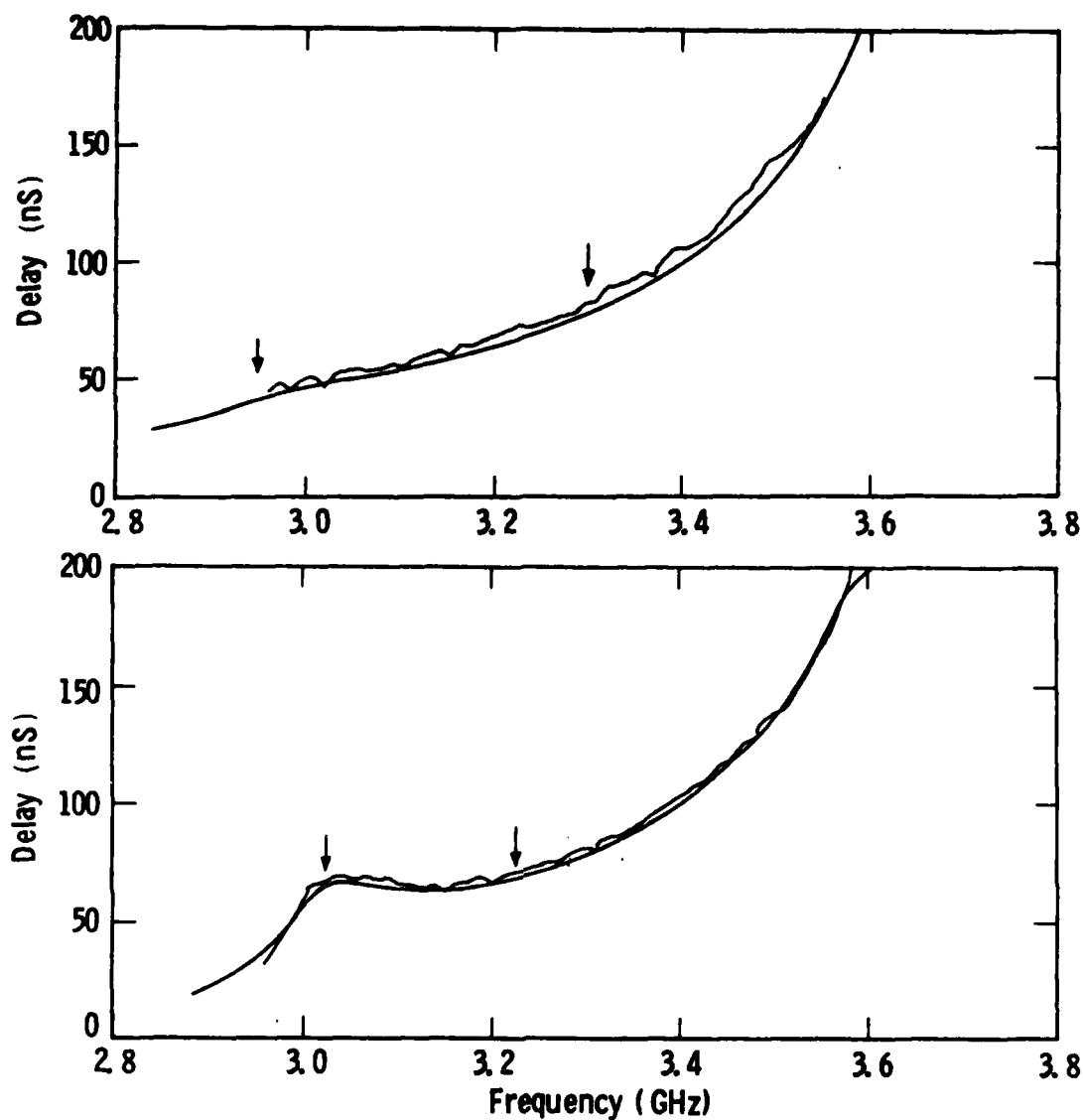
Figure 4. Upper: Delay versus frequency for a 20 μm thick film spaced
250 μm from a ground plane supporting -k surface waves.
Lower: as above, except supporting +k surface waves. "Wiggly"
curves are the experimental results.

lower limit. Because of the high coupling coefficient for SW's relative
to volume waves plus the advantages of uni-directionality insertion
losses of 3 dB or less may be anticipated with SW. The results were
taken at S-band to exploit the increased bandwidth for SW's at the lower
microwave frequencies.

163

The calculated curves of Figures 2 through 4 were all done using the original approach of Damon and Eshbach[4] with allowance for ground plane boundaries and finite sample width. The only adjustable parameters used to get the agreement between theory and experiment to within 5 nS were the internal bias field H and the magnetization $4\pi M$. The bias field was uncertain to the extent of having no exact knowledge of the internal anisotropy field H_A. H_A was typically in the range 10 to 100 Oersteds depending on the orientation of H. $4\pi M$ can depend on crystal growth conditions — it being typically in the range 1750 to 1800 Gauss.

The characteristics of the simple delay lines described here are probably not sufficiently well controlled to permit their immediate use in say microscan receiver applications or phased array radars without some technique to reduce the residual delay ripple. A sensitive and frequently quoted parameter to describe the delay ripple tolerance is the phase deviation or error over the operating bandwidth. Microscan receiver applications call typically for a limit of 20° phase deviation from quadratic for the dispersive delay lines whereas some phased array radar requirements will only tolerate a 2° phase error from linearity for the constant delay lines. Figure 5 is a calculation of the quadratic phase error for the FVW dispersive delay line of Figure 2. The delay data over a 1 GHz bandwidth were fitted to a least squares straight line. The phase deviation ($\Delta\phi$) from this straight line is shown in Figure 5 and shows $\Delta\phi_{max} = \pm 100°$. Thus, without correction, the dispersive delay line has a phase error within a factor of 5 of that required by the microscan receiver for example.

A constant but adjustable delay can be obtained from "up-chirp"
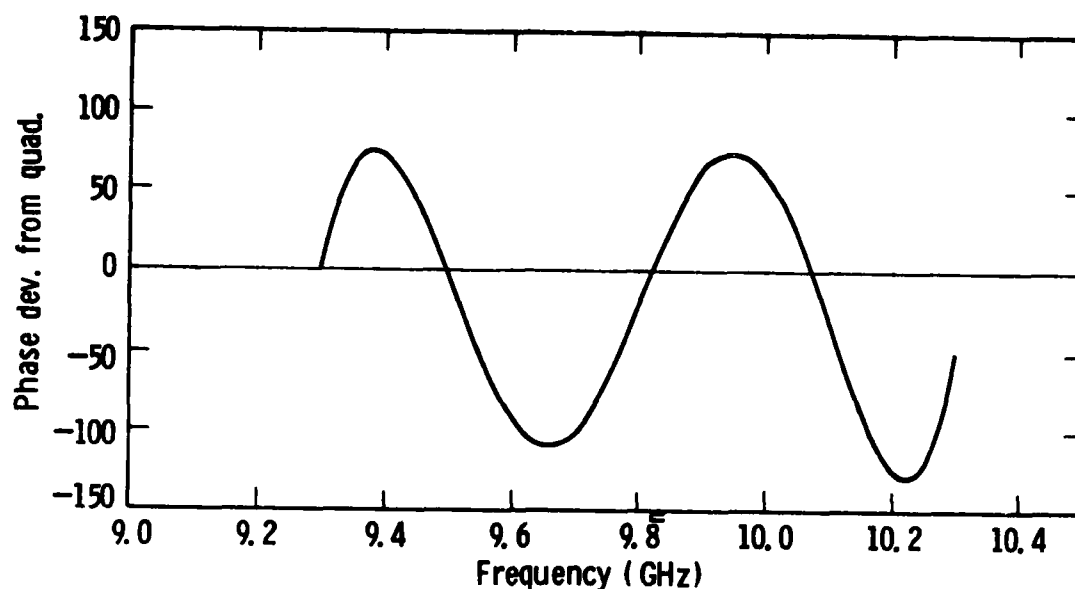
Figure 5. Phase deviation from ideal quadratic response versus frequency for the forward volume wave curve of Figure 2 (upper).
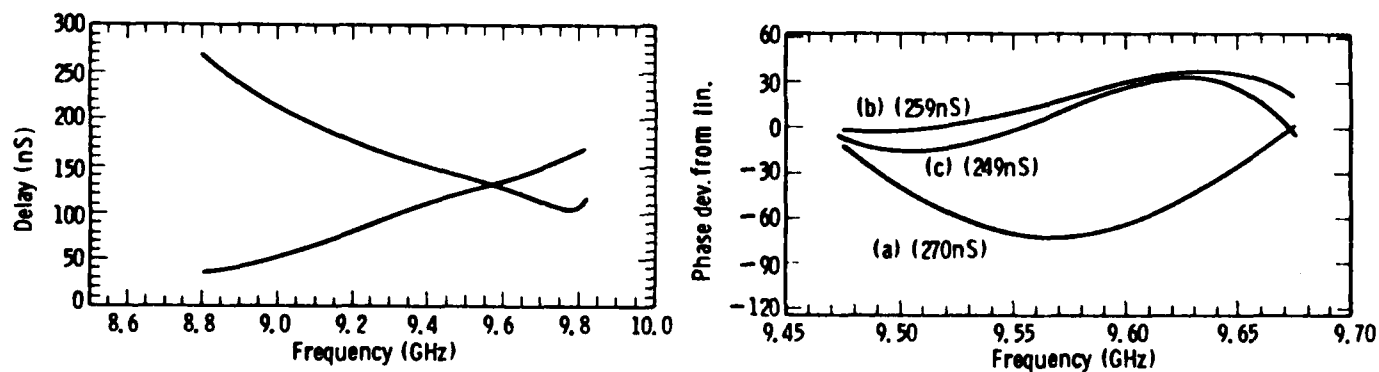
Figure 6. Left: Calculated delay responses versus frequency for the forward volume and backward volume curves shown in Figures 2 (upper) and 3 (upper). Right: Phase deviation from linearity versus frequency for the combined delay results of the upper curves, (a) FVW bias field 3041 Oe, (b) 3071 Oe, (c) 3101 Oe.

165

and "down-chirp" dispersive delay lines in series. Changing the bias field of, say, the "up-chirp" line slides its delay along the frequency axis causing the constant total delay to move up or down. In Figure 6 we show a calculation for the FVW and BVW delay lines. The lower curve shows, in terms of the phase error, how constant such a combined delay would be for $\pm$ 10 nS increments in delay adjustment. The calculation was done for 200 MHz of bandwidth with the most linear portions of the FVW and BVW curves. It gives another illustration of where these simple delay lines presently stand in terms of performance.

There are a number of possible techniques which could correct the second order delay ripple and in conclusion and as an illustration of one of these we show the effect of a small linear gradient (6%) in the bias field. Figure 7 (upper curve) is the same type of plot as Figure 5 except that the actual delay ripple is plotted rather than $\Delta\phi$. The lower curve shows that a 6% linear gradient in H over the path length of the delay line shifts the delay response down in frequency and away from the original least-squares fit straight line. However, substantial reduction in delay ripple does result but over a reduced bandwidth of about 500 MHz. A field gradient in H may not be the best solution to the delay ripple problem but it does illustrate that future developments and improvements can be expected in the performance of simple single transducer magnetostatic delay lines.

3. CONCLUSION

In conclusion, we have shown how both constant and linearly dispersive magnetostatic delay lines may be designed using single finger transducers which avoid the multiple reflection effects associated with
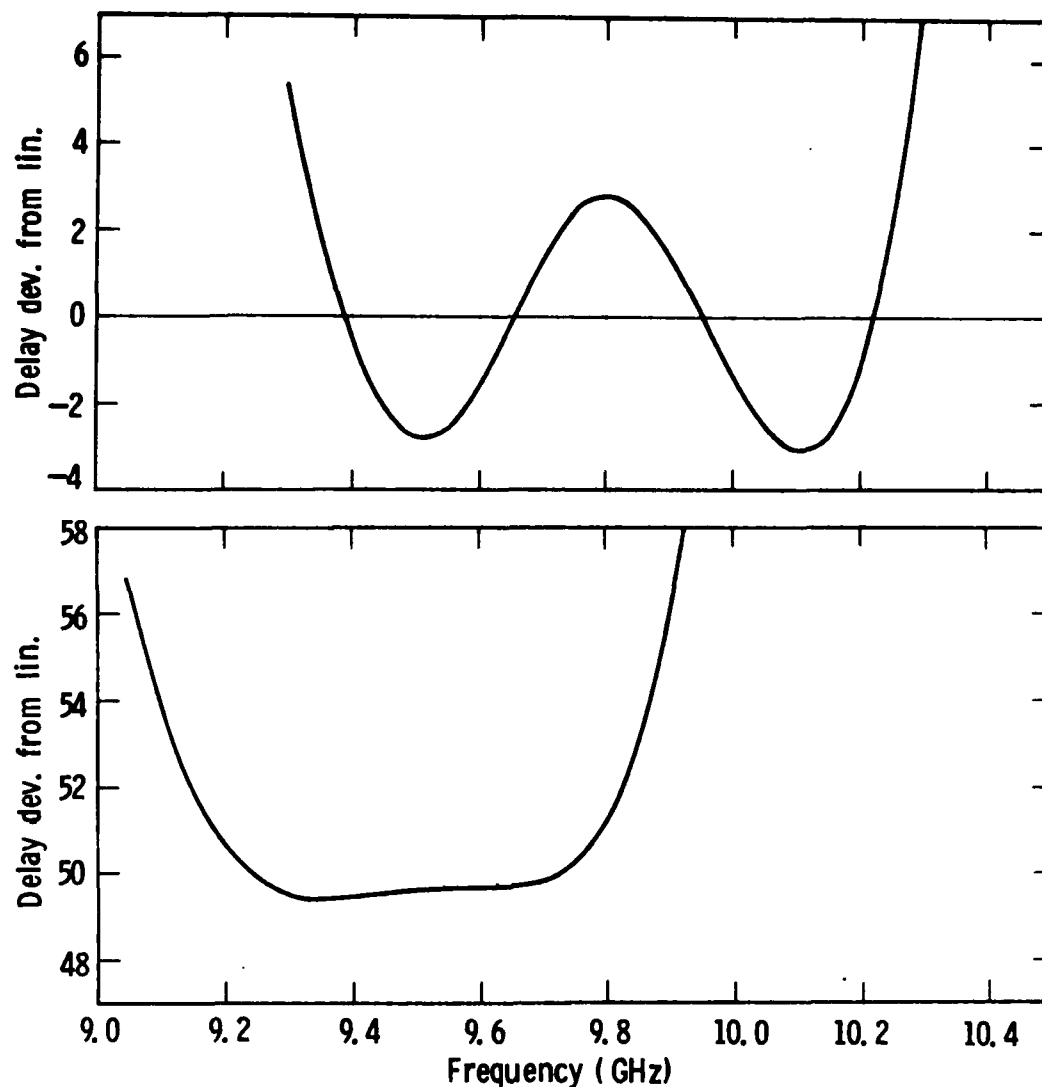
Figure 7. Upper: calculated delay ripple versus frequency for the
FVW dispersive delay of Figure 2 (upper). Lower: Effect of
a 6% linear bias field gradient along the path length of the
FVW dispersive delay line.

interdigital or reflective array transducers. The desired delay

characteristics were obtained through modification of the magnetostatic

dispersion by one or more close proximity ground planes. The limitations

of this approach in terms of delay ripple or phase error were shown.

Finally, an example of how the delay ripple might be reduced through a gradient in the bias field was given. At present, it is not known how to reduce the increased insertion loss which results from finite conductivity damping of the magnetostatic wave by the ground plane. This effect is more noticeable in the FVW dispersive delay line and the BVW constant delay line.

REFERENCES

1. W. L. Bongianni, J. Appl. Phys., 43, 2541 (1972).

2. Z. M. Bardai, J. D. Adam, J. H. Collins and J. P. Parekh, Magnetism and Magnetic Materials AIP Conf. Proc. No. 34, 268 (1977).

3. N. D. J. Miller, Phys. Stat. Solidi, (a) 37, 83 (1976).

4. R. W. Daman and J. R. Eshbach, J. Chem. Phys. Solidi, 9, 308 (1960).

NONDISPERSIVE AND LINEARLY DISPERSIVE MSW PROPAGATION ON MULTILAYER FILMS

L.R. Adkins and H.L. Glass

SUMMARY

The dispersive characteristics of magnetostatic waves propagating in multiple magnetic layer structures have been evaluated theoretically and experimentally. In general, the multiple layer surface wave (MSSW) mode is useful for nondispersive operation while the multiple layer forward volume wave (MSFVW) mode can be used to obtain linearly dispersive characteristics. Experimental confirmation of predicted behavior has been obtained for both modes of propagation.

1. INTRODUCTION

The fact that the natural dispersion characteristic of magnetostatic waves propagating in layered media is nonzero and nonlinear complicates device design. Techniques for tailoring this dispersion to achieve either linearly dispersive or nondispersive operation include multiple ferrite layers with identical magnetizations in a spacially dependent bias field[1], multiple layers with different crystallographic orientations[2], variable ground plane spacing[3], and multiple layers with different magnetizations[4,5]. In this paper theoretical and experimental results for the latter technique are discussed. The advantage of the multiple layer approach is that the dispersive characteristics are determined during the growth process, and thus simple magnetics and standard fabrication techniques can be employed for the device structures. It has been determined that the surface wave (MSSW) mode can be employed to obtain flat nondispersive operation, while the forward volume wave (MSFVW) mode can be used to obtain approximately linear dispersion. These two modes are discussed in turn.

2. MSSW PROPAGATION IN MULTIPLE LAYER FILMS

Theoretical analysis of and experiments with MSSWs propagating in multiple layer films have been previously reported[4,5] and only the major results will be discussed here. Briefly, a dispersion relation has been derived for a structure consisting of up to four layers with each layer having arbitrary magnetization ($4\pi M$) and thickness. Wave number or delay versus frequency curves are then calculated using a computer routine. In general, each magnetic layer will have its own characterization curve, and the shape of this curve will be modified by the presence of the other layers. The mechanism operating here is the perturbation of the bias field seen at a given layer by the precessing spins of the adjacent layers.

Typical experimental data and theoretical prediction are shown in Figure 1 for a two-layer structure. Here, one layer is nominally "pure" YIG ($4\pi M_3$ in the figure) while the magnetization ($4\pi M_1$) of the other layer has been lowered by substituting Lanthanum and Gallium (La and Ga) into the YIG lattice. From the figure it will be seen that the nondispersive region centered at 3.3 GHz is about 200 MHz wide. The experimental deviation from flatness is approximately 1% over this passband. The shape of the dispersion curve can be changed by changing the magnetization of either one or both of the layers as shown in Figure 2. Further modification is possible by varying the thickness.

169

It was concluded from this investigation of the MSSW mode that the total bandwidth of the dispersion cannot be increased by the multiple layer technique but that the nondispersive region can be flattened by manipulating the thickness and the magnetization of the constituent films. The maximum nondispersive pass-band obtainable with this technique is about 200 MHz in the 2 GHz to 4 GHz region.

3. MSFVW PROPAGATION IN MULTIPLE LAYER FILMS: THEORY

The forward volume mode will be discussed in more detail. The structure to be analyzed is shown in Figure 3. A conductor which serves as a ground plane supports four epitaxial layers. The layers may have any thickness and layers t_2 and t_4 may have any value of magnetization. In this analysis, t_1 and t_3 are nonmagnetic spacing layers and the structure is assumed to be infinite in the X and Y directions. Two distinct volume wave modes with opposite dispersion can be propagated along a structure of this type. A magnetostatic forward volume wave (MSFVW) is sustained when the magnetic bias field H_o is applied perpendicular to the surface of the magnetic medium, while a magnetostatic backward volume wave (MSBVW) propagates when H_o is applied parallel to the direction of propagation. In this analysis, only MSFVWs will be considered.

The analysis follows the basic approach previously presented in references (5-9). The magnetostatic assumption ($\nabla \times H = 0$) allows h (the applied RF field component) to be expressed as the gradient of a scalar potential ψ. Applying Gauss' law to ψ, one obtains the LaPlace relation which can be satisfied by a function with separable coordinates. For the coordinate system shown in Figure 3, H_o is along the Z axis and thus the propagating waves are X directed. Since MSFVWs are supported within the volume of the magnetic layers, the scalar potential will have a sinusoidal dependence in the Z direction anywhere within the magnetic medium. The X dependence will also be sinusoidal, as that is the direction of propagation. Finally, there will be no Y dependence, since the structure is assumed to be semi-infinite. The scalar potential thus has the form:

$$\psi = [C_1 \sin(\alpha_N |k| Z) + C_2 \cos(\alpha_N |k| Z)] e^{-ikx} \qquad (1)$$

in the magnetic layers. Here $\alpha_N^2 = \mu_N$, where μ_N is the Polder permeability tensor of the Nth layer. The components of μ_N are

$$\mu_{11}^N = \mu_{22}^N = \mu^N = 1 - \frac{4\pi M^N H_i^N}{(\omega/\gamma)^2 - (H_i^N)^2}$$

$$\qquad (2)$$

$$\mu_{12}^N = \mu_{21}^N = \chi^N = \frac{(\omega/\gamma) 4\pi M^N}{(\omega/\gamma)^2 - (H_i^N)^2}$$

170

H_i is the net internal field given by $H_i = H_O - 4\pi M^N + H_A^N$, where H_A^N is the anisotropy field of the Nth layer, ω and γ are the radial frequency and gyromagnetic ratio, respectively, and M^N is the saturation magnetization of the Nth layer.

In the nonmagnetic layers (t_1 and t_3 in Figure 1), the dependence of ψ is exponential. In these regions, the scalar potential will have the form:

$$\psi = [C_3 e^{-|k|Z} + C_4 e^{|k|Z}] e^{ikx} \tag{3}$$

Thus, the complete set of scalar potential functions for the various regions can be written as:

$$\psi_V = A \exp(-|k|Z) \exp(-ikx) \qquad\qquad Z > d_4 \tag{4}$$

$$\psi_{IV} = [B \sin(\alpha|k|Z) + C \cos(\alpha|k|Z)] \exp(-ikx) \quad d_4 > Z > d_3 \tag{5}$$

$$\psi_{III} = [D \exp(-|k|Z) + E \exp(|k|Z)] \exp(-ikx) \quad d_3 > Z > d_2 \tag{6}$$

$$\psi_{II} = [F \sin(\beta|k|Z) + G \cos(\beta|k|Z)] \exp(-ikx) \quad d_2 > Z > d_1 \tag{7}$$

$$\psi_I = [H \exp(-|k|Z) + I \exp(|k|Z)] \exp(-ikx) \quad d_1 > Z > 0 \tag{8}$$

The boundary conditions require the continuity of the tangential field component h_x and the normal induction component b_z at the layer interfaces and $b_z = 0$ at the conductor. Obtaining expressions for h_x and b_z in each of the five regions and applying the boundary conditions yields a set of equations which are functions of the wave number $|k|$, the frequency ω (through $[\mu^N]$), the magnetization $4\pi M^N$ and the thickness t_N of the layers, and the unknown constants A through I. Since we are interested in the dispersion relation only, it is not necessary to determine the constants and prepare the complete wave function. The relationship between ω, k and the various material parameters is therefore found by solving the determinent formed by the final set of equations. The complete dispersion relation is found to be:

$$\{[\beta^2(1+e^{-2|k|t_1}) - (e^{-2|k|t_1} + 1)] \sin\beta|k|t_2$$

$$+ 2\beta \cos\beta|k|t_2\} (1+\alpha^2)e^{-2|k|t_3} \sin\alpha|k|t_4$$

$$+ \{(1-\alpha^2) \sin\alpha|k|t_4 + 2\alpha\cos\alpha|k|t_4\}$$

$$\cdot \{[\beta^2(1+e^{-2|k|t_1}) + (e^{-2|k|t_1} + 1)] \sin\beta|k|t_2$$

$$- 2\beta\cos\beta|k|t_2\} = 0 \tag{9}$$

where $\alpha^2 = -u_{IV}$, $\beta^2 = -\mu_{II}$

171

Equation (9) is solved by means of a search routine. The dispersion may be presented either in terms of wave number (k) vs. frequency (ω) or as a group delay $(d\omega/dk)^{-1}$ vs. frequency (ω).

For volume mode propagation α and β must be real quantities. Thus, it can be shown from Equation (2) and (9) that volume mode coupling between two magnetic films is restricted to a frequency range lying between the lower frequency limit of the high magnetization film and the upper frequency limit of the low magnetization film. If $H = H_o + H_A - 4\pi M$, then the frequency limits for one film are given by:

$$\omega_u = \gamma[H(H+4\pi M)]^{\frac{1}{2}}$$

$$\omega_L = \gamma H \tag{10}$$

For two layers having magnetizations $4\pi M_1$ and $4\pi M_2$ with $M_1 > M_2$, the coupling limits would be:

$$\omega_u = \gamma[H_2(H_2+4\pi M_2)]^{\frac{1}{2}}$$

$$= \gamma[(H_o+H_A-4\pi M_2)(H_o+H_A)]^{\frac{1}{2}} \tag{11}$$

$$\omega_L = \gamma H_1 = \gamma(H_o+H_A-4\pi M_1)$$

Thus, one effect of the two layers will be to reduce the bandwidth. However, the advantage in using structures of this type is that a degree of control over the dispersion characteristics is provided. Of special interest is the use of the multiple layered structure to obtain linearly dispersive operation. If the non-magnetic layer III is given a thickness of 25μm and the two magnetic layers have $4\pi M$ values of 1771 Gauss and 1654 Gauss, a linearity dispersive region of about 1 GHz can be obtained in the X band ($\sim$ 10 GHz center frequency) region as shown in Figure 4. In this figure additional curves showing the variation of line shape as a function of the thickness of layer I are also shown. The shapes of the curves are also dependent on the $4\pi M$ values of the magnetic layers (as for MSSWs) and on the thickness of the nonmagnetic layer. Curves with these parameters variable are shown in Figures 5 and 6.

4. MSFVW PROPAGATION IN MULTIPLE LAYER STRUCTURE: EXPERIMENT

Delay lines fabricated from triple layer film structures have been evaluated experimentally. For these experiments the magnetic layers (II and IV in Figure 3) had $4\pi M$ values of 1654 Gauss and 1771 Gauss, respectively, and both were 15μm thick. The nonmagnetic layer was 25μm thick and was prepared by heavily substituting La and Ga into the YIG lattice. This decreased the value of the layer magnetization ($4\pi M$) to approximately 483G giving an $H_A-4\pi M$ of -433 Gauss and thus providing an effectively "nonmagnetic" layer. Film evaluation was carried out with an FMR spectrometer for single magnetic layer, magnetic-nonmagnetic layer, and magnetic-nonmagnetic-magnetic layer structures. For the triple layer structure, two main mode resonance lines corresponding to the two magnetic films were obtained as shown in Figure 7. These data convinced us that the "nonmagnetic" layer was behaving as required.

172

A delay vs. frequency curve for the triple layer delay line is shown in Figure 8. Clearly, the experimental data follow the theoretical cure quite closely in the linear region. The measurements were made at low frequencies because of apparatus limitations. In this frequency regime the center frequency inertion loss was about 22 dB increasing to about 30 dB over the complete pass-band.

5. CONCLUSION

The basic conclusion from this work is that the multiple layer technique can be useful in obtaining nondispersive characteristics with the MSSW mode and linearly dispersive characteristics with the MSFVW mode. Further, it has been shown that multiple layer structures with the required characteristics can be prepared using LPE techniques. The main questions at this point are: (1) how reproducibly can the required structures be grown; and (2) how does the multiple layer approach compare with alternate techniques? The basic answer to the first question is that results reproducible within the usual experimental error will be achieved if the thickness can be specified to within $1\mu m$ ($\sim 4\%$) and the magnetization can be specified within about 25 Gauss ($\sim 2\%$). This can be seen by examining the curves in Figures 4-6. We are currently able to control the thickness to the required tolerance and are approaching similar control with the magnetization parameter.

The major alternative technique for both nondispersive and dispersive operation involves varying the spacing between the ground plane and a single layer magnetic film. Our calculations show that virtually any dispersive characteristic obtainable by varying the ground plane spacing can also be realized with a multiple layer structure. Thus, any choice between the two approaches will depend on such factors as ease of fabrication, losses and reproducibility. In favor of the multiple layer approach is the fact that standard alumina wafers can be used as spacers and no close thickness tolerances need be obtained by polishing. It is also possible to use the nonmagnetic layer developed here as the ground plane spacer, eliminating the alumina wafer, if coplanar wave is employed as the coupling structure. This approach is now under evaluation.

REFERENCES

1. W. L. Bongianni, Microwave Journal 17, 49 (January 1974).

2. A. K. Ganguly and C. Vittoria, J. Appl. Phys. 45, 4665 (1974).

3. M. R. Daniel, J. D. Adam and T. W. O'Keefe, IEEE Trans. Mag., MAG-15, 1735-1737 (1979).

4. L. R. Adkins and H. L. Glass, Electronics Letters 16, 590 (1980).

5. L. R. Adkins and H. L. Glass, 1980 Ultrasonics Symposium, 80CH1602-2, 526 (1980).
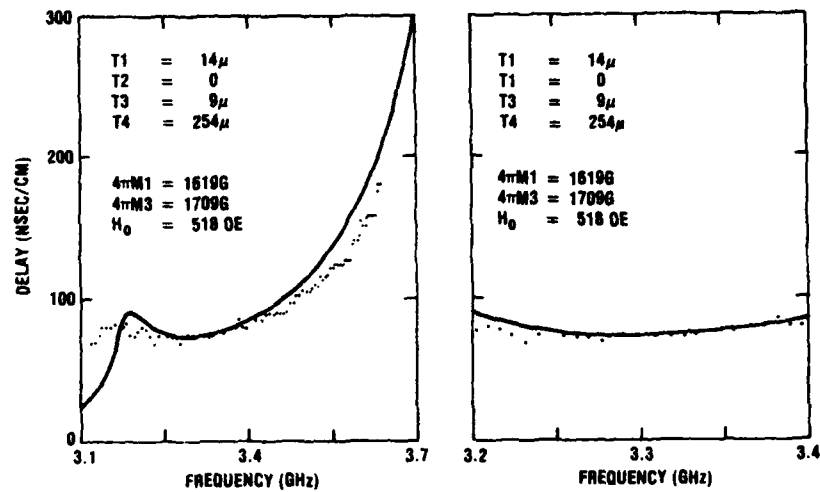
Figure 1. Delay per CM as a Function for a
Two Layer Delay Line with no Spacing
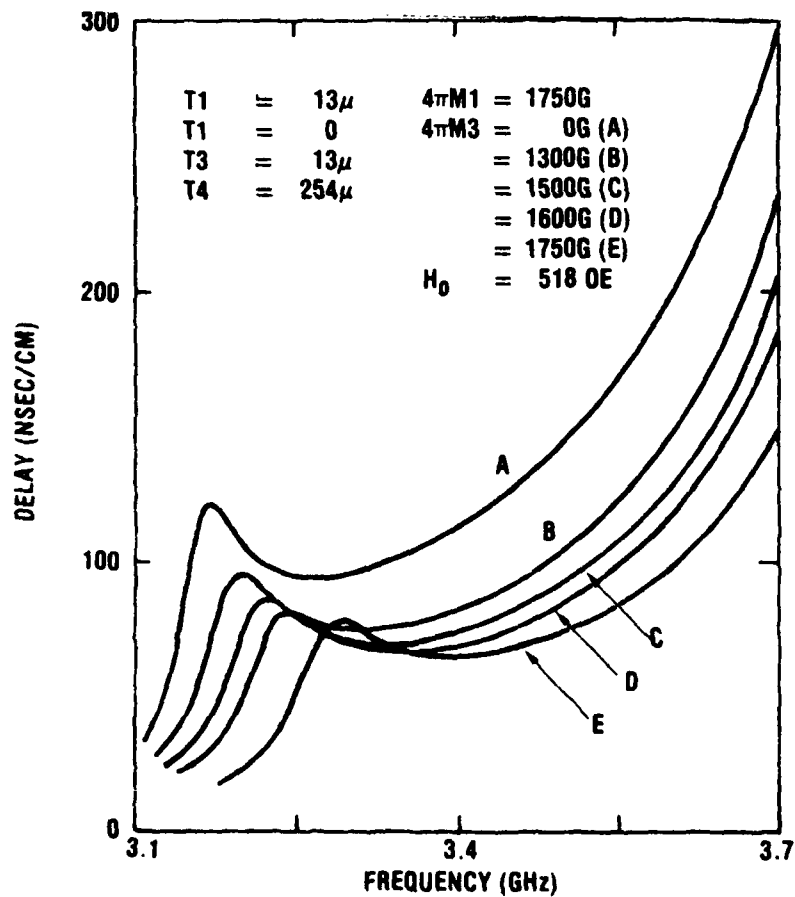
Figure 2. Delay as a Function of Frequency for a Two Layer Delay Line
with Constant Film Thickness and Spacing and Different
Magnetizations

174
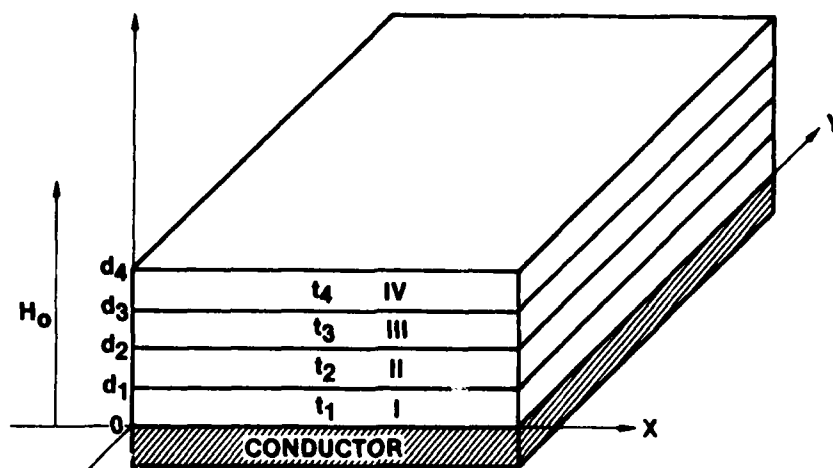
SCALAR POTENTIAL FUNCTIONS

$$\psi_V = A \exp(-|k|z) \exp(-ikx) \qquad z > d_4$$

$$\psi_{IV} = [B \sin(\alpha|k|z) + C \cos(\alpha|k|z)] \exp(-ikx) \qquad d_4 > z > d_3$$

$$\psi_{III} = [D \exp(-|k|z) + E \exp(|k|z)] \exp(-ikx) \qquad d_3 > z > d_2$$

$$\psi_{II} = [F \sin(\beta|k|z) + G \cos(\beta|k|z)] \exp(-ikx) \qquad d_2 > z > d_1$$

$$\psi_I = [H \exp(-|k|z) + I \exp(|k|z)] \exp(-ikx) \qquad d_1 > z > 0$$

Figure 3. Multiple Layer Structure for MSFVW Analysis

$4\pi M_{IV} = 1771$
$4\pi M_{II} = 1654$
$T_{IV} = 15\,\mu$
$T_{III} = 25\,\mu$
$T_{II} = 5\mu, 15\mu, 20\mu, 25\mu, 26\mu, 30\mu$
$T_I = 250\,\mu$
$H_1 = 4900\ Oe$
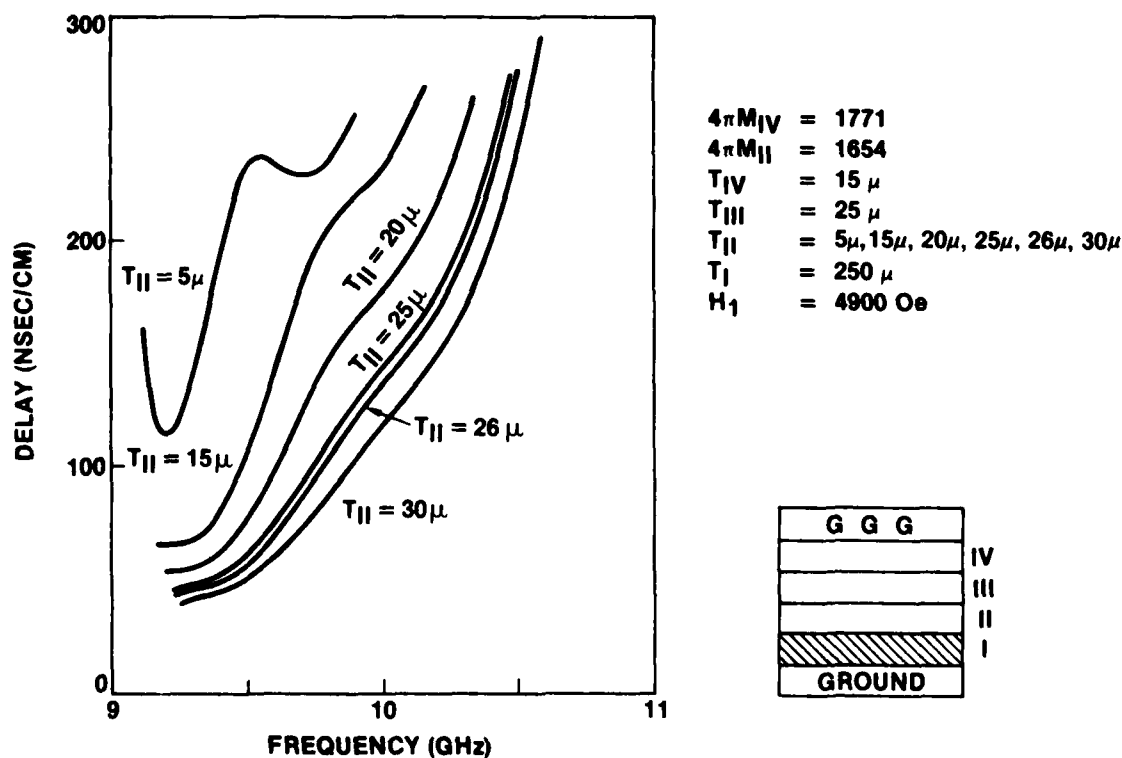
Figure 4. Multilayer MSFVW Dispersion as a Function of Layer Thickness

175

$4\pi M_{IV} = 1771$
$4\pi M_{II} = 1200\mu, 1300\mu, 1400\mu, 1500\mu, 1600\mu, 1700\mu$
$T_{IV} = 15\mu$
$T_{III} = 25\mu$
$T_{II} = 15\mu$
$T_{I} = 250\mu$
$H_O = 4900$ Oe

$4\pi M_{II} = 1200$
$4\pi M_{II} = 1300$
$4\pi M_{II} = 1400$
$4\pi M_{II} = 1500$
$4\pi M_{II} = 1600$
$4\pi M_{II} = 1700$
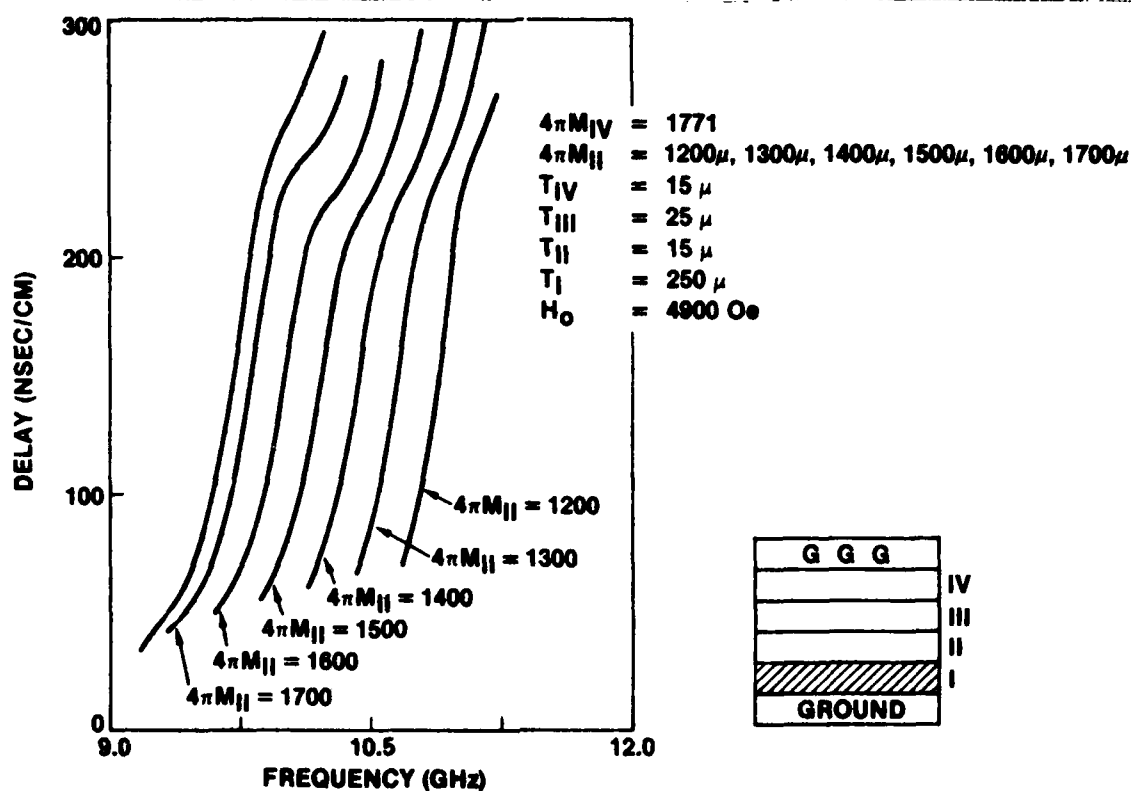
Figure 5. Multilayer MSFVW Dispersion as a Function of $4\pi M_{II}$

$4\pi M_{IV} = 1771$
$4\pi M_{II} = 1654$
$T_{IV} = 15\mu$
$T_{III} = 5\mu, 15\mu, 25\mu$
$T_{II} = 15\mu M$
$T_{I} = 250\mu M$
$H_O = 4900$ Oe

$T_{III} = 25\mu$
$T_{III} = 15\mu$
$T_{III} = 5\mu$

Figure 6. Multilayer MSFVW Dispersion as a Function
of Nonmagnetic Layer Thickness
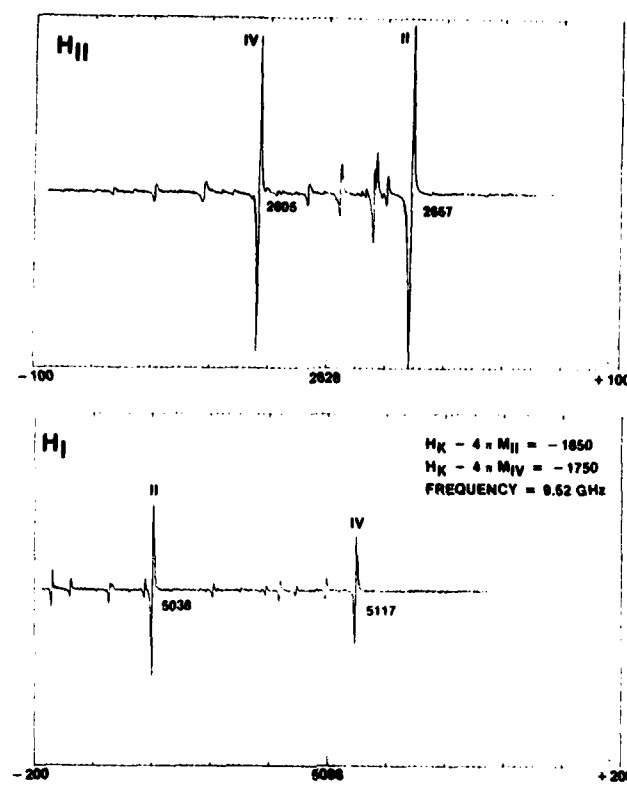
Figure 7. Ferromagnetic Resonance (FMR) Spectrum
of Triple Layer YIG and Ga,La:YIG Films
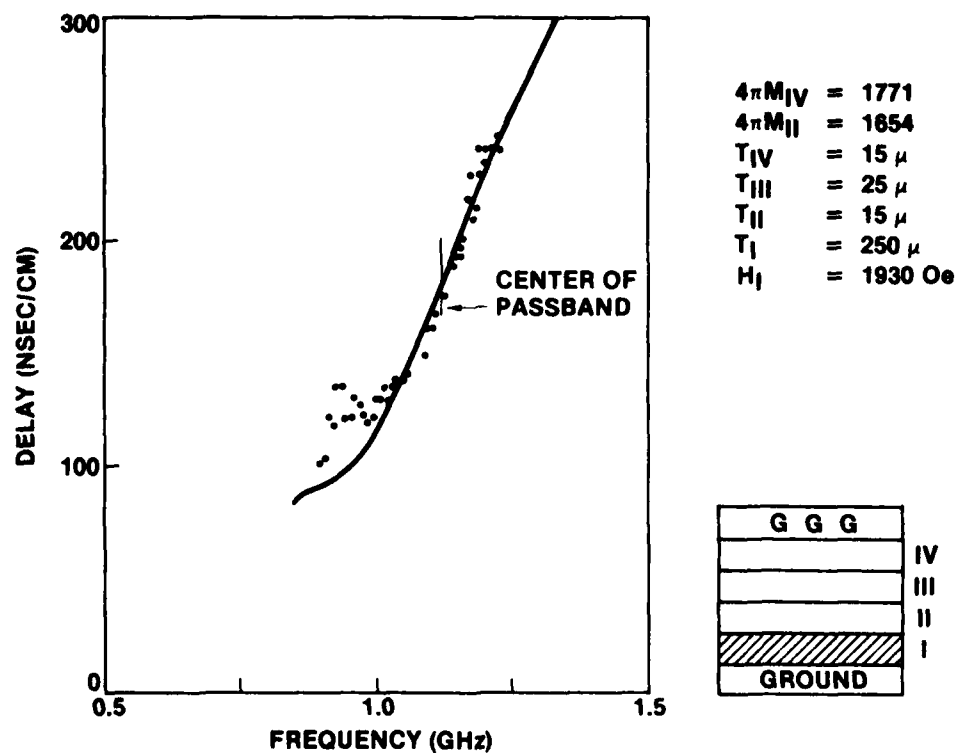
Figure 8. Delay versus Frequency Experiment and Theory for
a Three Layer MSFVW Delay Line

177

MAGNETOSTATIC WAVE TEMPERATURE COEFFICIENTS

J.P. CASTERA
THOMSON-CSF, Research Center
Domaine de Corbeville, 91401 Orsay, France

ABSTRACT

$\smile$ The design and applications of epitaxial yttrium iron garnet (YIG) magnetostatic wave devices will depend upon the variation of the device characteristics versus temperature. A theoretical expression of the delay line oscillator frequency temperature coefficient has been calculated for the three kinds of magnetostatic waves and a comparison between theoretical and experimental results has been done. Temperature stabilization of the frequency of a magnetostatic forward volume wave delay line oscillator has been obtained through the use of a permanent bias magnet made of magnetic materials with a suitable temperature coefficient. Its center frequency of 7.665 GHz is stable to within $\pm$ 1 MHz over the temperature range extending from + 46° C to + 111° C.

INTRODUCTION

Magnetostatic waves (MSW) are very promising to perform signal processing at microwave frequencies. However the application capability will depend upon the temperature stability of center frequency and delay time of these components. Assuming that the frequency versus temperature dependence is only due to the change of YIG magnetization $4\pi M$, a theoretical expression of the temperature coefficient of a delay line oscillator frequency has been determined for magnetostatic surface waves (MSSW), magnetostatic forward volume waves (MSFVW) and magnetostatic backward volume waves (MSBVW). The variation of the temperature coefficient versus frequency between 2 GHz and 20 GHz at a 300 μm wavelength has been calculated and compared to the experimental results. Mo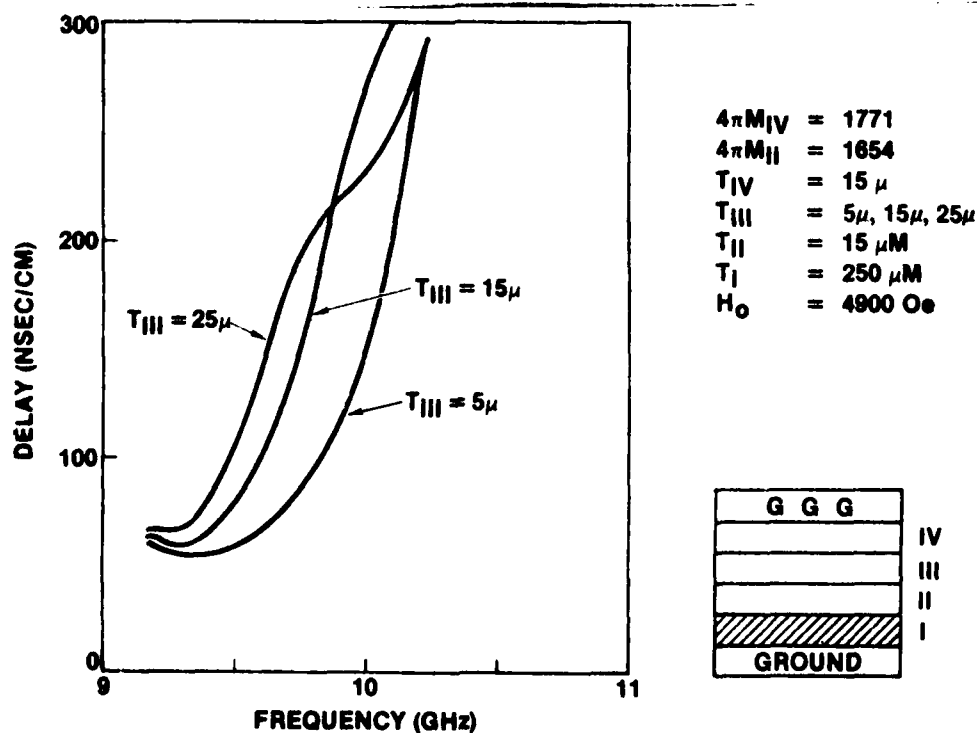reover the frequency of a MSFVW delay line oscillator has been stabilized using commercially available rare earth cobalt permanent magnets.

MSW TEMPERATURE COEFFICIENTS

A schematic representation of an oscillator using a magnetostatic wave delay line in the feedback loop of a solid-state amplifier is shown in Fig. 1. The conditions required for oscillation of a feedback loop oscillator are that the path length along the loop corresponds to a phase shift of $2\pi n$ radians, n being an integer, and that the loop gain exceeds unity at the operating frequency. If ζ is the delay time in the delay line and t_0 the delay time in the amplifier and connections, the oscillating frequency f may be written as :

$$f = \frac{n}{\zeta + t_0} \tag{1}$$

and the temperature coefficient C satisfies :

$$C = \frac{\Delta f}{f \, \Delta T} \tag{2}$$
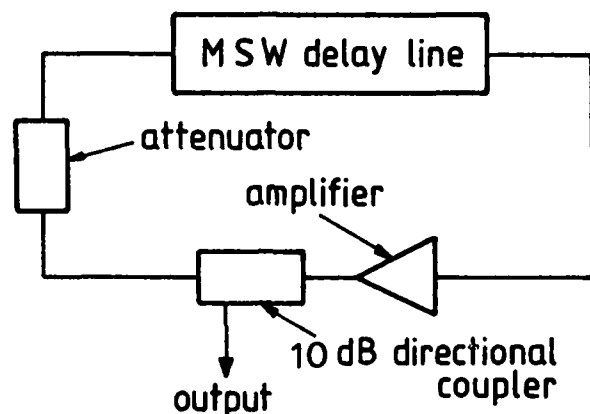
Fig. 1 - Typical block diagram of a delay line oscillator

Magnetostatic Surface waves

For these waves, the magnetic field is applied in the plane of the YIG film perpendicular to the propagation direction. The coefficient C is determined according to the following relationship :

$$C = \frac{- \gamma^2 \ L \ \left[H \ (H + 2\pi M) \ - \ (f/\gamma)^2 \right] \ \Delta \ 4\pi M \ / \ \Delta T}{4 \ \pi M \ f \ \left[Lf + 2\pi \ d \ \gamma^2 \left[(H + 2\pi M)^2 \ - \ (f/\gamma)^2 \right] \ t_0 \right]} \qquad (3)$$

where γ is the gyromagnetic ratio, L the length of the MSW delay line, H the applied magnetic field, $4\pi M$ the magnetization, f the oscillating frequency and d the film thickness. The intrinsic temperature coefficient of MSSW is given by relation (3) when $t_0 = 0$. This equation becomes :

$$C = \frac{- \gamma^2 \ \left[H \ (H + 2\pi M) - (f/\gamma)^2 \right]}{4\pi M \ \ f^2} \ \frac{\Delta 4\pi M}{\Delta T} \qquad (4)$$

which may be expressed as follows :

$$C = \frac{\gamma^2 \ \left[\sqrt{\left(\frac{f}{\gamma}\right)^2 + (2\pi M)^2} \ e^{-\frac{4\pi d}{\lambda}} - 2\pi M_e^{-\frac{4\pi d}{\lambda}} \right]}{2 \ f^2} \ \frac{\Delta 4\pi M}{\Delta T} \qquad (5)$$

where λ is the magnetostatic wavelength. The variation of C with frequency between 2 GHz and 20 GHz is shown in Fig. 2 for a 300 µm wavelength MSSW propagating in a 20 µm thick YIG film.
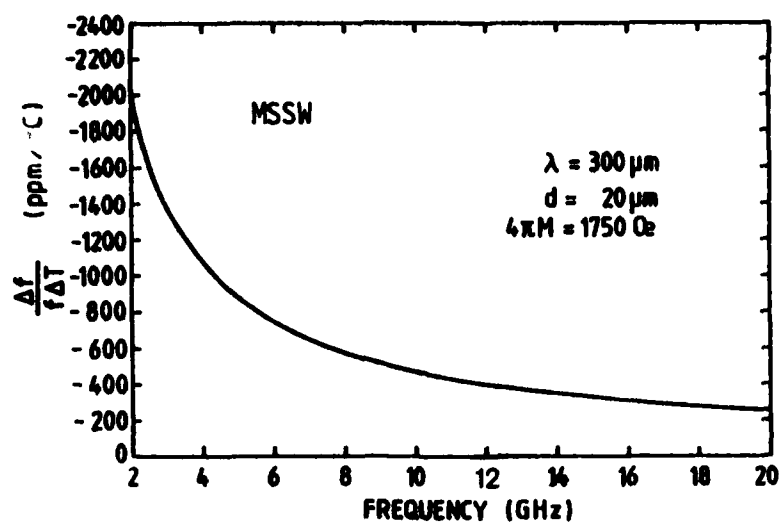
Fig. 2 - Calculated MSSW temperature coefficient versus
frequency

The value of $\Delta 4\pi M /\Delta T$ is deduced from the $4\pi M$ versus temperature measurements of P. Hansen et al.[1]   As shown on this figure, the MSSW temperature coefficient is negative and decreases when frequency increases. For instance, C = - 1375 ppm/°C at 3 GHz and C = - 376 ppm/°C at 13 GHz.
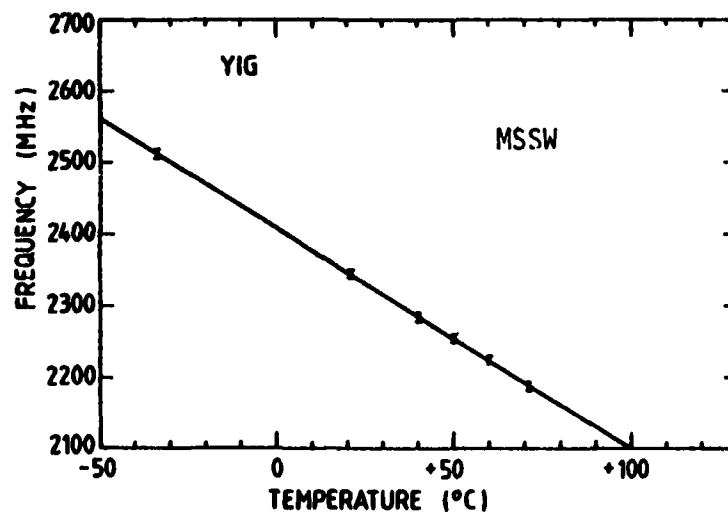
Fig. 3 - Experimental temperature variation of MSSW delay
line oscillator frequency for a constant bias
magnetic field

For the experiments, a 10 mm long delay line has been realized with a 10 μm thick YIG film. A constant bias magnetic field H = 187 Oe was applied in the plane of the film perpendicular to the propagation direction of the waves. At room temperature the oscillating frequency was f = 2346 MHz for a 214 μm wavelength and the delay time t_0 = 10 ns. Fig. 3 represents the oscillator frequency shift versus temperature. This frequency variation corresponds to an experimental temperature coefficient C_{exp} = - 1300 ppm/°C which slightly differs from the theoretical value C_{th} = - 1418 ppm/°C. The difference between theoretical and experimental coefficients may be attributed to the approximations made, i.e. the anisotropy field has been neglected and the magnetization 4πM is supposed to be equal to 1750 Oe.

Magnetostatic Forward Volume Waves

In this case, the magnetic field is applied perpendicular to the plane of the YIG film. The frequency temperature coefficient when t_0 is not zero is given by :

$$C = \frac{A \quad \Delta 4\pi M / \Delta T}{-Bf + \dfrac{\pi \ d \ \alpha \ f}{L \left[\dfrac{kd}{2} + \dfrac{1}{1 + \alpha^2} \right]} \ t_0} \tag{6}$$

with :

$$k = \frac{2}{d \ \alpha} \tan^{-1} \left[\frac{1}{\alpha} \right] \qquad ; \qquad k = 2\pi / \lambda$$

$$A = \frac{(H - 8\pi M) \ (f/\gamma)^2 - H \ (H - 4\pi M)^2}{2 \ \alpha \left[(f/\gamma)^2 - (H - 4\pi M)^2 \right]^2}$$

$$B = - \frac{4\pi M \ (H - 4\pi M) \ f}{\gamma^2 \ \alpha \left[(f/\gamma)^2 - (H - 4\pi M)^2 \right]^2} \tag{7}$$

$$\alpha^2 = \frac{H \ (H - 4\pi M) - (f/\gamma)^2}{(f/\gamma)^2 - (H - 4\pi M)^2}$$

If t_0 = 0, C has the following form :

$$C = \frac{\gamma^2}{2} \left[\frac{(H - 8\pi M) \ (f/\gamma)^2 - H \ (H - 4\pi M)^2}{4\pi M \ (H - 4\pi M) \ f^2} \right] \frac{\Delta 4\pi M}{\Delta T} \tag{8}$$

Fig. 4 shows the MSFVW temperature coefficient versus frequency between 2 GHz and 20 GHz. In this example, d = 20 μm and λ = 300 μm. C is positive and decreases with temperature going from + 3280 ppm/°C at 3 GHz to + 740 ppm/°C at 13 GHz.
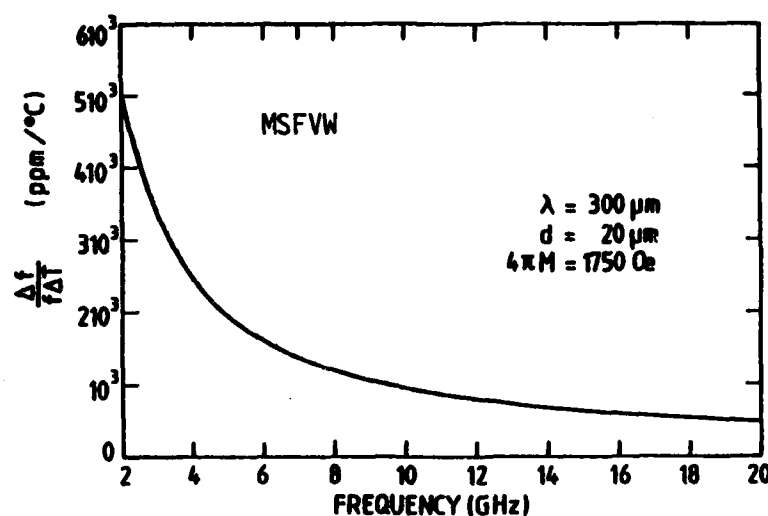
Fig. 4 - Calculated frequency dependence of MSFVW temperature
coefficient

A 10 mm long, 10 µm thick MSFVW delay line has been used to measure
the oscillator frequency versus temperature variation. A 4521 Oe magne-
tic field is applied to the YIG film corresponding to a frequency f =
8.050 GHz at the wavelength λ = 419 µm. For this experiment t_0 = 6,3 ns.
The experimental temperature coefficient for those waves, equal to
+ 1140 ppm/°C, is very close to the theoretical one C_{th} = + 1176 ppm/°C.

Magnetostatic Backward Volume Waves

For this kind of waves corresponding to a magnetic field applied in
the plane of the YIG film parallel to the propagation direction, the
temperature coefficient C satisfies the following relationship :

$$C = \frac{\left\{ \frac{k\ H}{2\ \left[H\ (H + 4\pi M) - (f/\gamma)^2\right]} + \frac{1}{4\pi\ Md} \right\}}{\left[\frac{2}{d\ (1 + \beta^2)} + k\right]\ \frac{f}{\beta}\ D\ -\ \frac{2\pi\ f\ t_0}{L}}\ \frac{\Delta 4\ \pi M}{\Delta T} \tag{9}$$

with :

$$k = \frac{2}{d\beta}\ \tan^{-1}\left(\frac{1}{\beta}\right)$$

$$D = \frac{4\pi\ M\ H\ f}{\gamma^2\ \beta\left[H\ (H + 4\pi M) - (f/\gamma)^2\right]^2} \tag{10}$$

$$\beta^2 = \frac{(f/\gamma)^2 - H^2}{H\ (H + 4\pi M) - (f/\gamma)^2}$$

This relationship when $t_o = 0$, is reduced to :

$$C = \frac{\gamma^2 \left[(f/\gamma)^2 - H^2 \right]}{8 \pi M f^2} \frac{\Delta 4\pi M}{\Delta T} \tag{11}$$

As shown by the previous relation, a zero frequency change with temperature is achieved for $f = \gamma H$ corresponding to the lower frequency limit.

The C variation versus frequency is presented in Fig. 5 for a 20 µm thick YIG film at a 300 µm magnetostatic wavelength. The MSBVW temperature coefficient is negative and decreasing with increasing frequency. It is equal to - 769 ppm/°C at 3 GHz and to - 267 ppm/°C at 13 GHz.
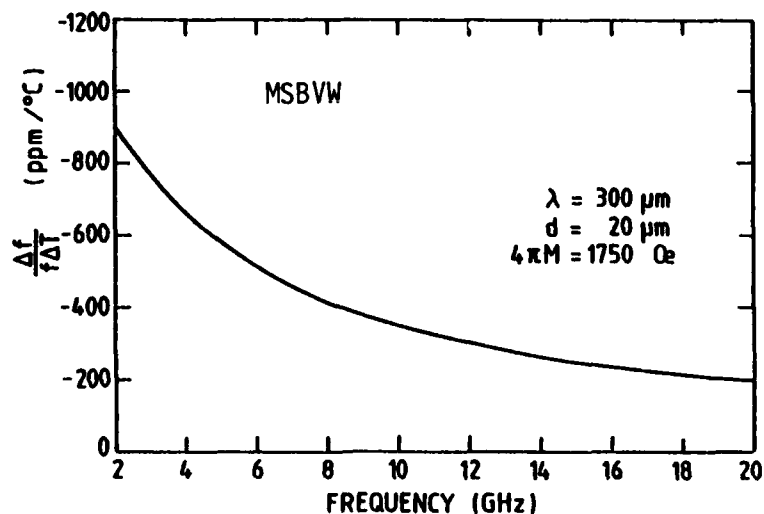
Fig. 5 - Calculated MSBVW temperature coefficient vs. frequency

So as to show the magnetostatic wavelength dependence of C, we have not registered the delay line oscillator frequency variation versus temperature as in the two previous experiments, but the overall transfert function of a MSBVW delay line with two narrow microstrip transducers. Fig. 6 is a multiple trace of the frequency response of a MSBVW delay line at several temperatures. The experiment has been realized on a 18.5 µm thick YIG film where two 30 µm wide aluminum transducers have been etched. As theoretically predicted the lower frequency limit for these waves is temperature independant. The upper frequency limit as a function of temperature is given in Fig. 7. The experimental temperature coefficient C_{exp} = - 804 ppm/°C is in good agreement with the theoretical one C_{th} = - 848 ppm/°C.

183
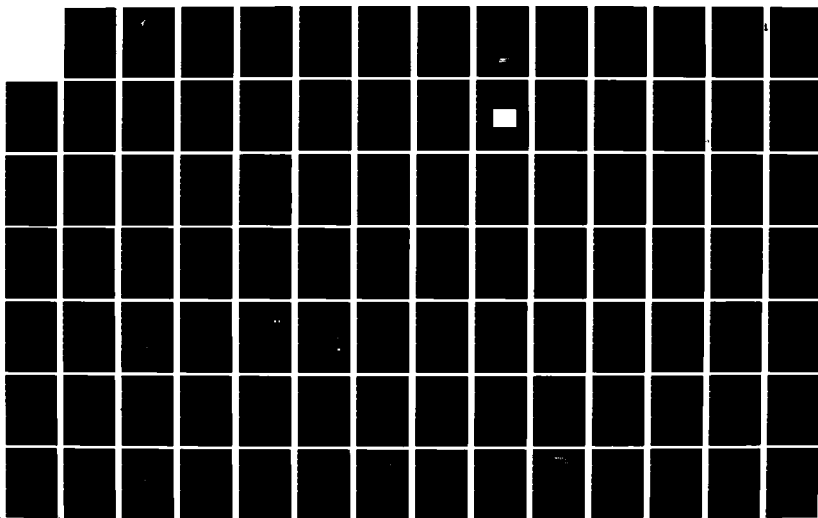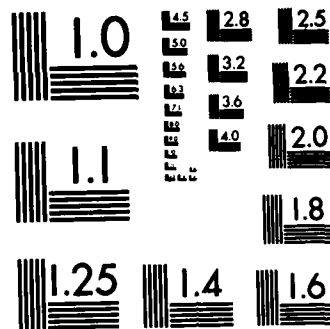
MICROCOPY RESOLUTION TEST CHART

NATIONAL BUREAU OF STANDARDS-1963-A
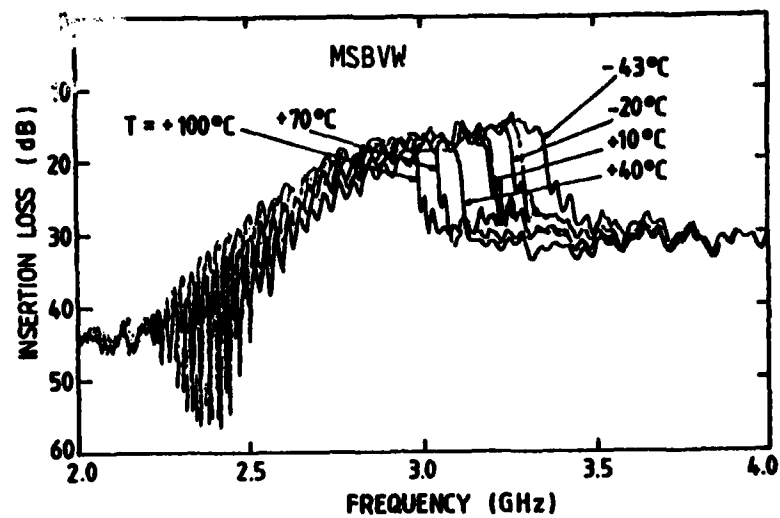
Fig. 6 - Frequency response of a MSBVW delay line registered at
several temperatures
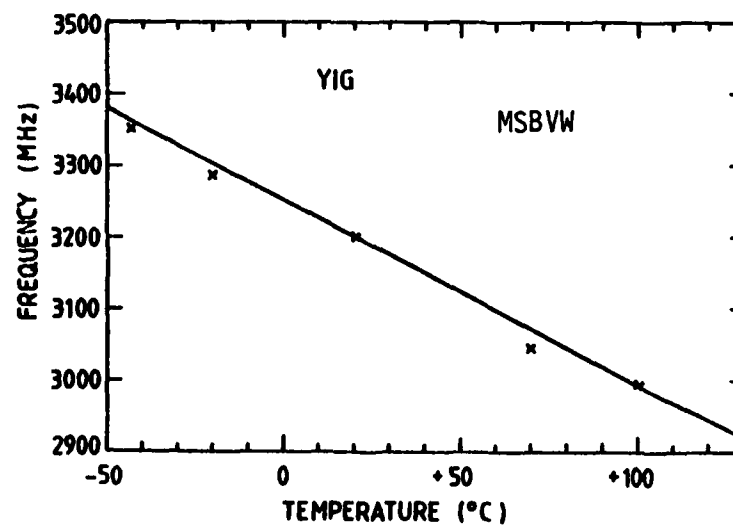
Fig. 7 - Measured upper frequency limit of a MSBVW delay line as
a function of temperature

TEMPERATURE STABILIZATION BY PERMANENT MAGNETS

Permanent magnets having a high negative temperature coefficient
of remanence (between - 0.04 %/°C and - 0.09 %/°C) are commercially
available. As shown by J.D. Adam[2,3], a combination of these materials
may be used to achieve temperature shift compensation of a MSFVW delay
line oscillator. The variation of internal field of YIG is compensated
by a change with equal amplitude and opposite sign in the bias magnetic
field. Adam[3] achieved a delay line oscillator at 8.84 GHz stable over a
65° C temperature range around room temperature. However the variation
of 4πM and anisotropy field are not linear functions of temperature. So
it seems impossible, for example, to stabilize a MSW oscillator over the
MIL operating temperature of - 55° C to + 85° C without oven. But if a
hybrid heater holding the YIG temperature variation to less than 10° C
over the MIL operating temperature range is used (as for Watkins Johnson
YTOs), a better frequency stability than with YIG sphere oscillators can
be obtained. In this case, the stabilization of the MSW device has to be
obtained at higher temperature than room temperature. So as to show the
feasibility, a delay line oscillator using a MSFVW delay line was imple-
mented. Multibar microstrip transducers were used to achieve a single
mode oscillator. The permanent magnet comprises a soft iron yoke and two
rare earth cobalt pole pieces. The first permanent magnet material is
"CORAMAG" with a coefficient of remanence of - 0.04 %/°C, the other one
is "RARENET-B" with a coefficient of - 0.09 %/°C. The magnet was designed
to produce a bias magnetic field of 4361 Oe at room temperature with tem-
perature dependence of - 0.072 %/°C. The corresponding oscillator fre-
quency is 7.665 GHz. Fig. 8 shows the variation in center frequency of
the oscillator with temperature over the range - 25° C to + 125° C. The
frequency is stable to within ± 1 MHz over a 65° C temperature range from
+ 46° C to + 111°C.
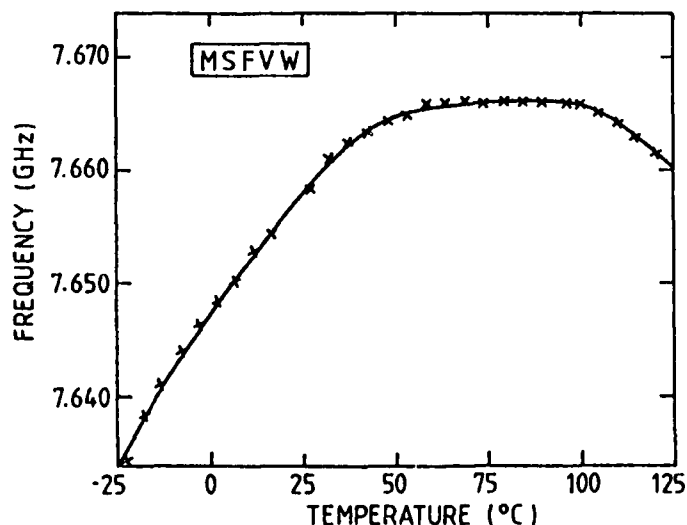
Fig. 8 - Frequency drift characteristics of the MSFVW delay line
stabilized oscillator vs. temperature

Temperature stabilization of MSSW and MSBVW devices by this technique
is not so easy and seems impossible with commercially available permanent
magnets which have too small positive coefficients of remanence.

CONCLUSION

The frequency variation of the temperature coefficient at a 300 μm wavelength for MSSW, MSFVW and MSBVW has been calculated. The center frequency stability of MSW devices can be improved through the choice of permanent bias magnetic materials with a suitable temperature coefficient. MSSW and MSBVW have a negative variation of frequency and it seems difficult to achieve temperature stabilization of these components with commercially available magnets which have too small positive coefficients of remanence. On the other hand, MSFVW frequency temperature coefficient is positive and this frequency change can be cancelled by the temperature dependence of rare earth cobalt permanent magnets. A MSFVW delay line stabilized oscillator at 7.66 GHz has been performed. The center frequency of this device is stable to within $^{+}_{-}$ 1 MHz over a 65° C range from + 46°C to + 111° C. Moreover, if a hybrid heater is used, a better frequency stability than with YIG sphere oscillators can be obtained over the MIL operating temperature of - 55° C to + 85° C.

ACKNOWLEDGEMENT

REFERENCES

1 P. Hansen, P. Röschmann and W. Tolksdorf, "Saturation magnetization of gallium-substituted yttrium iron garnet", Journal of Applied Physics, Vol. 45, N° 6, June 1974.

2 J.D. Adam, "A temperature stabilized magnetostatic wave device", Int. Microwave Symp., Proc. 79 CH 1439-9 MTT-S, p. 160, 1979.

3 J.D. Adam and M.R. Daniel, "The Status of magnetostatic devices", Intermag Conference, Grenoble, May 12-15, 1981, paper 20-1.

PROPAGATION CHARACTERISTICS OF MAGNETOSTATIC WAVES: A REVIEW

J.P. Parekh
Department of Electrical Engineering
State University of New York at Stony Brook
Stony Brook, N.Y. 11794

ABSTRACT — This paper reviews the propagation characteristics of guided magnetostatic waves (MSW's) in a YIG film magnetized beyond saturation. There exist three guided magnetostatic wave-types, viz., magnetostatic surface waves (MSSW's) and magnetostatic forward and backward volume waves (MSFVW's and MSBVW's). The orientation of the internal bias field determines the particular wave-type that can be supported by the YIG film. The frequency spectrum of the volume waves coincides with that over which magnetostatic plane waves are of the homogeneous variety. The frequency spectrum of the MSSW's is located immediately above the MSVW spectrum. MSW's are dispersive, with the dispersion properties alterable through modification in boundary conditions. The most explored dispersion control technique employs the placement of a ground plane somewhat above the YIG film surface. This dispersion control technique, which provides one method of realizing nondispersive MSW propagation, raises the upper bound of the MSSW spectrum but does not affect the bounds of the MSVW spectrum. Numerical computations illustrating the dispersion and polarization characteristics of MSW's are presented.

I. INTRODUCTION

The present paper represents a brief review of the propagation characteristics, i.e., the dispersion and polarization characteristics, of guided magnetostatic waves (MSW's) in a YIG film magnetized beyond saturation. The basic problem of determining the number of MSW modes or wave-types supported by a planar YIG geometry and their propagation characteristics was solved by Damon and Eshbach some twenty years ago[1]. The Damon-Eshbach (DE) study established the existence of three MSW wave-types, viz., magnetostatic surface waves (MSSW's) and magnetostatic forward and backward volume waves (MSFVW's and MSBVW's), which are dispersive, with the orientation of the internal bias field relative to the YIG film and the propagation direction determining which particular wave-type can exist. With the advent of low-loss high-quality epitaxial YIG films, these three MSW's have assumed enhanced significance and are, indeed, the basis for the growing current interest in exploiting MSW's for performing analog signal processing directly at microwave frequencies. The assumption made in the DE study of a uniform internal bias field in the YIG medium makes for enormous simplicity in analysis and, for YIG films (unlike bulk YIG), is an excellent one. The resulting simplicity and high accuracy of medium characterization for YIG films has led to close agreement between theory and experiment in a variety of MSW studies[2] and has spurred the growth of interest in MSW technology.

The DE work has subsequently been extended to studies of: i) MSW dispersion control techniques utilizing ground-plane placement in close proximity to the YIG film[3-6] or a layered geometry comprised of two or more YIG films[7]; ii) beam steering[8] and diffraction effects[9,10]; iii) finite-width waveguide effects[11]; and iv) propagation in inhomogeneously biased films[12]. The present paper is limited to a treatment of the propagation characteristics of the MSW modes of a single,

homogeneously-magnetized, infinite YIG film, i.e., effects due to the finite width of a YIG film, inhomogeneous bias field or the layering of two or more YIG films are excluded.

For the sake of generality, a two-ground-plane configuration is considered wherein a perfectly conducting ground plane is placed at an arbitrary distance on each side of the YIG film. The commonly used internal bias field orientations are treated, viz., H_o normal to the YIG film (MSFVW configuration) and H_o tangential to the YIG film (MSBVW and MSSW configurations). While the former bias-field orientation permits the existence solely of MSFVW's, with the latter bias-field orientation only MSBVW's can exist for propagation directions lying within an angle zone bisected by the bias-field direction and only MSSW's can exist for propagation directions lying within an angle zone bisected by an inplane normal to H_o.

Unlike the MSFVW, which is isotropic in the plane of the YIG film, the MSSW and MSBVW are anisotropic and exhibit a pronounced beam-steering effect that is reminiscent of the divergent lens effect in optics[13]. Since beam steering accentuates diffraction loss and is, therefore, undesirable for most applications, the MSSW and MSBVW experimental configurations usually utilize propagation along "pure-mode" directions, defined as propagation directions for which the phase and group velocities are collinear. The terminology "pure-mode directions" is borrowed from microwave acoustics[14]. The pure-mode directions for the MSBVW and MSSW are propagation along and at right angles, respectively, to a tangential bias field. While the MSSW and MSBVW propagation characteristics problems are solved for arbitrary propagation directions, the computations presented here emphasize the pure-mode directions.

In addition to being anisotropic, the MSSW's are nonreciprocal. In the absence of ground planes, the MSSW nonreciprocity is purely of the field displacement type, i.e., a switch occurs, with reversal in propagation direction or in bias field direction, in field localization from one YIG surface to the other, with the wavenumber for opposite directions of propagation being degenerate. The presence of a ground plane, while maintaining the field-displacement-type nonreciprocity, additionally removes this wavenumber degeneracy. MSBVW's are reciprocal for propagation along the pure-mode direction but exhibit a nonreciprocity for other directions of propagation provided at least one ground plane is present.

The frequency spectra of MSFVW's and of MSBVW's propagating along the pure-mode direction coincide with the spectrum over which magnetostatic plane waves (MSPW's) are of the homogeneous variety. As the MSBVW propagation direction is shifted away from the pure-mode direction, the lower bound of the MSBVW spectrum moves up but the upper bound remains invariant. The frequency spectrum of MSSW's is located immediately above the MSVW spectrum. As the MSSW propagation direction is shifted away from the pure-mode direction, the upper bound of the MSSW spectrum moves down but the lower bound remains invariant. On the other hand, for a given MSSW propagation direction, the upper bound of the MSSW spectrum is lifted monotonically as a ground plane is brought in towards the YIG surface of MSSW localization. The bounds of the MSVW spectra are unaffected by the presence of a ground plane.

II. MSW FIELD EQUATIONS

MSW's are electromagnetic (or spin) waves in a magnetically biased ferrite medium whose wavelengths are sufficiently small to permit the neglect of the retardation effect and yet sufficiently large to permit the neglect of the exchange effect. The first condition simplifies the Maxwell curl h equation to

curl $\underline{h}\approx o$ (1)

so that $\underline{h}$ may be expressed as the gradient of a scalar potential, i.e.,

$\underline{h}=-\text{grad } \phi$.   (2)

The second condition simplifies the spin equation of motion

$\partial \underline{M}/\partial t =- \gamma\mu_o \underline{M} \times \underline{H}_{eff}$ (3)

in that the space-dependent exchange field $\underline{h}_{exc}$ in the effective magnetic field $\underline{H}_{eff}$ may be ignored, yielding

$\underline{H}_{eff} \simeq \underline{H}_o + \underline{h}$.   (4)

In Eq. (3), $\gamma=2.8\text{MHz/G}$ is the gyro-magnetic ratio, μ_o is the permeability of free space and $\underline{M}$ is the magnetization vector. The dc bias field $\underline{H}_o$ in Eq. (4) will be taken to be z-directed and to saturate the sample, producing a z-directed saturation magnetization $\underline{M}_o = M_o \underline{z}$. The expression for $\underline{H}_{eff}$ in Eq. (4) which assumes a source-free problem and that the magnetic anisotropy and magnetoelastic fields may be ignored, is adequate for highlighting all the gross features of MSW's. Under small-signal conditions and for time-harmonic variation $\exp(j\omega t)$, Eq. (3) may be linearized to yield the constitutive relation

$\underline{b}\equiv\mu_o(\underline{h}+\underline{m}) = \mu_o \underset{\sim}{\mu}\cdot\underline{h}$ (5)

where the relative permeability tensor $\underset{\sim}{\mu}$ has the expression

$\underset{\sim}{\mu} = \mu(\underline{x}_o\underline{x}_o+\underline{y}_o\underline{y}_o) - j\kappa(\underline{x}_o\underline{y}_o - \underline{y}_o\underline{x}_o) + \underline{z}_o\underline{z}_o$ (6)

with

$\mu = (\omega_3^2-\omega^2)/(\omega_o^2-\omega^2)$ (7a)

and

$\kappa =-\omega_M\omega/(\omega_o^2-\omega^2)$.   (7b)

In Eq. (7), $\omega_3=[\omega_o(\omega_o+\omega_M)]^{\frac{1}{2}}$ with $\omega_o=\gamma\mu_o H_o$ (gyro-frequency) and $\omega_M=\gamma\mu_o M_o$ (magnetization frequency). An important simplification arising from the neglect of the exchange effect is that the elements μ and κ of the linearized constitutive parameter $\underset{\sim}{\mu}$ characterizing the YIG medium, while being functions of ω, ω_o and ω_M, are independent of the MSW wavenumber k.

The complete set of MSW field equations is comprised of Eq. (2), the Maxwell div $\underline{b}$ = o equation which may be rewritten as

$[\mu(\partial^2/\partial x^2 + \partial^2/\partial y^2) + \partial^2/\partial z^2] \phi=o$ (8)

and the Maxwell equation

curl $\underline{e} =- j\omega\underline{b}$ (9)

which yields the electric field $\underline{e}$ associated with a MSW once ϕ is found by solving Eq. (8) subject to appropriate boundary conditions.

III. MAGNETOSTATIC PLANE WAVES (MSPW's)

The simplest MSW is a uniform plane wave. The instantaneous spin distribution in such a wave is shown in Fig. 1 for the case of propagation in an arbitrary direction at an angle θ to the bias field. Since $\underline{H}_o$ defines an anisotropy or symmetry axis, the propagation characteristics of magnetostatic plane waves (MSPW's) depend only on θ. Thus, no loss of generality arises in making the assumption that the

189

MSPW's propagate in the xz plane with the harmonic plane-wave dependence $\exp j(\omega t - \underline{k} \cdot \underline{r})$ where $k = k_x \underline{x}_o + k_z \underline{z}_o$. The MSW field equation(8) then yields the MSPW dispersion relation which has the polar form

$$\omega^2 = \omega_o(\omega_o + \omega_M \sin^2\theta).\tag{10}$$
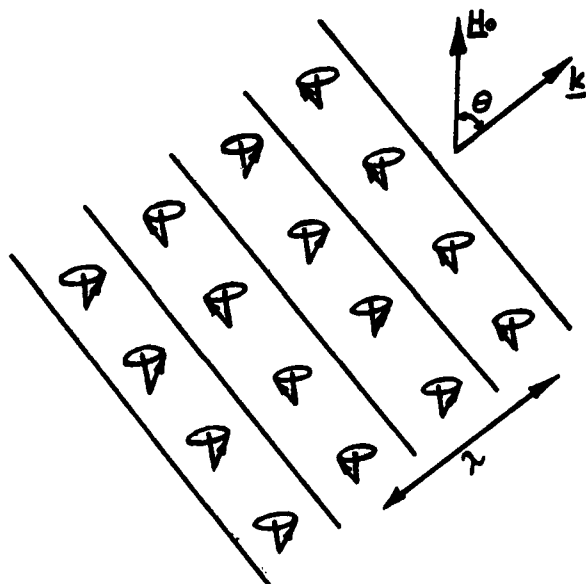
Fig. 1. Instantaneous spin distribution in a uniform MSPW propagating at an arbitrary angle θ relative to the bias field $\underline{H}_o$.

Equation (10) shows that ω depends only on the angle of propagation θ but not on k (see Fig. 2) and that the MSPW's are homogeneous within the spectrum $\omega_o < \omega < \omega_3$ but inhomogeneous outside. Since guided MSW's in a planar geometry are synthesized from MSPW's, it follows that guided MSW's can be of the volume-wave variety only within this spectrum (called the MSVW spectrum) and of the surface-wave variety only outside of this spectrum. It turns out that, when the boundary-value problem associated with MSW's in a YIG film is solved, volume waves of the forward and backward types are found to exist with spectra coinciding with or lying within the MSVW spectrum and a surface wave is found to exist within a frequency band (the MSSW spectrum) located immediately above the MSVW spectrum. Thus, although the MSPW is of the inhomogeneous variety for all frequencies outside of the MSVW spectrum, boundary conditions for a surface-wave solution are only satisfied within the MSSW spectrum.
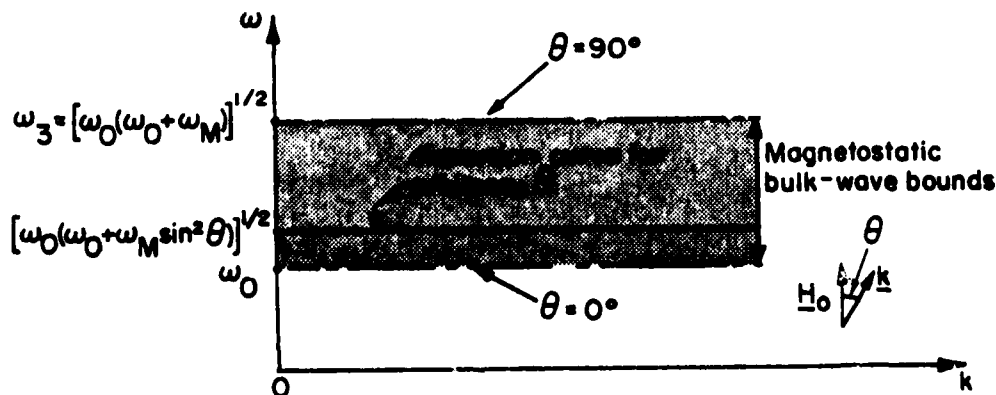
Fig. 2. Qualitative dispersion diagram for MSPW's

A constant-frequency locus of the dispersion relation (10) in the wave-vector or $\underline{k}$ space (the so-called wave-vector or refractive-index diagram) is readily seen

to be a cone with its axis lying along the k_z axis and the apex located at the origin. This simply means that the MSPW propagates at a fixed angle $\theta = \tan^{-1}(-\mu)^{-\frac{1}{2}}$ from $\underline{H}_o$ for a given frequency within the MSVW spectrum.

IV. GUIDED MSW'S IN A YIG FILM GEOMETRY

A. Dispersion relations

A two-ground-plane geometry is considered which is comprised of a YIG film of thickness d and two perfectly conducting ground planes spaced, respectively, by distances h and w from the opposite surfaces of the YIG film (see Fig. 3). A right-handed co-ordinate system is chosen with the x axis normal to the film for the MSSW and MSBVW configurations and with the z axis normal to the film for the MSFVW configuration. The bias field is taken to be z-directed in all the configurations so that the expression for the permeability tensor in Eq. (6) is invariant with rotation of the co-ordinate system. The MSFVW propagation direction is taken, with no loss of generality, to be along the x axis, i.e., the MSFVW propagation factor is expj(ωt-kx). For the MSSW and MSBVW configurations, the propagation is taken to be in an arbitrary direction in the yz plane, i.e., the corresponding propagation factor for these waves is expj(ωt-k_yy-k_zz). The distinction between the MSSW and MSBVW configurations lies in the choice of hyperbolic or sinusoidal variation of fields across the YIG film corresponding, respectively, to $\mu > o$ and $\mu < o$. While the fields in the air and GGG regions are a sum of two inhomogeneous MSPW's, in the YIG region the fields are a sum of two inhomogeneous MSPW's for MSSW's but of two homogeneous MSPW's for the MSFVW's and MSBVW's. By subjecting the general guided MSW field solutions, obtained by superimposing the plane-wave solutions of the MSW field equation (8) for the YIG region and the corresponding field equation for the air and GGG regions obtained by setting μ=1 in Eq. (8), to the boundary conditions, viz., the continuity of potential ϕ and normal magnetic induction b_n at the interfaces between air or GGG and YIG and the vanishing of b_n at the ground planes, the following dispersion relations are readily derived:

MSSW $\quad \tanh \xi kd = - \dfrac{\mu\xi(\tanh kh + \tanh kw)}{[\tanh kh \tanh kw + \kappa k_y'(\tanh kh - \tanh kw) + (\mu^2\xi^2 - \kappa^2 k_y'^2)]}$ (11)

MSFVW $\quad \tan \beta kd = - \dfrac{\beta(\tanh kh + \tanh kw)}{(\tanh kh \ \tanh kw + \mu)}$ (12)

The bias field $\underline{H}_o = H_o \underline{z}_o$ is applied along z axis in a right-handed co-ordinate system for all three configurations. The propagation is along x for MSFVW and in an arbitrary direction in the yz-plane for MSSW and MSBVW.

Fig. 3. The guided MSW two-ground-plane geometry.

191

MSBVW $\tan \eta kd = - \dfrac{\mu\eta(\tanh kh + \tanh kw)}{[\tanh kh \tanh kw + \kappa k_y'(\tanh kh - \tanh kw) - (\kappa^2 k_y'^2 + \mu^2\eta^2)]}$ (13)

In Eqs. (11) and (13), $k=(k_y^2+k_z^2)^{\frac{1}{2}}$, $\xi=[k_y'^2+(k_z'^2/\mu)]^{\frac{1}{2}}$, $\eta=[(k_z'^2/\beta^2)-k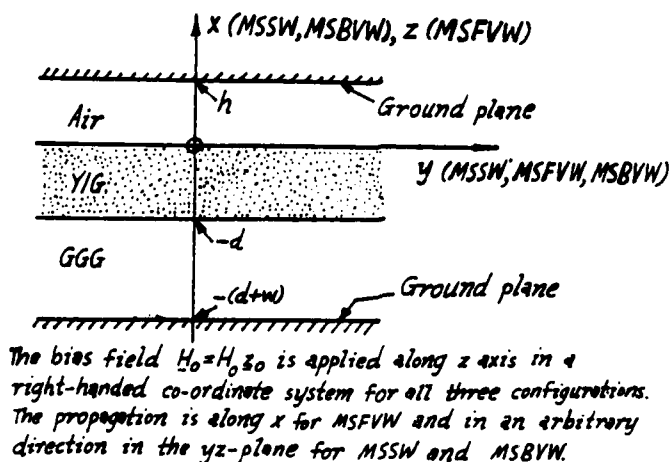_y'^2]^{\frac{1}{2}}$, $k_y'=k_y/k$, $k_z'=k_z/k$ and $\beta=(-\mu)^{\frac{1}{2}}$. The latter expression for β also applies to Eq. (12).

The special cases of Eqs. (11) and (13) corresponding to propagation along the pure-mode directions are

MSSW $\tanh kd = - \dfrac{\mu(\tanh kh + \tanh kw)}{[\tanh kh \tanh kw + \kappa(\tanh kh - \tanh kw) + (\mu^2-\kappa^2)]}$ (14)

MSBVW $\tan (kd/\beta) = \dfrac{\beta(\tanh kh + \tanh kw)}{(\tanh kh \tanh kw + \mu)}$.   (15)

The similarity between the MSSW and MSBVW dispersion relations (11) and (13) is expected since both relations refer to guided wave propagation in the same plane. A simple transformation of the MSFVW dispersion relation (12) is seen to yield the MSBVW dispersion relation (15) for propagation along the pure-mode direction. The transformation consists simply of substituting $1/\beta$ and β for β in the argument of the tangent function and $-\beta$ on the right-hand side of Eq. (12), respectively.

The dispersion relations for MSFVW's and pure-mode MSSW's and MSBVW's in a YIG film geometry without ground planes are obtained by simply letting $h \rightarrow \infty$ and $w \rightarrow \infty$ in Eqs. (12), (14) and (15) so that the right-hand side of each of these equations becomes independent of k. The latter simplification permits the dispersion relations to be written as

MSSW $k = \dfrac{1}{2d} \ln \dfrac{(\omega_M/2)^2}{[\omega_0+(\omega_M/2)]^2-\omega^2}$ (16)

MSFVW $k = (\beta d)^{-1} \tan^{-1} [-2\beta/(1+\mu)]$ (17)

MSBVW $k = (\beta/d) \tan^{-1} [2\beta/(1+\mu)]$ (18)

The dispersion relations (16)-(18) clearly do not require the use of an iterative procedure in a numerical determination of k. A similar simplification to Eqs. (16)-(18) obtains for a single-ground-plane configuration wherein the YIG film is directly metallized on its exposed surface. For all other cases, an iterative procedure would require to be used for a numerical determination of the dispersion characteristics.

The MSSW and MSBVW dispersion relations (11) and (13) are invariant under the substitution $k_z \rightarrow -k_z$ or the joint substitution $k_y \rightarrow -k_y$ and $H_0 \rightarrow -H_0$ (or $\kappa \rightarrow -\kappa$). The latter joint substitution implies nonreciprocal propagation, i.e., the MSSW or MSBVW wavenumber k is changed with a reversal effected in $\underline{H}_0$ without a reversal in k_y or equivalently with a reversal effected in k_y without a reversal in $\underline{H}_0$. If both ground planes are removed to infinity, the term proportional to κk_y in Eqs. (11) and (13) vanishes so that the k solutions to these equations for opposite directions of the bias field are degenerate. For such an ungrounded YIG film, while the MSBVW is always reciprocal, in the case of MSSW a nonreciprocity is still present which is

192

purely of the field-displacement type, i.e., the MSSW is localized at opposite surfaces of the YIG film for opposite directions of the bias field. If a ground plane is present, then the MSSW nonreciprocity is due both to the field-displacement effect as well as the nondegeneracy in k arising from a reversal in the bias field direction. Nonreciprocity in MSBVW propagation is seen to obtain only for propagation directions other than the pure-mode direction[15].

The effect of varying the thickness of the YIG film on the dispersion characteristics of the MSW's is readily seen from the dispersion relations (16)-(18) for a geometry without ground planes. The result that the wavenumber k at a given frequency varies inversely with d applies also when ground planes are present.

Equation (16) shows that the wavenumber k (as well as the derivative $dk/d\omega$) for the pure-mode MSSW in a geometry without ground planes increases monotonically from zero as the frequency ω is increased from ω_3, with a resonance corresponding to $k \to \infty$ obtaining at $\omega = \omega_0 + (\omega_M/2)$. The same result is obtained for a MSSW in a single-ground-plane or two-ground-plane configuration as long as the ground plane placed on the side of YIG surface of MSSW localization (if any) is electrically far away. A real solution k does not obtain outside of the spectrum $\omega_3 < \omega < \omega_0 + (\omega_M/2)$ which is called the MSSW spectrum corresponding to MSSW localization at an ungrounded YIG surface. On the other hand, the MSSW spectrum corresponding to MSSW localization at a metallized YIG surface with h=o is considerably wider, extending from $\omega = \omega_3$ where k=o to $\omega = \omega_0 + \omega_M$ where k exhibits a resonance ($k \to \infty$).

The transcendental nature of the MSFVW and MSBVW dispersion relations implies that an infinite number of modes can in principle exist. The dispersion curve for any particular MSFVW (or pure-mode MSBVW) mode corresponds to a monotonic increase (or decrease) in k and $dk/d\omega$ with increasing frequency over the MSVW spectrum, with a resonance ($k \to \infty$) occuring at the upper (or lower) bound of the MSVW spectrum. Note that the names forward and backward volume waves refer, respectively, to the phase and group velocities being co-directed or contra-directed. As the mode number for MSFVW or MSBVW is increased at a fixed frequency, the dispersion curve shifts in the direction of increasing k except for being pinned at the k=o point at $\omega = \omega_0$ (MSFVW) or $\omega = \omega_3$ (MSBVW). The dispersion curves for the non-pure-mode MSBVW's are similar to the dispersion curve for the pure-mode MSBVW except for the property that the resonance frequency goes up as the angle of propagation from the bias-field direction is increased.

B. Dispersion diagrams

The qualitative features of the MSSW and MSBVW dispersion diagrams corresponding to propagation in an arbitrary direction are shown in Figs. 4 and 5, respectively. While a single-ground-plane configuration is assumed in Fig. 4 with h=o and $w = \infty$, the dispersion curves in Fig. 5 are essentially the same with or without ground planes. The quantity ψ in Figs. 4 and 5 represents the propagation angle measured from the bias-field direction, with ψ_0 being the cut-off angle.

The resonance frequency for MSSW propagating at an arbitrary ψ is given simply[16] by the solution of the dispersion relation for MSSW's on a metallized or unmetallized YIG half-space which takes the form

$$(\mu^2 + \mu \cot^2 \psi)^{\frac{1}{2}} - \kappa + g = 0 \tag{19}$$

where g=o for MSSW localized at a metallized YIG surface and $g = (1 + \cot^2 \psi)^{\frac{1}{2}}$ for MSSW localized at an unmetallized YIG surface. A real solution ψ of Eq. (19) exists in in the frequency range $\omega_3 < \omega \leq \omega_0 + (\omega_M/2)$ for MSSW localized at an unmetallized YIG surface, with ψ increasing monotonically from $\psi_0 = \tan^{-1}(\omega_0/\omega_M)^{\frac{1}{2}}$ at $\omega = \omega_3$ to $\psi = 90°$ at $\omega = \omega_0 + (\omega_M/2)$. On the other hand, the solution of Eq. (19) for a MSSW localized at a metallized YIG surface has the simple expression

$$\psi = \cot^{-1}\{[(f_o+f_M)^2 - f^2]/(f^2-f_3^2)\}^{\frac{1}{2}} \qquad (20)$$

which indicates the existence of a real ψ for frequencies lying within the range $\omega_3 < \omega < \omega_o + \omega_M$, with ψ increasing monotonically from $\psi = o$ at $\omega = \omega_3$ to $\psi = 90°$ at $\omega = \omega_o + \omega_M$. Notice the MSSW wavenumber nonreciprocity (or nondegeneracy) imposed by the presence of a ground plane and that, while a MSSW localized at an unmetallized YIG surface can exist only over a limited angle zone that is bisected by the bias-field direction, a MSSW localized at a metallized YIG surface can propagate in all directions except $\psi = o°$.
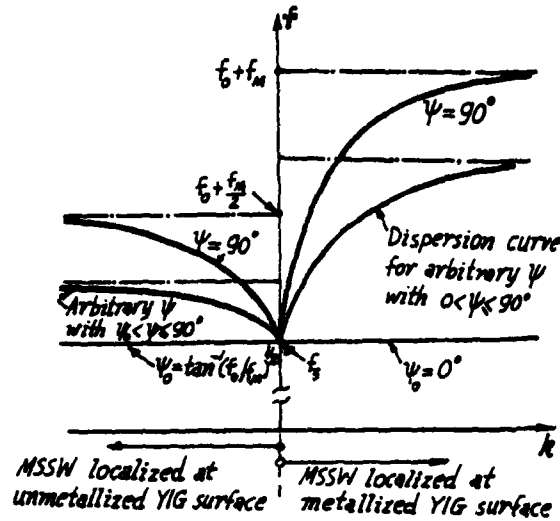
Fig. 4. Qualitative MSSW dispersion diagram for arbitrary propagation direction in a single-ground plane configuration with h=o and w=∞.
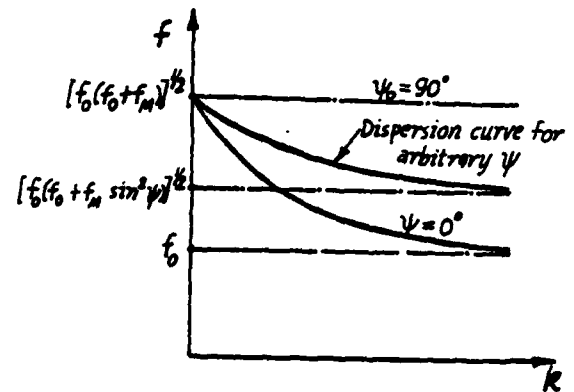
Fig. 5. Qualitative MSBVW dispersion diagram for arbitrary propagation direction.

The MSBVW has been shown[15] to exist for all propagation directions, with the resonance frequency for an arbitrary propagation angle ψ being $\omega = [\omega_o(\omega_o + \omega_M \sin^2\psi)]^{\frac{1}{2}}$.

The pronounced anisotropy of MSSW and MSBVW propagations is illustrated in the refractive-index diagrams given in Figs. 6 and 7, respectively. The computations of Fig. 6 and 7 as well as Figs. 10 to 16 are for a YIG film of thickness d=10μm, bias field $\mu_o H_o$ =500G and saturation magnetization $\mu_o M_o$ =1750G. While the curves in Fig. 6 are for a single-ground-plane configuration with h=o, the curves in Fig. 7 are for an unmetallized YIG film with h=∞ and w=∞ which supports reciprocal MSBVW's only. The portion of the MSBVW refractive index diagram in the third and fourth quadrants of Fig. 7 is thus simply the mirror image of the given portion in the k_y axis. The noncollinearity of the phase and group velocity vectors except for propagation along the pure-mode directions is evident from the recognition that the group velocity vector $v_g = \nabla_k \omega$ is normal to the refractive index curve and points in the direction in which the curve moves as the frequency is increased. In Fig. 6, the separation of the refractive-index curves for MSSW localized at a metallized YIG surface becomes accentuated as the frequency approaches $\omega = \omega_o + \omega_M$. Notice that the forward-wave and backward-wave characters of the MSSW and MSBVW, respectively, are exemplified by whether the phase velocity vector and the component along it of the group velocity vector are co-directed or contra-directed.

194
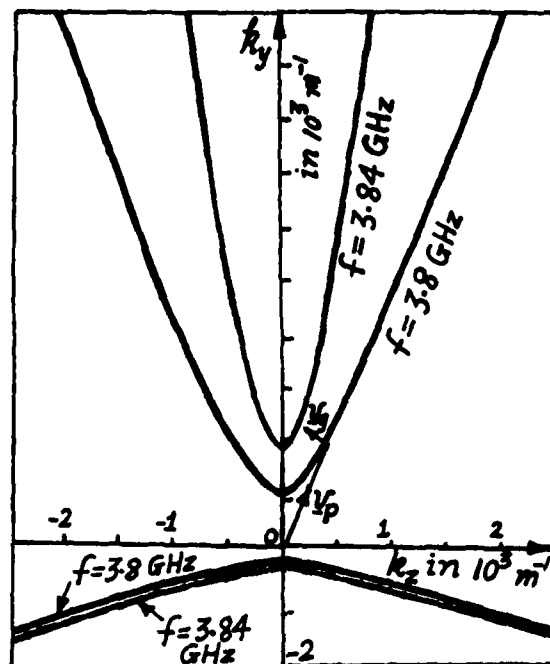
Fig. 6. Computed MSSW refractive-index curves
for f=3.8GHz and f=3.84GHz in a single-ground-
plane configuration corresponding to h=0 and
w=∞
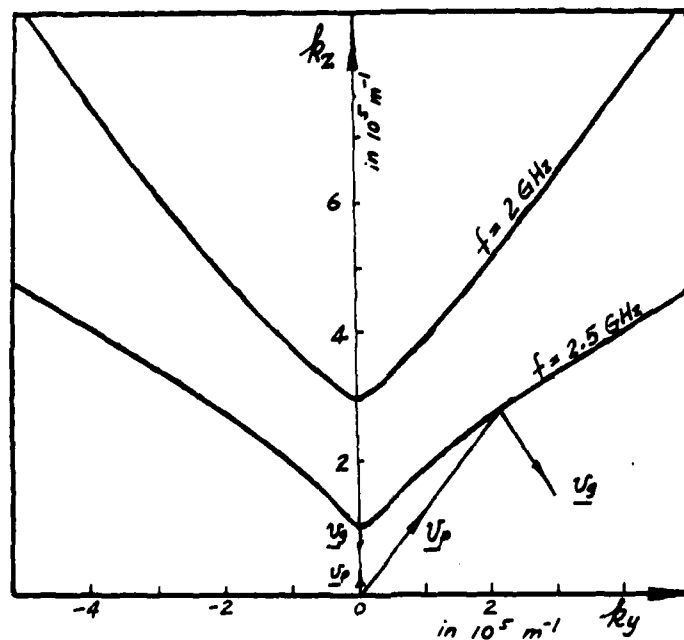
Fig. 7. Computed MSBVW refractive-index curves for f=2GHz and
f=2.5GHz in an ungrounded YIG film configuration.

195
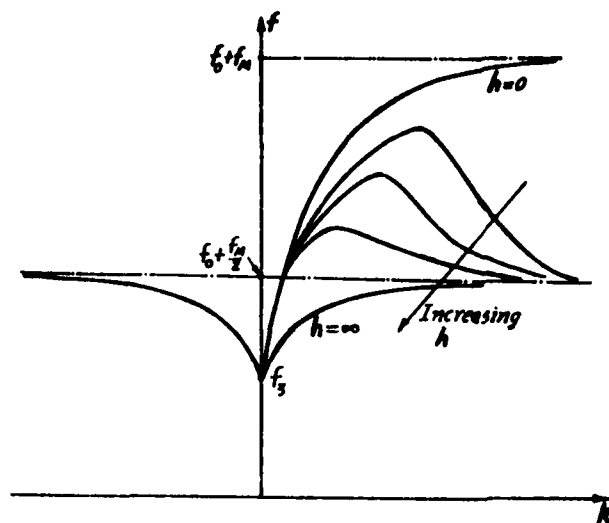
Fig. 8. Qualitative pure-mode MSSW dispersion curves in a single-ground-plane configuration with variable h.

In Fig. 8, the effect of moving the ground plane from h=o to h=∞ on the dispersion curves for pure-mode MSSW's in a single-ground-plane configuration are qualitatively illustrated. The effect appears primarily on the dispersion curve for MSSW localized on the YIG surface that is closer to the ground plane, and is readily interpreted from the limiting cases of MSSW dispersion characteristics corresponding to MSSW localization at a metallized and an unmetallized YIG surface. As k→o, the electrical separation kh of the ground plane with a finite physical separation h tends to zero, i.e., the MSSW assumes the properties of a MSSW localized at a metallized YIG surface. On the other hand, as k→∞, the same ground plane at physical separation h appears electrically to be removed to infinity, i.e., the MSSW assumes the properties of a MSSW localized at an unmetallized YIG surface. The limits of the dispersion curve at low and high values of k result in the MSSW assuming a backward-wave character at intermediate and high values of k, a feature that is accentuated as h is decreased. In practice, the frequency band over which the MSSW is of the backward wave variety is large only for h values of a few μm or less.
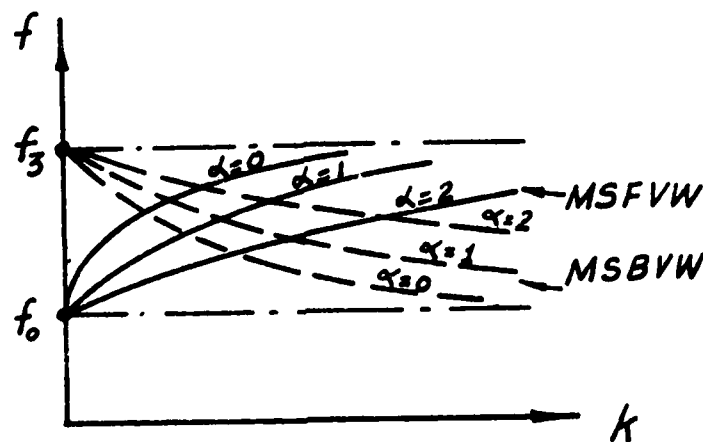
Fig. 9. Qualitative MSFVW and pure-mode MSBVW dispersion curves for the lowest three modes.

The dispersion curves for the lowest three MSFVW and pure-mode MSBVW modes are qualitatively illustrated in Fig. 9. While the MSVW's are analogous to the electromagnetic waveguide modes, a unique distinguishing feature of the MSVW dispersion curves is that they lie between the same frequency bounds, i.e., the MSVW spectrum, independent of the value of the mode number α, with each dispersion curve corresponding to a monotonic increase in k from the value k=o at one frequency bound to k=∞ at the other frequency bound. In Fig. 10, computed MSFVW dispersion curves are presented for the sake of quantitative illustration.
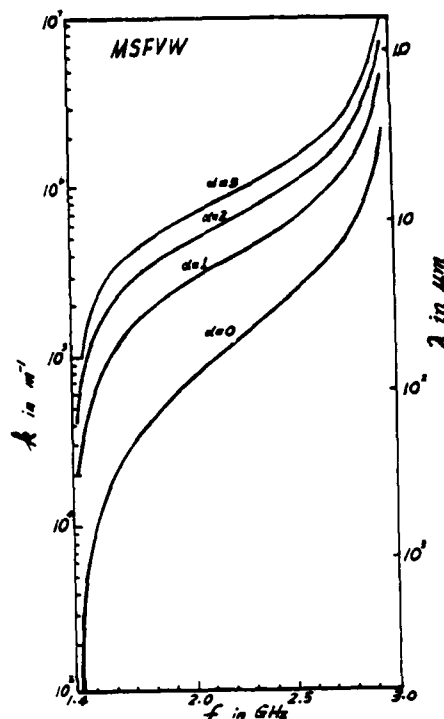
Fig. 10. Computed MSFVW dispersion curves for the lowest four modes in an ungrounded YIG film configuration.

Fig. 11. Computed frequency variation of group delay for the α=o MSFVW mode in a single-ground-plane configuration with variable h.

C. Dispersion control with ground planes

MSW dispersion control utilizing ground-plane placement in close proximity to the YIG film is illustrated in the computed group delay vs. frequency characteristics given for MSFVW's in Figs. 11 to 13 and for pure-mode MSBVW's in Fig. 14 where h is taken as a parameter. The computations of Figs. 11 and 12 are for the lowest (or α=o) MSFVW mode while those of Fig. 13 are for the α=1 MSFVW mode. A single-ground-plane configuration with w=∞ is assumed in the computations of Fig. 11 and a two-ground-plane configuration with w=550μm (which is a typical minimum value of the thickness of the GGG substrate that can be conveniently handled) is assumed in the computations of Fig. 12. In Fig. 11, the MSFVW group delay curves for finite values of h are seen to approach the h=o curve as ω→ω₀ and the h=∞ curve as ω→ω₃. The presence, for a range of h values, of constant group delay over a limited frequency band is evident at the low-frequency end of the MSVW spectrum for MSFVW's and at the high-frequency end for MSBVW's. The potential for achieving constant delay over a wider frequency band appears to exist with the α=1 MSFVW mode than with the α=0 MSFVW mode. Regions of linear dispersion are also seen to exist in Figs. 11 to 14. While the present results are indicative of the manner in which the placement of ground planes in close proximity to the YIG film affects the dispersion of MSW's, no attempt was made at optimizing parameter values. The use of ground planes for

197

realizing delay lines with constant delay or linear dispersion constitutes the most widely explored dispersion control technique, and close agreement between theory and experiment has been reported[5].
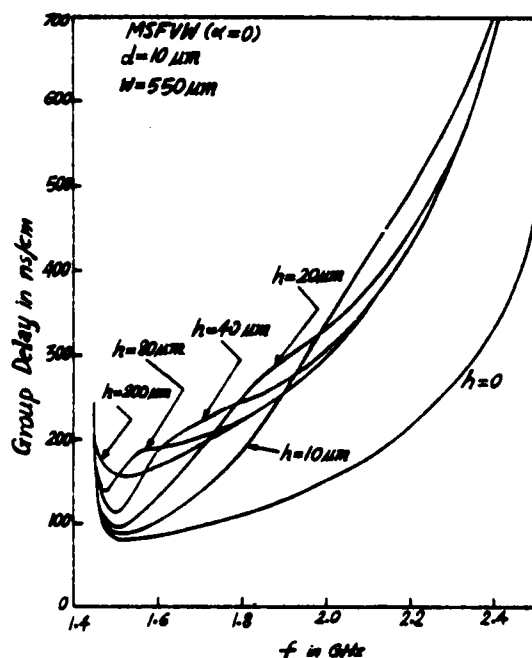
Fig. 12. Computed frequency variation of group delay for the $\alpha=0$ MSFVW mode in a two-ground plane configuration with w=550µm and h variable.
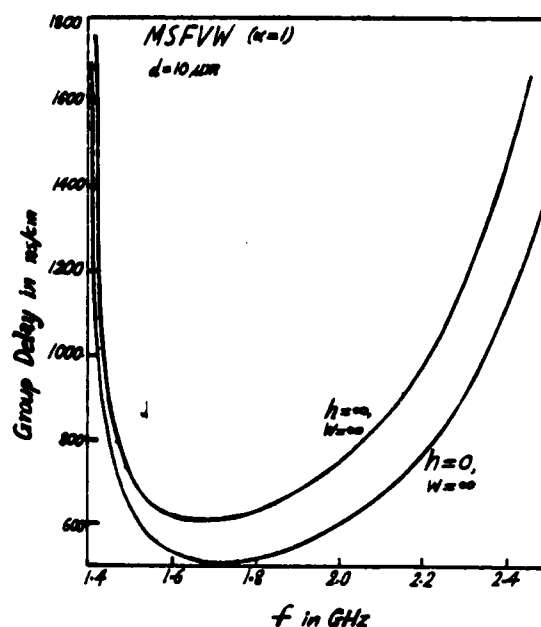
Fig. 13. Computed frequency variation of group delay for the $\alpha=1$ MSFVW mode.

D. Polarization characteristics

The MSW field or polarization profiles across the YIG film are readily computed from the field equations pertinent to specific configurations. Illustrative field profiles are presented for pure-mode MSSW's in Fig. 15 and for MSFVW's in Fig. 16. For the sake of simplicity, an ungrounded YIG film configuration is assumed in the computation of these figures. The MSSW computations in Fig. 15 are for a frequency f=3.75GHz which corresponds to a MSSW wavelength $\lambda=60.8$µm that is slightly larger than six times the YIG film thickness d=10µm. The hyperbolic variation within, and exponential decay outside of, the YIG film of the h_x and h_y components of rf magnetic field are apparent in Fig. 15. The MSSW rf magnetic field is circularly polarized outside, and elliptically polarized within, the YIG film, with the magnetic field being right-elliptically polarized about H_o within the YIG film. The localization of MSSW at one surface of the YIG film, apparent in Fig. 15, becomes accentuated as the frequency approaches the upper bound of the MSSW spectrum.

The MSFVW field profiles, given in Fig. 16 for the lowest three $\alpha=0,1,2$ modes, are for a frequency f=1.5GHz. The MSFVW wavelengths for the three modes at this frequency are 122µm ($\alpha=0$), 84µm ($\alpha=1$) and 45µm ($\alpha=2$). MSFVW modes with even mode numbers, i.e., $\alpha=0,2,4,\ldots$, possess odd symmetry about the YIG film midplane in the rf magnetic field component h_z normal to the film but even symmetry in the rf magnetic field component h_x in the direction of propagation. On the other hand, the h_z and h_x field profiles for the MSFVW modes with odd mode numbers, i.e., $\alpha=1,3,5,\ldots$, are symmetric and antisymmetric, respectively, about the YIG film midplane. The problem of defining symmetric and antisymmetric MSFVW modes is resolved by recognizing that the Poynting vector in the air, YIG and GGG regions is proportional to
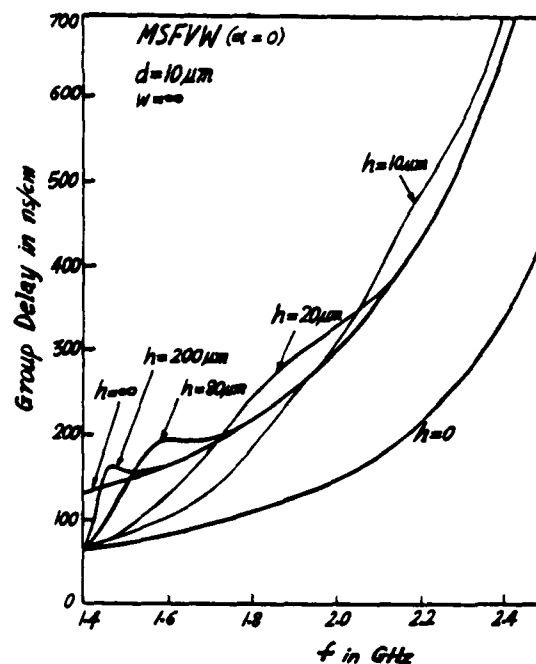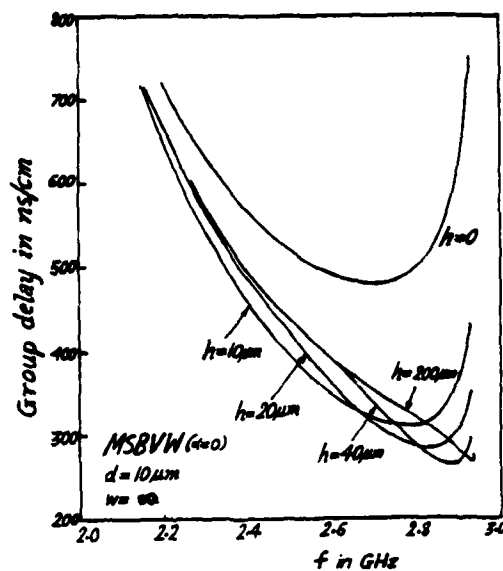
Fig. 14. Computed frequency variation of delay for the α=o MSBVW mode in a single-ground-plane configuration with variable h.
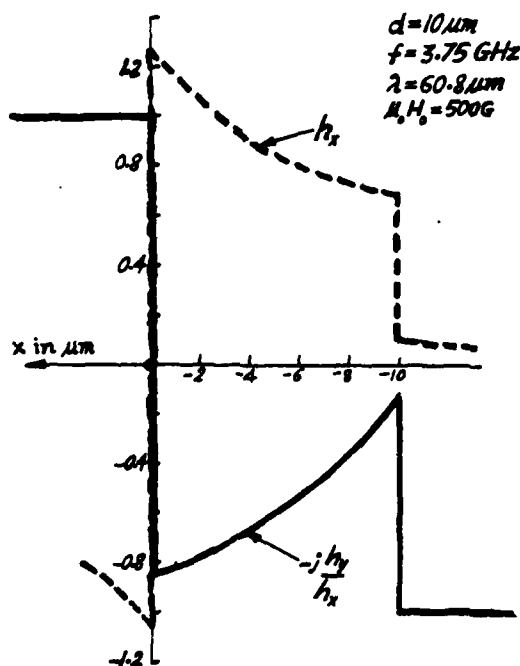
Fig. 15. Computed MSSW h_x and h_y profiles across the YIG film for an ungrounded YIG film geometry.

$|h_z|^2$. If the profile of h_z variation across the film is symmetric about the midplane of the YIG film, the mode in question is defined as a symmetric mode. A mode with antisymmetric h_z-profile is conversely defined as an antisymmetric mode. The qualitative symmetry properties of the h_z profiles in Fig. 16 are maintained as f is varied.
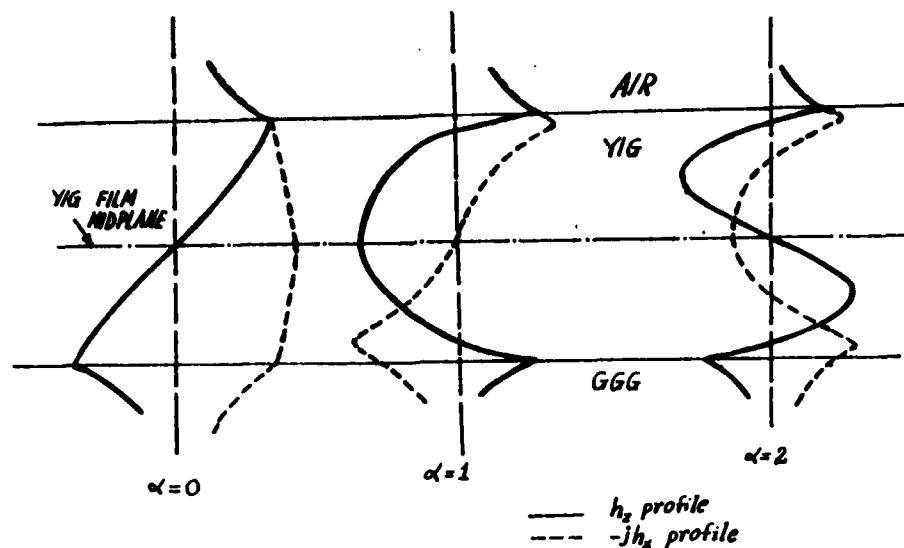
Fig. 16. MSFVW h_x and h_z profiles across the YIG film for the a=o, 1 and 2
modes in an ungrounded YIG film geometry.

REFERENCES

1. R.W. Damon and J.R. Eshbach, "Magnetostatic modes of a ferromagnet slab," J. Phys. Chem. Solids 19, 308 (1961)

2. J.M. Owens, R.L. Carter, C.V. Smith, Jr. and J.H. Collins, "Magnetostatic waves, microwave SAW's?," in Proceedings of the 1980 IEEE Ultrasonics Symposium

3. W.L. Bongianni, "Magnetostatic propagation in a dielectric layered structure," J. Appl. Phys. 43, 2541 (1972)

4. Z.M. Bardai, J.D. Adam, J.H. Collins and J.P. Parekh, "Delay lines based on magnetostatic volume waves in epitaxial YIG," AIP Conference Proc. 36, 268 (1976)

5. J.D. Adam, T.W. O'Keeffe and M.R. Daniel, "Magnetostatic wave devices for microwave signal processing," SPIE (Society of Photo-Optical Instrumentation Engineers) 241, 96 (1980)

6. J.C. Sethares, "Magnetostatics promise analog processing at microwave frequencies," Microwave Systems, p. 82, March 1981

7. L.R. Adkins and H.L. Glass, "Dispersion control in magnetostatic delay lines by means of multiple magnetic layer structures," in Proceedings of the 1980 IEEE Ultrasonics Symposium

8. F.A. Pizzarello, J.H Collins and L.E. Coerver, "Magnetic steering of magnetostatic waves in epitaxial YIG films," J. Appl. Phys. 41, 1016 (1970)

9. H.S. Tuan and J.P. Parekh, "Diffraction and beam steering of magnetostatic surface waves," in Proceedings of the 1980 Ultrasonics Symposium

10. J.P. Parekh and H.S. Tuan, "Beam steering and diffraction of magnetostatic backward volume waves," J. Appl. Phys. 52(3), 2279 (1981)

11. T.W. O'Keeffe and R.W. Patterson, "Magnetostatic surface-wave propagation in finite samples," J. Appl. Phys. 49(9), 4886 (1978)

12. F.R. Morgenthaler, "Synthesis of magnetostatic waves and modes using nonuniform bias fields," in Proceedings of the 1980 IEEE Ultrasonics Symposium

13. H.S. Tuan and J.P. Parekh, "Diffraction of magnetostatic surface waves," in this Proceedings of the RADC Microwave Magnetics Workshop (1981)

14. B.A. Auld, "Acoustic fields and waves in solids," J. Wiley and Sons (1973)

15. N.D.J. Miller, "Nonreciprocal propagation of magnetostatic volume waves," Phys. Stat. Sol. (a) 43, 593 (1977)

16. J.P. Parekh, "Magnetostatic surface waves on a partially metallized YIG plate," Proc. IEEE 61, 1371 (1973)

MSW-POTENTIAL SYSTEMS APPLICATIONS

Pradeep Wahi - Zygmond Turski
Litton Amecom
5115 Calvert Road
College Park, Maryland 20740

Electronic Warfare and Telecom systems operating at microwave frequencies often require low loss fixed and variable delay lines. Development of SAW devices addressed the needs in the low end of microwave spectrum, i.e., below 2 GHz. Bulk acoustic waves, however, have been successful above 2 GHz but these are quite expensive. The idea to use planar, SAW like technology above 2 GHz was revived with the appearance of MSSW devices.[1] Magnetostatic waves travel at velocities much slower than ordinary EM waves and an order of magnitude faster than the acoustic waves facilitating, therefore, realization of transducer geometeries. Of course, the ease of tuning the frequency with varying magnetic field makes MSW devices useful in many narrow band applications.[2]

Extensive work done indicates that all the magnetostatic modes are associated with varying degree of dispersion. The dispersion in three main modes, surface wave, forward volume wave and Backward volume wave, can be controlled by magnetic field, proximity of the ground plane and thickness of the film.[3]

Numerous papers have described applications necessitating either minimization or linearization of dispersion.[3,4] This paper describes two applications where dispersion is of great interest. In the first case only the magnitude of dispersion is important and the maximization of the dispersion was attempted. Preliminary results are presented.

1. Simultaneous Signals Separation - Although of general nature but with implications in EW systems is the ability to detect and characterize two or more simultaneous signals. Majority of the traditional receivers and spectrum analyzers would respond erroneously to such an input.

Highly dispersive delay line in front of the receiver could possibly lead to time domain separation of originally overlapping signals. Although investigated, the physical dimensions of a traditional quasi TEM delay lines were prohibitive. For example, line lengths greater than one meter would be needed to separate simultaneous signals, 200 MHz apart in frequency by only 5 ns in time domain using layered microstrip media.

Other dispersive transmission media for slow wave propagation such as helical guides and SAW devices were either narrow band or not suitable for microwave frequencies.

Laboratory applications of inherently dispersive Magnetostatic wave devices showed great promise. The preliminary results indicate that two simultaneous signals differing in frequency by less than 100 MHz can be easily separated by 40 - 50 ns depending upon the length of YIG film sample. Figure 1 shows separation of two signals, 400 MHz apart, using a one centimeter long delay line made from the sample film supplied by Allied Chemicals. No attempt was made to match the input/output couplers and no special terminations were used. A moderately low loss of 12 dB, mainly due to unmatched couplers, was observed over a band width of about 800 MHz.

Based upon the theoretical studies and initial experimental results a scheme has been proposed using a highly dispersive delay line to separate simultaneous signals as shown in Figure 2. Once again, dispersion should be maximum and not necessarily controlled for this application. Although an ample work is needed to precisely determine the effect of YIG film thickness on the dispersion and time bandwidth product and the development of the optimum, wide band transducer model, it seems that finally, a feasible signal processing scheme above 2 GHz has been unveiled.

2. MSW in Optical Communication - The optical data rates in future communication systems utilizing optical fibers will be inherently limited due to the spreading of the pulses resulting from dispersion in the low cost multimode fibers. The main dispersion mechanisms in fiber are related to waveguide effects, material properties and multimode propagation. Single mode fiber bandpass is limited primarily by material dispersion while multimode fiber bandpass is limited by the spread in mode group velocities. In most of the cases dispersion is characterized by the longer wave length components travelling faster than the shorter ones. In signal processing language this corresponds to upchirp response.

Various techniques have been proposed to compensate for this phenomenon including downchirping the modulation by propagating the light through metal vapors, a medium with opposite dispersion characteristics.[6] A scheme is being proposed to compensate for the pulse spreading using a magneto static wave device (Figure 3). The dispersion in MSW device corresponds to a downchirp response and is, therefore, of the opposite slope of that in optical fibers and it should be controlled and complimentarily matched to the chirped optical signal using device parameters such as the thickness of the film, proximity of the ground plane and an optimum design of the coupler. The device characteristics can be further matched by varying the magnetic bias field. The proposed scheme will prove especially useful in conjunction with low cost multimode fibers.

Acknowledgements

References

1. F. A. Olson and J. R. Yaeger "Microwave Delay Techniques using YIG"
    IEEE Transaction on Mic. Theo and Tech. Vol MTT-13, January 1965,
    p 63 - 69.

2. J. M. Owens, R. L. Carter, C. V. Smith and J. H. Collins "Magnetostatic
    Waves, Microwave SAW" Proceedings 1980 IEEE Ultrasonic Symposium,
    Boston, Mass.

3. W. L. Bongianni "Magnetostatic Propagation in Dielectric Layered
    Structure". Journal of Applied Physics Vol. 43, No. 6, June 1972,
    pp 25ul - 25 u8.

4. J. C. Sethares, C. V. Smith and J. M. Owens "MSW Time Delays"
    Proceedings 1980 IEEE Ultrasonics Symposium, Boston, Mass Paper No. E-3.

5. Thomas G. Giallorenzi "Optical Communication Research and Technology:
    Fiber Optics" Proceedings IEEE, Vol. 66, No. 7, July 1978 p 7uy-780.

6. "IBM Researchers Limit Dispersion in Glass Fibers" Optical Spectra
    February 81, p 42-u4.

—| |—
20NS

FIG 1: SIMULTANEOUS SIGNALS AT 2.4 AND 2.8 GHz
EXPERIMENTAL MSSW RESULTS
USING 1.2 CM LONG FILM
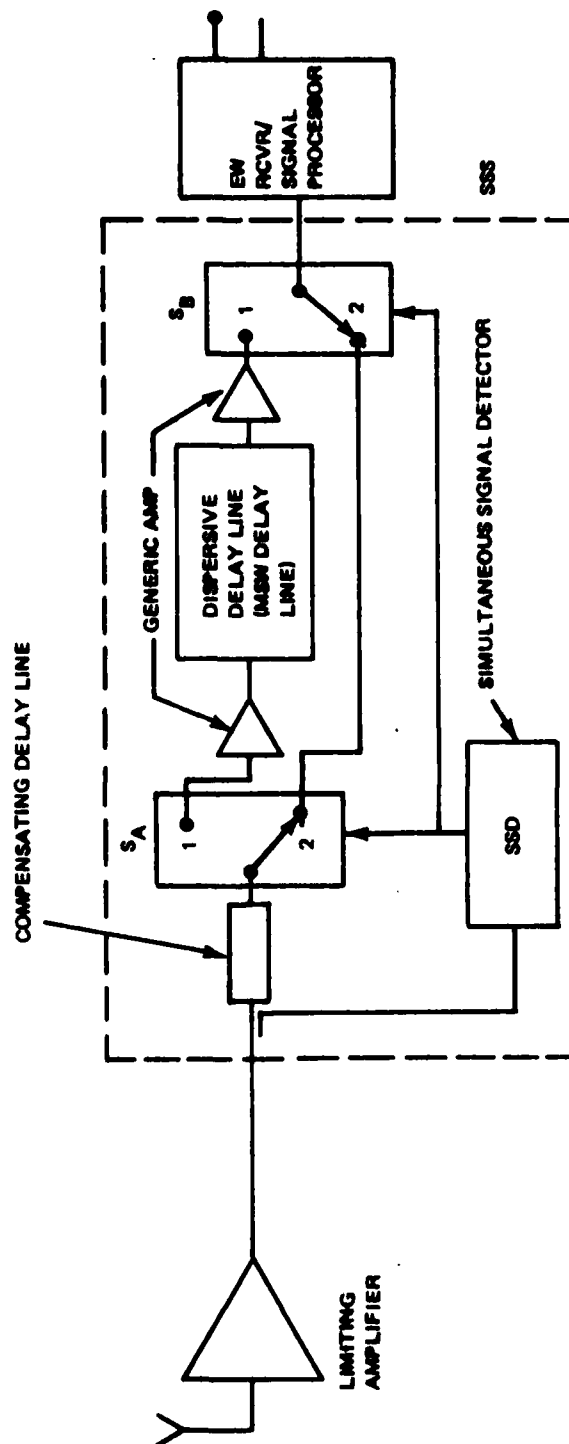
Figure 2. Simultaneous Signal Separator

MODULATING PULSES

LASER

OPTICAL FIBER

DISPERSED PULSE

DETECTOR

MS BVW DEVICE

COMPRESSED PULSE
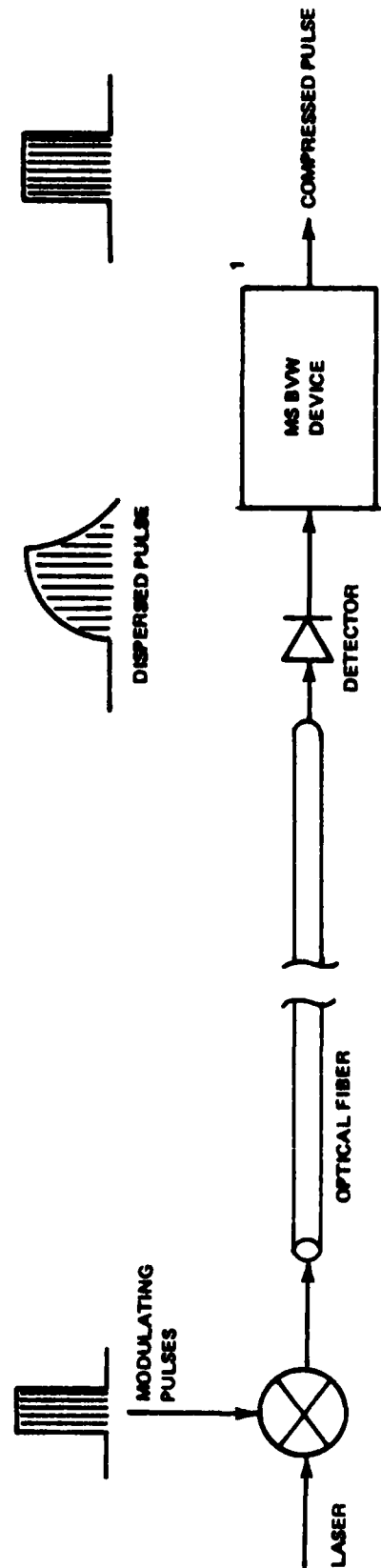
NOTE:

1. MAGNETOSTATIC BACKWARD VOLUME WAVE DEVICE

Figure 3. Magnetostatic Pulse Compression To Compensate The Broadening Of Pulses In Optical Fibers

206

DIFFRACTION OF MAGNETOSTATIC SURFACE WAVES

H.S. Tuan and J.P. Parekh
Department of Electrical Engineering
State University of New York at Stony Brook
Stony Brook, New York 11794

ABSTRACT

This paper reports theoretical computations of magneto-static-surface-wave (MSSW) diffraction resulting from the finite length of practical transducers and the pronounced anisotropy of MSSW propagation. The computed MSSW beam spreading is in good agreement with recently reported experimental results. While the MSSW's are found to suffer a significantly larger beam spreading than SAW's on YZ LiNbO$_3$, the total diffraction loss in a typical configuration comprised of two transducers on a YIG film spaced by a distance of 1cm, with both transducers having an overlapping aperture of 5mm, is at most in the order of a few dB. The diffraction loss is found to decrease with increasing frequency. The latter feature is consistent with the MSSW dispersion characteristics, viz, the MSSW wavelength decreases monotonically with increasing frequency. Thus, as the frequency is increased, a radiating MSSW transducer of given physical length becomes electrically longer so that MSSW collimation is improved and the diffraction loss is reduced.

INTRODUCTION

While a large body of literature exists on the diffraction and beam steering properties of surface acoustic waves (SAW's) on different piezoelectric substrates,[1] analogous calculations for magnetostatic waves (MSW's) have only recently begun to emerge.[2,3] Theoretical treatments of MSW transduction have hitherto assumed infinitely long transducers that radiate straight-crested waves so that the diffraction effects have been excluded. A theoretical calculation of MSW diffraction loss is clearly essential in delineating the minimum realizable insertion loss in a practical two-port structure. The present paper reviews a theory of MSW diffraction that is restricted to magnetostatic surface waves (MSSW's). The computed MSSW beam spreading is found to be in good agreement with recently reported experimental results.[4] The present computations show that the largest MSSW diffraction loss, occuring at frequencies near the lower-frequency bound of the MSSW spectrum, is in the order of a few dB in practical MSSW two-port structures. The MSSW diffraction loss is found to decrease with frequency, a feature explained in terms of improved MSSW collimation

at higher frequencies which is caused by the fact that, as the frequency is increased, the MSSW wavelength decreases so that the <u>electrical</u> length of a radiating transducer of given physical length is increased. The present diffraction loss results are in line with the experimental realization in a MSSW two-port structure of a minimum insertion loss of about 3dB.

THEORY

An ungrounded YIG film geometry is considered in which an electromagnetic transducer in the form of a microstrip of aperture 2a is placed directly on the top surface of the YIG film (see Fig. 1). The transducer is oriented to
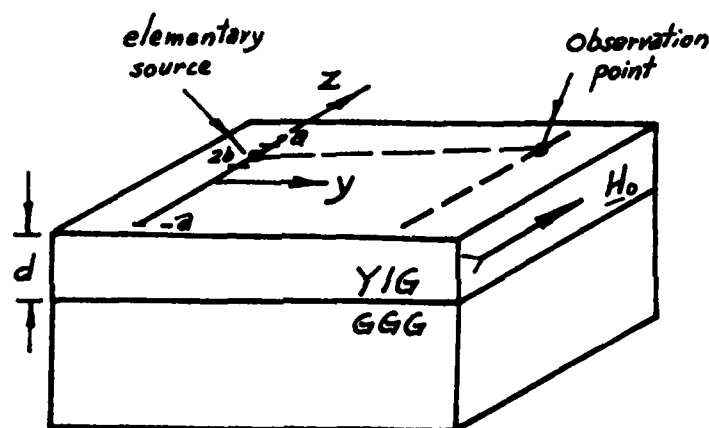
Fig. 1. Geometry of the Problem

lie parallel to a z-directed bias field $H_0\vec{z}_0$, with the desired direction of MSSW propagation being along the y direction.

The pronounced anisotropy of MSSW propagation is illustrated in the MSSW refractive-index diagram (or a constant-frequency locus in the k_y-k_z plane of the MSSW dispersion relation) given in Fig. 2 for an unmetallized YIG film. Only the portion of the MSSW refractive-index diagram in the first and fourth quadrants of the k_y-k_z plane is shown, with that in the second and third quadrants simply being the mirror image of the given portion about

208
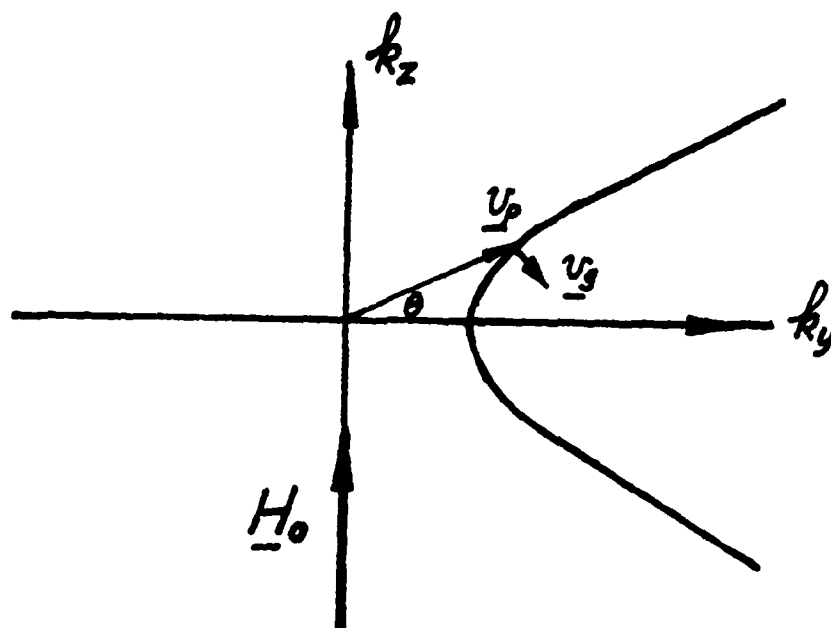
Fig. 2   Qualitative features of a MSSW refractive-index diagram.

the k_z axis.   The unique resonance behaviour of the MSSW gives
rise to the open branches of Fig. 2.   The noncollinearity of the phase and
group velocity vectors except for propagation along the y direction is evident
from the recognition that the group velocity vector $\underline{v}_g = \nabla_k \omega$ is normal to the
refractive-index curve and points in the direction in which the curve moves as
the frequency is increased.   As the frequency is increased, the refractive-
index curve in Fig. 2   shifts in the $+k_y$ direction and a simultaneous reduction
in the allowed angle zone of propagation that is bisected by the k_y axis takes
place. [5]

The monotonic decrease in MSSW phase velocity v_{ph} with increase in propa-
gation angle Θ measured from the y direction is reminiscent of the divergent-
lens effect in optics.   The divergent-lens effect is evidently accentuated
as the frequency is increased.

An exact field theory calculation of the MSSW radiation characteristics
of a finite microstrip transducer is extremely complicated.   Considerable

simplification is achieved in the present work by assuming a **uniform** aperture illumination, i.e., by assuming that the excited MSSW fields are constant at all points on the YIG surface directly below the transducer. This is an excellent assumption since in practice the length of the transducer is much shorter than the electromagnetic wavelength along its length, i.e., the current in the transducer is essentially constant over its length.

Since each elementary source radiates an angular spectrum of MSSW's, the total magnetostatic potential $\phi(y,z)$ at any point (y,z) on the surface of the YIG film may be written as

$$\phi(y,z) = (2\pi)^{-1} \int_{-\infty}^{\infty} \phi(k_z a) \exp[-j(k_y y + k_z z)] dk_z \qquad (1)$$

where

$$\phi(k_z a) = \int_{-a}^{a} \phi_s(z) \exp(jk_z z) dz \qquad (2)$$

is a weighting function which may be determined if the aperture illumination function $\phi_s(z)$ measured along the line $y=0$ is known. Although a uniform illumination function is assumed, i.e., ϕ_s = constant c_o for $|z| \le a$ and $\phi_s = 0$ for $|z| > a$, for all practical values of aperture 2a and separation distance y, a determination of $\phi(y,z)$ using Eq. (1) entails numerical integration. Note that, for the uniform aperture illumination case, Eq. (2) has the limiting expression $\lim_{a \to \infty} \phi(k_z a) = c_o \, \delta(k_z)$ which upon substitution into Eq. (1) yields the expected result that an infinite constant-current source oriented parallel to the z axis can only radiate a straight-crested wave in the y direction.

Considerable simplification is achieved in evaluating the integral in Eq. (1) by characterizing the MSSW refractive-index curve for a given frequency by the approximate expression

$$k(\theta) \approx k_o (1 + \Gamma \theta^2) \qquad (3)$$

where Γ is a constant and $k_o = 2\pi/\lambda_o$ is the MSSW wavenumber for the case of propagation along the y axis, i.e., $\theta=0$. By dividing the aperture 2a into 2m+1 elementary radiators each of length 2b (See Fig. 1) and employing the stationary phase integration technique, an explicit evaluation of the integral has been performed which yields

$$\phi(y,z) = \sum_{i=-m}^{m} \phi_i(y,z) \qquad (4)$$

210

where

$$\phi_i(y,z) = c_o A_1 A_2 \exp[-jk_o y f(\Theta_{si})/\cos \alpha_i] \tag{5}$$

The various quantities appearing in Eq. (5) have the expressions

$$\alpha_i = \tan^{-1}[(z-z_i)/y] \tag{6a}$$

$$\Theta_{si} = [Q-(Q^2+4\alpha_i k_2)^{1/2}]/2k_2 \tag{6b}$$

$$Q = k_2 \alpha_i + k_1 - 1 \tag{6c}$$

$$A_1 = 2k_o b\left(\frac{\sin\Theta_1}{\Theta_1}\right)h(\Theta_{si}) \tag{6d}$$

$$A_2 = [j\cos\alpha_i/(2\pi k_o y f''(\Theta_{si}))]^{1/2} \tag{6e}$$

$$f(\Theta_{si}) = (1+\Gamma\Theta_{si}^2)\cos(\Theta_{si}-\alpha_i) \tag{6f}$$

$$f''(\Theta_{si}) = [\Gamma(2-\Theta_{si}^2)-1-(8\Gamma^2\Theta_{si}^2)/(1+\Gamma\Theta_{si}^2)]\cos(\Theta_{si}-\alpha_i) \tag{6g}$$

$$\Theta_1 = k_o b(1+\Gamma\Theta_{si}^2)\sin\Theta_{si} \tag{6h}$$

$$h(\Theta_{si}) = 2\Gamma\Theta_{si}\sin\Theta_{si}+(1+\Gamma\Theta_{si}^2)\cos\Theta_{si} \tag{6i}$$

where z_i is the z co-ordinate of the center of the source element, Θ_{si} is the stationary phase point, and k_1 and k_2 (as well as Γ) are constants determined by the frequency f, film thickness d, bias field $\mu_o H_o$ and saturation magnetization $\mu_o M_o$.

NUMERICAL RESULTS AND DISCUSSION

Sample numerical computations indicating the nature of MSSW beam spreading are presented in Figs. 3 to 7 and Table I. The computations are for a YIG film of thickness d=21μm, bias field $\mu_o H_o$=375G, saturation magnetization $\mu_o M_o$=1750G and radiating transducer aperture 2a=4mm. The frequency bounds of the MSSW spectrum in the present work are 2.5GHz and 3.5GHz.

The computations of Figs. 3 and 4 are for signal frequency f=2.84 GHz which together with the foregoing parameter values corresponds to the parameters applicable to the reported experimental measurement employing an induction probe[4] of the beam spreading of a [$\bar{1}\bar{1}2$]-propagating MSSW with [$\bar{1}10$]-oriented tangential bias field. The constant k_o, Γ, k_1 and k_2 corresponding to Figs. 2 and 3 have values k_o=8590.8m^{-1} (λ_o=731.4μm), Γ=1.55, k_1=3.219 and k_2=1.0183. In Fig. 2, the diffraction or intensity profiles are given for three successive values of y, i.e., y_1=4.5mm, y_2=6.75mm and y_4=11.25mm. The computations yield
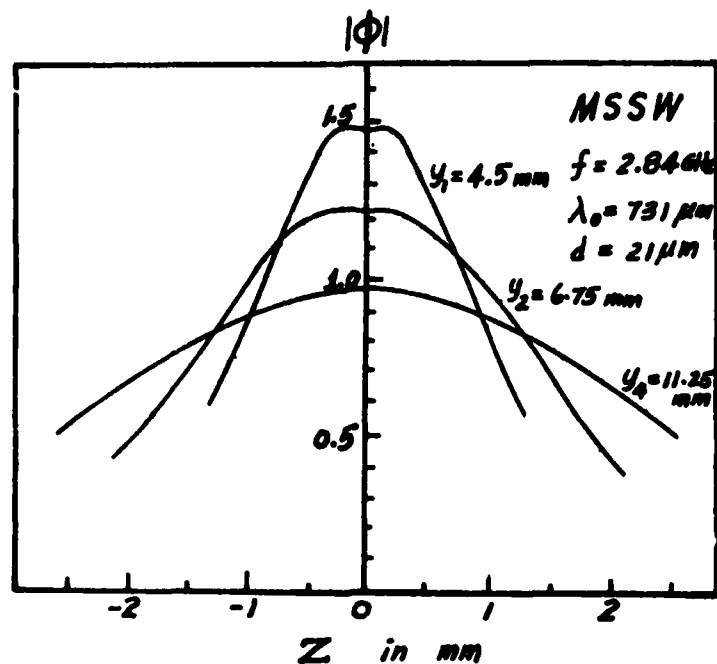
Fig. 3.   Computed MSSW diffraction patterns, i.e.
variation of $|\phi(y,z)|$ with z for fixed values of
y on the YIG surface.   The computations are for
f=2.84 GHz, 2a=4mm, d=10 μm, $\mu_o H_o$=375G and $\mu_o M_o$=1750G.

MSSW   f = 2.84 GHz
λ_o = 731 μm
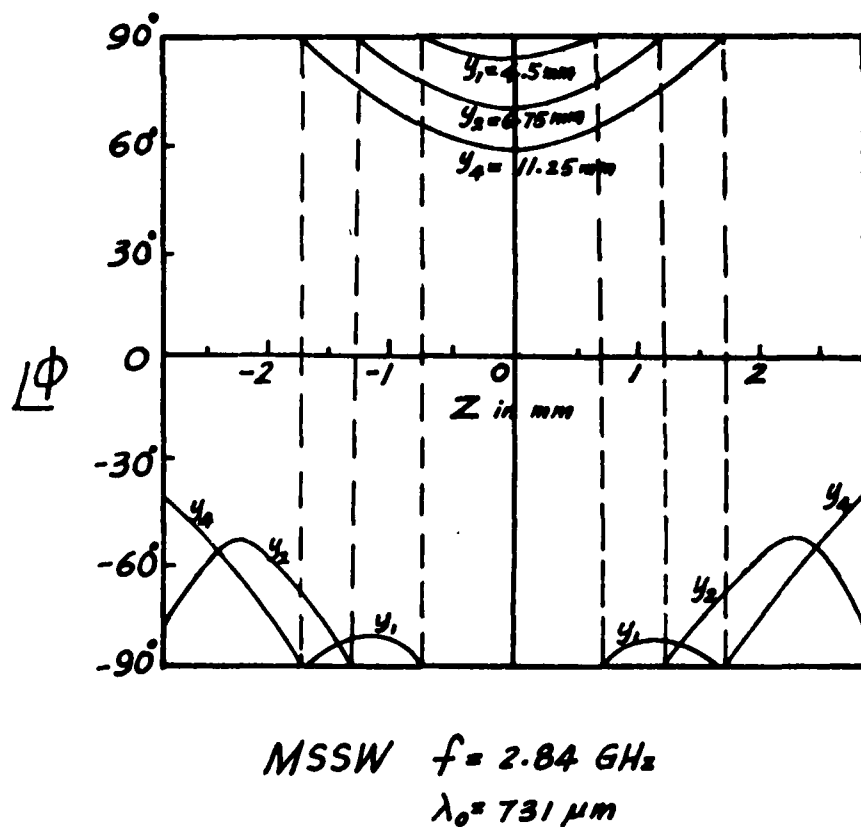
Fig. 4.   Computed z-variation of $\angle\phi(y,z)$ for fixed values
of y on the YIG film surface.   The computations are for the
same parameter values as Fig. 3.

212

$|\phi(y_2,0)|/|\phi(y_1,0)| = -1.5\text{dB}$ which is in good agreement with the corresponding experimentally measured value of amplitude decrement of $\simeq -1.7\text{dB}$. The agreement between theory and experiment on the beamwidth of the field intensity profiles is poorer than on the amplitude decrement with propagation. Thus, for example, the experimental and theoretical 3dB beamwidth values for $y=y_1$ are 2.535mm and 1.725mm, respectively, implying that the present theory predicts slower beam spreading than in the experiment. This discrepancy may be caused by the fact that, unlike the uniform aperture illumination assumed in the present work, the experimentally measured field intensity profile along a line parallel and close to the input transducer shows a monotonic decrease away from the center point of the transducer.

In Fig. 4, computed phase profiles, i.e., variation of $\angle\phi$ with z for fixed values of y, are given for f=2.84 GHz. In the large amplitude region of the diffraction profiles, the variation of phase with z, in agreement with expectation, is slow. The 180° phase change obtained in the phase profiles is not of much consequence since it affects only the "tail" or low-amplitude region of the corresponding diffraction profiles.

The frequencies corresponding to the field intensity profiles given in Figs. 5 to 7 are f=2.7 GHz, 3.0 GHz, and 3.25 GHz, respectively. In each of these figures, intensity profiles are given for four successive values of y, i.e., $y_1=4.5\text{mm}$, $y_2=6.75\text{mm}$ $y_3=9\text{mm}$ and $y_4=11.25\text{mm}$.

The frequency variation of MSSW diffraction loss is summarized in Table I for various fixed values of y. The diffraction loss is the ratio $P(y)/P(0)$ where $P(y)$ is the power intercepted at y by a receiving transducer with the same aperture 2a=4mm as the radiating transducer and $P(0)$ is the power emanating from the radiating transducer at y=0. It is readily seen that the diffraction loss may be expressed as $P(y)/P(0) = [\int_{-a}^{a}|\phi(y,z)|^2 dz]/[\int_{0}^{a}|\phi(0,z)|^2 dz]$ where $\int_{0}^{a}|\phi(0,z)|^2 dz = c_0^2 a$.

Two competing diffraction loss processes may be identified. One process is the divergent-lens effect which becomes accentuated, leading to increase in the corresponding diffraction loss component, as the frequency is increased. On the other hand, since the MSSW wavelength λ_0 decreases (or the electrical length of a radiating transducer of given physical aperture increases)
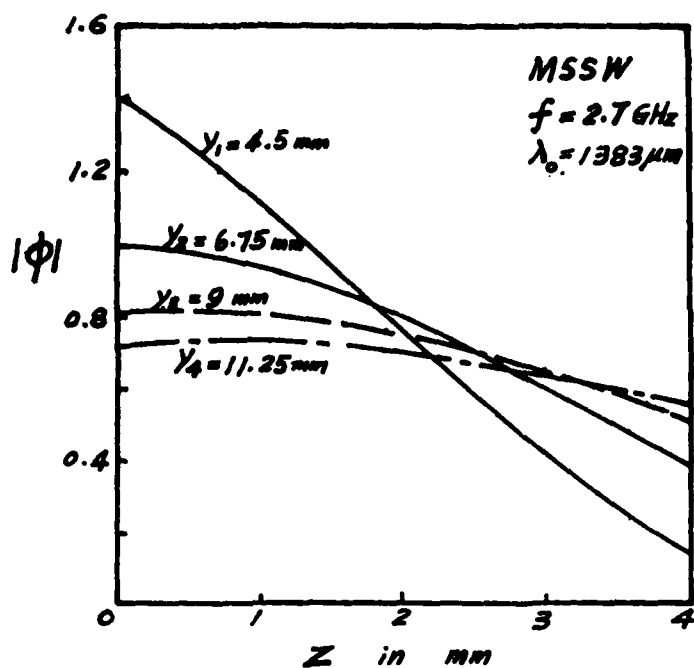
Fig. 5. Computed MSSW diffraction patterns for
signal frequency f=2.7GHz, with other parameters
same as for Fig. 3.
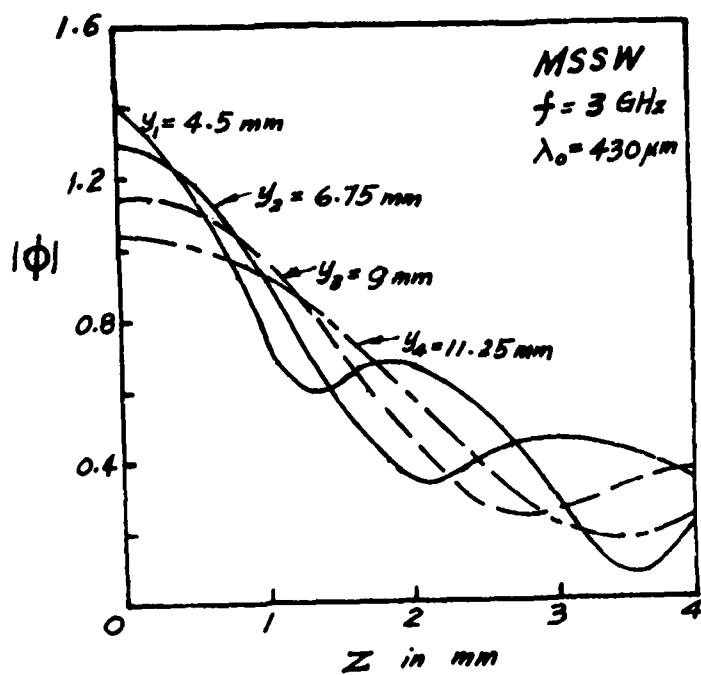
Fig. 6. Computed MSSW diffraction patters for
signal frequency f=3.0GHz, with other parameters
same as for Fig. 3.

214

monotonically with increasing frequency, improved MSSW collimation, leading
to decrease in the corresponding diffraction loss component, is obtained.

The diffraction loss computations in Table 1 show, in agreement with ex-
pectation, that for a fixed frequency, as the receiving transducer is moved
away from the radiating transducer the diffraction loss goes up. If, on the
other hand, the frequency is increased for a given y, then the diffraction
loss goes down. The latter result is indicative of the property that improve-
ment in MSSW collimation dominates over the divergent-lens effect as the frequency
is increased.

The contribution of beam steering to MSSW diffraction at a given frequency
becomes progressively more pronounced as a receiving transducer with fixed
aperture is moved closer to the radiating transducer. This feature is qualitat-
ively readily interpreted using the MSSW refractive-index diagram (see Fig. 2). One
first recognizes that the maximum value of the observation angle θ subtended
with the y-axis by the line joining an element of the radiating transducer with
an element of the receiving transducer increases monotonically from 0° as the
separation between the two transducers is reduced from infinity. The beam steering
effect is now seen from Fig. 2 to become progressively more pronounced as θ is
increased. It follows that the beam-steering effect may be ignored when the distance
separating the two transducers is large but must be taken into account when this
distance is short. Furthermore, if the receiving transducer is far away from the
radiating transducer, the MSSW diffraction problem is essentially one of diffraction
of an <u>isotropic</u> wave-type.

The ripples in the MSSW intensity profiles (see Figs. 5 to 7) which make
appearance as the frequency is increased and the observation plane is brought
closer to the radiating transducer are a consequence of two factors: i) a radiating
transducer of given physical length becomes electrically longer at higher frequencies;
and ii) the beam-steering effect which becomes important as the separation between
the radiating transducer and the observation plane is reduced.

A salient feature of the MSSW field intensity profiles is that MSSW beam
spreading is significantly faster than SAW beam spreading on YZ $LiNbO_3$ or on
(111)-cut [110]-propagating $Bi_{12}GeO_{20}$.[1] SAW propagation in the latter crystals is
well-known to approach almost perfect auto-collimation (SAW beam profile is essen-
tially undergraded for many hundred SAW wavelengths of propagation), a condition
resulting from the unique nature of SAW slowness diagrams for these crystals. This
comparatively deleterious MSSW beam-spreading property is somewhat mitigated by
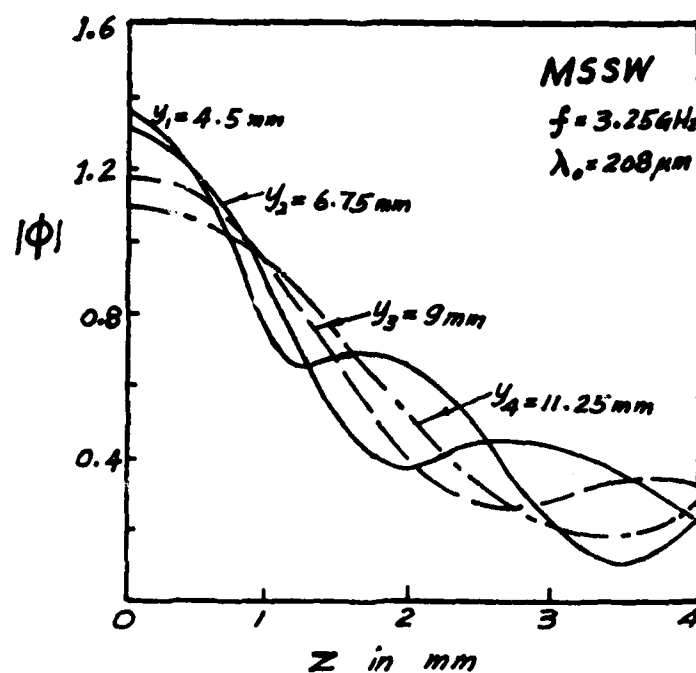
Fig. 7. Computed MSSW diffraction patterns for
signal frequency f=3.75GHz, with other parameters
same as for Fig. 3.

Table 1. Diffraction loss calculations *

f (GHz)	Γ	2a	y_2	$P(y_2)/P(0)$ (dB)	y_3	$P(y_3)/P(0)$ (dB)	y_4	$P(y_4)/P(0)$ (dB)
2.7	1.45	3.25	4.88	0.7	6.5	1.8	8.13	2.75
3	1.86	9.3	15.7	0.58	20.9	0.6	26.2	0.8
3.25	2.99	19.2	32.45	0.5	43.3	0.57	54.	0.68

* The distance quantities 2a, y_2, y_3, and y_4 are expressed in terms of the MSSW wavelength λ_o at the frequency in question.

the fact that the pathlength between the input and output transducers measured in wavelengths is much shorter for MSSW structures than for SAW devices. In fact, the diffraction loss computations given in Table I show that the worst MSSW diffraction loss occurs at frequencies near the lower-frequency bound of the MSSW spectrum where it is in the order of few dB for a typical configuration comprised of two transducers spaced by a distance of 1cm, with both transducers having an overlapping aperture of 5mm. As the frequency is increased, the MSSW wavelength decreases or the electrical length of a radiating transducer of given physical aperture increases, leading to improved MSSW collimation and reduction in MSSW diffraction loss. The present diffraction loss results are within the lowest experimentally realized insertion loss in a MSSW two-port of about 3 dB.

REFERENCES

1. A. J. Slobodnik, Jr. "Materials and their influence on performance," in Acoustic Surface Waves, ed. by A. A. Oliner (Springer Verlag, 1978).

2. H. S. Tuan and J. P. Parekh, "Diffraction and beam steering of magnetostatic surface waves," in Proceedings of the 1980 IEEE Ultrasonics Symposium.

3. J. P. Parekh and H. S. Tuan, " Beam steering and diffraction of magnetostatic backward volume waves," J. Appl. Phys. 52(3), 2279 (1981).

4. C. V. Smith, Jr., J. M. Owens, T.J. Mears, II and N.D. Parikh, "Induction probing of magnetostatic delay line fields," IEEE Trans. Magnetics MAG-15, 1738 (1979).

5. J. P. Parekh, "Magnetostatic surface waves on a partially metallized YIG plate," Proc. IEEE 61, 1871 (1973).

MAGNETOSTATIC WAVE RESONATORS

J.P. CASTERA and P. HARTEMANN
THOMSON-CSF, Research Center,
Domaine de Corbeville, 91401 Orsay, France

ABSTRACT

✓ The purpose of this paper is an overview of recent advances about tunable two-port microwave resonators using the propagation of magnetostatic waves. These waves propagate in yttrium iron garnet films grown by liquid phase epitaxy on gadolinium gallium garnet substrates. 8 dB insertion loss magnetostatic surface wave resonators have been achieved with a loaded Q close to 450 and an out of band rejection of about 10dB. By decoupling the resonator from the transducers, Q values greater than 800 can be obtained with 15 dB insertion loss and a rejection of the off-resonance frequencies greater than 10 dB. Volume wave resonators have a higher Q value of about 1200 and 16 dB insertion loss for a rejection equal to 4 dB. Some experimental results on metal dot array cavity are presented and limitations related to power saturation, frequency versus temperature variations and off-resonance transmission are discussed. ,

INTRODUCTION

Magnetostatic wave (MSW) devices form the basis for a new emergence of microwave analog signal processing. Among these devices, MSW resonators offer over surface acoustic wave (SAW) resonators simple transducers not needing narrow-line-width photolithography and broad frequency tunability by an externally applied magnetic field. Over yttrium iron garnet (YIG) sphere resonators which operate well at microwave frequencies, but which require tedious and expensive fabrication procedures, MSW resonator techniques provide means for obtaining very small, high Q resonators allowing MSW oscillator and complex filter functions. This resonator is the MSW counterpart of the SAW Fabry-Perot interferometric cavity. It is based on magnetostatic wave propagation in a YIG film grown by liquid phase epitaxy on a gadolinium gallium garnet (GGG) substrate. These devices have been studied by two laboratories : the University of Texas at Arlington in the U.S.A. and the Thomson-CSF Research Center in France. This paper is a review of the configurations and performances obtained with MSW resonators for magnetostatic surface waves (MSSW), magnetostatic forward volume waves (MSFVW) and magnetostatic backward volume waves (MSBVW). Resonators implemented with etched groove gratings or using metal dot arrays as distributed reflectors have been considered. The configuration of etched groove grating resonators has been optimized. Finally, limitations related to power saturation and frequency versus temperature variations of MSSW resonators are presented.

MSW RESONATORS

The basic element of this device is a periodic grating which reflects the MSW at specific wavelengths. Initial studies by Sykes et al.[1] of the University of Edinburgh, U.K., demonstrate that etched groove periodic structures could be used to yield more complex structures such

as resonators. A single port MSSW resonator was achieved by Collins et al.[2] with a quality factor Q of 500 at 3 GHz. This device has been realized in a 9 µm thick YIG film where a 38 parallel grooves (each 30 µm wide by 4 mm long and separated by 120 µm) periodic array was etched with a groove depth to film thickness ratio close to 11 %. But the one-port configuration suffers the same difficulty as its SAW analog, when used for frequency control in an oscillator, that of spurious oscillations. The problem is avoided by the two-port configuration shown in figure 1.
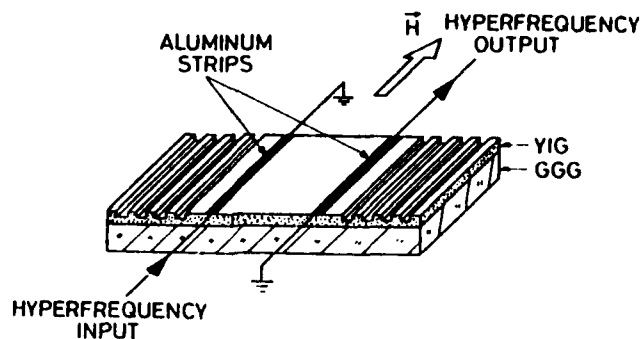
Fig. 1 - Schematic of two-port MSW resonator

The two-port resonator consists of a pair of such distributed mirrors separated by a propagating spacing. This structure is of particular interest due to its inherent isolation between input and output ports. Efficient distributed reflectors can be formed by several types of discontinuity : chemically or ion beam milled etched groove arrays or metal dot arrays. The tested resonators are designed to operate at a 300 µm wavelength. The transducers are two aluminum microstrip couplers deposited directly on the YIG film or on an alumina substrate and the YIG film is located on this transducer pair in a "flipped" configuration.

MSSW resonators

MSSW mode corresponds to the bias magnetic field applied in the plane of the YIG film, perpendicular to the propagation direction of the waves. This magnetic field has a direction so that the off-resonance transmission between the transducers is realized by waves propagating at the bottom face of the YIG film. A lot of MSSW two-port resonators has been designed, fabricated and tested in the two previously mentioned laboratories by J.M. Owens, C.V. Smith et al. at the University of Texas and by J.P. Castéra et al. at Thomson-CSF. Table 1 gives the characteristics and summarizes the experimental performances obtained with these devices.

The MSSW resonators described in Table 1 are all tunable by bias field adjustment over an octave between 2 GHz and 4 GHz. These results show that an important value of h/d is necessary to obtain low insertion loss and that the loaded Q is better when the resonator is decoupled from the transducers by a dielectric film. To obtain better rejection of the off-resonance transmission, Castéra et al.[7] of Thomson-CSF, France, have investigated a new configuration which is similar to that of a single mode laser. It consists of two cavities : the first

resonator is long with two high reflection coefficient arrays and is mul-
timoded but has a high Q, the second one is single moded but has a lower
Q. A mode of the first resonator is filtered by the second giving overall
single-mode resonator with high Q. The device has been realized in a 16μm
thick YIG film for a 300 μm wavelength. The transducers are deposited on
an alumina substrate and there is one transducer per cavity. At 3 GHz,
the insertion loss is 15 dB and the rejection of the off-resonance trans-
mission is 15 dB. The Q value is about 500 and the resonator is tunable
from 2 GHz to 4 GHz. The double cavity resonator has 4 dB more rejection
than the single cavity device byt its Q value is smaller and it has 3 dB
more insertion loss.

d (μm)	10	10		20.5	8	10	16
h/d (%)	2.5	2.8		4.4	3.6	6	11
D (mm)	3.6	3.6		3.6	3	3	1.5
N	40	40		40	56	66	50
t (μm)	0	0	35	0	0	0	0
F (GHz)	3	3	3	3.2	2.25	2.50	3
P (dB)	≃ 16	16	16	≃ 12	13	9	12
R (dB)	≃ 10	9	11	≃ 12	9	8	11
Q	830	775	805	500	314	665	600
Chemical etching	x	x		x			
Ion beam milling					x	x	x
Laboratory	University of Texas[3]	University of Texas[4]		University of Texas[5]	Thomson-CSF[6]	Thomson-CSF[6]	Thomson-CSF[7]

Table 1 - Characteristics and experimental performances obtained with MSSW
two-port resonators. d is the thickness of the YIG films, h/d the groove
depth to film thickness ratio, D the distance between the gratings, N the
number of grooves per array, t the spacing between the YIG and the trans-
ducers, F the resonance frequency, P the insertion loss at resonance, R
the rejection of the off-resonance transmission and Q the loaded quality
factor.

N°	1			2		3	4
d (µm)	15			15		15	17
h/d (%)	11			11		11,3	11
D (mm)	1,5			1,5		1,5	1,5
N	50			50		50	50
t (µm)	30	≃ 50	30	0	26	10	0
F (GHz)	3	3,63	4,075	3,2	3	3	3
P^λ (dB)	8	15	10,5	6	7,5	7,5	6
$P^{\lambda/2}$ (dB)	27,5	40	34	20	28	23	20
Q	450	800	530	280	440	410	290
R (dB)	> 10	> 10	> 10	< 10	> 10	≃ 10	< 10

Table 2 - Characteristics and experimental performances of four optimized MSSW two-port resonators

In order to estimate the possibility of MSSW resonator, we have conducted an experimental study of etched groove gratings, particularly evaluating the depth and the base bandwidth of the rejection notches at 300 µm wavelength as a function of N and h/d. This work has shown that for a resonator using a pair of 50 groove arrays, a value of h/d between 10 % and 12 % allows single mode operation with low insertion loss. Several devices have been realized. Their characteristics together with their experimental performances are summarized in Table 2.

When the YIG is positionned directly on the transducers, insertion loss can be as low as 6 dB but the Q, of the order of 300, and the rejection are not as high as for the decoupled case. For a resonator decoupled by a 30 µm thick dielectric layer, insertion loss of about 8 dB with a Q of 450 can be obtained. If the spacing between YIG and the transducers is increased, Q reaches 800 but with 15 dB insertion loss. Moreover, we can see in Table 2 that insertion loss at half wavelength are very sensitive to the spacing between YIG and transducers. To illustrate this work, the experimental frequency response of these devices are shown in the following figures : Fig. 2a shows the experimental insertion loss versus frequency for a coupled resonator (resonator 4), Fig. 2b represents the same function for a decoupled device (resonator 1 with t ≃ 50 µm), the difference of the frequency responses for the applied magnetic field in one sense and in the opposite sense showing the highly anisotropic propagation of MSSW in the film plane are illustrated in Fig. 3a and Fig. 3b for resonator 1, and a multiple trace obtained by variation of the bias magnetic field intensity (plotted for resonator 1 with t = 30 µm) from 2 GHz to 5 GHz gives in Fig. 4 the typical tuning range of an MSSW resonator.

221
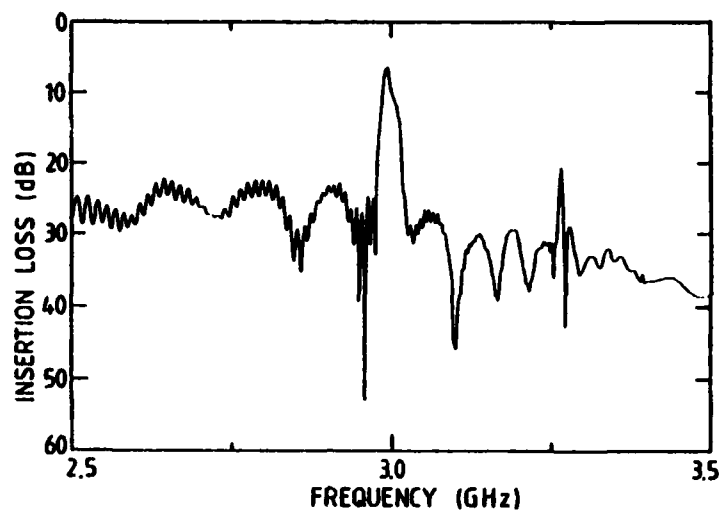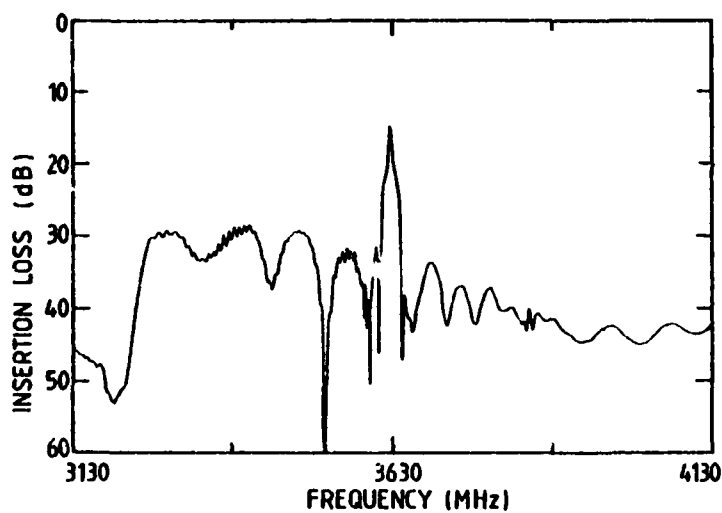
Fig. 2 - Experimental insertion loss versus frequency of MSSW resonators :

(a) coupled configuration

(b) decoupled configuration
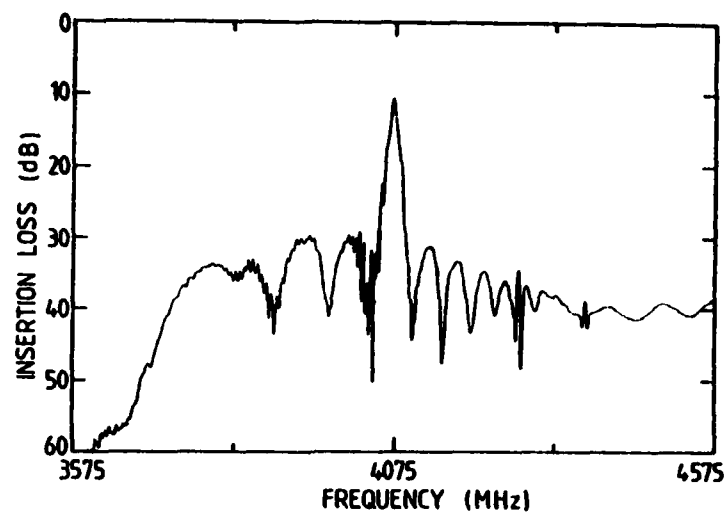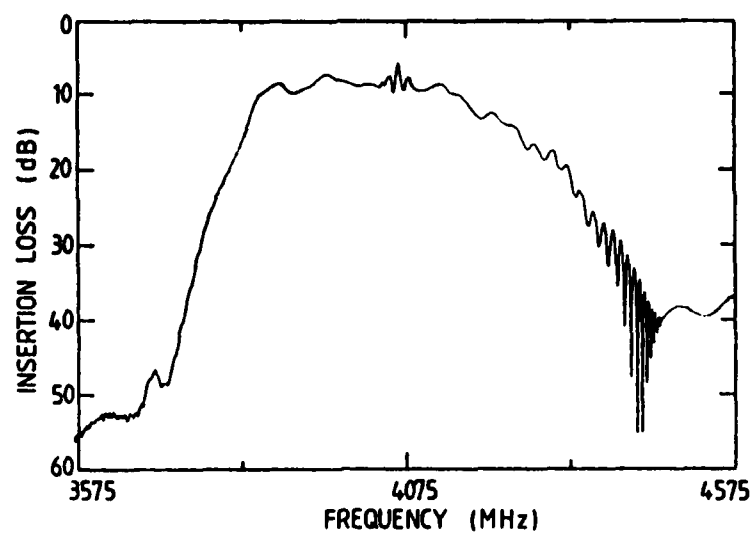
Fig. 3 - Frequency response of a MSSW two-port resonator for the applied magnetic field :

(a) in one sense and (b) in the opposite sense
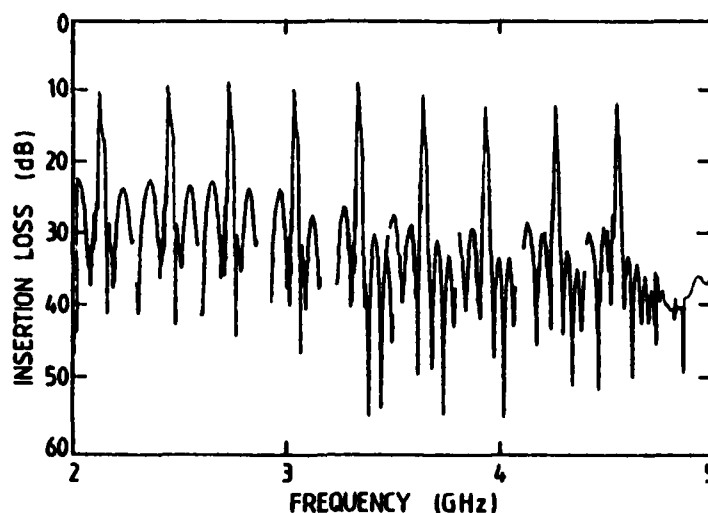
Fig. 4 - Field tuning characteristics of an MSSW two-port
resonator

We have realized some experiments with metal dot array resonators.
For a given device implemented on a 18.5 μm thick YIG film, 69 μm in
diameter aluminum dots, 100 μm spaced along a row and designed to ope-
rate at a 300 μm wavelength were deposited on a glass plate and placed
in contact with the YIG surface. At 2.5 GHz, insertion loss are 21 dB
with a rejection of the off-resonance frequencies of about 6 dB and a
loaded Q of 115. The high insertion loss at resonance and the low Q
value are due to the metal since metallizing the YIG surface makes the
propagation of MSSW strongly non reciprocal. Moreover additional loss
are introduced by the propagation under metal dot arrays as shown by
Volluet[8] in the case of MSFVW.

MSVW resonators

In 1979, Castéra of Thomson-CSF reported results on two-port
MSVW resonators. Ion beam milled periodic etched groove gratings were
used in both magnetostatic forward volume wave (MSFVW) and magnetos-
tatic backward volume wave (MSBVW) configurations.

MSFVW resonators

In this case, the magnetic field was applied perpendicular to the
plane of the YIG film. The characteristics and experimental results
about insertion loss, rejection and loaded Q for these resonators are
summarized in Table 3.

For resonator 1, transducers were deposited directly on the YIG
film while for resonator 2, they were etched on an alumina substrate
and the YIG film placed in contact with the alumina. Resonator 1 was
multimoded while device 2 had a single resolved mode. In contrast to
MSSW resonators, these devices had larger off-resonance transmission
due to the reciprocal nature of MSVW.

224

N°	1		2	
d (μm)	10		8	
h/d (%)	6		3.5	
D (mm)	3		3	
N	66		56	
MSW	MSFVW	MSBVW	MSFVW	MSBVW
F (GHz)	2.4	4.21	2.2	4.35
P (dB)	12	19	13	24
R (dB)	.-	8	6	7
Q	-	830	550	870

Table 3 - Characteristics and experimental results for MSVW two-port resonators

Measurements of the amplitude of reflection notches due to a periodic etched groove grating show that for a given h/d ratio, the reflection is greater for MSFVW than for MSSW. Consequently, we have designed a 2-port MSFVW resonator having a lower groove depth. The device has been realized on a 22 μm thick YIG film where two groove arrays 8.25 mm distant have been ion beam milled. The 50 grooves of each array are 0.44 μm deep corresponding to h/d = 2 %. The input and output aluminum microstrip transducers (30 μm-wide, 7 mm long and 3 mm distant) are deposited on a 250 μm thick alumina substrate and the YIG film is positioned on the transducers. The frequency response of this device is shown in figure 5. The insertion loss, at 3 GHz, is 16 dB and the rejection of the off-resonance frequencies is close to 4 dB. The loaded Q is approximately 1200 at 3 GHz and the resonator is tunable over an octave.
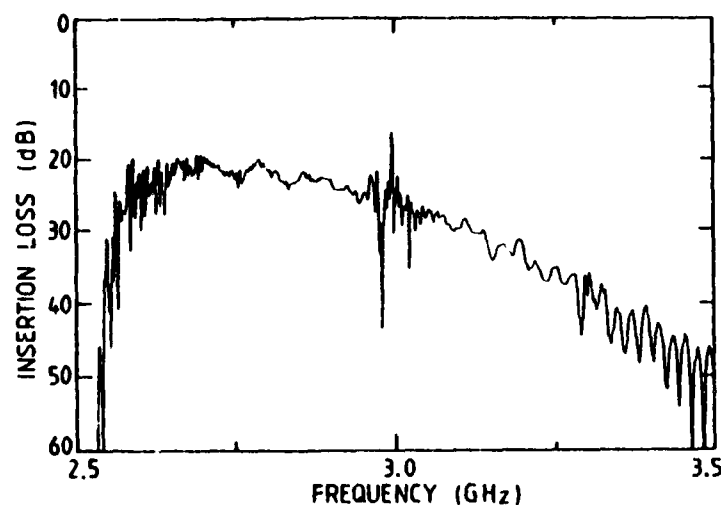
Fig. 5 - Frequency response of an MSFVW two-port resonator

225

MSBVW resonator

The same devices were experimented with MSBVW for which the magnetic field was applied in the plane of the YIG film, parallel to the propagation direction of the waves. As given in Table 3, these resonators presented greater insertion loss than their MSFVW counterparts but with higher Q values.

Both the MSFVW and MSBVW resonators were tunable by bias field adjustment over an octave.

DISCUSSION

Reflection by etched groove gratings is greater for MSVW than for MSSW. In consequence, the groove depth to film thickness ratios of MSSW and MSVW resonators are very different, typically 11 % for surface wave devices and 2 % for volume wave resonators.

With MSSW, the resonator is operated so that the direct transmission between transducers is via the "bottom" surface wave. Use of the "bottom" surface wave further decouples the resonator and reduces off-resonance transmission. This operation is not possible for volume waves and, in consequence, the off-resonance rejection for the conventional two-port configuration is too small.

The power saturation levels of MSSW resonators depends upon frequency. We have measured, on a 18.5 μm thick YIG film, a saturation level of about - 10 dBm below 4.25 GHz. Above this frequency, the MSSW saturate at + 20 dBm. On the other hand, MSFVW allow operation at + 20 dBm power levels and do not present a low power saturation frequency range.

Coupling to spin waves is theoretically allowed both for MSSW and MSFVW but is not allowed for MSBVW. Surface waves show weak coupling whereas this coupling is very strong with MSFVW. But for a YIG film of given thickness and groove depth, the spin wave spectra can be calculated[9] and these parameters chosen to avoid that the resonator frequency corresponds to a spin wave mode.

The variation of the resonator center frequency with temperature is different for the three kinds of magnetostatic waves. MSFVW frequency temperature coefficient is positive. This frequency change due to the variation of the 4 πM can be cancelled by the temperature variation of rare earth cobalt permanent magnets[19]. On the other hand, MSSW and MSBVW have a negative variation of frequency, so it seems impossible to achieve temperature stabilization with commercially available permanent magnets which have a negative or a very small positive coefficient of remanence. Nevertheless, MSW devices may have a lower temperature coefficient by the use of gallium substituted YIG films.

MSVW resonators exhibit greater Q values than MSSW devices. This feature is attributed to the great sensitivity of MSSW to surface defects.

CONCLUSION

Grooved grating Fabry-Perot type resonators using the propagation of magnetostatic waves could have significant impact in the future on microwave systems such as tunable oscillators and filters. Surface wave resonators using metal dot arrays have high insertion loss and a low Q value. The best results for MSSW have been obtained with grooved array resonators. It has been shown that depending on the coupling between the resonator and the transducers, insertion loss as low as 6 dB and Q values greater than 800 can be obtained with these devices, the rejection of the off-resonance level being 10 dB. With MSVW, Q of the order of 1200 have been demonstrated, the insertion loss being 16 dB and the rejection 4 dB. The resonators are bias magnetic field tunable over more than an octave bandwidth in S-band. However, a number of problems remain in the utilization of MSW resonators including power saturation of MSSW devices below 4.25 GHz, temperature stability of MSSW and the large off-resonance transmission of MSVW resonator due to the reciprocal nature of volume waves.

Flat magnetostatic wave resonators would overcome several problems encountered with YIG spheres namely just because they are spheres and because MSW resonators would avoid the considerable problem of orienting the crystalline sphere within the external magnetic field. This planar geometry is suitable to realize complex tunable filter function. Moreover, feedback oscillator based on these devices could theoretically have noise performance better than the equivalent YIG sphere oscillator. The growth technology utilized is a result of magnetic bubble domain research and is highly developed. Furthermore, transducer and periodic structure dimensions permit easy fabrication and good reproducibility by conventional microelectronic techniques.

While problems remain in the MSW resonators mainly about the off-resonance rejection of volume waves, further work to overcome these difficulties must be undertaken.

ACKNOWLEDGMENT

REFERENCES

1 C.G. Sykes, J.D. Adam and J.H. Collins, "Magnetostatic wave propagation in a periodic structure", Appl. Phys. Letters, 29, p. 388, 1976

2 J.H. Collins, J.D. Adam and Z.M. Bardai, "One-port magnetostatic wave resonator", Proc. IEEE (Lett.), 65, p. 1090, 1977

3 J.M. Owens, C.V. Smith, Jr. and J.H. Collins, "Magnetostatic wave bandpass filters and resonators", IEEE circuit sy., IEEE CH 1358-1, p. 563, 1978

4 J.M. Owens, C.V. Smith, Jr. and E.P. Snapka, "Two-port magnetostatic wave resonators utilizing periodic reflective arrays", Int. Microwave Symp., Proc. IEEE 78 CH 1355-7 MTT, p. 440, 1978

5   J.H. Collins and J.M. Owens, "Magnetostatic wave and SAW devices - similarities, differences and trade-offs", IEEE circuit sy., IEEE CH 1358-1, p. 536, 1978

6   J.P. Castéra and P. Hartemann, "Magnetostatic surface wave oscillators and resonators", 8th European Microwave Conference Proc., p. 658, 1978

7   J.P. Castéra, G. Volluet and P. Hartemann, "New configurations for magnetostatic wave devices", Ultrason. symp. Proc., Cat. 80CH1602-2, p. 514, 1980

8   G. Volluet, "Magnetostatic forward volume wave reflective dot arrays" Intermag Conference, Grenoble, May 12-15, 1981, paper 20-4

9   J.D. Adam, T.W. O'Keeffe and R.W. Patterson, "Magnetostatic wave to exchange resonance coupling", J. Appl. Phys., Vol. 50, N° 3, 1979

10 J.D. Adam, "A temperature stabilized magnetostatic wave device", Int. Microwave Symp., Proc. 79 CH 1439-9 MTT-S, p. 160, 1979

BURIED MAGNETOSTATIC-FORWARD-VOLUME-WAVE TRANSDUCERS

AD P000936 Parekh and H.S. Tuan
Department of Electrical Engineering
State University of New York at Stony Brook
Stony Brook, N.Y. 11794

ABSTRACT

This paper reports theoretical computations of the magneto-static-forward-volume-wave (MSFVW) excitation characteristics of transducers that are buried within a YIG film. The frequency varia-tion of the radiation resistance of a line-current source and a micro-strip transducer is calculated over the entire magnetostatic-volume-wave (MSVW) spectrum. The expectation that the symmetry of transducer location relative to the YIG film must determine whether symmetric or antisymmetric MSFVW's are selectively excited is borne out in the present work. Thus, while a surface-localized microstrip transducer selectively excites the lowest (or $\alpha=0$) mode which is found to be an antisymmetric mode, a microstrip transducer buried half-way across the film selectively excites the lowest symmetric (or $\alpha=1$) mode. The suppression of <u>unwanted</u> modes is far superior with the latter buried microstrip transducer than with a surface-localized microstrip trans-ducer. While the technological problem of implementing buried trans-ducers remains to be resolved, the present results are of relevance to the MSFVW layered structure wherein the transducer is sandwiched between two YIG films.

INTRODUCTION

The transduction of magnetostatic waves is usually performed utilizing a microstrip transducer localized at the surface of a YIG film. Previous theoretical studies[1-3] and confirming experiments[1,4] have shown that a surface-localized magnetostatic-forward-volume-wave (MSFVW) microstrip transducer suppresses all modes except the lowest (or $\alpha=0$) mode. An examination of the field profile of the $\alpha=0$ MSFVW mode reveals that this mode is an antisymmetric mode. Thus, in retrospect, it is not surprising, based on considerations of the symmetry of transducer location relative to the YIG film, that this mode is selectively excited by a <u>surface-localized</u> transducer.

In an analogous fashion to the problem of mode slectivity of electromagnetic waveguide modes, one expects that selective excitation of antisymmetric or symmetric MSFVW modes may be achieved through the use of a <u>buried</u> transducer whose placement relative to the YIG film possesses appropriate symmetry. This MSFVW mode-selectivity property is verified in the present calculations. Thus, while a surface-localized microstrip transducer selectively excites the $\alpha=0$ MSFVW mode, a microstrip transducer buried half-way across the film selectively excites the lowest symmetric (or $\alpha=1$) MSFVW mode. The suppression of <u>unwanted</u> modes is found to be far superior with the latter buried microstrip transducer than with a surface-localized microstrip transducer.

229

While the technological problem of implementing buried transducers is a difficult one, the present work is of relevance in modelling the MSFVW layered structure wherein the transducer is sandwiched between two YIG films, and has further clarified the antisymmetric and symmetric nature of the MSFVW modes of a YIG film. The motivation for looking into the question as to whether the $\alpha=1$ mode can be selectively excited lies in the advantages offered by the $\alpha=1$ mode over the $\alpha=0$ mode, e.g., longer time delay per unit distance of propagation and improved constant-delay and linear-dispersion characteristics.
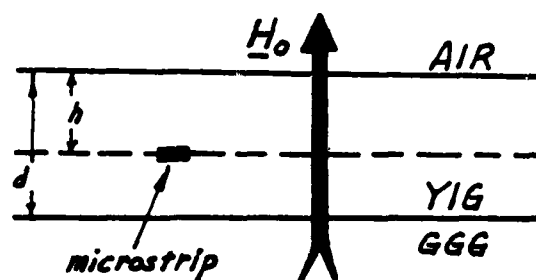
Fig. 1. Geometry of the problem

THEORY

The geometry of the problem treated here is shown in Fig. 1. An ungrounded YIG film of thickness d is magnetized beyond saturation by a bias field $H_o=H_o z_o$ applied normal to the film. A thin microstrip of width b carrying a current I_o assumed uniformly distributed over the micrstrip is buried in the YIG film at a depth h.

The standard Fourier transform technique yields integral expressions for the magnetostatic potential functions ϕ_{AIR}, $\phi_{YIG}^{(+)}$, $\phi_{YIG}^{(-)}$ and ϕ_{GGG} for the air region, two YIG regions and the GGG region, respectively, which satisfy appropriate interface boundary conditions at the three interfaces and the radiation condition at $z \to \pm\infty$. The potential functions $\phi_{YIG}^{(+)}$ and $\phi_{YIG}^{(-)}$ are for the YIG regions lying above and below the dashed line in Fig. 1 drawn through the microstrip, respectively. Recognizing the bidirectionality of MSFVW transduction, the total power P_{MS}/I_o^2 transduced by a micro-strip per unit length of the microstrip into MSFVW propagating in either direction may be expressed in terms of the total power P_{LC}/I_0^2 transduced into MSFVW propagating in either direction by a single infinite line-current source carrying a current I_0 per unit length along the line current by the expression

230

$$P_{MS}/I_o^2 = g^2 (P_{LC}/I_o^2) \tag{1}$$

where g is the microstrip array factor

$$g = \sin(kb/2)/(kb/2). \tag{2}$$

Notice that $g=1$ in the limit $b\to 0$ which is consistent with the fact that a line-current source is a limiting case of a thin microstrip transducer corresponding to $b\to 0$. In Eq. (2), k is the MSFVW wavenumber whose value for the various modes described by the mode numbers $\alpha=0,1,2,\ldots$ is the solution of the dispersion relation

$$|k| = (1/\beta d) \tan^{-1} [-2\beta/(1-\beta^2)] \tag{3}$$

where β^2 is the negative of the xx or yy component of the relative permeability tensor characterizing the YIG medium.

The power P_{LC}/I_0^2 is comprised of the powers carried in the four regions defined above by MSFVW propagating in either direction, i.e.,

$$P_{LC}/I_0^2 = P_{AIR}/I_0^2 + P_{YIG}^{(+)}/I_0^2 + P_{YIG}^{(-)}/I_0^2 + P_{GGG}/I_0^2 \tag{4}$$

where

$$P_{AIR}/I_0^2 = (\pi f \mu_0/2) A^2 \tag{5a}$$

$$P_{YIG}^{(+)}/I_0^2 = Q_1 (P_{AIR}/I_0^2) \tag{5b}$$

$$P_{GGG}/I_0^2 = (\pi f \mu_0/2) D^2 \tag{5c}$$

$$P_{YIG}^{(-)}/I_0^2 = Q_2 (P_{GGG}/I_0^2) \tag{5d}$$

In Eq. (5), μ_0 is the permeability of free space and the quantities A, D, Q_1 and Q_2 have the expressions

$$A = (\beta/k\Lambda_1) [\cos\beta k(d-h) - \beta\sin\beta k(d-h)] \tag{6a}$$

$$D = (\beta/k\Lambda_1) (\beta\sin\beta kh - \cos\beta kh) \tag{6b}$$

$$Q_1 = (1+\beta^2)kh - 1 + \cos 2\beta kh + ((1-\beta^2)/2\beta) \sin 2\beta kh \tag{6c}$$

$$Q_2 = (1+\beta^2)k(d-h) - 1 + \cos 2\beta k(d-h) + ((1-\beta^2)/2\beta)\sin 2\beta k(d-h) \tag{6d}$$

with

$$\Lambda_1 = \beta d[(1-\beta^2)\cos\beta kd - 2\beta\sin\beta kd] \tag{6e}$$

The power expressions in Eqs. (4) and (5) reduce in the limit $h\to 0$ to the previously reported [3] expressions for a surface-localized transducer. The quantity Q_1 and thus $P_{YIG}^{(+)}$, in agreement with expectation, become zero in the limit $h\to 0$.

The total radiation resistance of a transducer is

$$R_i = 4P_i/I_0^2 \tag{7}$$

where the subscript i stands for MS (microstrip) or LC (line-current).
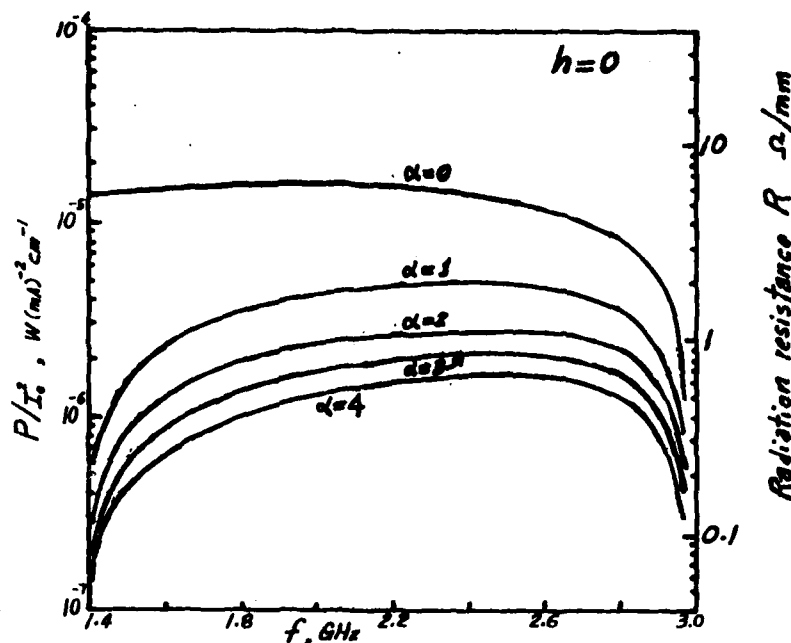
Fig. 2. Frequency variation of the MSFVW radiation resistance of a **surface-localized line-current source**

NUMERICAL RESULTS AND DISCUSSION

Computed MSFVW transduction properties of a line-current source are presented in Figs. 2 and 3 and of a microstrip transducer in Figs. 4 and 5. The computations in these figures are for a YIG film of thickness $d=10\,\mu m$, internal bias field $\mu_0 H_i = 500G$ and saturation magnetization $\mu_0 M_0 = 1750G$, with the frequency varied over the entire MSVW spectrum, i.e., $1.4GHz < f < 2.96GHz$. These computations are presented as the frequency variation of the radiation resistance $R_i = 4P_i/I_0^2$ defined in Eq. (7). A microstrip transducer width of $b=50\,\mu m$ is assumed in the computations of Figs. 4 and 5. The computations of Figs. 2 and 4 are for a surface-localized transducer representing optimum transducer location for selective excitation of the lowest (or $\alpha=0$) MSFVW mode. On the other hand, the computations of Figs. 3 and 5 are for a transducer buried half-way across the YIG film representing optimum transducer location for selective excitation of the $\alpha=1$ mode.

232
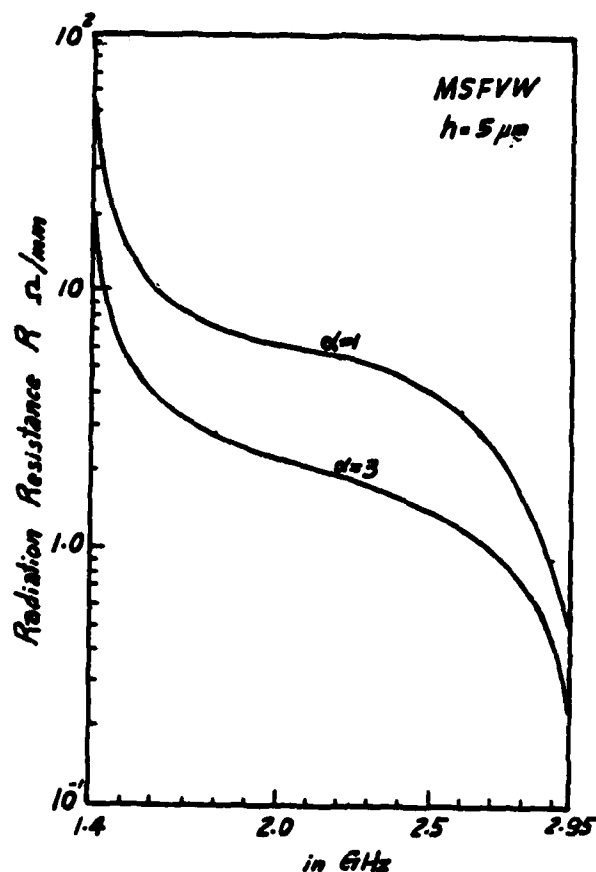
Fig. 3. Frequency variation of the MSFVW
radiation resistance of a line-current
source buried half-way across the YIG film.

A surface-localized line-current source is seen from Fig. 2 to be broadband and
to excite the lowest (or α=0) mode most strongly, with the excitation of the higher-
order modes (α=1,2,3,...) being progressively less pronounced with increase in mode
number but nevertheless not insignificant. A line-current source buried half-way
across the YIG film is seen from Fig. 3 to selectively excite modes with odd α values
(α=1,3,5,...), with the excitation of these modes becoming progressively weaker with
increase in the mode number. The latter transducer configuration excites modes
with even α values (α=0,2,4,...) too weakly to be shown on the ordinate scale of
Fig. 3.

The array factor g, representing the extended nature of a microstrip transducer
in comparison to a line-current source, permits the following predictions when taken
in conjunction with the MSFVW dispersion characteristics, viz., k increases monotoni-
cally with increasing frequency (with a resonance k→∞ occuring at the top bound of

233
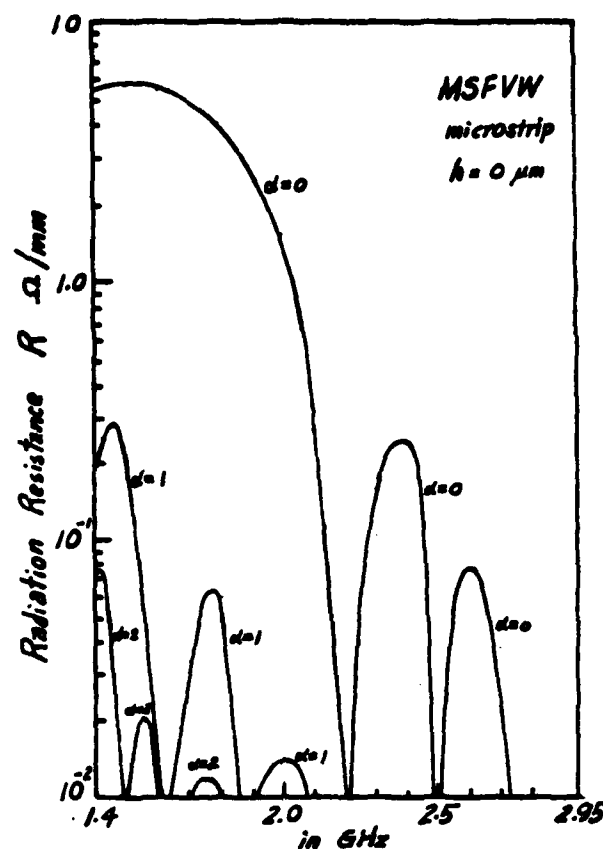
Fig. 4. Frequency variation of the MSFVW
radiation resistance of a surface-localized
microstrip transducer.

the MSFVW spectrum): i) the R_{MS} vs. f characteristic for a given mode is comprised of
an infinite number of lobes whose level and frequency spacing decreases monotonically
with increase in frequency, with only the lowest few lobes being significant in practice;
ii) the microstrip radiation resistance R_{MS} cannot exceed the corresponding line-
current radiation resistance R_{LC}, i.e., $R_{MS} \leqslant R_{LC}$; and iii) the use of a microstrip
transducer leads to higher-order mode suppression since, at a given frequency, the
MSFVW wavenumber k increases (or the corresponding value of array factor g decreases)
with increase in the mode number. These predictions are confirmed in the computations
of Figs. 4 and 5. The selective excitation of the $\alpha=0$ mode by a surface-localized
microstrip transducer and of the $\alpha=1$ mode by a microstrip transducer buried half-way
across the film is apparent in these figures. The latter microstrip location yields
a suppression of modes other than the $\alpha=1$ mode that is far superior to the suppression
of modes other than the $\alpha=0$ mode achieved with a surface-localized microstrip trans-

234
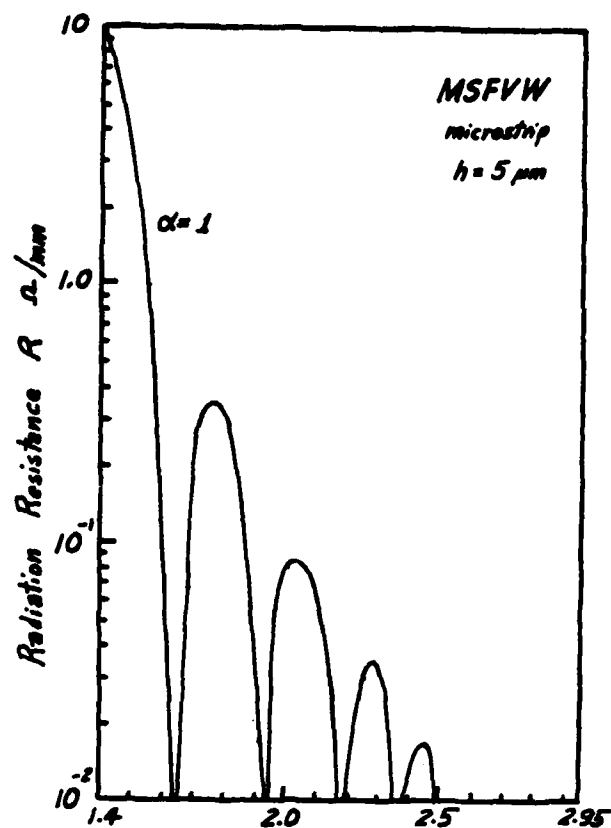
Fig. 5. Frequency variation of the MSFVW radiation resistance of a microstrip transducer buried half-way across the YIG film.
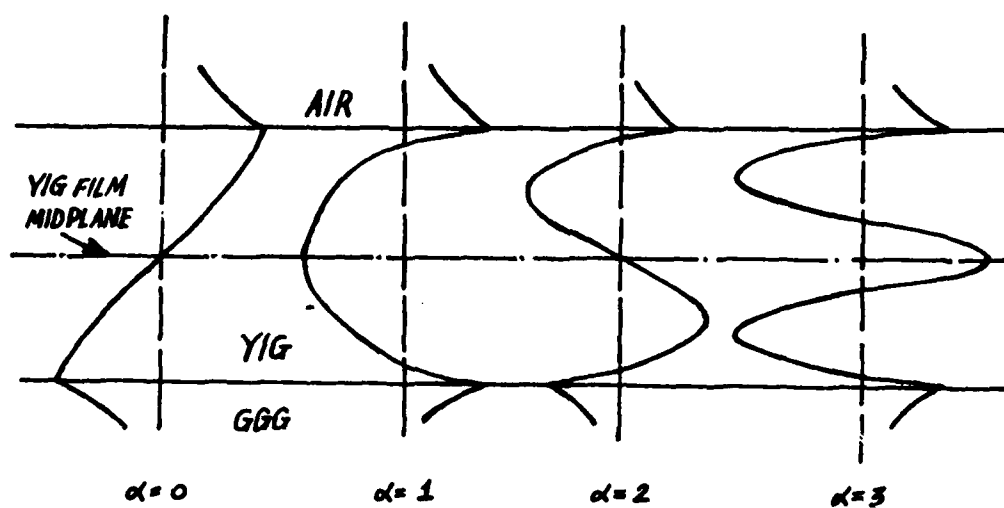
Fig. 6. Variation of rf magnetic field h_z normal to the YIG film with position across the film for the lowest four MSFVW modes.

235

ducer. Notice that only the α=1 curve appears in Fig. 5 for the chosen range of variation of the ordinate scale, with R_{MS} for the α=0 mode being smaller than $10^{-16} \Omega/mm$ over the entire MSVW spectrum.

The problem of identifying the symmetric or antisymmetric nature of a MSFVW mode with a given mode number has been treated by recognizing that the Poynting vector in the air, YIG and GGG regions is proportional to the square of the magnitude of the rf magnetic field h_z normal to the film. If the profile of h_z variation across the film is symmetric about the midplane of the YIG film, the mode in question is defined as a symmetric mode. A mode with an antisymmetric h_z-profile is conversely defined as an antisymmetric mode. Sample z-variations of h_z for the lowest four modes are given in Fig. 6 for a YIG film of thickness d=10 μm and frequency f = 1.5GHz, with the other parameters chosen the same as in the preceding calculations. The MSFVW wavelengths for the four modes at f=1.5GHz are 722μm (α=0), 84μm (α=1), 45μm (α=2) and 30μm (α=3). The qualitative symmetry properties of the h_z profiles in Fig. 6 are maintained as f is varied. It is evident that MSFVW modes with even α values are antisymmetric modes while modes with odd α values are symmetric modes.

REFERENCES

1. J.M. Owens and C. V. Smith, Jr., "Magnetostatic wave devices: a status report," in Proceedings of the 1978 IEEE Ultrasonics Symposium.

2. P.R. Emtage, "Interaction of magnetostatic waves with a current," J. Appl. Phys. 49, 4475 (1978).

3. J. P. Parekh, "Theory for magnetostatic forward volume wave excitation," J. Appl. Phys. 50(3), 2452 (1979).

4. G. Volluet, "Undirectional magnetostatic forward volume wave transducers," IEEE Trans. Magnetics MAG-16, 1162 (1980).

THE EFFECTS OF WIDTH MODES IN MAGNETOSTATIC
FORWARD VOLUME WAVE PROPAGATION*

J. D. Adam

Westinghouse Electric Corporation
Research & Development Center
Pittsburgh, PA   15235

ABSTRACT

Delay line amplitude ripple and out-of-band filter response in magnetostatic forward volume wave devices are shown to be due to the transduction and propagation of width modes, which at low wavenumbers have different phase and group velocities, but at high wavenumbers become degenerate. Various techniques which minimize the effects of width modes are suggested and results obtained on the preferential attenuation of higher order width modes by thin resistive strips are described.

INTRODUCTION

The effects of finite sample width on magnetostatic surface wave propagation has been discussed previously[1, 2] and under certain conditions gives rise to significant changes in wave velocity when compared to propagation in an infinite sample. Similar effects

237

are observed with magnetostatic forward volume waves (FVW) and here measurements and calculations performed for FVW propagation in epitaxial YIG samples of different widths are described. The motivation for this study was the observation that FVW delay lines formed from strips of epitaxial YIG always show significantly more undesirable amplitude and delay ripple than is obtained when using only a limited area of a larger sample, e.g. a 1 cm propagation path in the center of a 2.5 cm diameter YIG disc.

DISPERSION

The dispersion relation for FVW propagation in a YIG film of finite width has been derived before[3, 4] and is given by

$$\tan(\beta N d) = \frac{\beta[\tanh(Nt) + 1]}{[\beta^2 - \tanh(Nt)]} \tag{1}$$

where $N = \left[k^2 + \left(\frac{m\pi}{w}\right)^2\right]^{1/2}$ and $\beta^2 = \frac{4\pi MH}{((\omega/\gamma)^2 - H^2)} - 1.$

m is an integer 1, 2, 3 etc. and k is the wavenumber in the direction of propagation, w is the YIG film width, d is the YIG film thickness and t is the spacing of a conducting plane from the YIG film. $4\pi M$, H, ω and γ are the saturation magnetization, internal magnetic field, signal frequency and gyromagnetic ratio respectively. Because the term tan ($\beta N d$) in equation 1 is multivalued, higher order thickness modes can result but here only the lowest order thickness mode is assumed.

The roots of the dispersion equation were computed and the variation of wavenumber with frequency for the m = 1, 3 and 5 width modes is shown in Figure 1. The YIG film was 18.3 μm thick, 1 mm wide and spaced from the ground plane by 0.635 mm. The frequency where k = 0 for a FVW in an infinite sample (or m = 0) is 9.002 GHz. Only the odd numbered width modes are shown in Figure 1 since it was assumed that even numbered modes would not be launched to a significant extent owing to the transducer symmetry. The frequency spacing between the m = 1 and m = 3 modes at k = 0 is approximately 140 MHz. m = 5, 7, 9 etc. modes are not shown but do exist and the spacing between adjacent modes slowly decreases with increasing mode number. Narrower samples result in a wider frequency separation and conversely width modes in wider samples have a smaller frequency separation. The corresponding variation in group delay with frequency for a 1 mm wide strip is shown in Figure 2. Note that the delay for each mode tends to infinity when k = 0 and the curves become virtually degenerate at high frequencies.
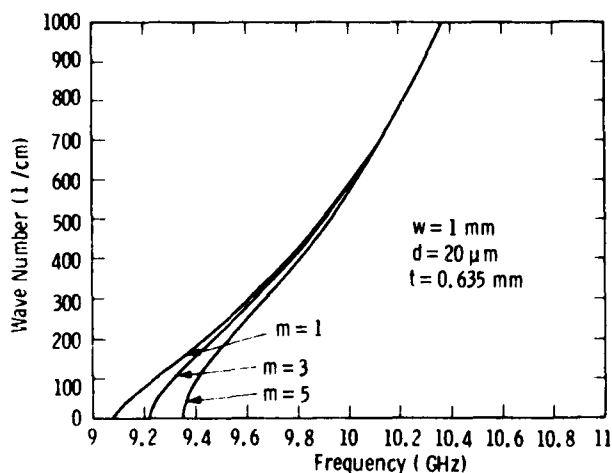
Figure 1. Variation of wavenumber with frequency for width modes m = 1, 3 and 5 in a 1 mm wide and 20 μm thick YIG film.
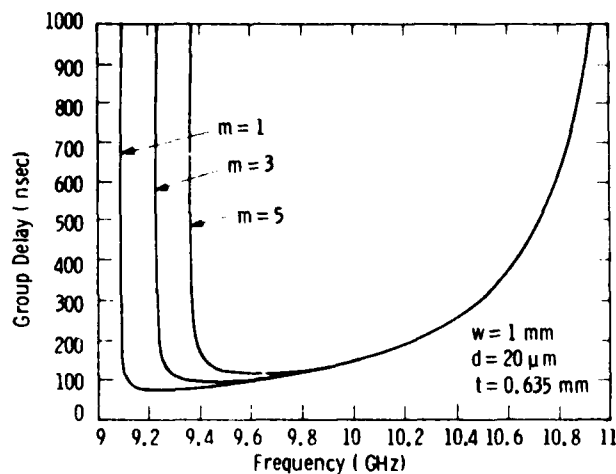
Figure 2. Variation of group delay with frequency for width modes m = 1, 3 and 5 in a 1 mm wide and 20 μm thick YIG film.

239

RESULTS

As mentioned earlier, delay lines formed from narrow YIG

strips show significantly more ripple than delay lines using wide

strips. This is illustrated in Figure 3a and b which shows the

measured insertion loss as a function of frequency for YIG films of

thickness (d) 18.3 µm and width (w) of 5 mm and 1 mm respectively.

The transducers were 5 mm long and 50 µm wide, open circuited at one

end and supported on an alumina substrate 0.635 mm thick. Apart from
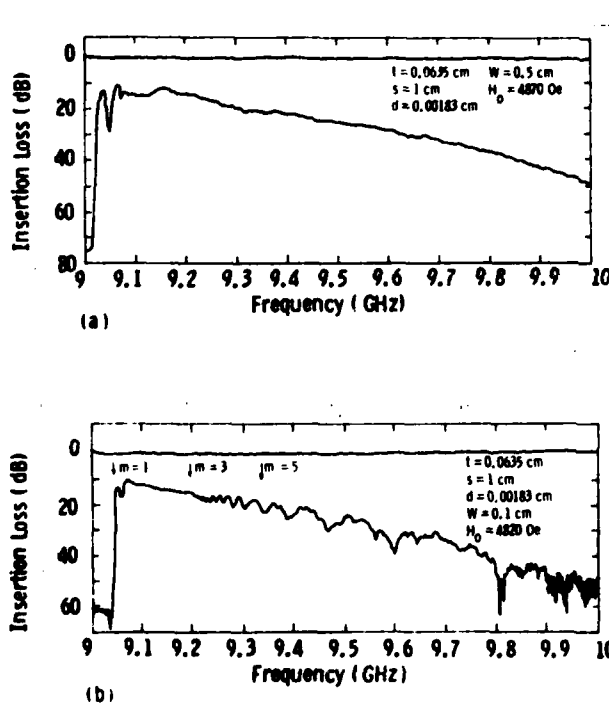
Figure 3. Measured variation of transmission loss with frequency in 18.3 µm thick YIG films: (a) width (W) = 5 mm; (b) width (W) = 1 mm.
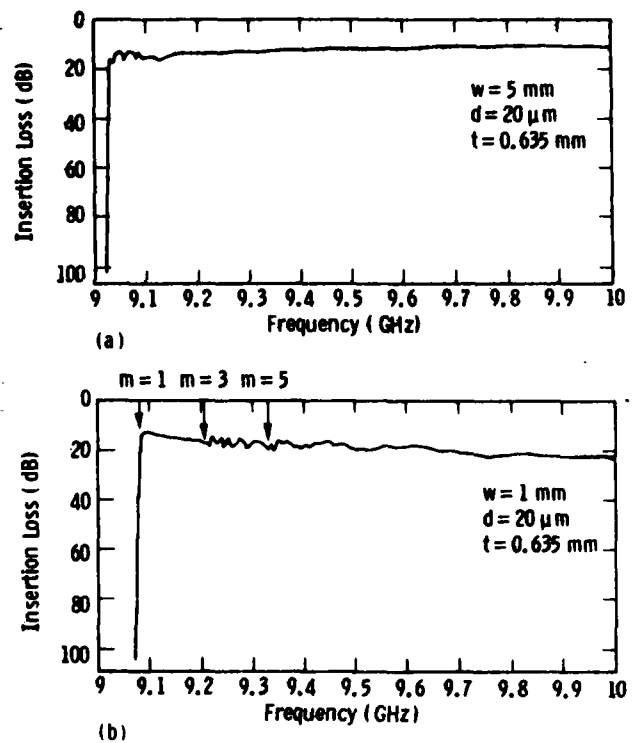
Figure 4. Calculated variation of insertion loss with frequency in 20 µm thick YIG films: (a) width (W) = 5 mm, (b) width (W) = 1 mm.

large amplitude ripple below 9.1 GHz, the response of the 5 mm wide delay

line is relatively smooth. Results on 4, 3 and 2 mm wide samples of the

same thickness showed progressively more severe ripple with a complicated

structure. However the results on a 1 mm wide sample, Figure 3b, show

clearly that the complicated ripple structure is due to interference

between different width modes. The calculated low frequency limits for

the width modes with m = 1, 3 and 5 are indicated by arrows in Figure 3b.

In order to further confirm that the observed ripple was due

to width mode interference, the insertion loss was calculated with

the radiation resistance[5] of each width mode weighted by the

(Fourier coefficient)^2 of the assumed field distribution of the

mode. The current distribution in the microstrip transducer was taken

to be uniform along its length. The calculated results for 20 µm thick

YIG films of width 5 mm and 1 mm are shown in Figure 4a and b respectively.

Only the m = 1, 3 and 5 moves were included in the calculation but the

results are in good qualitative agreement with the measurements shown

in Figure 3. The most significant discrepancy is the difference in the

increase in insertion loss with frequency between the calculated and

measured results which is not related to the width modes being

discussed here.

Narrow pass band characteristics can be obtained if the

transducer is suitably spaced from the YIG film. The measured

transmission loss as a function of frequency is shown in Figure 5

for an 18.6 µm thick YIG film, 1 mm wide. The gold transducers were

5 mm long, 0.635 mm wide on 0.635 mm thick alumina. The YIG film was

spaced from the transducers by a glass slide 160 µm thick and the bias

field was 4880 Oe. Note that a series of pass bands with increasing

insertion loss are observed and correspond to the low wavenumber

range of the m = 1, 3, 5, etc. width modes. Wider YIG strips yield

reduced mode separation and hence overlap of the pass bands and interference.
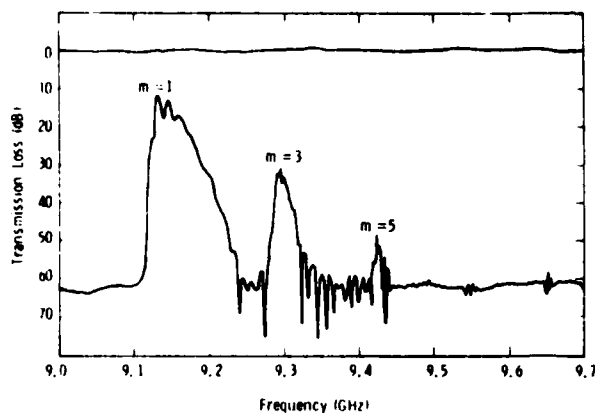
Figure 5. Measured transmission loss as a function of frequency for an 18.6 μm thick YIG film, 1 mm wide. Transducers were 5 mm long 0.635 mm wide on 0.635 mm thick alumina. YIG film spaced 160 μm from transducer and bias field 4880 Oe.
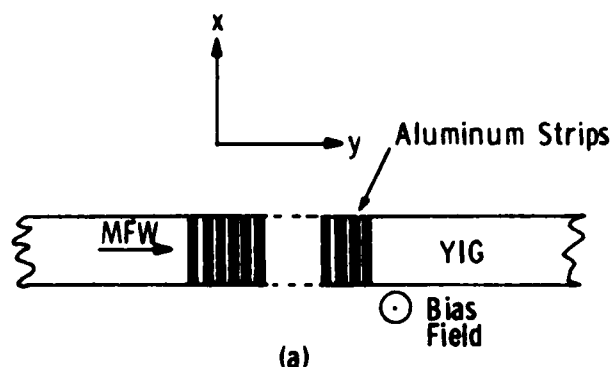
Figure 6. Aluminum strips for preferential attenuation of higher order width modes.

SUPPRESSION

In most applications the presence of width modes other than the lowest mode is not desired. The effects of width modes can be minimized through use of wide samples $\left(\dfrac{w}{d} > 500\right)$ or by use of absorbing techniques, such as bevelling, on all sample edges. In addition, a transducer current distribution which spatially matches the field distribution of the desired mode should result in preferential transducion of that mode. A further technique has been investigated which preferentially attenuates the higher order width modes. It was found that an array of thin aluminum strips evaporated onto the YIG as shown in Figure 6 were effective in preferentially attenuating the higher order width modes.

It has been shown[6] that the attenuation of FVW by a

242

resistive plane in contact with a YIG film increases rapidly with
wavenumber. Thus, the preferential attenuation properties of the
aluminum strips can be qualitatively explained if each width mode is
considered as having two componentns k_x and k_y. In all modes, providing
the aluminum strip period is less than π/k_y, the aluminum strips have
an infinite effective resistance and hence zero attenuation for waves
directly along the y direction. However for waves directed along the
x-direction, the aluminum strips have a finite effective resistivity
and will thus attenuate the wave. For width modes, $k_x = \frac{m\pi}{w}$ so that
in a 1 mm wide YIG strip, $k_x(m=1) = 10\pi$, $k_x(m=3) = 30\pi$ and $k_x(m=5) = 50\pi$ cm^{-1}.
Thus modes with m > 1 are attenuated more than the desired m = 1 mode.
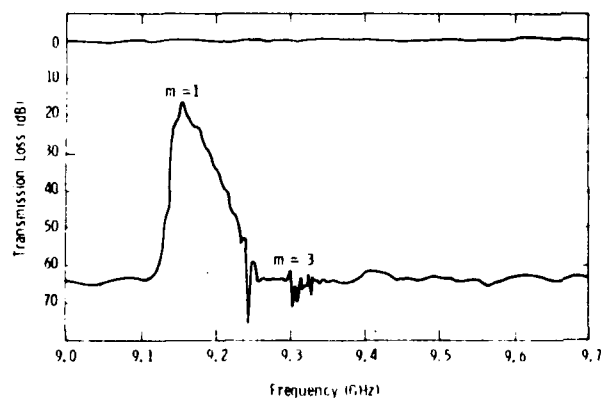
Figure 7. Attenuation of higher order
width modes as a function of aluminum
thickness. Measured on an 18.5 μm
thick YIG film spaced from 0.635 mm
wide transducers by 160 μm: (a) 18
strips; (b) continuous film of length
equivalent to the strips.
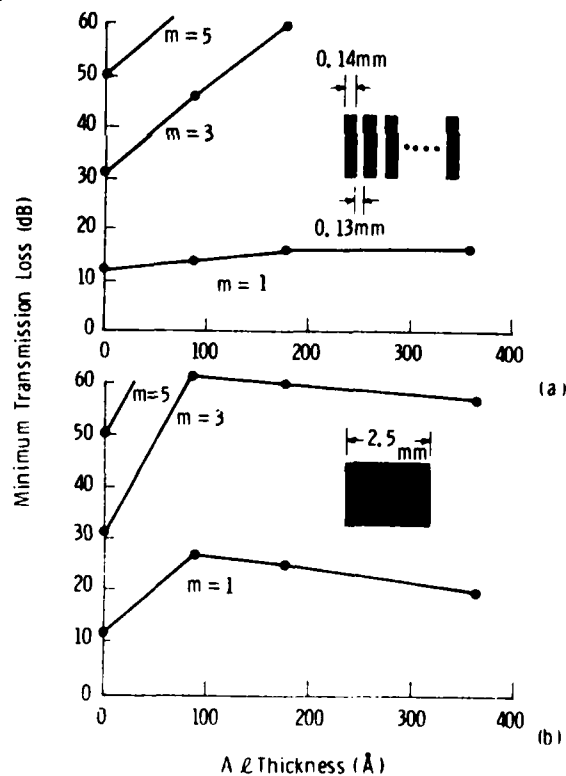
Figure 8. Measured transmission loss
as a function of frequency for an
18.5 μm thick YIG film with the same
parameters as in Figure 5, but with
18 aluminum strips 364Å thick evaporated
onto the surface.

243

Measurements of the attenuation of the width modes as a function of aluminum thickness were performed using a delay line with the same parameters as Figure 5 and are shown in Figure 7. Aluminum was evaporated onto the YIG film through a shadow mask so as to produce an array of 18 strips, each 0.14 mm wide and separated by 0.13 mm. Viewed as a reflective array, these strips would have a stop band at $k = 150 \text{ cm}^{-1}$ which is well outside the delay line pass band. The minimum transmission loss for FVW propagating under the strips as a function of aluminum thickness is shown in Figure 7a. Note that there is only a slight increase in loss for the m = 1 mode but a significant increase for m = 3 and 5 modes. For comparison, the minimum transmission loss through a continuous aluminum film of length equivalent to the array of aluminum strips is shown in Figure 7b. Here the m = 1 mode as well as the m = 3 and m = 5 modes experience significantly increased attenuation with increasing aluminum thickness. The transmission loss of a delay line with 18 aluminum strips of thickness 364Å is shown in Figure 8. Other parameters are the same as in Figure 5. Note that the m = 3 mode is just visible and is approximately 50 dB below the m = 1 transmission peak.

CONCLUSIONS

Delay line amplitude ripple and out of band responses occuring in band pass filters[6] have been identified with higher order FVW width modes. Several techniques are available to minimize the effects of width modes, these include wide YIG samples, absorbing edges on the YIG and preferential transduction using a transducer current distribution

which matches the fields of the desired mode. However in many situations
space or other requirements may preclude the use of these techniques.
Then structures, such as arrays of resistive strips may be used to
preferentially attenuate the higher order width modes.

REFERENCES

1. J. D. Adam, Electronics Letters 6, 718 (1970).

2. T. W. O'Keeffe and R. W. Patterson, J. Appl. Phys. 49, 4886 (1978).

3. Z. M. Bardai et al., AIP Conf. Proc. No. 34, 268 (1977).

4. N.D.J. Miller, Phys. Stat. Solid (a) 37, 83 (1976).

5. A. K. Ganguly and D. C. Webb, IEEE Trans. MTT-23, 998 (1975).

6. "Magnetic Surface Wave Device Technology," J. D. Adam et al., Final
    Report to USAFSC, Aeronautical Systems Division, Wright Patterson AFB,
    OH 45433; Contract No. F33615-77-C-1068.

AD P000938

MAGNETOSTATIC WAVE PROPAGATION IN YIG DOUBLE FILMS[*]

Michael R. Daniel and P. R. Emtage
Westinghouse Research & Development Center
Pittsburgh, PA 15235

ABSTRACT

Using the technique of "surface permeabilities." an expression is derived for the dispersion of a magnetostatic wave propagating in two close proximity magnetic films. Two modes of propagation are identified respectively as the symmetric and antisymmetric modes from the symmetry of the rf magnetic field. Useful group delay behavior is shown to result from films of equal thickness. Some measurements are reported using two Yttrium Iron garnet films sandwiching simple single finger transducers. Difficulties in exciting the symmetric forward volume mode are explained in terms of the coupling coefficients for these double film structures.

1. Introduction

Work reported on yesterday at this workshop showed how single Yttrium Iron Garnet (YIG) films and simple single finger transducers may be exploited to give practical microwave delay lines. However, one penalty for simplicity is the attendant increased insertion loss of these devices by the necessary near-by ground plane. We report here on magnetostatic wave propagation in the YIG double films with the primary motivation being to see if they offer any useful device characteristics

which would render them superior to the single YIG film delay lines. Some work on YIG double films has already been reported.[1],[2] We give here a more complete account both theoretically and experimentally of both forward volume wave (FVW) and backward volume wave (BVW) magneto- static propagation. Additionally we emphasize the very useful approach of "surface permeabilities"[3] as a technique for solving the dispersion relation in magnetostatic problems.

2. Calculations

Figure 1 sets out the geometry and defines most of $\iota_{\iota\sigma}$ arameters for the double film structure. The magnetic bias field H would lie along the Y-direction (Figure 1) for the FVW or alternatively along the X-direction for the BVW. The surface permeability approach was defined in Reference 3 and is briefly summarized here in Figure 2. A magneto- static wave of unspecified form (FVW or BVW) is assumed propagating in the X-direction of the YIG film of thickness d. Associated with the wave are the usual rf magnetic induction $\underline{b}$ and magnetic field $\underline{h}$ vectors. These are related by the permeability tensor $\underline{\mu}$. Since the normal component of $\underline{b}$, b_y, and the tangential component of $\underline{h}$, h_x, is conserved across a boundary it follows that the ratio b_y/h_x is also conserved and this ratio defines a surface permeability, μ_s. μ_s as defined in Figure 2 has, at present, no known physical significance[4] and exists only as a computational aid. Using the definition of μ_s and the Damon and Eshbach[5] approach to magnetostatic wave propagation a relation between $\mu_s(o)$, at the lower surface of the film, and $\mu_s(d)$, at the top of the film, may be derived as in Figure 2. This relation was applied to the geometry of Figure 1 starting at the lower ground plane and working up, step-wise, to the upper ground plane. At each step the

$$\begin{bmatrix} b_x \\ b_y \end{bmatrix} = \begin{bmatrix} \mu_{11} & \mu_{12} \\ -i\mu_{12} & \mu_{22} \end{bmatrix} \begin{bmatrix} h_x \\ h_y \end{bmatrix}$$

$$\left| \frac{b_y}{h_x} \right|_{\substack{outside \\ film}} = \left| \frac{b_y}{h_x} \right|_{\substack{inside \\ film}}$$

Define $\mu_s = -i\dfrac{b_y}{h_x}$ which guarantees that

1. $\mu_s = 1$ in vacuo

2. μ_s is conserved across a magnetic boundary

$$\mu_s(0) = \frac{\mu_s(d) + [\mu_{11}\,\mu_{22} - \mu_{12}^2 - \mu_{12}\,\mu_s(d)]\left(\dfrac{1}{\mu_{22}}\right)\tanh\beta\,kd}{1 + \left[\mu_s(d) \quad \mu_{12}\right]\left(\dfrac{1}{\mu_{22}}\right)\tanh\beta\,kd}$$

Fig. 1 Double YIG film configuration for the excitation of FVW's.

Fig. 2 Development of the surface permeability, μ_s, appropriate to a magnetostatic wave propagating in a magnetic layer of thickness d.

appropriate tensor components of $\underline{\mu}$ must be used for either a magnetic film or a space. A number of related equations result. However, they number only half of those which result from the more conventional "determinant of coefficients" approach.

For FVW's, the resulting dispersion relation is:

$$[(\alpha_1^2 - t_1)\sin\alpha_1 kd_1 - (1 + t_1)\alpha_1\cos\alpha_1 kd_1] \cdot [\#2\ film]$$

$$[(\alpha_1^2 + t_1)\sin\alpha_1 kd_1 + (1 - t_1)\alpha\cos\alpha_1 kd_1] \cdot [\#2\ film]\ \exp(-2kt).....(1)$$

In the relation #2 film means replace the subscript 1 by a 2; additionally

248

$\alpha^2_1 = -\mu_{11}$, $t_1 = \tanh ks_1$ and $\mu_{11} = 1 - 4\pi M_1 H/[\frac{f^2}{\gamma^2} - H^2]$. The RHS of equation (1) is the product of the dispersion relations for each single film in isolation. Thus the LHS of this equation may be identified as a coupling or interaction term between the films. Equation 1 generates two sets of solutions for k and f; each set being the usual series of thickness modes for magnetostatic wave propagation. We identify the two sets respectively as the symmetric and antisymmetric modes, where the symmetry derives from the field components $h_x(y)$ and $b_x(y)$ for FVW's or $h_y(y)$ and $b_y(y)$ for BVW's. These components have been caluclated for 20 µm equal thickness films spaced 40 µm apart and supporting either FVW's or BVW's. The results are shown in Figures 3 and 4 for FVW's and BVW's respectively at a particular k and f value. One interesting feature peculiar to double films is shown in Figure 5. Films of different magnetization may support a magnetostatic wave at a particular bias field and frequency which normally for one of the films alone would be outside the excitation bandwidth. Film number 1 in Figure 5 has a magnetization of 1.8 kG and an internal field of 3.214kG. In film number 2 the magnetization is 1.4kG and thus its internal field is (3.214 + 1.8 - 1.4)kG or 3.614kG. This second film, on its own, could not support a magnetostatic wave at a frequency of 9.4GHz and a bias field of 3.614kG. In the double film structure the first film of magnetization 1.8kG carries most of the wave amplitude which then decays exponentially in the second film much like a surface wave. In Figure 5 the terms symmetric and antisymmetric have rather lost their original meaning. In fact, the "antisymmetric" mode corresponds more to the first thickness overtone for a single film.
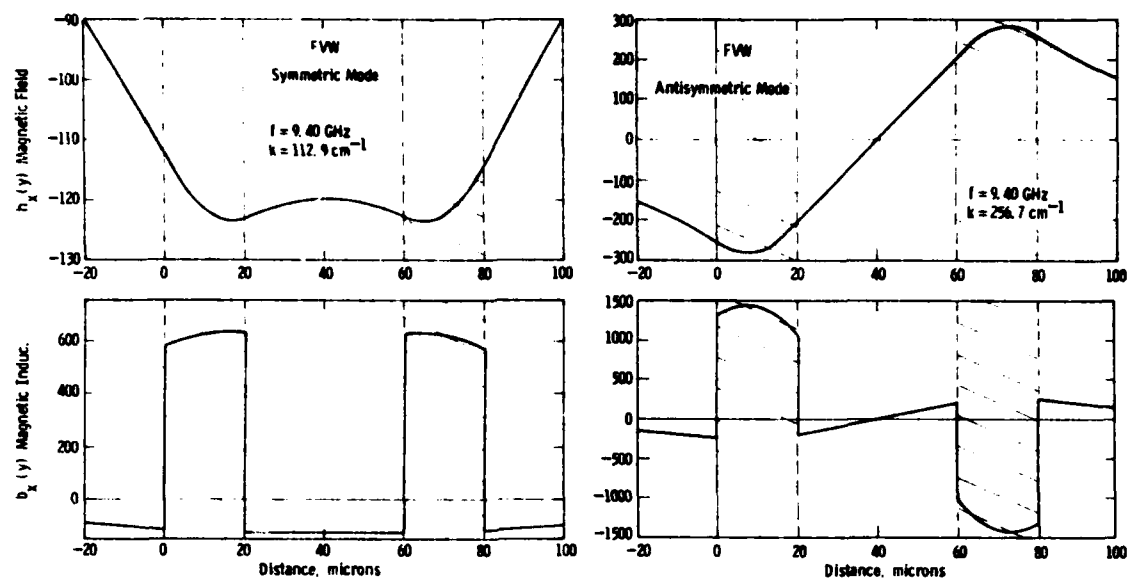
Fig. 3   Normalized plots of the magnetostatic rf magnetic field and
         induction for a FVW propagating in coupled films of equal
         thickness 20 μm and separated by 40 μm.
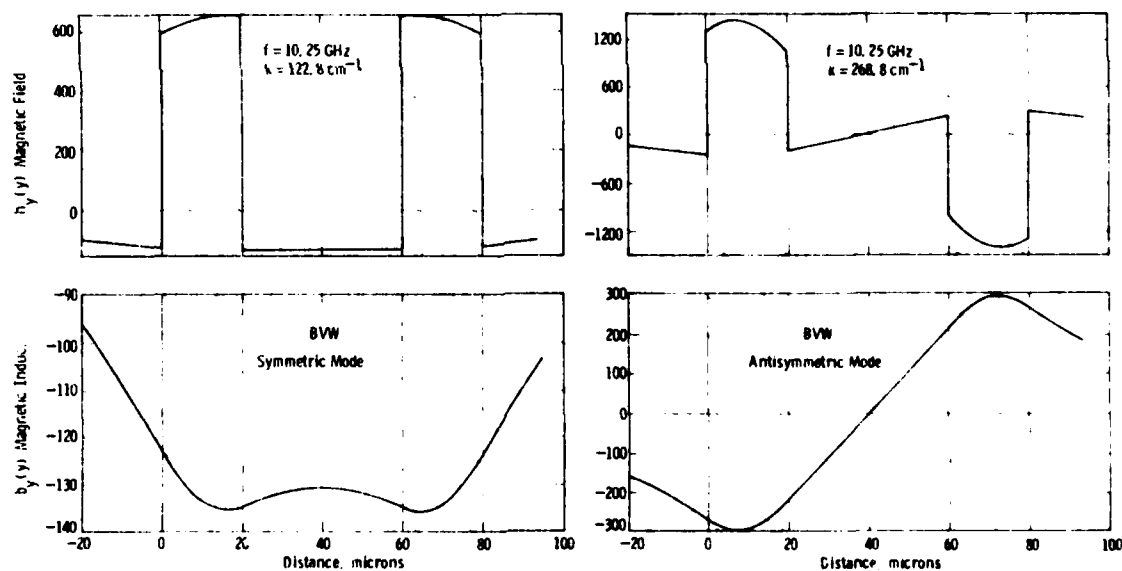
Fig. 4   Normalized plots of the magnetostatic rf magnetic field and
         induction for a BVW propagating in coupled films of equal
         thickness 20 μm and separated by 40 μm.

250
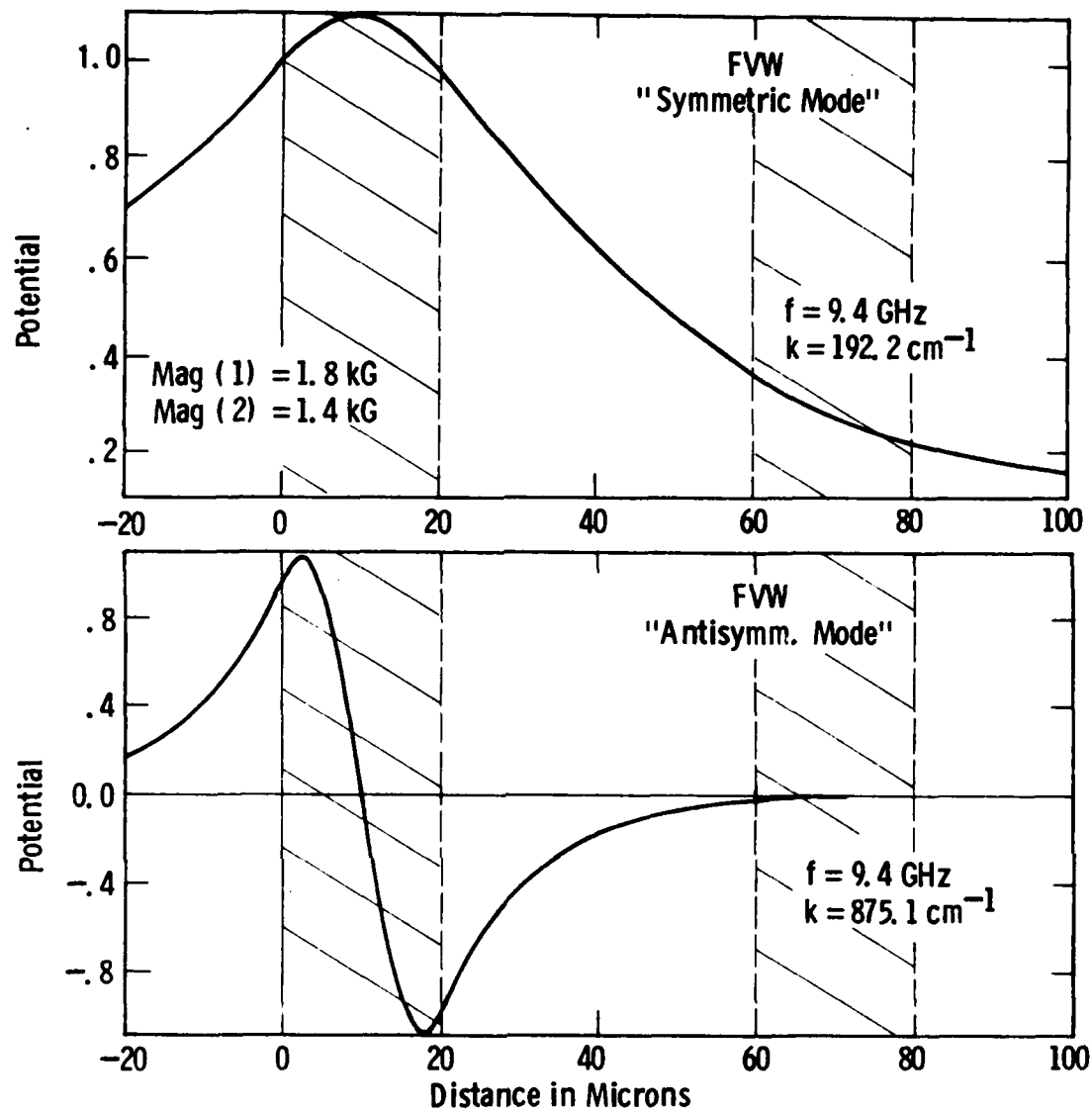
Fig. 5 Normalized plots of the magnetostatic potential for a FVW propagating in 20 μm thick films separated by 40 μm with magnetizations of 1.8kG and 1.4kG respectively.

3. Results

As mentioned in the introduction the real interest in double films is to examine their behavior for useful device possibilities. A general search of Equation (1) to get f-k curves and hence group delay by differentiation is a big undertaking due to the many parameters it contains.

However, several comments seem valid. Equation (1) gives interesting results i.e., different from single film results, when the film thicknesses are comparable and the films are close but not touching. Widely disparate d values (see Figure 1) give results dominated by one of the films much like a single film. Widely separated films only interact significantly at low k values. With these in mind we illustrate some double film results for equal thickness films fairly close together. Figure 6 shows that both FVW's and BVW's can give approximately linear delay results over 1GHz of band width. They can also give constant delays over about 0.4GHz to within ±5nS. Both sets of results occur with the ground planes far removed and so an immediate advantage results in a lower insertion loss. The dispersive delay results are quite good as is shown in Figure 7 where the phase deviation from quadratic response is plotted over the frequency range of greatest delay linearity.
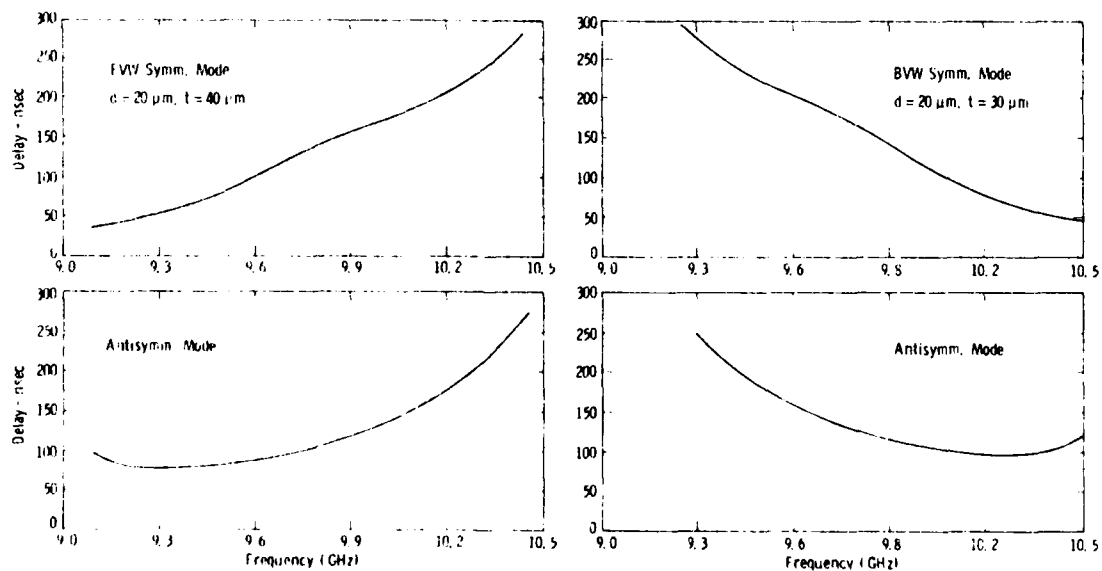
Fig. 6 Delay versus frequency for FVW's in 20 μm films separated by 40 μm and for BVW's in 20 μm films separated by 30 μm.
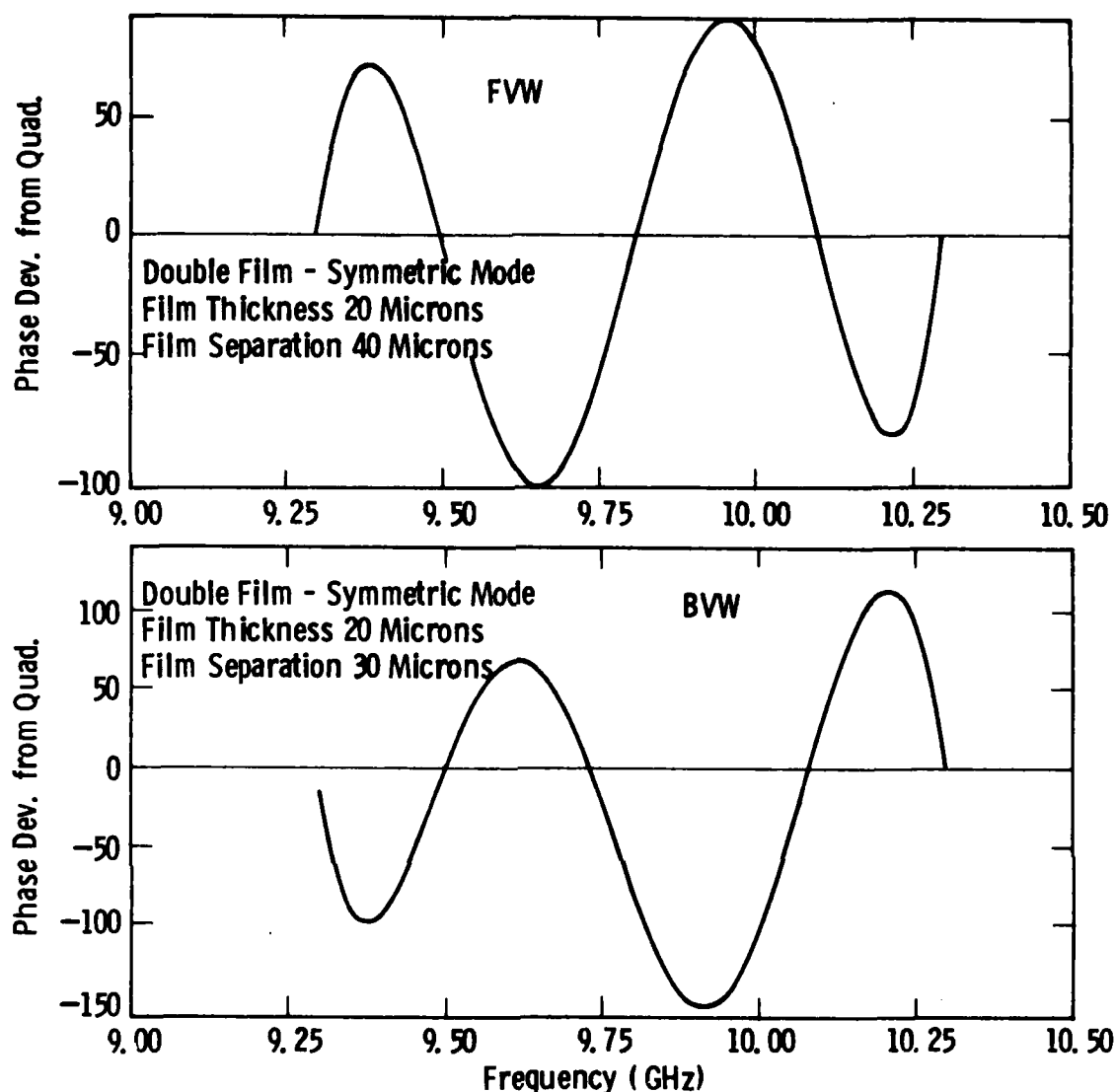
Fig. 7   Phase deviation in degrees from a quadratic response versus
frequency for the upper delay curves of Figure 6.

Some experimental results have been taken using the geometry of

Figure 8.   Two 20 μm films were separted by 1 mil(25μm) diameter Au wire

transducers.   The symmetry of the rf h-field components which the

wire produces shows that for FVW's the antisymmetric mode should be excited

whereas for BVW's the symmetric mode is expected.   The delay results

of Figures 9 and 10 confirm this wherein the FVW antisymmetric mode

displays some region of quasi-constant delay and the BVW symmetric mode

253
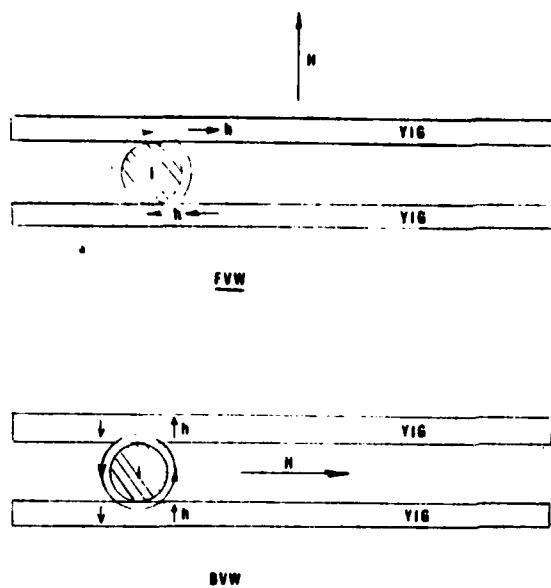
Fig. 8 rf h fields from a wire
transducer required to generate FVW's
(upper figure) or BVW's (lower figure).
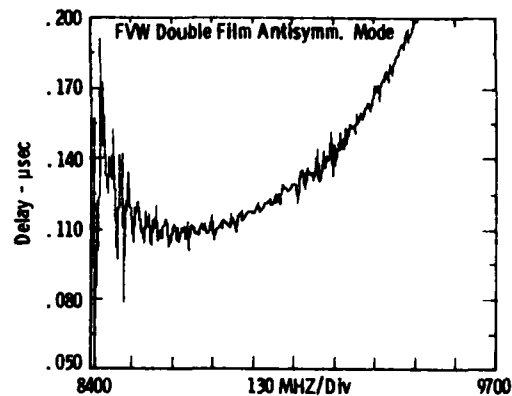
Fig. 9 - Delay versus frequency for
FVW antisymmetric mode in 20μm films
separated by 25μm.

shows linear delay variation. An attempt was made to excite the FVW symmetric

mode using the transducer arrangement of Figure 11(a). The transducer wires

were actually Au tape 2 mils x 0.5 mils in cross section sandwiched between

the YIG films and separated by a double layer of Saran Wrap (commercial

polymer film) to prevent them from shorting. The results of Figure 12

were not expected and strongly suggested that mainly antisymmetric mode

was being excited with perhaps a weaker symmetric mode causing much

interference. At this juncture a coupling constant calculation was

performed which gave some revealing results. The constant, K, was defined

and calculated in the manner described in reference 3. For double films

such a calculation cannot readily be done except, fortunately, for equal

thickness films. We define two constants: $K_{internal}$ for the transducers

in contact with the YIG films internally as in Figure 11(a); and

$K_{external}$ when the transducers lie outside the double film sandwich

but in contact with the YIG outer surfaces. Figure 13 shows the results

254
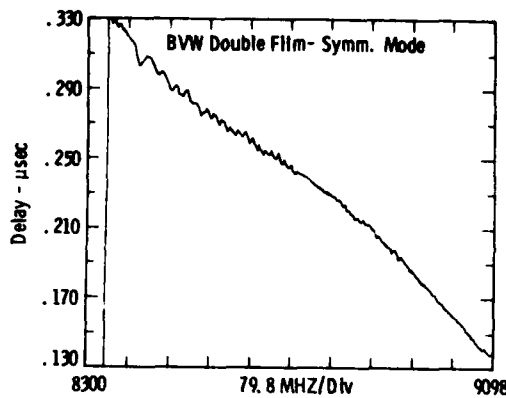
Fig. 10 Delay versus frequency for BVW symmetric mode in 20 μm films separated by 25 μm.
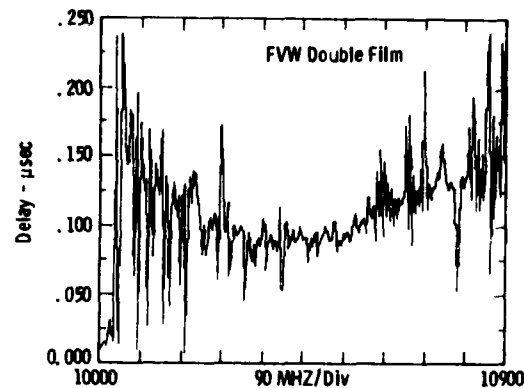
Fig. 12 delay versus frequency for FVW excitation using the transducer configuration of Figure 11(a); 20 μm thick films spaced about 50 μm apart.
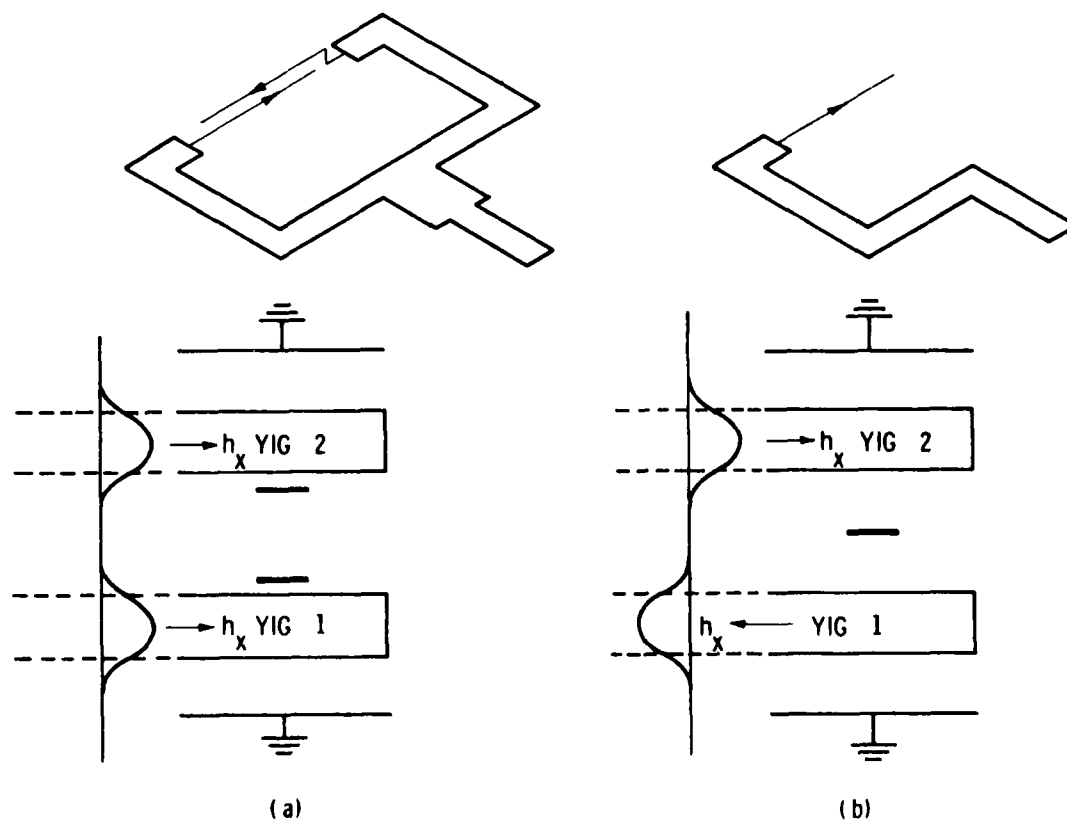
Fig. 11 Possible transducer configurations for exciting FVW (a) symmetric modes and (b) antisymmetric modes.

of these calculations for FVW's and BVW's. The upper left figure shows that $(K_{int})_{symm} \ll (K_{int})_{anti}$ except at high k values for FVW's and thus the results of Figure 12 are not now suprising. A more satisfactory approach would be to use external coupling as shown by the lower left curves of Figure 13. In the experiment of Figure 12 the equal but opposite currents in each of the transducer wires tend to produce cancelling rf h-fields particularly as the wires come together. This makes $(K_{int})_{symm}$ small, also a small error in the position of the internal wires can produce a relatively strong antisymmetric mode and this is presumably the reason for the results shown in Figure 12.
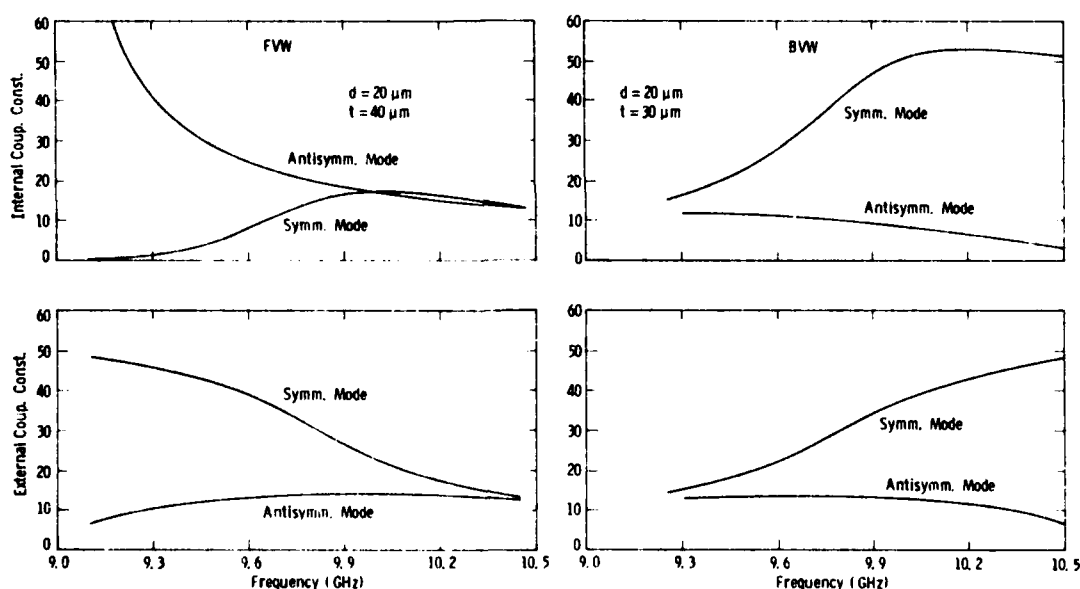
Fig. 13 Internal and external geometry coupling coefficients (%) versus frequency for both FVW's and BVW's in 20 μm films.

4. Conclusions

The propagation of magnetostatic waves in YIG double films has shown some useful delay characteristics for microwave delay lines. Films of equal thickness support two types of volume modes. The

256

first or symmetric mode can exhibit a linear delay with frequency over 1GHz of bandwidth. The second or antisymmetric mode shows a constant delay over 0.4 GHz of bandwidth. Double films are characterized by a coupling coefficient which varies with wave vector. They can also support a magnetostatic wave in films of different magnetizations at frequencies normally outside the band of the lower magnetization film.

REFERENCES

1. L. R. Adkins and H. L. Glass, Electronics Letters, 16, 503 (1980).

2. P. Grunberg, Journal of Applied Physics, 51, 4338, (1980).

3. P. R. Emtage, Journal of Applied Physics, 49, 4475, (1978)

4. This concept of surface permeability is similar to that of surface impedance used in electrical engineering problems.

5. R. W. Damon and J. T. Eshbach, Journal of Physics, Chemistry and Solids, 19, 308 (1961).

GUIDING MAGNETOSTATIC SURFACE WAVES

WITH NONUNIFORM IN-PLANE FIELDS*

by

D. D. Stancil and F. R. Morgenthaler

Department of Electrical Engineering and Computer Science
and the Research Laboratory of Electronics
Massachusetts Institute of Technology, Cambridge, MA 02139

Abstract

We have recently reported the observation of magnetostatic surface waves (MSSW's) in a rectangular YIG film placed between strips of mu-metal and in the plane of the strips. However, the interpretation of this experiment was complicated by the fact that the field was nonuniform not only in the transverse direction but along the direction of propagation as well. This latter nonuniformity resulted because the microstrip antenna structure did not allow the strips to extend along the entire path of propagation. We here report experiments using a rectangular slab and a different antenna structure which minimizes this difficulty. These experiments suggest that nonuniform in-plane fields can be used to alter the dispersion characteristics of the waves.

In addition, new experiments are described in which nonuniform fields caused by a slot in a mu-metal covering layer are used to guide MSSW's through a turn of 160°.

1. Introduction

The prospect of guiding magnetostatic waves is of considerable interest because of possible device applications.[1,2] Such guided waves might be used to increase the delay time realizable on a given size sample by meandering the path, or to make a resonator by guiding the waves along a closed loop. In addition, controlling the coupling between adjacent waveguides could make possible signal routing devices such as directional couplers.

Guiding magnetostatic surface waves (MSSW's) is complicated by the fact that MSSW propagation is highly anisotropic. Specifically, turns approaching 180° would normally require conversion to backward volume waves. However, unidirectional energy flow in such a transition would be prohibited since phase matching between the forward and backward waves would not be possible[3]. Hence the wave would be reflected from the transition region rather than guided through the turn.

It is possible to overcome this difficulty by employing gradients which arise from a change in the direction of the bias field. As an example, consider a YIG film that is covered with mu-metal containing a slot of controlled width. If the mu-metal is at a different magnetostatic potential on either side of the slot, the dc magnetic field will be parallel to the film in the region underneath the slot but normal to the film surface in those portions directly underneath the mu-metal.

The in-plane fields permit magnetostatic surface wave propagation; the normal fields do not. Therefore the surface wave energy should be localized under the air-filled slot rather than under the conducting mu-metal; eddy current dissipation is thereby minimized. The slots can be curved or even meandered with the in-plane field automatically adjusting direction to maintain the surface wave conditions.

In the event that either eddy current dissipation or radiation to volume waves beneath the mu-metal causes difficulty, the mu-metal can be placed on both sides of the meandering narrow ribbon of the YIG film to maintain the necessary field conditions for surface wave propagation .

If the above geometry is examined closely, however, there is a gradient of the in-plane field in the slot in addition to that caused by a change in direction. The magnitude of the in-plane field will vary in a bowl-shaped fashion across the slot reaching maxima at the edges of the mu-metal. It is possible that this gradient further localizes the wave to the center of the YIG ribbon minimizing scattering from the rough sample edges and/or eddy current losses.

Also, it has been previously shown that magnetic bias field gradients can alter the dispersion of magnetostatic surface waves.[4,5] In these previous analyses, the field varied along the direction normal to the surface to which the wave was bound. This is to be contrasted with the present situation of field variations along the in-plane direction, but the experiments reported here indicate that

using an in-plane gradient to control the dispersion also appears possible.

We have recently reported the experimental observations of MSSW propagation in a rectangular YIG film centered in the slot between strips of high permeability metal foil.[6] However, the interpretation of this experiment was complicated by the presence of longitudinal as well as transverse gradients. The gradients along the direction of propagation resulted because the micro-strip coupling structures prevented the mu-metal strips from extending along the entire propagation path[7]. We here report experiments using different coupling structures which minimize this difficulty.

In addition, we describe an experiment in which a nonuniform in-plane field is used to guide MSSW's through a turn of 160°.

2. Straight Path Experiment

The geometry of the straight path experiment is shown in Figure 1. The sample is a 4.5 micron thick film of YIG approximately .300 cm wide and 1.13 cm long on a .05 cm thick substrate of GGG.

The sample was cut from a one inch disk in such a way that a portion of the disk's curvature remains at one end, helping to minimize coherent end reflections. (This probably means that the film thickness is not as uniform as it would have have been had it been cut from near the center of the disk, however.) The fine wire antennas are 50 microns wide with .025 cm square bonding pads at each end. The total length of each antenna (including bonding pads) is .285 cm, and the two antennas are separated by .75 cm. The antennas were formed by first evaporating 100 $\overset{o}{A}$ of Cr followed by approximately 10000 $\overset{o}{A}$ (1 micron) of Aℓ directly on the surface of the YIG. The antennas were then etched using standard photo-lithography. Connections are made to the antennas using .001 inch diameter gold wire.

The mu-metal strips are 1.27 cm wide, 100 microns thick, and were cut from standard magnetic shielding foil (Eagle AAA foil, Eagle Magnetic Co.). The strips were placed on top of three layers of .018 cm plastic tape in order to offset the substrate thickness and place the strips approximately in the plane of the film. The separation between the strips was .5 cm.

The mu-metal was found to saturate at the field strengths of interest, so that the nonuniform field due to the strips can be calculated using a finite length magnetic line charge model[6]. Figure 2 shows in-plane field profiles at either antenna as well as midway between the antennas calculated in this way. These calculations show that the field minimum is uniform to within approximately 2.7% along the propagation path, referenced to the field at the center of the film (similar calculations carried out for the configuration of reference 6 indicate a variation of approximately 10%).

Figure 3 compares the insertion loss of the experimental delay line with and without the mu-metal strips. The field of the laboratory magnet (H_{dc}) in part (b) was chosen so that the field minimum at the center of this film (cf. Fig. 2) coincided as closely as possible to the uniform field in part (a).

A comparison of these uniform and nonuniform field insertion loss curves leads us to make the following observations. First, in part (b) there is evidence of an interference pattern suggesting multipath or multimode propagation. If it were due to multipath propagation (as in the case of end reflections) it would seem that the interference should be pronounced in part (a) also. Hence the absence of such interference makes this explanation seem unlikely.

On the other hand, the delay characteristics of the lowest order modes of a finite width slab in a uniform field are so similar at these frequencies that interference between them should not be a strong effect.[8] Since the modes have

different spatial distributions, however, the presence of a gradient could lift this degeneracy causing increased interference between these modes. Hence we interpret the presence of an interference pattern in (b) and the relative absence of one in (a) to be evidence of multimode propagation.

Secondly, the presence of the gradient appears to slightly increase the insertion loss. This, no doubt, is in part a result of the interference discussed above. In addition, the presence of the gradient should change the field distributions of the modes thereby affecting the radiation efficiency of the microstrip antennas. This latter effect could presumably be compensated for by proper modification of the microstrip coupling structures.

The delay characteristics for the two cases are illustrated in Figure 4. The data were actually obtained by measuring the slope of the phase as a function of frequency using a network analyzer. The offset in frequency between the the two curves is believed to be due to small descrepancies between the actual and computed gradients, though this has not been definitely established.

It is clear that for the higher frequencies the delay curve has essentially the same form with or without the gradient. However, it should be noted that the gradient does have a significant effect near the bottom of the band.

3. Curved Path Experiment

The geometry used to investigate guiding a surface wave through a turn of 160° is shown in Figure 5. The YIG film is in the shape of a half disk one inch in diameter. The film is approximately 4.5 microns thick and is present on both sides of a .05 cm GGG substrate. The removal of the film on one side was not attempted due to a limited supply of samples and the possibility of damaging the remaining side. Although the possibility of interaction between the two sides may complicate the detailed interpretation of the experiment, it is felt that it should not be a sufficiently strong effect to prevent a valid investigation of the basic waveguiding concept.

The antennas are the same size as those used in the straight path experiment and were fabricated in a similar way, except that the Cr adhesion layer was omitted. The inner radius of the channel is .399 cm and the outer radius is .899 cm resulting in a channel width of .500 cm, and a mean radius of .649 cm. The mean circumferential path between antennas is 1.82 cm.

The mu-metal pole pieces are .127 cm thick and were machined from standard magnetic shielding material (NETIC S3-6 alloy stress annealed sheet, Magnetic Shield Div., Perfection Mica Co.). These sheet mu-metal pole pieces are connected directly to the poles of a small electromagnet as shown in Figure 6. In contrast to the procedure used in the straight path experiment, this assembly was not placed in the field of a large laboratory magnet; all of the flux is supplied by the small magnet shown.

A rather large amount of hysteresis in the electromagnet complicated the process of precisely setting the magnetic field. Experimentally, it was found that even when the magnet current was varied so as to follow a specific hysteresis path, the required current to repeat a particular spectrum could vary by on the order of 10%.

The relatively thick mu-metal sheet and the above mentioned alloy were chosen in an attempt to minimize the saturation problem encountered with the very thin foil used in the straight path experiment. Saturation was still a severe problem, however, and limited operation to frequencies below 1GHz. It was particularly important to avoid saturation in the present experiment since the YIG film extended beneath the mu-metal as well as in the channel. Hence it was crucial for the mu-metal to exhibit a high permeability in order to cause the desired change in the direction of the field. It should be possible to minimize this saturation problem either through a suitable choice of pole piece material and design or by using properly shaped permanent magnets.

263

Typical dc magnetic field profiles are shown in Fig. 7. The fields were measured using a samll Hall probe oriented so as to be sensitive to the in-plane component of the flux. The active area of the probe is approximately .102 cm in diameter and was centered in the plane containing the lower surface of the mu-metal sheets. No corrections for field averaging due to the finite active area of the probe have been made.[6] Since field measurments must necessarily be made in the absence of the sample and precise field repeatability has been found to be a problem, these field contours should be viewed as typical only.

It is clear from Figure 7 that the curvature of the channel causes a pronounced asymmetry in the field profile (cf. Figure 2). The difference between the profiles near the antennas and halfway between them is due to the transition from a straight to a curved path. The effect of this longitudinal nonuniformity could be minimized by adjusting the width of the channel so as to make the magnitude of the field minimum constant everywhere. Such a nonuniformity would not appear, of course, in the case of a resonator formed by a closed circular path.

The transmission characteristics associated with the field profiles of Figure 7 are shown in Figure 8. It should be noted that the observed bandwidth is only a small fraction of that expected from uniform field surface wave theory. The reason for this is not completely understood at present. Note also that the delay increases sharply near the bottom of the band in a manner reminiscent of that observed in the straight path experiment (cf. Figure 4). Thus this feature is due most likely to the in-plane gradient rather than the radius of curvature. The fluctuations in the delay could be due to the effects of multimode propagation and/or end reflections.

Since the YIG exists beneath the mu-metal as well as in the channel, other propagation paths than the channel are conceivable, though unlikely due to the change in field direction. In order to verify that the signal was indeed

264

propagating around the curved path, the wave was probed using a small induction loop at several points along the path. The loop is .2 cm wide and .1 cm high and is made from .003 inch diameter wire. In addition to verifying the presence of the wave at various points along the path, the loop was used to determine the local direction of the k vector. This was done by making use of the fact that the loop is most sensitive to k vectors directed normal to its plane; hence the direction of $\overline{k}$ can be approximately determined by rotating the loop. The results of these measurements are shown in Figure 9. Although the vectors are not all precisely circumferentially directed, it is felt that the results strongly support the waveguiding interpretation.

The deviation from the circumferential direction could be due in part to multimode propagation as well as anisotropy. Anisotropy in particular should be expected to have a relatively large effect on the propagation characteristics in view of the small applied magnetic fields.

4. Summary and Conclusion

We have discussed the problems associated with guiding MSSW's and how they may be overcome using nonuniform magnetic fields. The possible use of nonuniform in-plane fields for dispersion control has also been discussed.

We have described experiments using nonuniform in-plane fields in both straight and curved path geometries. The curved path experiment is believed to be the first demonstration of the ability to guide MSSW's.

Acknowledgement

265

References

1. J. D. Adam and J. H. Collins, "Microwave Magnetostatic Delay Devices Based on Epitaxial Yttrium Iron Garnet," _Proc. IEEE_, Vol. 64, No. 5, p. 794, May 1976.

2. D. A. Zeskind and F. R. Morgenthaler, "Localized High-Q Ferromagnetic Resonance in Nonuniform Magnetic Fields," _IEEE Trans. on Mag._, Vol MAG-13, No. 5, p. 1249, September 1977.

3. J. H. Collins and F. A. Pizzarello, "Propagating Magnetic Waves in Thick Films: A Complementary Technology to Surface Wave Acoustics," _Int. J. Electronics_, Vol. 34, No. 3, pp. 319-351 (1973).

4. F. R. Morgenthaler, "Magnetostatic Waves Bound to a DC Field Gradient," _IEEE Trans. on Mag._, Vol. MAG-13, No. 5, p. 1252, September 1977.

5. F. R. Morgenthaler, "Bound Magnetostatic Waves Controlled by Field Gradients in YIG Single Crystal and Epitaxial Films," _IEEE Trans. on Mag_, MAG-14, No. 5, p. 806, September 1978.

6. D. D. Stancil and F. R. Morgenthaler, "Magnetostatic Surface Modes in a Thin Film with Nonuniform In-plane Fields," _IEEE Trans. on Mag._, Vol. MAG-16, No. 5, . 1156, September 1980.

7. D. D. Stancil and F. R. Morgenthaler, "The Effects of Nonuniform In-plane Fields on the Propagation Characteristics of Magnetostatic Surface Waves," _1980 Ultrasonics Symposium Proceedings_, IEEE Cat. No. 80CH 1602-2, P. 547 (1980).

8. T. W. O'Keefe and R. W. Patterson, "Magnetostatic Surface-Wave Propagation in Finite Samples," _J. Appl. Phys._, Vol. 49, No. 9, p. 4886, September 1978.
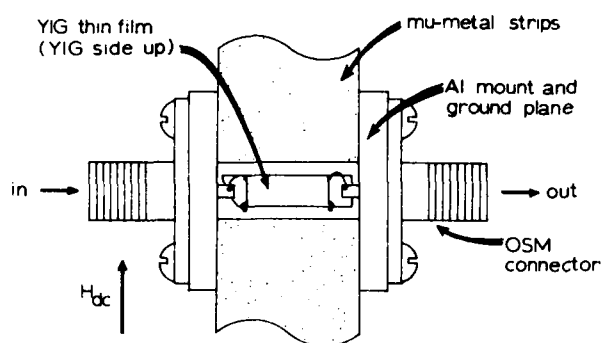
Figure 1.   Geometry of straight
path experiment.
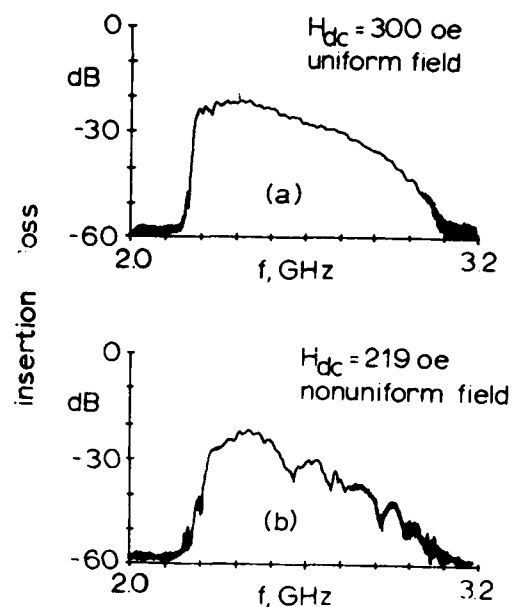
Figure 3.   Effects of in-plane
gradient on insertion
loss.
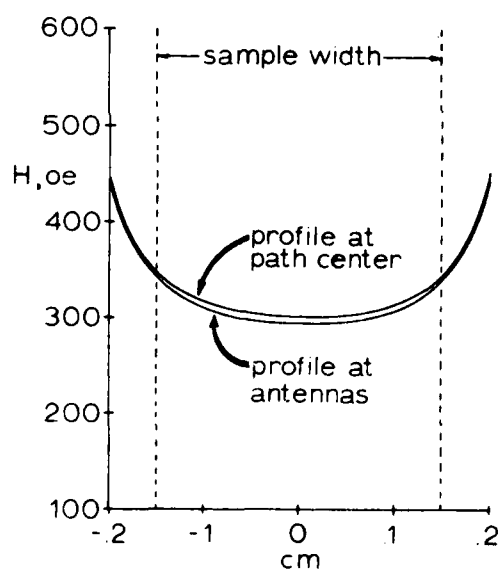
Figure 2.   Calculated magnetic field
profiles for straight path
experiment, H_{dc} = 219 oe.
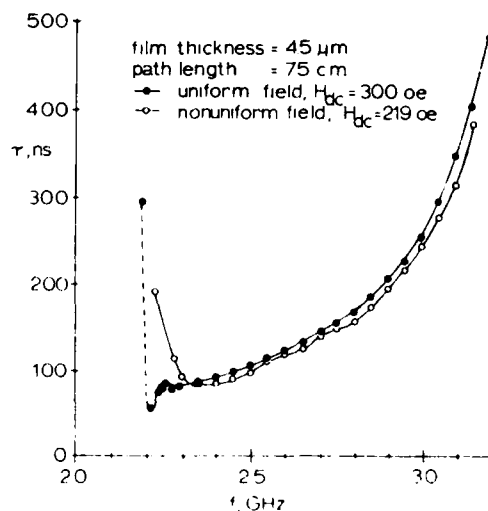
Figure 4.   Effects of in-plane
gradient on delay
characteristics.

267
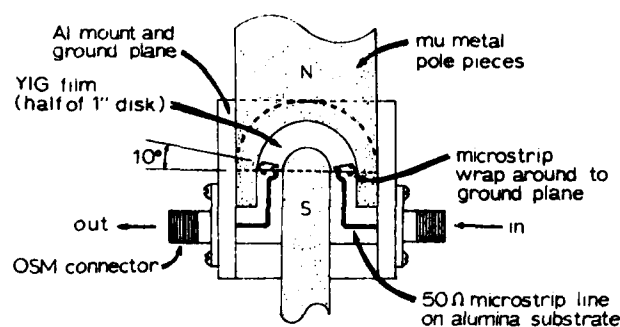
Figure 5. Geometry of curved path experiment.

Figure 8. Transmission characteristics of curved path delay line.

Figure 6. Electromagnet and pole piece assembly.
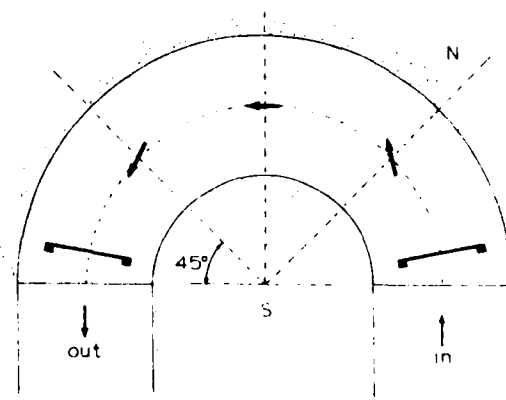
Figure 9. Direction of $\bar{k}$ at points along propagation path at fixed frequency (the frequency was chosen near the peak of the transmission spectrum).

Figure 7. Measured field profiles for the curved path experiment. $r_<$ = inside radius of slot, $r_>$ = outside radius.

OCTAVE BANDWIDTH
MAGNETOSTATIC SURFACE WAVE SIGNAL-TO-NOISE ENHANCER*

Steven N. Stitzer
Westinghouse Electric Corp.
Advanced Technology Laboratories
Baltimore MD 21203

INTRODUCTION

The signal-to-noise enhancer[1,2] is a passive two-port device which performs the function opposite that of the frequency selective microwave power limiter. Incoming signals falling below some threshold power level suffer insertion loss up to 30 dB or more. Signals exceeding the threshold, which is on the order of 1 mW, are attenuated by a significantly smaller amount. The difference in insertion loss can be more than 25 dB for signals 20 dB or more above threshold.

ENHANCER CONSTRUCTION

Figure 1 is a sketch of the device. A single microstrip transmission line, connecting the input and output ports, is placed over a sample of ferrimagnetic material. This material is typically YIG epitaxially grown on a GGG substrate. A pair of permanent magnets supplies an in-plane static magnetic bias field parallel to the microstrip. Magnetostatic surface waves (MSSW) excited in the YIG by the RF magnetic fields surrounding the microstrip propagate perpendicularly away from the microstrip.

At low RF power levels, the MSSW excitation is linear, and the MSSW carry RF energy toward the edge of the film. Much of this energy would ordinarily be reflected at the edge of the YIG/GGG substrate and would eventually be coupled back into the microstrip line. This is prevented by providing a lossy layer on the microstrip substrate under the YIG. A film of nichrome having a surface resistivity of about $30\,\Omega/\square$ absorbs virtually all of the MSSW energy. The result is high absorption of low-level RF signals.

Above a critical RF power level, the spinwave amplitudes saturate, and no additional RF power can be coupled into the film. The excess power travels along the microstrip to the output port. The measured insertion loss thus decreases as the input power rises above the threshold. Since the RF power is coupled to spinwaves on a frequency selective basis, only those spinwaves near the RF signal frequency saturate. Weak signals separated from the above-threshold signal by more than a few spinwave linewidths are still strongly attenuated. If the input consists of a strong coherent signal in the presence of broadband low-level noise, the ratio of the coherent signal to the broadband noise will be greater at the output than at the input, hence the name of the device.

If we define enhancement as the ratio of the insertion loss below threshold to that at a given power level, we find the following expressions for enhancement E (in dB):

$$E = 0 \qquad\qquad\qquad\qquad\qquad\qquad P_{in} < P_{th}$$

$$E = 4.34\,(P_{in}/P_{th} - 1) - 10\,\log(P_{in}/P_{th}) \qquad P_{th} < P_{in} < (1+C_1)P_{th}$$

$$E = 10\,\log(1 - C_1\,P_{th}/P_{in}) + 4.34\,C_1 \qquad\qquad P_{in} > (1+C_1)P_{th}$$

where C_1 is found from the below-threshold loss: $L_0 = 4.34\,C_1$ (dB).

SINGLE BAND ENHANCEMENT

The instantaneous bandwidth of an individual enhancer is controlled by 1) the frequencies over which MSSW can propagate and 2) the requirement that half-frequency spin waves must coexist with the MSSW. These criteria are illustrated in figure 2, which shows the operating frequency as a function of the magnetic bias strength. Enhancers can be operated in the shaded regions of the graph.

The below-threshold insertion loss is given by

$$L=0.08686 \ (c/v_{ph}) \ \text{Im}(1 + j\mathcal{R}/\omega\mathcal{L}) \ \ \text{dB/cm}$$

where c is the speed of light in vacuum and v_{ph} is the phase velocity in the microstrip. $\mathcal{R}$ is the radiation resistance per unit length[3] and $\mathcal{L}$ is the inductance per unit length of the microstrip. The amount of enhancement possible increases directly as the below-threshold loss is raised. The low-level absorption can be increased by lowering the phase velocity in the microstrip. Since the dielectric does not affect the low-level or saturation characteristics of the MSSW, we have used a high dielectric constant ceramic, magnesium-calcium-titanate*, having $\epsilon_r=70$, as the microstrip substrate for this purpose.

To obtain strong coupling at high wavenumbers, the microstrip must be narrow. A typical width is 1-2 mils. These narrow lines, when etched on the high dielectric constant material described above, have an impedance near 50 ohms. This largely eliminates any impedance matching problems at the input and output ports.

We constructed two enhancers having 1 mil transducers on MCT-70 substrates, with 35-50 micron YIG films. One was biased at 375 Oe and the other at 620 Oe. Swept frequency response curves for the two devices are shown in figures 3 and 4. The low-level absorption band corresponds to the calculated MSSW band for each. Over 10 dB enhancement was obtained at +15 dBm input. Subsidiary resonance limiting can be seen above the MSSW band.

From figure 2, we find that the useable bandwidth in an isolated (ungrounded) YIG film goes to zero at 4.9 GHz. Theoretically, more than an octave band could be covered if one surface of the YIG film is metallized. Only one surface of an epitaxial film is accessible, so the metallization must be broken for a transducer. So far, we have not found a transducer capable of operation over the full metallized MSSW band.

We have used two experimental techniques to extend the upper frequency limit in narrow band enhancers. The first is a coplanar waveguide transducer, shown in figure 5. Initial tests with a single 1 mil wide center conductor separated from the coplanar groundplanes by 1 mil gaps showed strong resonant responses in the MSSW band. Also, the lower limit of operation with this transducer is much higher than the lower MSSW band edge. Both of these problems are due to the symmetry of the RF magnetic fields around the center conductor, which effectively cancels the coupling at long wavelengths and at discrete frequencies throughout the MSSW band. The observed nulls are not unlike those observed in the multiple finger transducers used in delay lines and filters. To eliminate these nulls, three cascaded sections of coplanar waveguide were etched on an alumina substrate. Each section is about 0.25 inch long. The center conductor widths and center conductor-to-coplanar groundplane spacings are 1, 2 and 5 mils in the three sections. Any resonance in one section tends to be masked by smooth response in the other sections at that frequency. The response of this enhancer is shown in figure 6.

*Trans-Tech MCT-70.

270

The second technique used is an effort to provide a metallized mode from the MSSW point of view, while simultaneously providing a nonmetallized environment for the microstrip. Figure 7 shows the basic structure. The surface of the YIG film is metallized, as in coplanar waveguide, but the metallization is divided into isolated cells. The linear dimensions of the cells are large compared to the MSSW wavelength, while the 1-mil gaps are small compared to the MSSW. Thus the film acts as though it is continuously metallized. The cells are much smaller than the (quasi-)TEM microstrip wavelength, which is $c/f\sqrt{\epsilon_{eff}} \approx 1$ cm. The gaps disrupt the coplanar groundplane currents whose field distributions cause the troublesome resonances in pure coplanar waveguide transducers. A relatively smooth response was obtained across 4.2-5.2 GHz, as seen in figure 8.

OCTAVE BANDWIDTH ENHANCEMENT

Three enhancers were constructed, covering 2.6-3.5, 3.5-4.2, and 4.2-5.2 GHz, respectively, with about 50 MHz overlap at the band edges. The individual enhancers gave a minimum 10 dB minimum enhancement across their respective bands. A network consisting of a pair of three-port circulators and a pair of steep-skirt bandpass filters for each subband was used to interconnect the three enhancers, as shown in figure 9. The filter passbands correspond to the enhancer bands, and were made contiguous. Signals applied to the input port are directed to the appropriate enhancers by the filters and circulators. The signals recombine at the single output port.

The overall swept response is shown in figure 10. A worst-case enhancement of 7 dB is obtained across the full octave band, 2.6-5.2 GHz, for an input power level of +20 dBm. Enhancement is greater than 10 dB at most frequencies, but is degraded near the subband edges. This is because 1) the triplexing network attenuates signals at the crossover frequencies by about 3 dB and 2) the enhancement factor falls off slightly near the MSSW band edges. Several dB greater enhancement is obtained if the input level is increased to +25 dBm, but equipment limitations prevented us from supplying greater levelled power across the full octave band. Above +25 dBm, a limiting effect takes place, and enhancement factor starts to decrease.

CONCLUSION

Signal-to-noise enhancers have been built covering one-third octave bands between 2.6 and 5.2 GHz. A new metallization technique has been developed to allow YIG to be used above 4.9 GHz. Over 7 dB enhancement was obtained across a full octave with three enhancers connected in a frequency splitting/recombining network.

REFERENCES

1. J.D. Adam and S.N. Stitzer, "A Magnetostatic Wave Signal to Noise Enhancer, Appl. Phys. Lett., 36, March 15, 1980, pp. 485-487.

2. S.N. Stitzer, J.D. Adam, H. Goldie and P.R. Emtage, "Magnetostatic Surface Wave Signal-to-Noise Enhancer," 1980 International Microwave Symposium Digest, pp. 238-240.

3. P.R. Emtage, "Interaction of Magnetostatic Waves with a Current," J. Appl. Phys. 49, August, 1978, pp. 4475-4484.
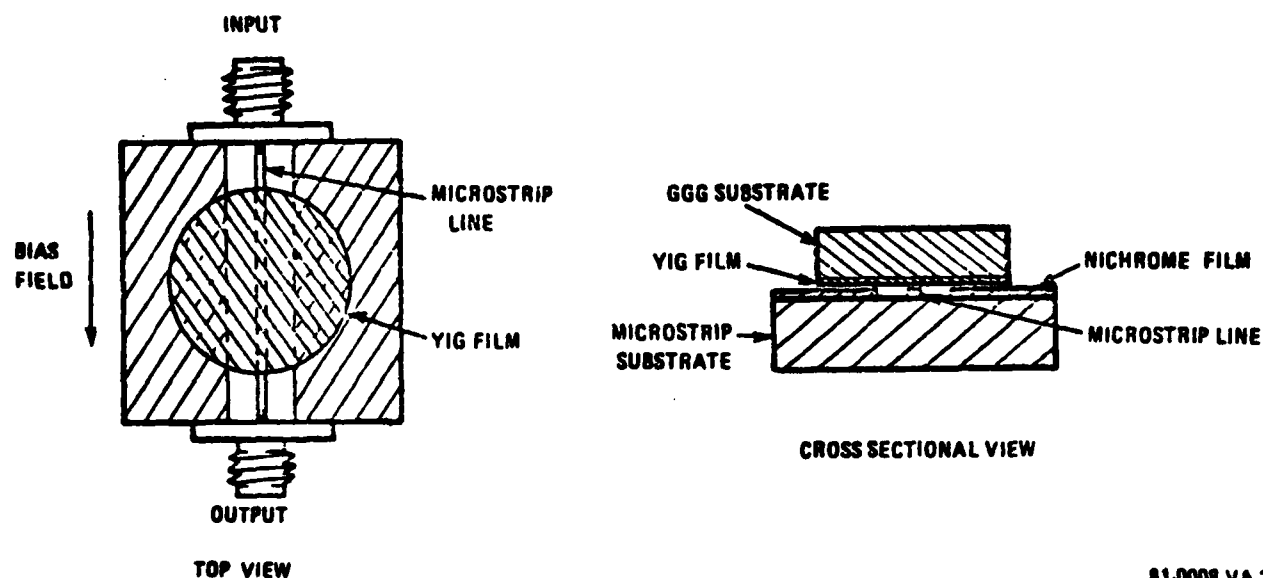
Figure   1.   Magnetostatic Surface Wave
Signal-to-Noise Enhancer
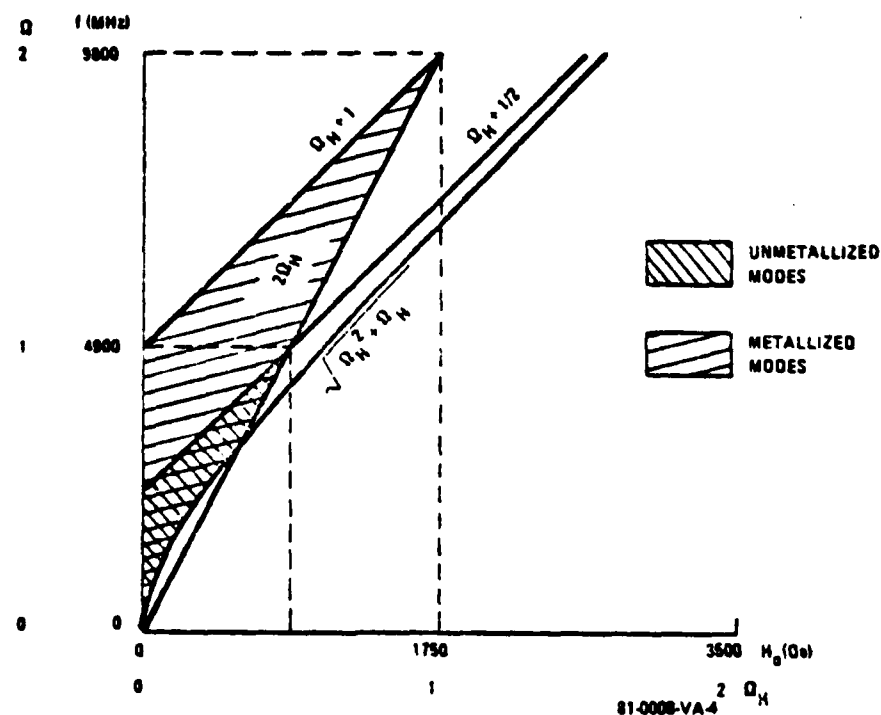
Figure   2. Magnetostatic Wavebands for YIG Enhancers

49 μm Pure YIG
$H_o = 310$ Oe
1 mil Line, $\epsilon_R = 70$
30Ω/□NiCr
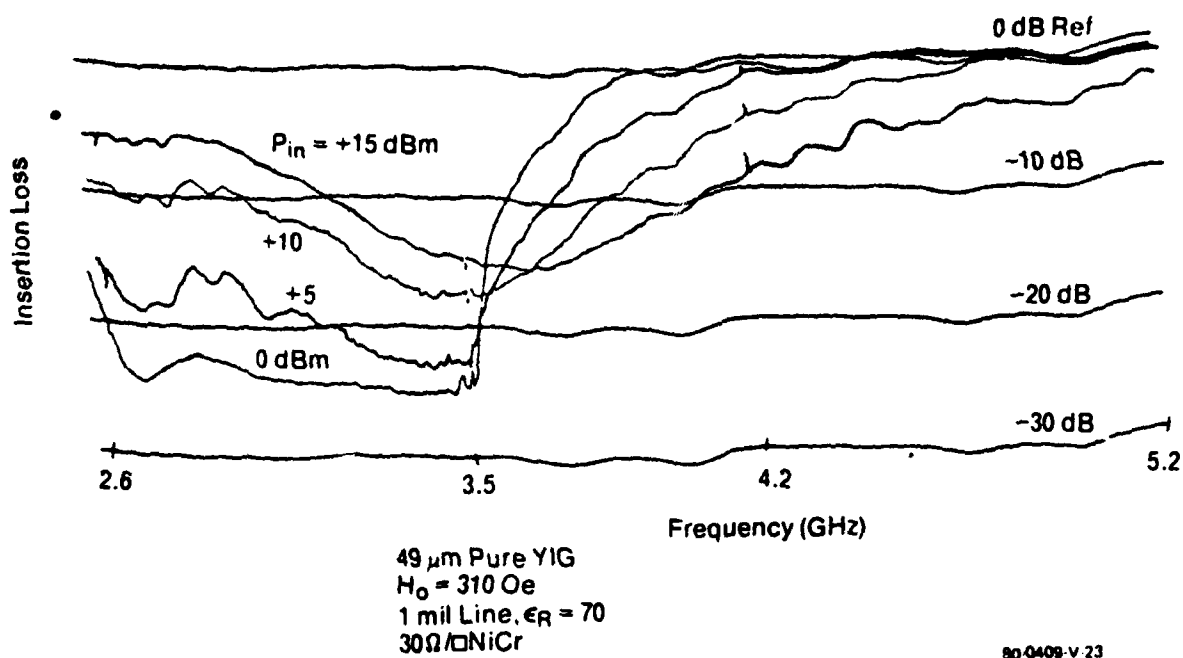
80-0409-V-23

Figure 3. Subband A Swept Insertion Loss

80-0157-VA-4
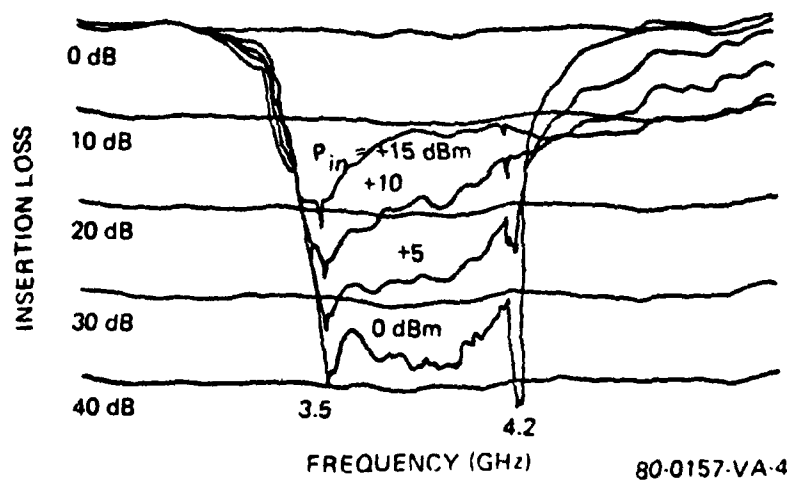
Figure 4. Subband B Swept Insertion Loss

273
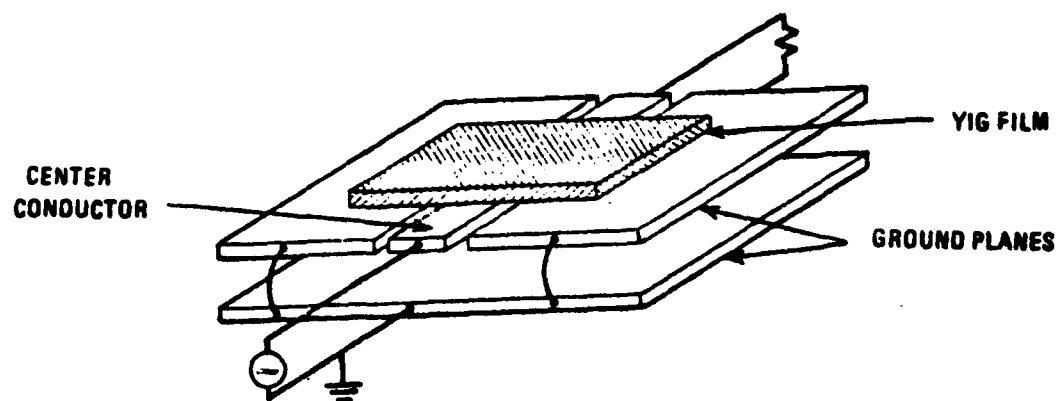
Figure 5. Coplanar Waveguide Transducer
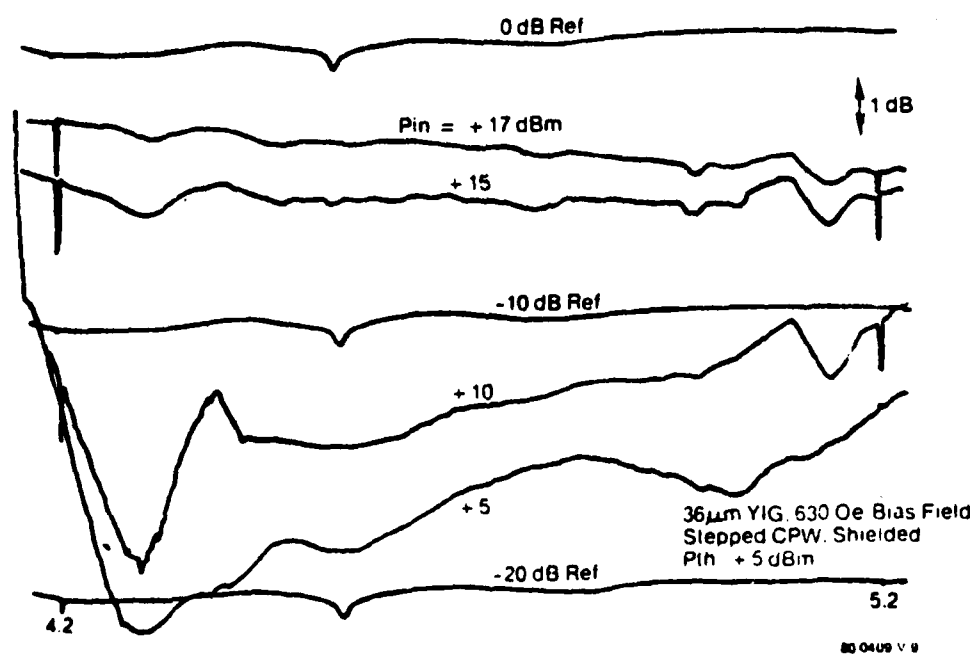
Figure 6. Frequency Response of 3 Cascaded Coplanar
Waveguide Stages

274
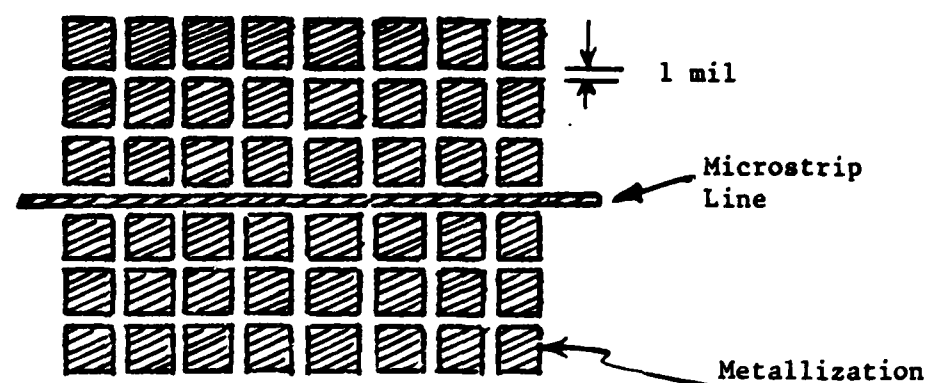
Figure 7. Plan view of Cellular Metallization Coplanar Transducer. (Not to scale.)
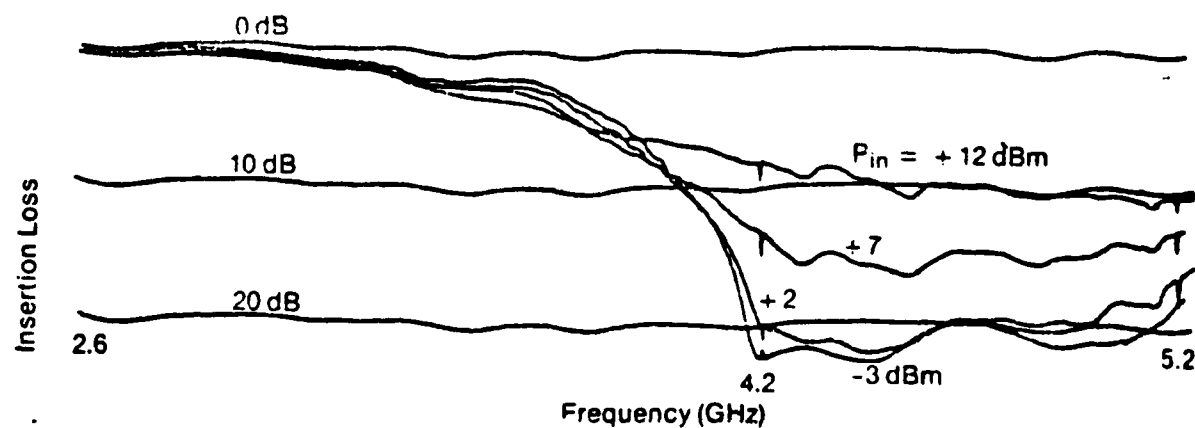
36.0μm Pure YIG; Ground Edge
80 mil Square Cell Metall. on A1$_2$O$_3$; Unshielded
H$_o$ = 570 Oe

80-0409-V-24

Figure 8. Frequency response of cellular metallization enhancer.

275
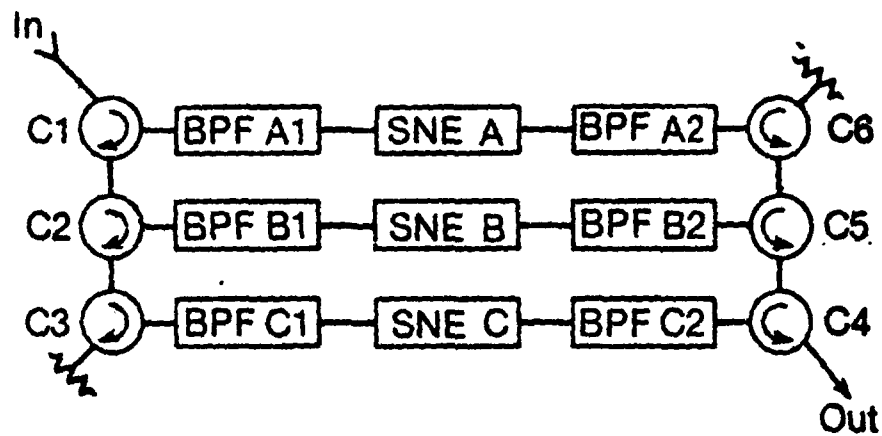
80-0409-V-48

Figure 9.   Frequency Triplexing Scheme
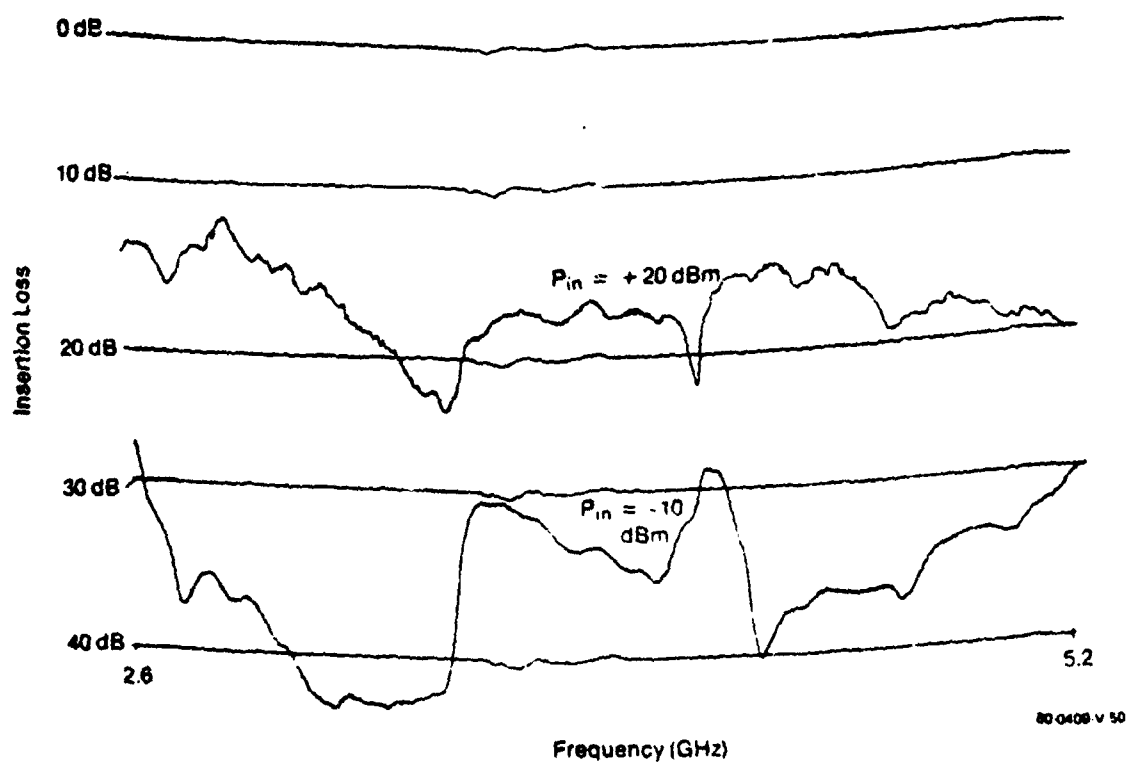
Figure 10.   Octave Band Enhancement

MICROWAVE PULSE COMPRESSION LOOPS

USING MAGNETOSTATIC WAVE DELAY LINES

C. V. Smith, Jr., J. M. Owens, R. L. Carter, and K. W. Reed

ELECTRICAL ENGINEERING DEPARTMENT,

THE UNIVERSITY OF TEXAS AT ARLINGTON,

ARLINGTON, TEXAS 76019

Abstract

Pulse compression systems utilizing surface acoustic wave (SAW) devices have been under intensive investigation for the past 10 years. These studies have concentrated primarily on linear chirps and the achievement of low time-sidelobes by appropriate amplitude weighting. Both active and passive generation have been utilized in the compression loops, and time-bandwidth products over 1000 with greater than 40 dB sidelobe suppression have been obtained. In general, SAW devices achieve large processing gains by large time delays (1-100 μsec) with bandwidths of 50-500 MHz and comparable center frequencies. A new technology based on "slow" magnetostatic wave (MSW) propagation in a magnetically biased epitaxial yttrium iron garnet (YIG) is emerging as a complementary technology to SAW at microwave frequencies (1-20 GHz). Spin coupling in the magnetostatic modes results in electromagnetic wave propagation at group velocities two orders of magnitude below the speed of light. This dispersive slow wave structure makes the investigation of MSW devices in pulse compression logical.

MSW devices achieve comparable processing gains through large bandwidths (nominally 0.5-1.0 GHz) accompanied by typical group delays of up to 1000 nsec/cm, depending on the bias field and film thickness used. The 1-20 GHz center frequency range makes processing possible directly at radar carrier frequencies. Center frequencies are electronically tunable by adjusting the magnetic bias field strength (375 Oe at 3 GHz with MSSW).

An experimental pulse compression loop has been built using a magnetostatic surface wave (MSSW) delay line as the compression filter and a microwave voltage controlled oscillator driven by a programmable voltage sweeper to provide the 3 GHz chirp signal. The recompressed pulse was observed at the output of the MSSW delay line using a sampling oscilloscope.

Initially, a single-bar transducer MSSW delay line was investigated with a 570 MHz bandwidth (based on the half-pulse width), centered at

2.9 GHz (16 dB insertion loss), with 53 nsec of delay dispersion, giving a time-bandwidth product of 30. Measured time-sidelobes were 15.d dB below the main pulse with a theoretically predicted peak-to-sidelobe ratio of 19.6 dB. Doppler peak-to-sidelobe degradation was less than 0.16 dB for simulated 1800 MPH target velocities and a 95 GHz carrier.

A first-order improvement in peak-to-sidelobe ratio was achieved using loop transducers for mild spectral shaping. The experimental device had 400 MHz bandwidth centered at 2.8 GHz (10 dB insertion loss), yielding -24 dB sidelobes and a theoretical compression gain of 44. Doppler studies resulted in 0.d dB sidelobe degradation at 1800 MPH target velocity with 95 GHz carrier.

This work demonstrates both theoretically and experimentally that the intrinsic MSW dispersion occurring in a simple MSSW delay line can be utilized effectively in a low loss pulse compression filter operating directly at microwave frequencies (1-20 GHz). Effects of Doppler shifts, delay line characteristics, and spectral weighting have been included. Theoretical studies indicate sidelobe suppression greater than 30 dB is attainable by using rack weighted MSW delay lines.

INTRODUCTION

Pulse compression as a signal processing technique had its initial beginning at the end of World War II when the radar system designers [1-4] realized that detectability (i.e., absolute range) was a function of signal energy while resolution (i.e., range resolution) was a function of signal bandwidth. It is interesting to note that all these early proposals provided an increase in signal bandwidth by a linear sweep of carrier frequency during transmission; this encoding clearly yields a correlation between time and frequency which can be exploited at the receiver. This particular form of signal encoding has proven most useful and continues to be applied in diverse systems such as radars and compressive receivers, as well as being discovered in natural settings where search, detection, and jamming are also matters of survival [5]. Other methods used for signal encoding, as first described in a unified manner by Woodward [6], include nonlinear FM, discrete frequency-shift, polyphase codes, compound Barker codes, code sequencing, complementary codes, pulse burst and stretch; these methods are discussed by Skolnik [7].

The basic reasoning as cited in the referenced patents gives a heuristic understanding as to why pulse compression works. A signal of time duration T is swept linearly in frequency over a bandwidth B. The various instantaneous frequencies in the signal are then in a direct correspondence with time occurrence within the pulse duration. If a "matched" filter [8], that is, a filter whose impulse response is a delayed, time-inverted replica of the signal to be matched, is considered; it is discovered that a compression filter with a constant amplitude spectrum and linear time delay (i.e., quadratic phase) is required. For such a dispersive delay line filter the early arriving frequency components of the signal are delayed more than the later

278

arriving frequency components, so the total signal energy is accumulated in time at the filter output. It may be shown that the peak output to input power ratio is given by (figure 1),

$$Po/Pi = TB,$$

where the parameter TB is known as the time-bandwidth product and represents a signal processing gain or figure of merit for this encoding scheme. In a matched filter the peak signal-to-noise ratio is proportional to the input signal energy, independent of signal shape, and the effective output pulse width for the compression filter is inversely proportional to the encoding bandwidth; this means that detectability is proportional to input signal duration and the resolution is proportional to the input signal bandwidth. The time-bandwidth product TB is then a figure of merit for detectability-resolution.

Figure 1: (a) The frequency swept transmitter pulse (down-CHIRP).
(b) The reverse delay characteristic of the compression filter.
(c) The recompressed pulse obtained by passing (a) through (b).

Pulse compression systems utilizing surface acoustic wave (SAW) devices have been under intensive investigation for the past 10 years. These studies have concentrated primarily on linear chirps and the achievement of low time-sidelobes by appropriate amplitude weighting. Both active and passive generation have been utilized in the compression loops, and time-sidelobes of greater than 40 dB down and time-bandwidth products >1000 have been obtained. In general, SAW devices achieve large processing gains by large time delays (1-100 μsec) with bandwidths from 50-500 MHz [9]. A new technology based on "slow" magnetostatic wave (MSW) propagation in a magnetically biased epitaxial yttrium iron garnet (YIG) is emerging as a complementary technology to SAW at microwave frequencies (1-20 GHz). Spin coupling in the magnetostatic modes results in electromagnetic wave propagation at group velocities two orders of magnitude below the speed of light [10]. This dispersive slow wave structure makes the investigation of MSW devices in pulse compression loops logical.

279

END

MICROCOPY RESOLUTION TEST CHART

NATIONAL BUREAU OF STANDARDS-1963-A

MSW devices achieve comparable processing gains through large bandwidths (nominally 0.5-1.0 GHz) accompanied by typical group delays of up to 1000 nsec/cm, depending on the bias field and film thickness used. The 1-20 GHz center frequency range and 2 GHz bandwidth capability of this technology makes processing possible directly at radar carrier frequencies. Center frequencies are electronically tunable by adjusting the magnetic bias field strength (375 Oe at 3 GHz with MSSW) [10].

This review focuses on use of the intrinsic MSW dispersion in a pulse compression loop formed from an active chirp generator and a simple magnetostatic surface wave (MSSW) delay line.

Experimental objectives were to establish performance limits for the simplest possible system. Although performance gains can be realized with added complexity, such as metalized arrays for spectral weighting and delay linearization, a simple delay line could be adequate for numerous less demanding applications at considerable cost and manufacturing savings.

MSW PROPAGATION AND DISPERSION CONTROL

The propagation characteristics of magnetostatic waves have been extensively investigated both experimentally and theoretically since the initial study by Damon and Eshbach [11] in 1961. Dispersion control by ground plane proximity has received much attention. Bongianni [12] at Rockwell International first showed that Magnetostatic Surface Wave (MSSW) dispersion characteristics could be significantly altered to produce both non-dispersive and linearly dispersive regions by placing a ground plane in close proximity to the YIG layer. Subsequent work by Tsai et al [13] of the University of Texas at Arlington and Daniel et al [14] at Westinghouse have shown that a similar situation exists for Magnetostatic Forward Volume Waves (MSFVW) and Magnetostatic Backward Volume Waves (MSBVW). Adams et al [15] of Westinghouse has shown experimentally using MSFVW that constant delay devices with a 100 nsec/cm delay and a bandwidth of 400 MHz are possible at 8 GHz and that linearly dispersive delays of greater than 1 GHz bandwidth at 10 GHz with time-bandwidth products of 230 can be realized with an insertion loss of 30 dB. Glass et al [16] of Rockwell International has demonstrated that dispersion control can be accomplished through the use of layered magnetic structures. These structures consist of two or more magnetic layers of slightly different magnetization spaced by a dielectric layer (either the substrate or an epitaxially grown nonmagnetic layer). This technique produces non-dispersive regions with 200 MHz bandwidths at S-band and 1% delay flatness is acheivable with lower propagation loss than is available with metal layered structures. Morgenthaler [17] of Massachusetts Institute of Technology has shown dispersion can be accurately controlled by bias field gradients.

DISPERSIVE FILTERS

Work on linearly dispersive filters has centered on two techniques. First, control of the existing dispersion characteristic by layering, and second, reflective array devices. Adams et al [15], achieved a MSFVW device with >1 GHz bandwidth at 10 GHz and a time-bandwidth product of 230, with a linearity of ±5 nsec over the bandwidth.

arriving frequency components, so the total signal energy is accumulated in time at the filter output. It may be shown that the peak output to input power ratio is given by (figure 1),

$$Po/Pi = TB,$$

where the parameter TB is known as the time-bandwidth product and represents a signal processing gain or figure of merit for this encoding scheme. In a matched filter the peak signal-to-noise ratio is proportional to the input signal energy, independent of signal shape, and the effective output pulse width for the compression filter is inversely proportional to the encoding bandwidth; this means that detectability is proportional to input signal duration and the resolution is proportional to the input signal bandwidth. The time-bandwidth product TB is then a figure of merit for detectability-resolution.
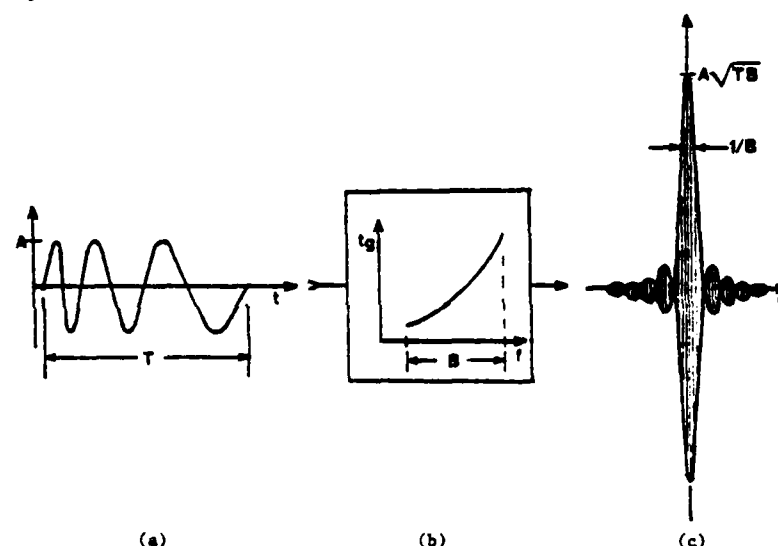

Figure 1: (a) The frequency swept transmitter pulse (down-CHIRP).
(b) The reverse delay characteristic of the compression filter.
(c) The recompressed pulse obtained by passing (a) through (b).

Pulse compression systems utilizing surface acoustic wave (SAW) devices have been under intensive investigation for the past 10 years. These studies have concentrated primarily on linear chirps and the achievement of low time-sidelobes by appropriate amplitude weighting. Both active and passive generation have been utilized in the compression loops, and time-sidelobes of greater than 40 dB down and time-bandwidth products >1000 have been obtained. In general, SAW devices achieve large processing gains by large time delays (1-100 μsec) with bandwidths from 50-500 MHz [9]. A new technology based on "slow" magnetostatic wave (MSW) propagation in a magnetically biased epitaxial yttrium iron garnet (YIG) is emerging as a complementary technology to SAW at microwave frequencies (1-20 GHz). Spin coupling in the magnetostatic modes results in electromagnetic wave propagation at group velocities two orders of magnitude below the speed of light [10]. This dispersive slow wave structure makes the investigation of MSW devices in pulse compression loops logical.

279

Insertion loss was 30-45 dB. Also, a backward wave down chirp device has been built with 800 MHz bandwidth and a time-bandwidth product of 90. Using reflective array technology Owens et al [18] achieved a 250 MHz bandwidth device at 3 GHz with a time-bandwidth product of 70, and a linearity of better than ±2 nsec. While these devices have large instantaneous bandwidths, the phase accuracy is still far from that seen in SAW RAC's. Initial studies of ion-implanted structures indicate that they show promise for controlled RAC devices.

THEORY OF CHIRP GENERATION AND COMPRESSION

Both delay lines were modeled theoretically with 25 μm thick YIG on a 0.51 mm, 15 mm long, and 3.0 mm wide GGG substrate. In the single-bar experiment a pair of narrow shorted microstrip transducers, 50 μm wide and 3.0 mm long were deposited photolithographically in 2.0 μm aluminum directly on the YIG surface, which was spaced from ground by the GGG substrate (figure 2). The weighted device used a similar processing to
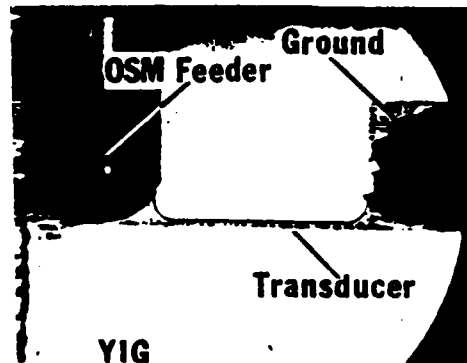
Figure 2: 20x magnification of the experimental single-bar transducer.

deposit a hair-pin transducer pair with 150 μm center-to-center spacing on the alumina substrate which then had a YIG film flipped over on top (figure 3). Earlier work by Wu [19] provided the amplitude responses
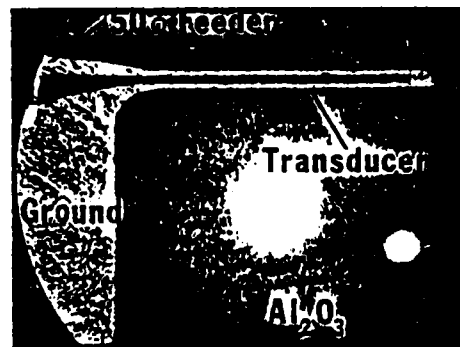
Figure 3: 20x magnification of the experimental loop transducer.

and group delays used in the theoretical predictions. Wu modeled the transducers (mainly responsible for the roll off) as low-loss microstrip transmission lines, with MSW excitation corresponding to a radiation loss. The theoretical group delay was calculated using a four layer dispersion relation after Collins, et al [10]. These two characteristics completely define the delay line transfer function,

$$A(\omega) = |A(\omega)| \exp[j1\ k(\omega)]$$

For best signal-to-noise in the recompressed pulse, the VCO must be swept so that the transform of its chirp,

$$S(\omega) = (1/\sqrt{2\pi}) \int a(t)\cos[\omega_0 t + \theta(t)]\exp(j\omega t) \, dt,$$

$$a(t) = \text{chirp envelope}$$
$$\theta(t) = \text{sweep function}$$

conjugately matches the delay line characteristic,

$$S(\omega) = A^*(\omega)$$

Since most high power radar transmitters operate class-C, $a(t)$ was considered constant in amplitude for the pulse duration allowing only phase matching in the transforms. A stationary-phase approximation,

$$\theta(t) = \omega_0 t + 1 \int |dk(\omega)/d\omega|^{-1} \, dt,$$

valid for large time-bandwidth products, was used to facilitate calculation of the required conjugate sweep [20].

Separate programs were written for the digital computer to model the swept VCO and delay line. The results from the first program verified the stationary phase approximation by using $a(t)$ and $\theta(t)$ to calculate $\arg[S(\omega)]$ and $|S(\omega)|$. This transform of the chirp, $S(\omega)$, then served as the input for the second program which modeled the delay line compression using,

$$r(t) = (1/\sqrt{8\pi m}) \int S(\omega/m - \omega_0) F(\omega) \, d\omega$$

where

$$F(\omega) = A(\omega - \omega_0)\cos[\omega t + 1 \langle k_R(\omega) - k_T(\omega/m) \rangle]$$

For an unweighted delay line this second program predicted a 19.6 dB upper bound on the peak-to-sidelobe ratio for the MSSW delay line pulse compressor. Simple weighting yields an improved sidelobe ratio of 28 dB. Of particular concern was the effect of Doppler shifts in conjunction with the nonlinear delay on this sidelobe level. In the compression integral,

$$m = 1 + 2v_{object}/c$$

models the Doppler effect. Computer runs with target relative velocities up to 1800 MPH with an assumed 95 GHz radar carrier frequency showed less than 0.5 dB of peak-to-sidelobe degradation for either filter.

282

As shown in figure 4, the experimental setup consists of four basic blocks. In the transmitter portion of the compression loop, both active and passive generation were considered. Impulsing either forward or reverse volume wave delay lines looks promising for passive generation and recompression (as corresponding delay time-frequency curves have opposite slopes), and active generation using a programmable sweep generator offers the possibility of sidelobe reduction by fm-predistortion after tuning out nonlinearities in the VCO and matching the receiver delay. Active generation was used for this work.
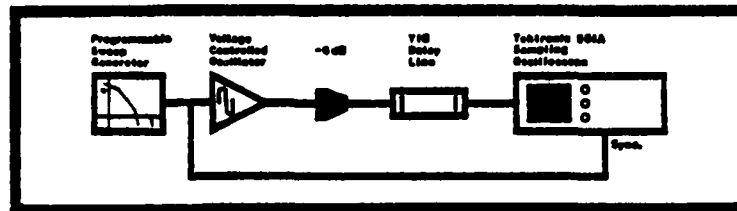
Figure 4: Block diagram of the compression loop used in this study.

A programmable voltage sweeper which approximated a continuous sweep with seven linear segments whose slopes and cut-on points could be independently set was designed. The sweep repetition rate was 70 KHz, and since the nominal sweep time was 100 nsec, this repetition rate allowed ample idling time for transients from the previous pulse to subside. The 23 V sweep drove the VCO output well beyond both sides of the delay line passband, eliminating need for pin-diode pulse truncation.

A Watkins-Johnson WJ-V302 VCO covering a 2 to 4 GHz frequency range with a minimum power output of 13 mW, and a 20 MHz FM bandwidth was used. A 6 dB divider was inserted before the delay line as a safeguard against saturation. Nonlinearities in the voltage-frequency curve of the VCO were lumped with the nonlinearity of the delay line group delay to generate the required time-voltage characteristic. Dynamic measurement of the chirp envelope revealed ripple >15 dB down, verifying the validity of the constant envelope assumption. Thus, the required time-voltage relation for the sweep generator could be found graphically from the measured delay line characteristic and the measured VCO voltage-frequency curve.

The MSSW delay lines described previously were biased transverse to the propagation direction in the plane of the film by a small horseshoe
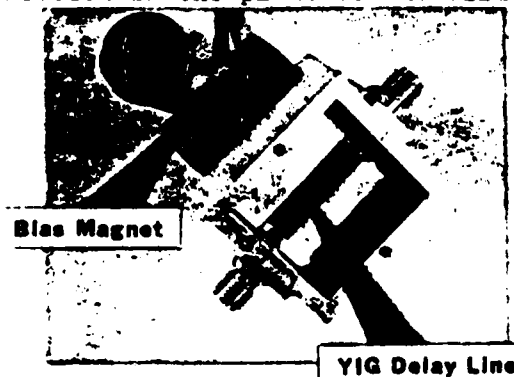
Figure 5: The experimental device mounted in its shielded case, with bias magnet.

magnet mounted outside the shielding case, with the pole-faces straddling the line (figure 5).

283

A Hewlett Packard 8410B network analyzer was used to measure the delay line spectral amplitude, $|A(\omega)|$, and group delay,

$$t_{group} = 1 \, dk(\omega)/d\omega$$

via the slope of the phase characteristic. As seen in figure 6 for the single-bar device, the amplitude response was centered at 2.9 GHz with a 16 dB minimum insertion loss for the single bar device. Reciprocating
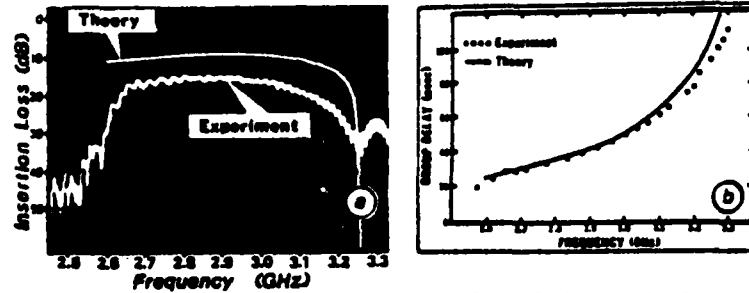
Figure 6: (a) Measured versus theoretical single-bar passband.
(b) Measured versus theoretical single-bar group delay.

the first zero crossing of the compressed pulse resulted in a 570 MHz effective bandwidth, spanning 53 nsec of delay dispersion, for a time-bandwidth product of 30. Need for down conversion of the recompressed pulse was eliminated by using a Tektronix 564/2S2/S4 sampling oscilloscope to view the recompressed pulse directly out of the delay line. Synchronism was obtained by triggering from the sweep generator. An oscilloscope trace of the recompressed pulse along with a comparison to the theoretical prediction is shown in figure 7. The
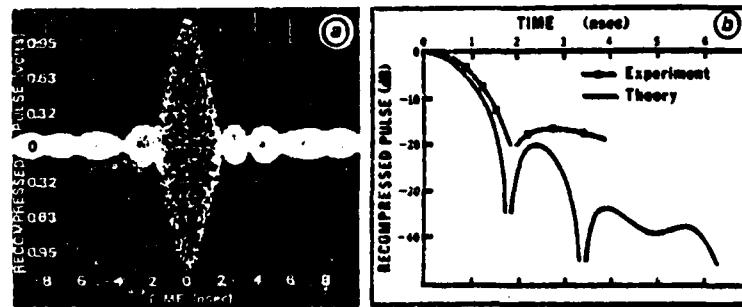
Figure 7: (a) Experimentally recompressed pulse from single-bar device.
(b) Comparison of experiment to theory.

sweep generator was initially programmed for the theoretical sweep and then fine tuned to maximize the peak-to-sidelobe ratio to 15.8 dB. In good agreement with theory the first zero crossing occured at 1.85 nsec.

Passband and recompressed pulse measurements are compared to theory for the improved loop-transducer device in figures 8 and 9. Spectral shaping reduced the bandwidth to 400 MHz, but improved the time-bandwidth product to 44. The experimental peak-to-sidelobe ratio was 24 dB compared to 28 dB predicted by theory.

Paired echo analysis [21] provides a useful way of interpreting some differences between theory and experiment. Consider the following transmitter signal and compression filter transforms,

$$T(\omega) = |T(\omega)| \, \delta(\omega) \exp[k(\omega) + \Delta(\omega)]$$

$$R(\omega) = |R(\omega)| \exp[-jk(\omega)].$$

284
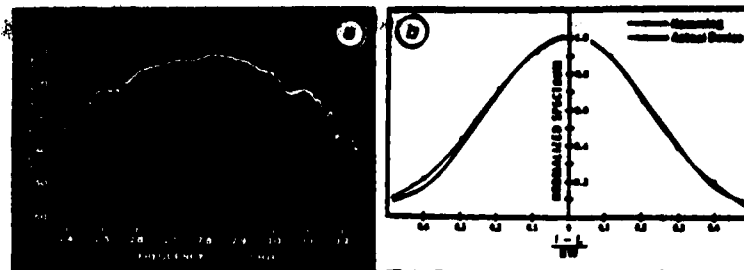
Figure 8: (a) Improved Hamming-like loop transducer device passband.
(b) Comparison of experiment to theory.
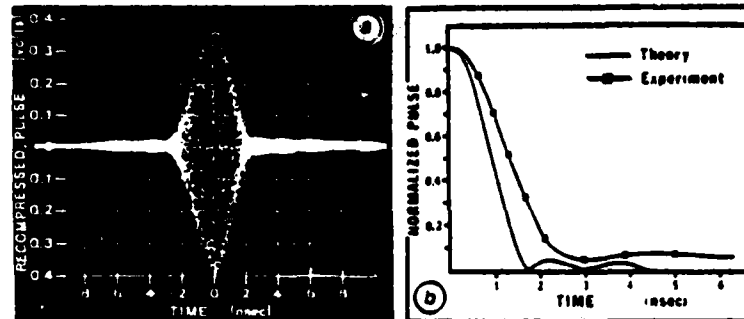
Figure 9: (a) Experimental compressed pulse from loop transducer device.
(b) Comparison of experiment to theory.

The receiver output is then,

$$S(\omega) = \delta(\omega)|T(\omega)||R(\omega)|\exp[j\,\Delta(\omega)].$$

Now, $|T(\omega)||R(\omega)|$ represents $s_0(t)$, the recompressed pulse waveform intended by the designer. $\delta(\omega)$, unless constant, is an undesired envelope modulation or ripple, and $\Delta(\omega)$ denotes an undesired phase mismatch or ripple. These distortion terms are represented by their ideal values, $\delta(\omega) =$ constant and $\Delta(\omega) =$ linear in ω, appended by Fourier series of their distortions (even amplitude, odd phase – for realizability),

$$\delta(\omega) = a_0 + \sum a_n \cos(nc\omega)$$

$$\Delta(\omega) = b_0\omega + \sum b_n \sin(nc\omega)$$

Typically the first order distortion terms are sufficient,

$$\delta(\omega) = a_0 + a_1 \cos(c\omega)$$

$$\Delta(\omega) = b_0\omega + b_1 \sin(c\omega).$$

The system is assumed linear allowing superposition to obtain the resultant receiver output, which may be interpreted as an infinite series of "paired echos" symetrically situated about the desired response. For $b_1 < 0.4$ rad, only two significant echos remain, and

$$s(t) = a_0 s_0(t)$$

$$+(a_0/2)[(a_1/a_0+b_1)s_0(t+b_1+c)-(a_1/a_0-b_1)s_0(t+b_1-c)].$$

285

Figure 10 shows the paired echo level - placing a minimum bound on the sidelobe level for given phase and amplitude ripple. This analysis is in good agreement with the observed experimental ripple and the recompressed pulse sidelobe degradation from theory seen in figures 7 and 9.
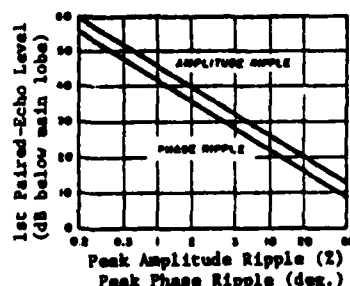
Figure 10: First paired-echo level vs amplitude and phase distortion.

Doppler shifts were simulated by varying the DC level at the VCO sweep input. Voltage offset was translated into a frequency shift by using the slope of the VCO characteristic, f(V), at 2.9 GHz. Both positive and negative shifts were used resulting in less than 0.16 dB peak-to-sidelobe degradation for simulated target velocities up to 1800 MPH, as predicted by theory for the single bar device (figure 11).
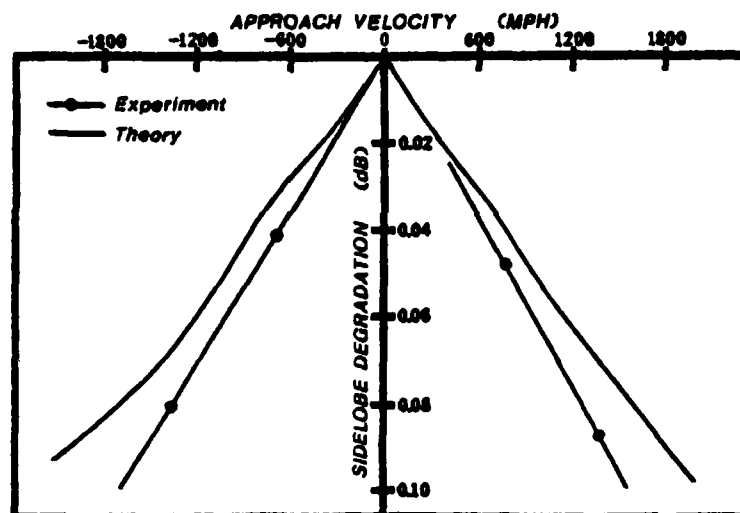
Figure 11: Theoretical versus experimental Doppler sidelobe degradation for the single-bar device.

Doppler performance for the improved device (loop-transducers) is given in figure 12, showing less then 0.8 dB degradation for 1800 MPH and 95 GHz carrier.
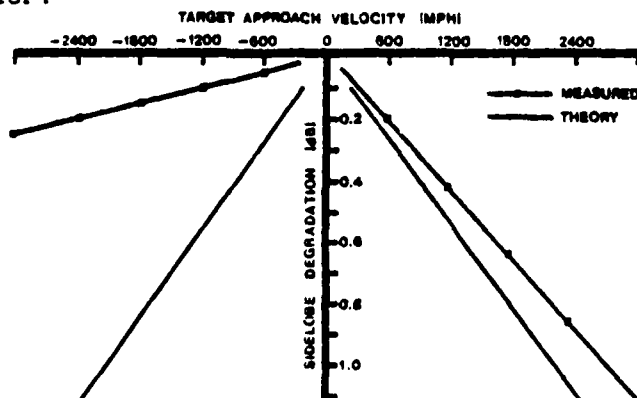
Figure 12: Theoretical versus experimental Doppler sidelobe degradation for the loop-transducer weighted device.

286

RESULTS AND CONCLUSIONS

Overall, model predictions were in good agreement with experimental results. The approximation of the sweep function in the actual compression loop is the most likely source of differences between theoretical predictions and experimentally observed pulse 3 dB width and peak-to-sidelobe ratio. A paired-echo model gives excellent prediction of the observed peak-to-sidelobe degradation. Since the zero crossings are mainly fixed by the amplitude response, reduction in the height of the main lobe due to the sweep approximation would cause the pulse to be wider at the 3 dB points. In addition, if the sidelobes were not identically effected by the approximation, a degradation in the peak-to-sidelobe ratio could result. Better delay matching could be attained by going to a longer delay (thinner film) recompression line, since this would result in a larger time-bandwidth product.

A particularly important result of this work was the peak-to-sidelobe immunity to Doppler shifts reflected in both theory and experiment (<0.8 dB degradation for $v \leq 1800$ MPH and 95 GHz carrier). The effect of nonlinear group delay on Doppler sensitivity had been a major concern for investigation in this work since radars intrinsically operate in a Doppler environment.

Further improvement in the peak-to-sidelobe ratio is possible by Hamming weighting the spectrum amplitude. With large time-bandwidth products, the stationary phase approximation,

$$|S(\omega)| = d[(\omega_0 + d\theta(t)/dt)^{-1}]/d\omega ,$$

provides an easy way to achieve spectral weighting by predistorting the sweep function, $\theta(t)$ [22]. Such predistortion is accompanied by unavoidable delay mismatch, so it is imperative that it be used in moderation. The amount of predistortion required could be minimized if the transducers were designed to give a passband already approximating the Hamming weighting.

		Sidelobes (dB)	Pulse Width (ns)	Doppler * Sens. (dB)	Band-Width(MHz)	TBW Product
SINGLE BAR	Exp.	15.8	1.85	0.16	540	28.8
	Thy.	19.6	1.75	0.09	571	29.7
LOOP	Exp.	24.0	2.55	0.68	392	———
	Thy.	28.0	1.75	0.80	571	44.0

*$v_0 = 1800$ MPH & $f_c = 95$ GHz

287

REFERENCES

1. Huttman, E., German Patent No.768,068, March 22, 1940.

2. Cauer, W. A., German Patent No.892,772, Dec. 19, 1950.

3. Dicke, R. H., U.S. Patent No.2,624,876, Jan. 6, 1953.

4. Darlington, S., U.S. Patent No.2,678,997, May 18, 1954.

5. Fenton, M. B., and Fullard, J. H., "Moth Hearing and the Feeding Strategies of Bats", American Scientist Vol. 69, No. 3, 1981, pp. 266-275.

6. Woodward, P. M., "Probability and Information Theory, with Application to Radar", Pergamon Press, Oxford, 1953.

7. Skolnik, M. I., "Introduction to Radar Systems", McGraw Hill Book Company, 1980, pp. 431 ff.

8. Skolnik, M. I., ibid., Chapter 10, pp. 369 ff.

9. J. D. Manes and E. G. S. Paige, Proc. IEEE, 64, 639-652, 1976.

10. J. H. Collins, J. M. Owens, and C. V. Smith, Jr., 1977 Ultrasonics Symp. Proc., IEEE Cat. No. 77CH1265-1SU, 541-561, 1977.

11. R. W. Damon and J. R. Eshbach, J. Phys. Chem. Solids, 19, 308-320, 1961.

12. W. L. Bongianni, J. Appl. Phys., 93, pp. 2541, 1972.

13. M. C. Tsai, H. J. Wu, J. M. Owens, and C. V. Smith Jr., A.I.P. Conf. Proc. #34, pp. 280, 1976.

14. M. R. Daniel, J. D. Adams, and T. W. O'Keeffe, Proc. 1979 IEEE Ultrasonics Symp., CH 1482-9/7910000-0800, pp. 806-809.

15. J. D. Adams, T. W. O'Keeffe, and M. R. Daniel, Proc. 1980 SPIE Conf., Vol. 111, pp. 241.

16. H. L. Glass and L. R. Adkins, "Dispersion Control in Magnetostatic Delay Lines by Means of Multiple Magnetic Layer Structures", 1980 Ultrasonics Symposium, pp. 526.

17. F. R. Morgenthaller, "Synthesis of Magnetostatic Waves and Modes Using Non-uniform Bias Fields", 1980 Ultrasonics Symposium, IEEE Cat. No. 80CH1602-2, pp. 532, November 1980.

18. J. M. Owens, C. V. Smith Jr., and T. J. Mears II, International Microwave Symp. Proc. IEEE #79 CH1439-9-MTTS, pp. 154-156.

19. H. J. Wu, C. V. Smith Jr., and J. M. Owens, J. Appl. Phys., 3 PT 11, 2455-2457, 1979.

20. C. E. Cook and M. Bernfeld, Radar Signals, Academic Press, New York, London, 34-56, 1967.

21. Klauder, J. R., Price, A. C., Darlington, S., and Albersheim, J., "The Theory and Design of Chirp Radars", Bell Sys. Te Jour., Vol. 39, No. 4, 1960, pp. 777 ff.

22. C. E. Cook and J. Paolillo, Proc. IEEE, 52, 377-389, 1964.

CRYSTALLOGRAPHIC EFFECTS IN YTTRIUM-IRON-GARNET ON

MAGNETOSTATIC SURFACE WAVE PROPAGATION

R.E. Floyd

Rome Air Development Center
Hanscom AFB, MA 01731

ABSTRACT

Magnetostatic surface waves (MSSW) were propagated on a
1-inch diameter yttrium-iron garnet (YIG) thin film disc with
adjustable coupling transducers. These adjustable transducers
enabled the film to be rotated underneath in order to investigate
crystallographic influence. Experiments are described and data
is plotted for signal power, time delay, beam steering and fre-
quency shifts. A correlation technique was used to evaluate the
resulting data, which reveals a 6θ dependence in some character-
istics.

INTRODUCTION

In order to help identify some of the problems associated with variable coupling of fine wire transducers, this project was undertaken to determine effects of crystalline anisotropy on propagation characteristics of magneto-static surface waves (MSSW) in yttrium-iron-garnet (YIG). Experiments involving rotation rate sensing, using MSSW's on a thick YIG ring, were performed by Poturalski in 1979.[1] Recommendations were to determine and model non-uniform behavior of the YIG medium. Experiments were done to resolve the amount of dependence on crystalline anisotropy of several characteristics, including signal power, time delay and frequency shift.

The propagation media for the magnetostatic surface waves is yttrium-iron-garnet (YIG). The crystallographic axes of YIG are of a single cubic structure. The YIG thin films were all grown by liquid phase epitaxy on a gadolinium-gallium-garnet substrate. The films tested had (111) surfaces ([111] direction is normal to the surface of the sample). See Figure 1. A top-down view of the cube reveals that the lattice structure exhibits three high symmetry directions. These three directions are where variations, if
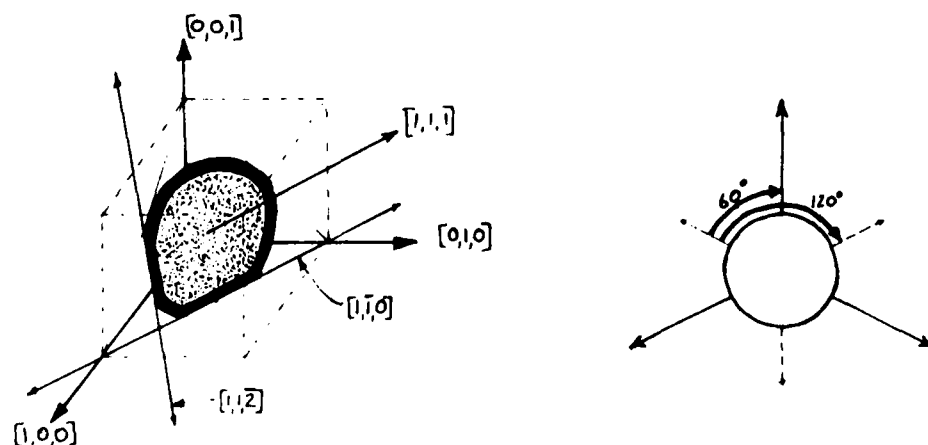
Figure 1. Crystallographic orientation of YIG samples.

291

IN PLANE RESONANCE
(111) LPE-YIG FILM
SAMPLE 5-18-8-2   (10 μm thick by 1 mm diameter)

FERROMAGNETIC RESONANCE IN MHZ

3900
3898
3896
3894
3892
3890

<211>

<110>

H = 755 oersteds
4 π M = 1750 gauss

K_1/M = -31 oersteds
—— THEORY (modified
        Everett)
•••• EXPERIMENT

0   30°   60°   90°   120°   150°   180°

ANGLE BETWEEN H AND (211) CRYSTAL AXIS IN (111) PLANE
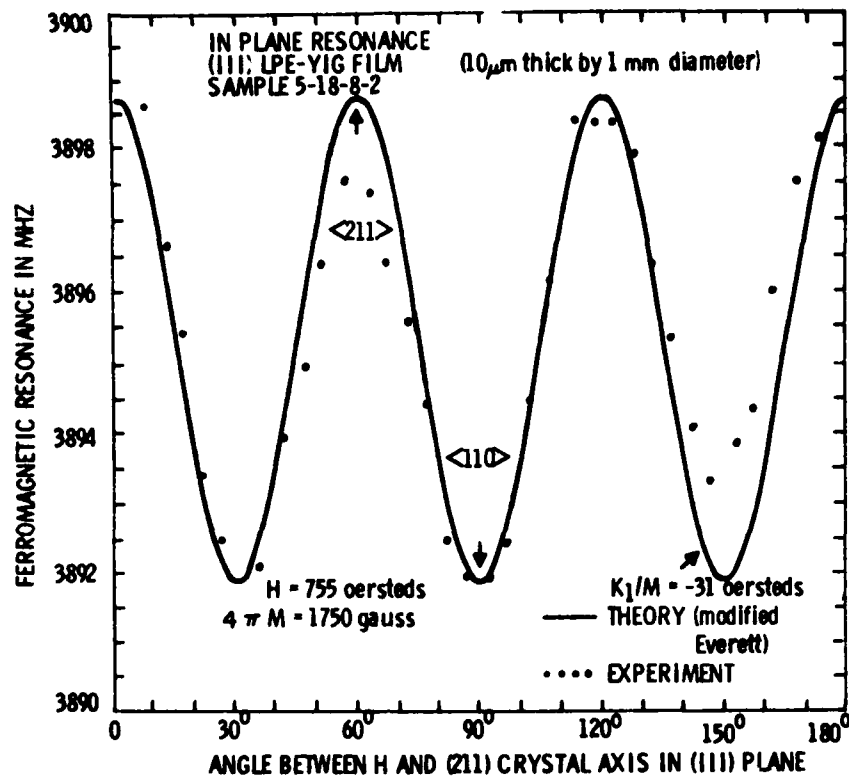
Figure 2. 6θ dependence for in plane resonance.

any, of the MSW would be expected. Since the experiment involves a 360 degree
rotation of samples, the three fold symmetry is expected to lead to a 6θ
dependence.

Work published by Sethares and Tsai provides an example of 6θ dependence
for in plane resonance.[2] (See Figure 2). The bias field H was rotated 180°,
with ferromagnetic resonance plotted in MHz. This same type of dependence is
anticipated for propagation characteristics of surface waves.

EXPERIMENTS

Three different configurations were used to test the YIG thin-film samples.
The samples, all one inch discs, were used in simple delay line configurations,
with fine wire transducers for input and output. The transducers were capable
of variable liftoff distances which allowed rotation of the samples underneath

Figure 3. Top and side view of test apparatus.

(see photos of test apparatus). In the first configuration, pulse measurements were made to test the samples (see Figure 4). Measurements of signal power, time delay and beam steering were taken using a 20 nanosecond input pulse.

Since crystallographic dependences were sought, an effort to make all measurements relative to a maximum of each characteristic were made. The measurement data was stored in computer files for easy access and evaluation. In Fig. 5a, one should note the randomness at which the signal power amplitude occurs; this data was taken every 10 degrees. Figures 5b and 5c show time
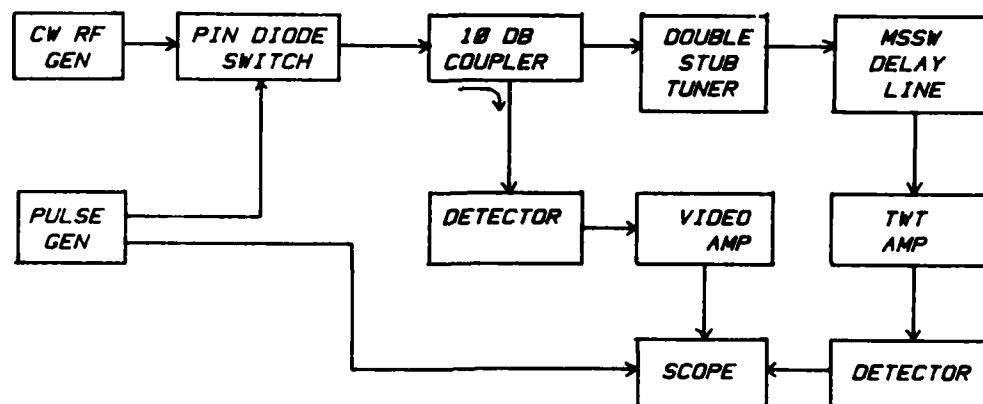
Figure 4. Circuit diagram for pulse measurements
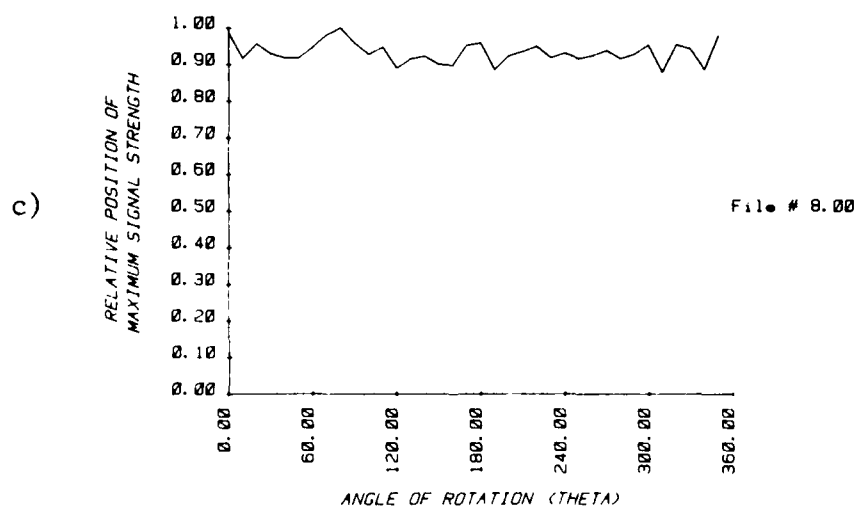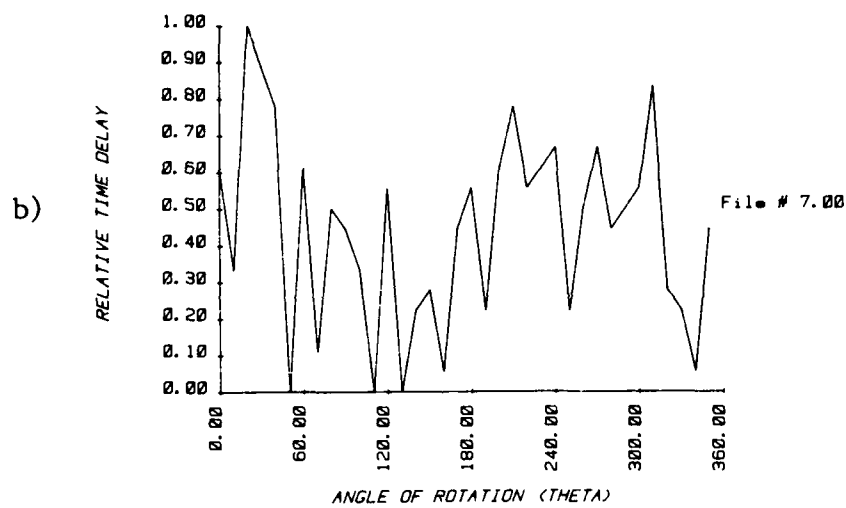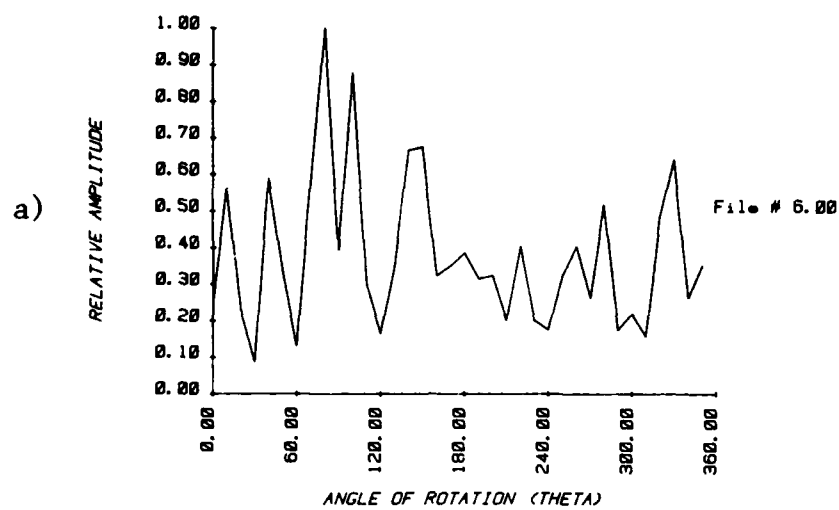
Figure 5.   Pulse measurements of a) signal power, b) time delay   and
            c) beam steering.

294
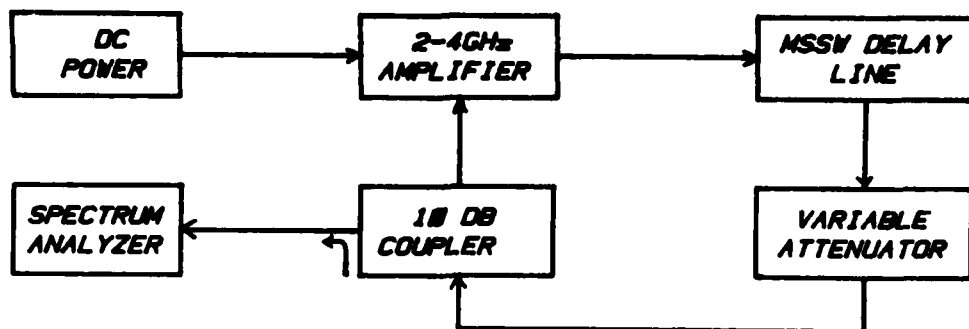
Figure 6. Circuit diagram for oscillator measurements.

delay and position of maximum signal strength (a beam steering measurement of distance from a reference). Evaluation of the data will be discussed in the results section.

Device characteristics were tested on a network analyzer and some interesting results led to the second configuration of testing. Observation of the delay line's passband shifting up and down in frequency, when the film samples were rotated underneath the transducers, gave indication to investigate frequency shifting with some oscillator measurements. The oscillator circuit diagram is shown in Figure 6. This delay line configuration was used since no alterations to the test apparatus or samples were needed. The DC magnetic bias field was held constant at approximately 300 oersteds while the only variable was the rotating sample. From the results shown in Figures 7a and 8a, one can easily see a definite crystallographic dependence.

ANALYSIS OF RESULTS

Visual inspection of the pulse measurement results show how hard it would be to deduce much of anything. The data is somewhat random in nature. In order to fully interpret what data there is, an analysis technique for correlating random data is used. The autocorrelation function in digital form is:

$$R_x(\theta) = \frac{1}{N-\theta} \sum_{n=1}^{N-\theta} X_n X_{n+\theta} \qquad \theta = 0°, 10°, 20°---350°$$

where $\theta = \phi * 10^o$ and is called the lag "angle", X is the appropriate set of data and R_x is the estimate of the true autocorrelation at lag θ. One should choose $N \gg \theta$ to decrease uncertainty of the estimates.[3] As the lag "angle" is moved, a plot of the autocorrelation function versus lag "angle" (autocorrellogram) is obtained.

In order to compare the strength of one correlation with another, the autocorrelograms were individually normalized to their maximum value. Even with this adjustment, one must be careful because periodicity at one frequency may tend to hide another. This occurrence is demonstrated in Figures 7 and 8. Figure 7a shows the frequency shift data from one sample, its autocorrelation in Fig. 7b and then its cross-correlation with a non-random 6θ function. Even though Fig. 8b shows no sign of a 6θ dependence, when the data from this sample is cross-correlated with the same 6θ function, its 6θ dependence becomes evident. When these two cross correlations are compared against each other, we see relatively the same amount of 6θ influence.

A 2θ dependence is introduced when the film was mounted at a tilt. Thus, when data was taken as the film rotated, a 2θ dependence resulted. Autocorrelograms for the pulse measurements are shown in Figure 9. The beam steering data (Figure 9a) shows no dependence at all. The time delay data does show a 2θ dependence but no prevalent 6θ dependence. Again, the 2θ dependence is present since propagating characteristics are similar when the wave is travelling in the opposite direction. The signal power measurements show the 2θ dependence and some evidence of a a 6θ influence. Notice the peaks near $\phi * 10^o = 60^o$, 120°, ...

SUMMARY AND CONCLUSIONS

From the presented data, the oscillator measurements were the most susceptible to the crystallographic influence. Data showed a clear 6θ dependence, with
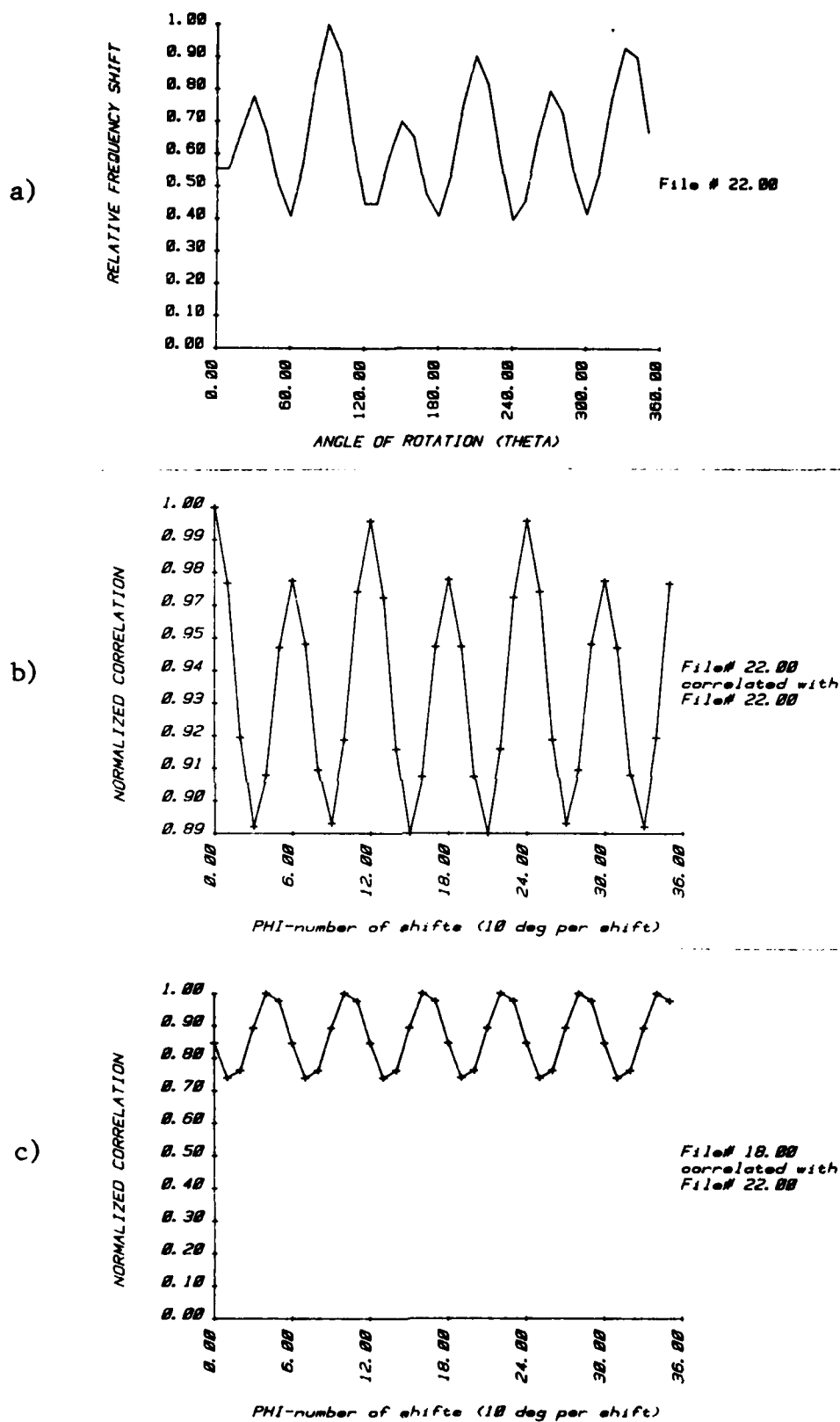
Figure 7. Oscillator measurements of sample A; a) data b) auto-
correlation and c) cross-correlation.
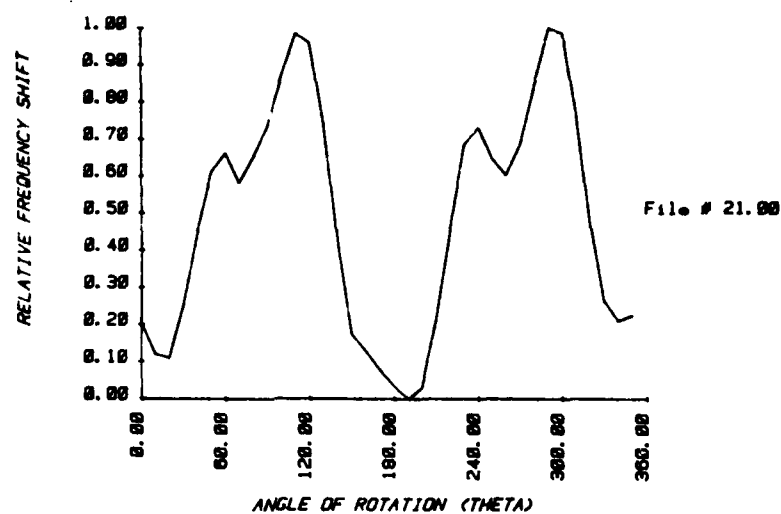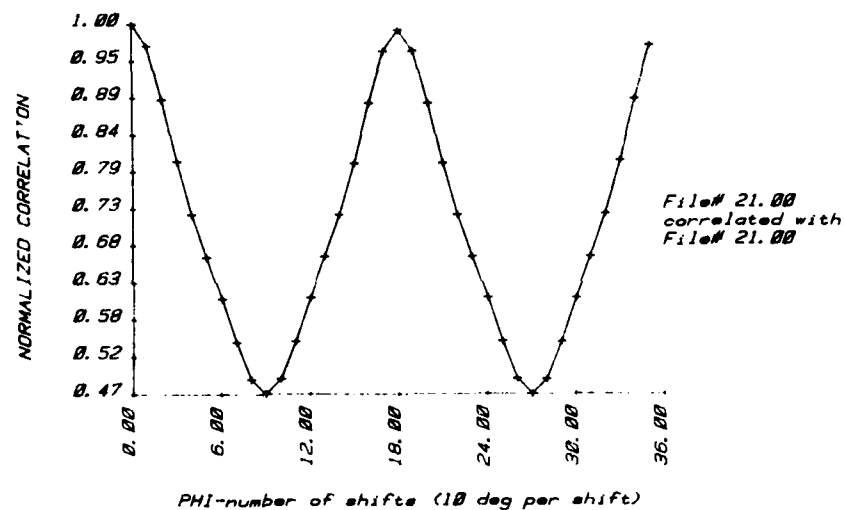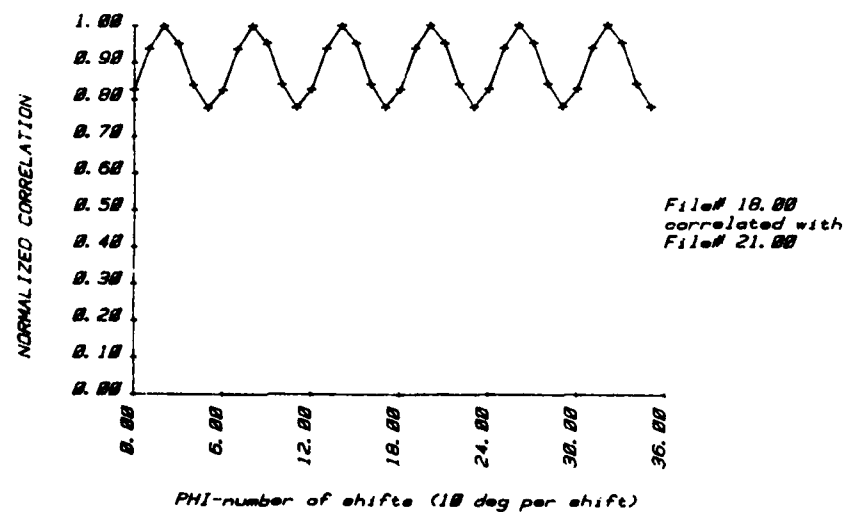
Figure 8. Oscillator measurements of sample B; a) data b) auto-correlation and c) cross-correlation.
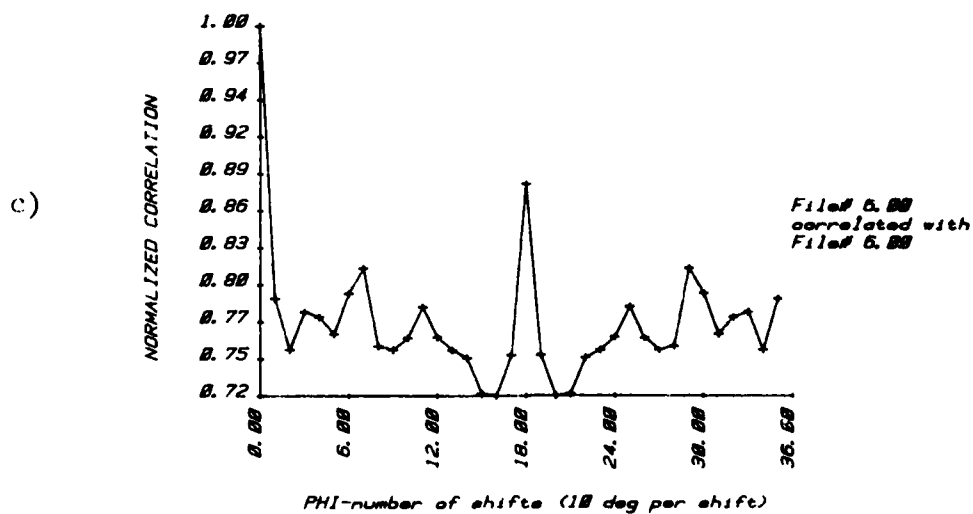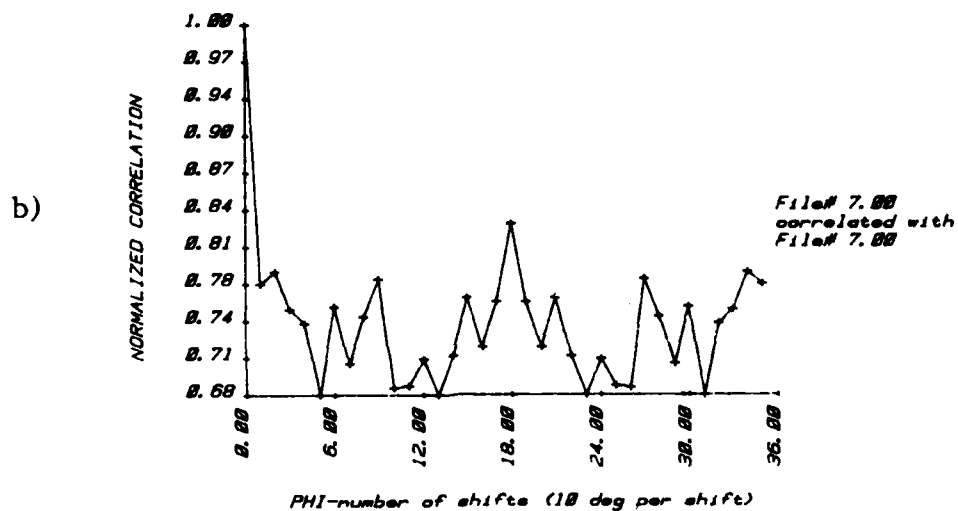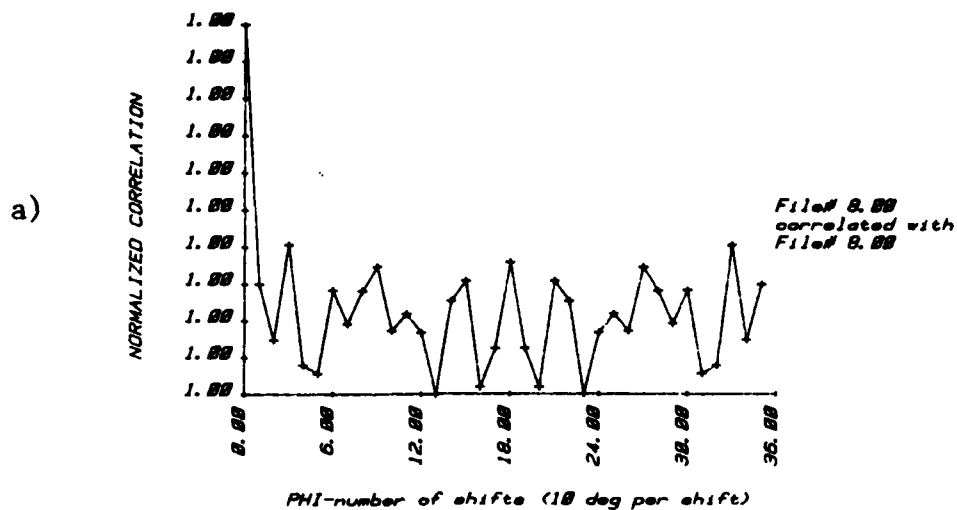
Figure 9. Autocorrelograms for pulse measurement data.

a change of 10-12 MHz at 2630 MHz. This is not a large amount but maybe enough to be considered in the design of oscillators. With the quite random or noisy data that was taken, the pulse measurements seem to have not been influenced greatly by the crystallography. Although not seen here, it seems there should be an ideal direction for propagation. If experiments were performed on a better test apparatus (i.e. very stable input and output transducers to prevent random coupling distances) it could be shown whether the hints of 6θ dependence on signal power will be truly significant.

ACKNOWLEDGEMENTS

REFERENCES

1. Poturalski, R.J., Rotation Rate Sensing Via Magnetostatic Surface Wave Propagation on a Thick YIG Ring, MSEE Thesis, Wright-Patterson AFB, OH: School of Engineering, Air Force Institute of Technology, December 1979.

2. Sethares, J.C. and Tsai, T, "Magnetic Anisotropy of (111) LPE-YIG Films on G^3 in Parallel Resonance," IEEE Transactions on Magnetics, Vol. MAG-13 (5) 1236-1237, September 1977.

3. Bendat, J.S. and Piersol, A.G. Measurement and Analysis of Random Data New York: John Wiley and Sons, Inc., 1966.

Magnetostatic Wave Dispersion Relations

I. J. WEINBERG

UNIVERSITY OF LOWELL

Introduction

The results presented here summarize and expand earlier results for magnetostatic wave dispersion relatons [1] and for magnetostatic wave oscillators [2].

In what follows is presented the dispersion relations for generalized volume waves and generalized surface waves for a thin YIG film bounded by two ground planes. Computer produced curves for volume waves and surface waves are presented. In particular, for volume waves in the plane $\phi = 0$ there is indicated an application to nondispersive electronically tunable time delay elements. Also presented is a comparison between a theoretically obtained dispersion curve for surface waves and one obtained by computer controlled experiment at RADC, Hanscom AFB.

There is also presented an analysis for magnetostatic wave oscillator frequencies for surface waves and for forward and backward volume waves. We take into account the possibility of obtaining multiple modes for volume waves. Comparisons are made between the curves obtained from theoretical considerations and those obtained experimentally at RADC, for surface waves and forward and backward volume waves.

301

Dispersion Relations

We here consider a magnetostatic wave transducer consisting of a thin YIG film sandwiched between two dielectric layers of arbitrary thicknesses subject to an arbitrarely directed applied magnetic field as shown in Figure 1.

Writing the total magnetic field and magnetization vectors as

$$\bar{H}_T = \bar{H} + \bar{h}\, e^{j\omega t} \quad ; \quad \bar{M}_T = \bar{M} + \bar{m}\, e^{j\omega t} \tag{1}$$

where

$$M = 1750 \quad Oe \tag{2}$$

and utilizing the gyromagnetic expression in the YIG region

$$\frac{\partial \bar{M}_T}{\partial t} = \gamma\, H_T \times M_T \tag{3}$$

where

$$\gamma = 2.8 \quad mhz/Oe \tag{4}$$

we are led to a matrix equation of the form

$$\bar{m} = \left[\chi \right] \bar{h} \tag{5}$$

by neglecting higher order terms in the products of components of $\bar{m}$ and $\bar{h}$.

Applying the consitutive relations in the YIG region

$$\bar{b} = \mu_e (\bar{h} + \bar{m}) \tag{6}$$

and substituting (5) we obtain

$$\begin{pmatrix} b_x \\ b_y \\ b_z \end{pmatrix} = \mu_o \begin{pmatrix} \mu_{xx} & \mu_{xy} & \mu_{xz} \\ \mu_{yx} & \mu_{yy} & \mu_{yz} \\ \mu_{zx} & \mu_{zy} & \mu_{zz} \end{pmatrix} \begin{pmatrix} h_x \\ h_y \\ h_z \end{pmatrix} \tag{7}$$

where all the components in (7) are shown earlier [1]. Also see Appendix.

302

The components needed in the analysis are, with $f = \omega/2$,

$$\mu_{xx} = 1 + \gamma^2 HM \frac{(\sin^2\theta \sin^2\phi + \cos^2\theta)}{\gamma^2 H^2 - f^2}$$

$$\mu_{xy} = j\gamma M \sin\theta \frac{(f \sin\phi + j\gamma H \cos\phi \cos\theta)}{\gamma^2 H^2 - f^2} \tag{8}$$

$$\mu_{yx} = -j\gamma M \sin\theta \frac{(f \sin\phi - j\gamma H \cos\phi \cos\theta)}{\gamma^2 H^2 - f^2}$$

$$\mu_{yy} = 1 + \frac{\gamma^2 HM \sin^2\theta}{\gamma^2 H^2 - f^2}$$

In the non YIG regions we employ the relations

$$\bar{b} = \mu_0 \bar{h} \tag{9}$$

Proceeding as in earlier analysis [5] with the magnetostatic approximation and no variation in the z direction, the field equations in each region

$$\nabla \times \bar{h} = 0 \quad , \quad \nabla \cdot \bar{b} = 0 \tag{10}$$

become

$$\frac{\partial h_x}{\partial y} - \frac{\partial h_y}{\partial x} = 0 \quad , \quad \frac{\partial b_x}{\partial x} + \frac{\partial b_y}{\partial y} \tag{11}$$

so that a potential function is assumed for $\bar{h}$

$$\bar{h} = \nabla \Psi \tag{12}$$

In the non YIG regions (9),(11), and (12) are satisfied by

$$\Psi = e^{-jKx} (A e^{|K|y} + B e^{-|K|y}) \tag{13}$$

where A and B are to be determined from continuity or boundary conditions and K is the wave number to be determined. The solution representes a wave propagating in the x direction.

To satisfy (7), (11), and (12) in he YIG region we define

$$\delta = -\frac{(\mu_{yx} + \mu_{xy})}{2\mu_{yy}} \quad , \quad c^2 = \frac{(\mu_{xy} + \mu_{yx})^2 - 4\mu_{xx}\mu_{yy}}{4\mu_{yy}^2} \tag{14}$$

The solution form will now depend on the sign of c^2.

For c^2 positive the solution is of the form

$$\psi = e^{-jk(x+\delta y)}(A\cos c|k|y + B\sin c|k|y) \qquad (15)$$

producing volume waves. Wave propagation can have a component in the y direction. For standard forward and backward volume wave configurations δ is 0 and wave propagation is in the x direction.

By trying to satisfy continuity conditions for h_x and b_y at region junctions and the vanishing of b_y at the ground planes we are required to satisfy the dispersion relation

$$\left[(\coth |k|t_1 + 1) - e^{-2|k|\ell}(\coth |k|t_1 - 1)\right] c \,\mu_{yy}\cot c|k|d =$$
$$\coth |k|t_1 \left[c^2\mu_{yy}^2 - (\mu_{yx} + \delta\mu_{yy})^2\right] - 1 + j\frac{|k|}{k}(\coth |k|t_1 - 1)(\mu_{yx} + \delta\mu_{yy})$$
$$+ e^{-2|k|\ell}\left\{\coth |k|t_1 \left[c^2\mu_{yy}^2 - (\mu_{yx} + \delta\mu_{yy})^2\right] + 1 - j\frac{|k|}{k}(\coth |k|t_1 + 1)(\mu_{yx} + \delta\mu_{yy})\right\} \qquad (16)$$

This general expression reduces to more familiar expressions for standard cases. For forward volume waves, $\theta = 0$, with one ground plane, $t_1 = \infty$, we obtain

$$2c\cot c|k|d = c^2 - 1 + e^{-2|k|\ell}(c^2 + 1) \qquad (17)$$

where

$$c^2 = -\left(1 + \frac{\gamma^2 HM}{\gamma^2 H^2 - f^2}\right) = -\mu_{xx} \qquad (18)$$

and for backward volume waves, $\theta = \pi/2$ and $\phi = 0$, with one ground plane, $t_1 = \infty$, we have

$$2c\cot c|k|d = c^2 - 1 - e^{-2|k|\ell}(c^2 + 1) \qquad (19)$$

where

$$c^2 = -\left(1 + \frac{\gamma^2 HM}{\gamma^2 H^2 - f^2}\right)^{-1} = -\frac{1}{\mu_{yy}} \qquad (20)$$

304

The bandwidth for the existence of volume waves has been shown to be[6]

$$\gamma \sqrt{H(H + M \sin^2\theta \sin^2\phi)} < f < \gamma \sqrt{H(H+M)} \tag{21}$$

Computerized results of (16) are shown in Figure 2 for generalized forward volume waves, Figure 3 for generalized backward volume waves and Figures 4, 5 for the biasing field in the plane $\phi = 0$. The dispersion relation in the latter cases consists of a backward volume wave changing abruptly to a forward volume wave. The frequency at which this change occurs is given by [6]

$$f_c = \gamma \sqrt{H(H + M \sin^2\theta)} \tag{22}$$

We observe from Figure 5 the feasibility of obtaining nondispersive electronically tunable time delay elements from a configuration such as for $\theta = 43^0$ which for H=2500 oe, is the midpoint of the frequency spectrum.

Returning to (14); if c^2 is negative the solution in the YIG takes the form

$$\psi = e^{-j\kappa(x + \delta y)} (A e^{\beta |\kappa| y} + B e^{-\beta |\kappa| y}) \tag{23}$$

where

$$\beta^2 = -c^2 \tag{24}$$

producing surface waves. Here too, wave propagation can have a component in the y direction. For standard surface waves, $\theta = 90^0$ and $\phi = 90^0$, δ is o and propagation is in the x direction.

305

By attempting to satisfy the continuity conditions for h_x and b_y at region junctions and the vanishing of b_y at the ground planes we are required to satisfy the dispersion relation

$$e^{2\beta|K|d} = \frac{(\alpha_2 - \tanh |K|t_1)\,(\alpha_1 - \tanh |K|\ell)}{(\alpha_2 + \tanh |K|\ell)\,(\alpha_1 + \tanh |K|t_1)} \tag{25}$$

where

$$\alpha_1 = \beta \mu_{yy} - j\frac{|K|}{K}(\mu_{yx} + \delta \mu_{yy})$$

$$\alpha_2 = \beta \mu_{yy} + j\frac{|K|}{K}(\mu_{yx} + \delta \mu_{yy}) \tag{26}$$

This general expression reduces to the previously obtained[5] dispersion relation for standard surface waves, $\Theta = 90^0$ and $\phi = 90^0$ which is given by (25) where here

$$\begin{pmatrix} \alpha_1 \\ \alpha_2 \end{pmatrix} = \left(1 + \frac{\gamma^2 HM}{\gamma^2 H^2 - f^2}\right) + \frac{|K|}{K}\frac{\gamma M f}{\gamma^2 H^2 - f^2} \tag{27}$$

(The minus sign goes with α_1 and the plus sign goes with α_2.)

The bandwidth for surface waves in the standard case, $\Theta = 90^0$ and $\phi = 90^0$, is [1]

$$\gamma\sqrt{H(H+M)} < f < \gamma\left(H + \frac{M}{2}\right) \tag{28}$$

Computerized results of (25) and (26) are shown in Figure 6 for generalized surface waves. Also shown in Figure 7 is a comparison of the dispersion relation curve for surface waves obtained from (25) and (27) and one obtained by computer controlled experiment at RADC.

Magnetostatic Wave Oscillator Frequencies

Magnetostatic wave oscillator frequencies for surface waves, forward and backward volumes waves were obtained experimentally by employing LPE-YIG delay lines as in Figure 8. Comparisons were made between the experimentally obtained curves of frequency as a function of biasing field and those obtained theoretically by employing (17) and (18) for forward volume waves, (19) and (20) for backward volume waves and (25) with (27) for surface waves.

For surface waves an analytical expression for the frequency is given[3] for no ground planes, $t_1 = \infty$ and $l = \infty$, which is

$$f^2 = \gamma^2 H^2 + \gamma^2 HM + \frac{\gamma^2 M^2}{4}\left(1 - e^{2|k|d}\right) \tag{29}$$

and was here employed.

Another expression[4] for the consideration of one ground plane is also available. The theoretical and experimental data for surface waves are shown in Figure 9 .

The expressions for volume waves (17)-(20) do not lend themselves to analytic expressions for the frequency as a function of biasing field. In seeking a numerical solution one should be aware that many solution modes exist for volume waves. In fact, two modes are obtained experimentally for backward volume waves.

An iterative numerical scheme was devised to take into account the possibility of obtaining several solution modes. Combining the equations for forward volume waves and backward volume waves we obtain from (17) and (19)

$$C_{i+1} = \frac{1}{|k|d}\left[\tan^{-1}\frac{2 C_i}{C_i^2 - 1 \pm e^{2|k|t}(C_i^2 + 1)} + n\pi\right] \qquad \begin{array}{l} i = 0,1,2, \\ n = 0,1,2, \end{array} \tag{30}$$

which is an iterative procedure to find C.

and then, from (18) and (20), we have

$$f = \left(\frac{\alpha \gamma^2 H M}{c^2 + 1} + \gamma^2 H^2 \right)^{1/2}$$

(31)

where, for forward volume waves we take the plus sign in (30) and α is 1 in (31) while, for backward volume waves we take the minus sign in (30) and α is c^2 in (31). An initial guess c_0 is needed. Different solutions are found for different n values. Figure 10 compares the experimentally obtained curves for forward volume waves and the one obtained from (30) and (31) for n=0. The translational difference between the two curves is to be expected and is not significant. Figure 11 shows the experimentally obtained curves and the curves obtained from (30) and (31) for backward volume waves for n=0 and n=2. In all of these cases the YIG thickness is 30 um and there is one ground plane spacing of 254 um. The wavelength is 300 um.

Summary

In this paper is summarized the dispersion relation expressions for surface waves and volume waves for arbitrary orientation of the of the biasing field and arbitrary thicknesses of the dielectrics. Computerized curves are obtained for surface waves and volume waves. RADC is currently obtaining some similar curves by experimental means. Also shown are magnetostatic wave oscillator frequency curves for surface waves and forward and backward volume waves. Comparisons are made between computer obtained curves and curves obtained by experimental means at RADC.

References

1. Weinberg, I.J., "Dispersion Relations for Magnetostatic Waves"; 1980 Ultrasonics Symposium Proceedings.

2. Sethares, J.C. Stiglitz, M.R. and Weinberg, I.J., "Magnetostatic Wave Oscillator Frequencies", 1980 MMM Conference.

3. Sethares, J.C., "Magnetostatic Surface Waves on a Cylinder"; AFCRL-TR-75-0380.

4. Bongianni, W.L., "Magnetostatic Propagation in a Dielectric Layered Structure"; J. Appl. Phys., 1972.

5. Weinberg, I.J. and Sethares, J.C., "Magnetostatic Wave Transducers with Variable Coupling"; RADC-TR-78-205.

6. Bajpai, S.N., "Excitation and Propagation of Magnetostatic Microwaves in Ferrimagnetic Structures"; Ph.D. Thesis, Indian Institute of Technology, 1980.

309

VOLUME WAVES
H=2500(OE),D=10(UM),L, AND T INFINITE

$\phi=90°$
$\theta=30°$

$\theta=0°$

FREQUENCY (MHz)

WAVE NUMBER K(+) (1/METER) (×10⁴)
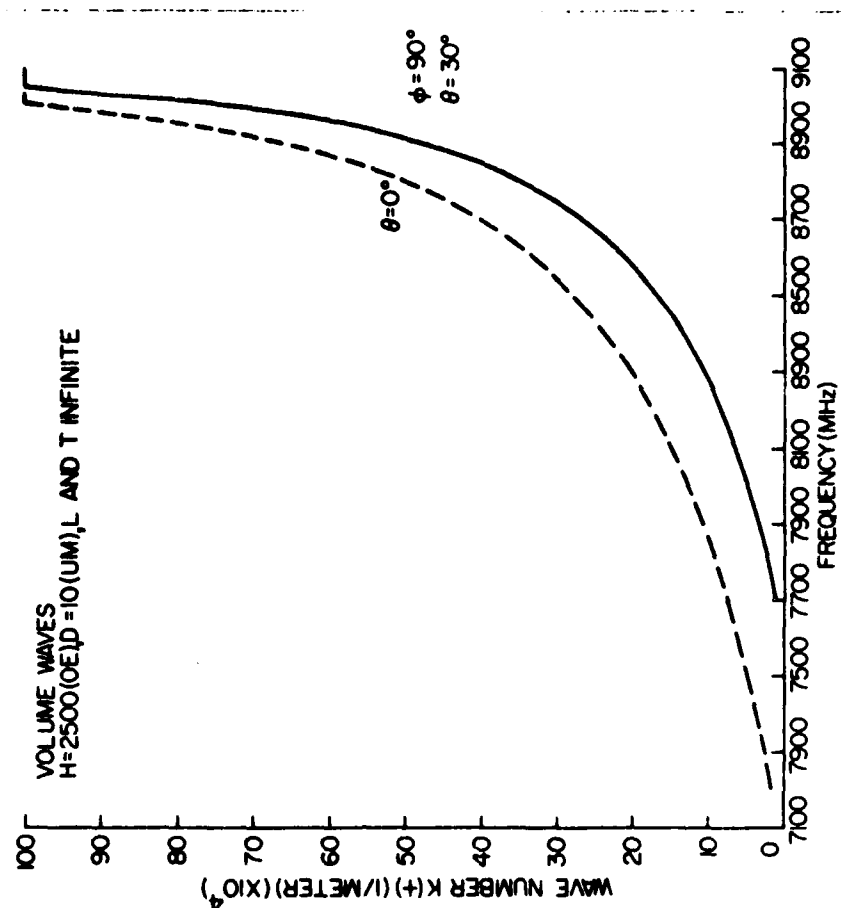
Figure 2 — Generalized forward volume waves.

GROUND PLANE

$y=t_1$

$\overline{H}$

θ

y

x

YIG

ϕ

$y=-d$

GROUND PLANE

$y=-(d+\ell)$

z
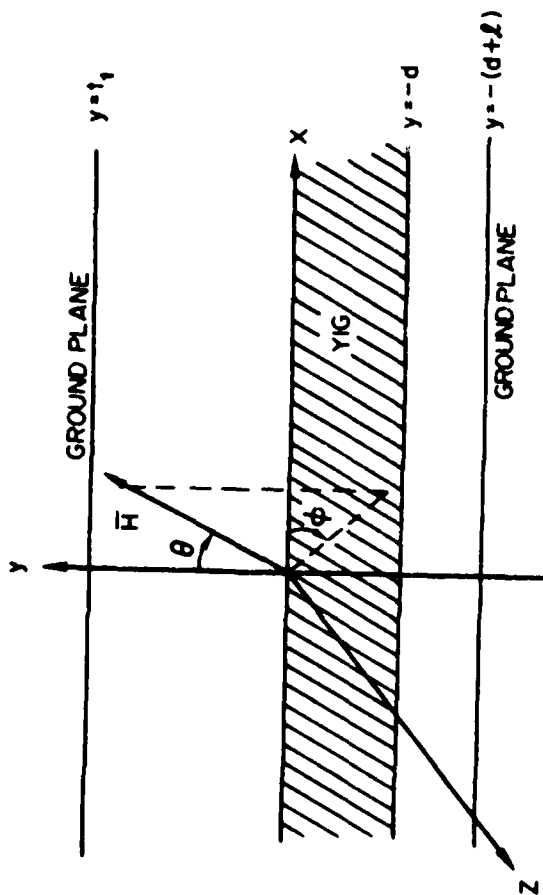
Figure 1 — Transducer Configuration.

310

Figure 4 — Results for $\phi = 0$.
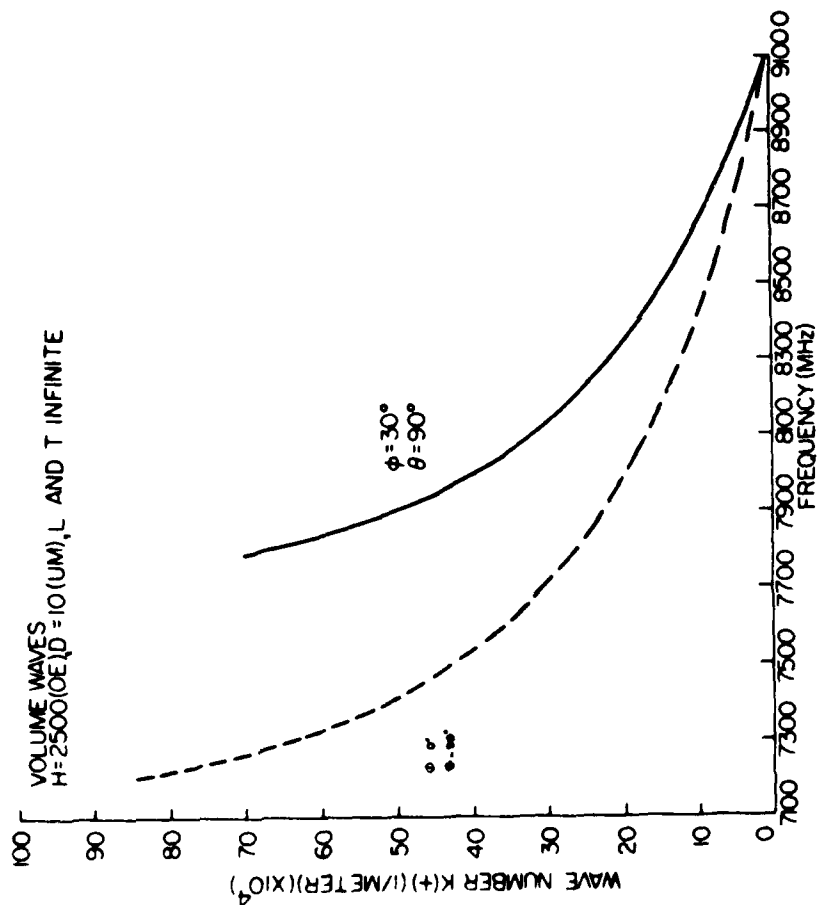
Figure 3 — Generalized backward volume waves.
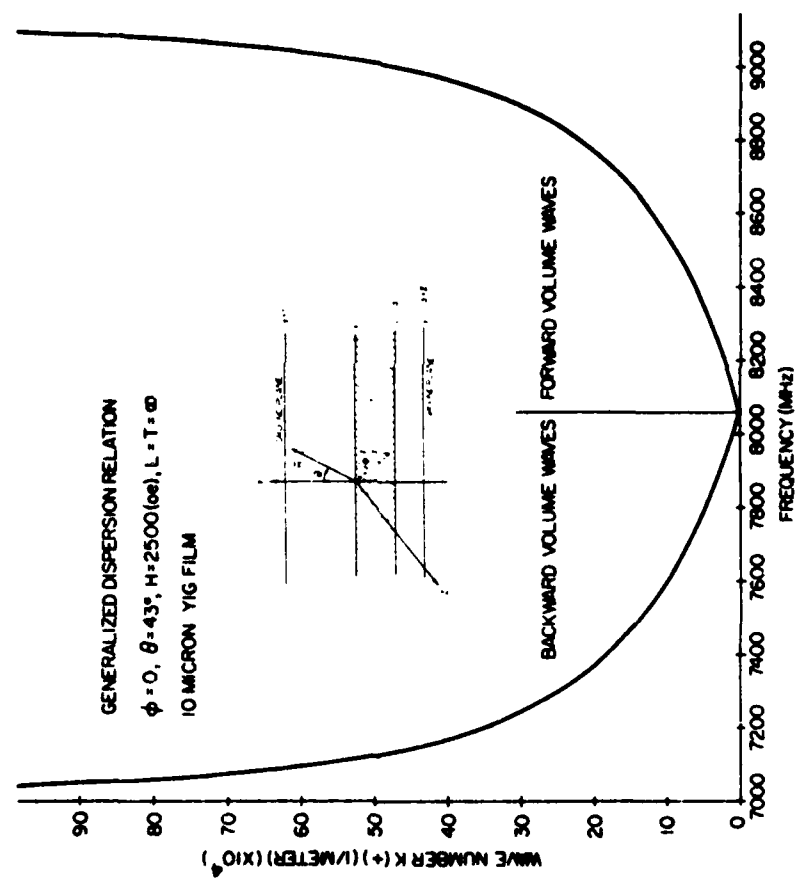
Figure 5 - Results for $\phi = 0$.

Figure 7 - Theoretical and experimental
surface waves.
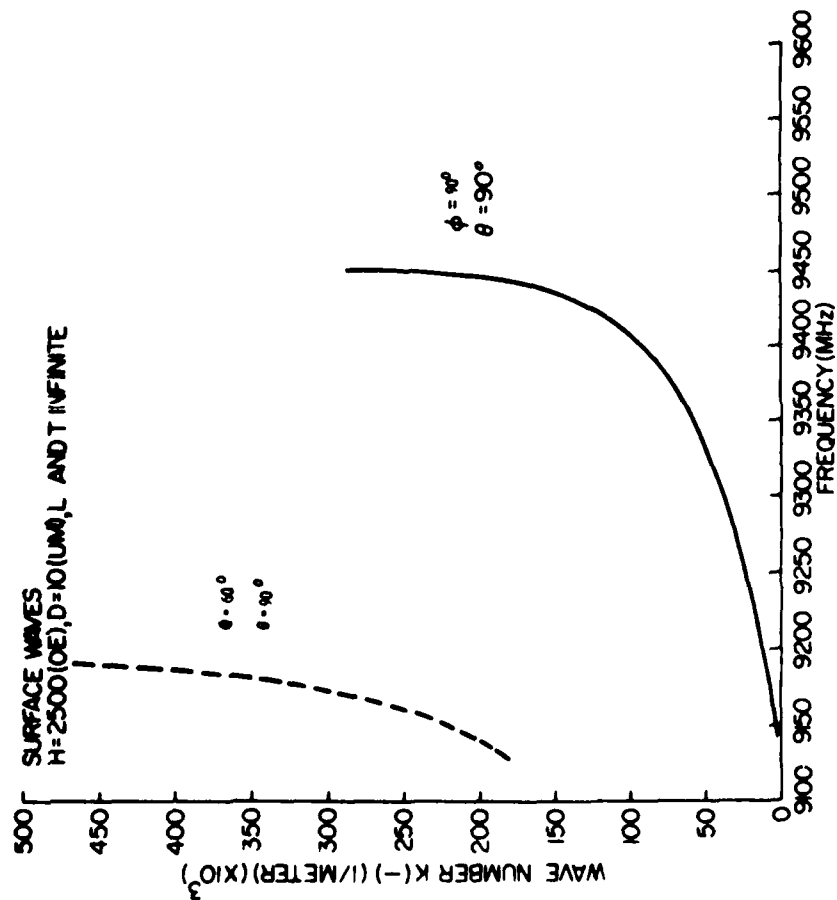
Figure 6 - Generalized surface waves.

313

BLOCK DIAGRAM FOR MSW OSCILLATOR

A, AVANTEK MODEL ABG—4005 AMPLIFIERS, 35dB GAIN

R, VARIABLE ATTENUATOR

H_{DC} DIRECTION OF DC BIAS FIELD

Figure 8 - Magnetostatic wave oscillator.
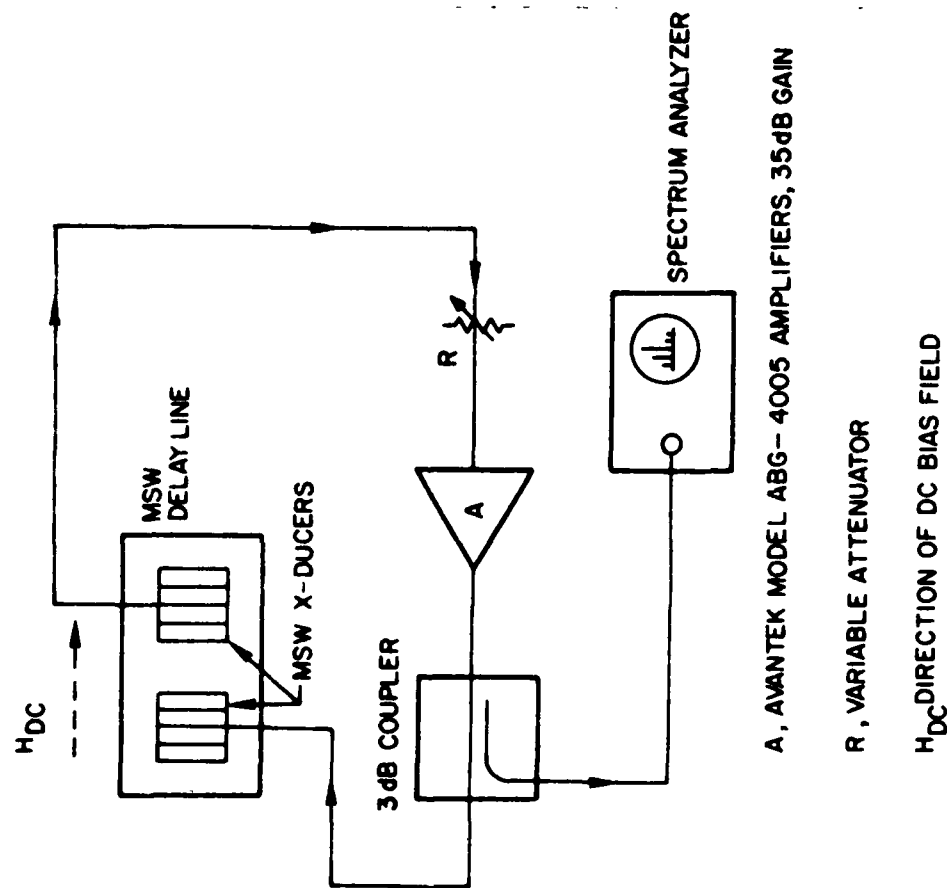
Figure 9 - Magnetostatic surface wave oscillator frequencies.

314

Figure 11 – Magnetostatic backward volume
wave oscillator frequencies.
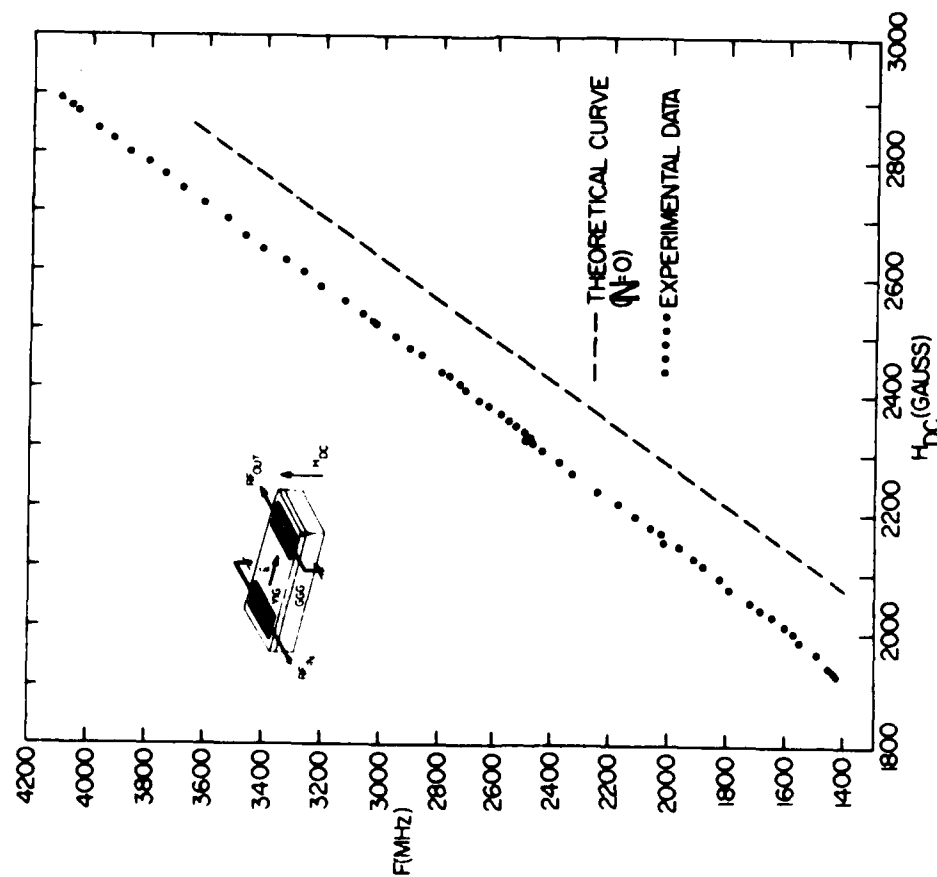
Figure 10 – Magnetostatic forward volume
wave oscillator frequencies.

All the components of Eq. (7) are given here.

$$\mu_{xx} = 1 + \frac{\gamma^2 H M (\sin^2\theta \sin^2\phi + \cos^2\theta)}{\gamma^2 H^2 - f^2}$$

$$\mu_{xy} = j\gamma M \sin\theta \frac{(f\sin\phi + j\gamma H \cos\phi \cos\theta)}{\gamma^2 H^2 - f^2}$$

$$\mu_{xz} = \frac{-j\gamma M (f\cos\theta - j\gamma H \sin^2\theta \sin\phi \cos\phi)}{\gamma^2 H^2 - f^2}$$

$$\mu_{yx} = -j\gamma M \sin\theta \frac{(f\sin\phi - j\gamma H \cos\phi \cos\theta)}{\gamma^2 H^2 - f^2}$$

$$\mu_{yy} = 1 + \frac{\gamma^2 H M \sin^2\theta}{\gamma^2 H^2 - f^2}$$

$$\mu_{yz} = \frac{j\gamma M \sin\theta (f\cos\phi + j\gamma H \sin\phi \cos\theta)}{\gamma^2 H^2 - f^2}$$

$$\mu_{zx} = \frac{j\gamma M (f\cos\theta + j\gamma H \sin^2\theta \sin\phi \cos\phi)}{\gamma^2 H^2 - f^2}$$

$$\mu_{zy} = \frac{j\gamma M \sin\theta (f\cos\phi - j\gamma H \sin\phi \cos\theta)}{\gamma^2 H^2 - f^2}$$

$$\mu_{zz} = 1 + \frac{\gamma^2 H M (\cos^2\theta + \sin^2\theta \cos^2\phi)}{\gamma^2 H^2 - f^2}$$

MAGNETOSTATIC WAVE

PANEL DISCUSSION*

Richard W. Damon
Chairman

Panel Members

J. Douglas Adam	Westinghouse Research Center, PA
Jeff H. Collins	Univ. of Edinburgh, Scotland
Howard Glass	Rockwell International, Anaheim, CA
Frederic Morgenthaler	Mass. Institute of Technology
John Owens	University of Texas at Arlington
Charles Smith	University of Texas at Arlington

*Transcribed from tape recordings, by J.C. Sethares and R.E. Floyd

Panel Discussion

SETHARES   Well, we've had two days of very interesting talks and I would like to thank all of you who contributed to this workshop. I'd like to thank you very much. I think the work that's going on is very significant and I was impressed with many of the results I've seen here in the last couple of days. I'd also like to thank Dick Damon for taking time out of a really busy schedule to be with us today.

The format for this afternoons' panel session will be mainly up to the panel. However, I would like to ask that at some point after the panel has a chance to say what they want to say, if they could open it up to questions and comments from the audience, and I will pass this mike around so that the question can be heard by everyone. Before we get started we have a photographer here who would like to take a picture of the group.

DAMON- It's a real pleasure for me to be here and I'm sorry I haven't been here more. That allows me to come in with a completely open mind, and challenge these guys to tell me why we should be doing magnetostatic surface wave work, and I think that's the object of the meeting anyway. But most of you are probably IEEE members, at least I hope so, and since I'm working for you I have not been able to be at more of this. But, we have here on the panel, why don't I ask them first to introduce themselves.

Jeff Collins - Univ of Edinborough

Howard Glass - Rockwell

John Owens - Univ TX at Arlington

Douglas Adam - Westinghouse

Charles Smith - Univ TX at Arlington

Rick Morgenthaler - MIT

313

DAMON- I think its an outstanding panel and looking at the titles and the authors of the papers I know its been an outstanding program and I commend you on putting it all together. I understand that Jeff Collins has <u>not</u> yet had an opportunity to speak at this conference and usually he has some provocative remarks. I would like to give Jeff an opportunity to present these and then I will ask other panel members to make formal statements if they wish, or we can just go into a discussion. So why don't you start it off Jeff.

COLLINS-Well thank you very much Dick. As you all know I'm an imposter because I haven't worked in this subject since I had a pleasurable year at the University of TX at Arlington (76-77) I didn't know what was going to be said here the last two days. I found myself really having to struggle on occasions from the depths of adaptive antennas, which takes seven years of training to understand, followed immediately by Howard Glass and his in depth discussion of materials. If I can help you on the adaptive area, read Microwave Systems News June-July-August where there are three excellent tutorial articles on the subject, written by people from, guess where, University of Edinborough. Now, Jim Sethares mentioned yesterday when he kicked off the meeting some things like what I have here on this viewgraph which I put together last week while sitting in my office in Edinborough. He made very similar statements to this up front, and I'd like to preface my remarks with these statements:

> Where are we? (in this technology)
> What is the competition? (is there any)
> What unique roles can MSW play???
> How do we get there?

What are the good things. Well Howard Glass would say we have a strong hand on materials technology and I would agree. I think another big "up" side is that people have demononstrated, unambiguously, non-recursive transversal filtering at <u>microwave</u> frequencies; and now back to the real world. What's

2

319

on the "down" side? Well a lot of us in this room can remember the bad history

of those 1 cm long 3mm diameter YIG rods of the early 60's and I don't think that

they have ever found the way to any systems socket as of today. So that's bad

history of the 60's which probably the system designers don't forget. The second

point which you may disagree with, but I hope to prove is correct in a moment, is

that devices we have today are, excuse the phrasology, "crude" and performance is

modest and I may be wrong on the third point but there is no identifiable or sold

success in a systems socket. Now, what is the competition? We've heard some very

interesting statements today about MSW resonators, the most outstanding work from

Thomson-CSF. But the triumph of YIG technology is the YIG sphere filter, as a

filter and as a resonator for microwave oscillators. People really do make and

sell these things today and have done so for twenty years, since 1960. But the

business, I would say is flat. Another competition which I'll demonstrate is that

in 1970 there was built an active filter channelizer, and finally good old surface

acoustic waves, which we've built in really very high fidelity devices, TV filters

and pulse compression filters, since at least 1974. There are three areas of

competition. YIG sphere filters are generally microwave. The active filters I've

described are also generally microwave, and of course SAW is UHF & VHF. For a

quick summary here is a three stage YIG resonator from YIG-tek, circa 1972. I

would be very happy in the discussion to say what this filter will do versus what

the current MSW resonators will do. I think it is important to know what the claim

of records is. One obvious statement to make is that this filter has a rejection

for spurious modes of 45 dB. Here is a contiguous filterbank based on inverted

common collector bi-polar transistor technology. I don't know what that means

either, but if you can focus your minds on the top right here, can you see it, here

is an active filter, contiguous --it has zero insertion loss per channel, because

its active, and it has a 3 dB overlap of the channels, its actually running from

3

360 to 435 megahertz and I stole this picture from the 1969 MTT symposium digest and
it was held in Dallas, Texas, and, here, is the box, pretty impressive. What Douglas
Adam has described on his channelizer, I think is extremely impressive, but you've
got to convince those ESM (electronic support measurement) designers to actually
put channelizers in systems, and I'll tell you right now that they'll do that rather
than put this gentleman's pulse compression filter in. Now here is a pulse compression
filter from Hughes with a time bandwidth of 1280, it's a surface acoustic wave
device, and the RMS phase error is on the order of $3°$ over the band, not like the
$100°$ for MSW that Mike Daniels presented earlier.

Now here we have a 51 dB sidelobe pulse compression filter and we can make
them everyday. So thats some of the competition.

What unique roles can MSW play? Well let me give my opinion on this. Repeat,
we have the non-recursive transversal filter for operation at microwave frequencies,
also frequency selectivity or programmability, something that SAW's do not have.
There are two things that SAW's don't have, microwave frequency operation and
frequency selectivity. Now its a pleasure to acknowledge Prof Smith and Owens who
are going to present a paper at MTT in LA next week where they are claiming that
the phase noise of a MSSW resonator based oscillator is superior to Avantek's YIG
sphere oscillator. There you are. I'm sure Larry will be very pleased to hear
that. He is the president of Avantek. Also low-cost phased array antennas present
an enormous challenge. I have been convinced for a long time that this new technology
must somehow have something to do with ECM receivers and I am glad to recognize
that even Westinghouse and Litton agree with me. The channelizer is an important
add on to an ECM receiver. Microscan, I'm not so sure about that because, tell me
how you get the data out, and the final one and perhaps the most important one and perhaps
the first one to get into a systems socket-maybe it has, Westinghouse won't tell
us, is the excellently described signal-to-noise enhancer, a very significant

device and a very simple device to design in principle. So I think we have seen today three things which give us great hope. The signal-to-noise enhancer for frequency-memory loops which no doubt Watkins-Johnson and Pete Kennedy will be interested in, the channelizers if the systems designers can really get down to the point that they are prepared to use a channelizer to do this time coincidence pulse sorting, where the pulses are different in the frequency domain, and the terrifically significant area of the low-phase noise oscillators, and during the discussion I think we'll have a lot more to say about that. But I'll not say much more except that you will have to worry about short, medium and long term stability. You'll have to look at the lessons of the SAW people. We've heard nothing on the low-phase noise at this meeting but Prof Smith & Owens will report it next week, Doug Adam gave an excellent pitch on the medium term stability, the temperature stability he achieved of ± 1 MHz at 9 GHz. None of you are saying anything about long-term stability, are they? (we haven't been around long enough).

How do we actually get MSW to play unique roles in a systems socket, and secondly to in fact replace some of the existing technology, like the oscillator may well do. Here are some thoughts I wrote down, totally at random, it sounded to me as if MSW was like SAW revisited. I heard so many prolifierations of the same thing I was getting confused. I think you really need to look straight through at what needs to be done to reduce the device options. We need to dramatically improve our theory. Let me give you one example of that, the lowest insertion loss delay line is an MSSW one. Four or five years ago we made one with 3 dB loss. Did anybody ever tell you where the 3 dB went to? In SATCOM 3dB is pretty important. Well Professor Tuan gave an excellent paper on diffraction and explained to us where about 1 dB went. I don't really know what the linewidth in this material is. Nobody has measured it for me or will tell me about it, and I'm not sure we've got the radiation resistance argument right, we have no scattering model for

the transducers. For example, I think to convince the systems people, we really need to dramatically improve our theoretical understanding then build and test these devices. The testing we are doing on the MSW devices is extremely poor. In my view, they are bad. We certainly need to get one device in a systems socket. Otherwise the Air Force will never put any money in it. I think the implications in all this are that we need to educate academic theoreticians. What I mean by this is that we've got to be clear on the goals. There is some very important and fundamental work to be done, which only the academic community are capable of doing. That leads to another point concerning tightly coordinated programs. You guys as I understand aren't even trading computer programs for dispersion. Somewhere there has to be a big brother that says this is where we are going and everybody has their role. But we need to coordinate and transfer the information much more effectively. Well thank you Dick, that's all I have to say, for now anyway.

Oh, I'm sorry there's more. This was prepared after the last talk this morning by Prof Smith and his friends. It's not in a logical order but we'll start with applications. We think MSW could have a role in getting rid of bulky coax cables with high loss that lie around in lots of real systems hardware. But of course the MSW has to do certain things for that to happen. It is a 1980's way of dealing with a 1940's problem. Phased array antennas present an enormous challenge, which has been identified by Hanscom AFB, and really an enormous amount of work to be done, can it or can it not have a role here? Nobody at this stage knows. But what one has to do, which Jim helped remind me, please remember you can't put kilowatts through these devices. I was very intrigued by John Graniero's talk on adaptive antennas which is a fantastically growing area. I think there is a very key role there for MSW which you can say is the, again coax role, which is the transversal equalizer, the programmable transversal equalizer, where the programability will be in silicon technology.

323

Now I have put down a provocative remark which the others didn't want me to put in. I listened with great care to Hunter Chilton on circulators and I don't think you should try to replace his circulator with this technology. Now, Paul Carr (RADC) reminded me that in the early 1970s, certain people demonstrated convolvers with magnetostatic waves. But there is the point that if there is signal processing technology you've only talked about handling pulse waveforms and chirp waveforms, whatever happened to multistrip coupling and all the good things that SAWs play with. And there is an interrogation system, which I can't talk about, because I don't understand, and if I did I wouldn't be allowed to, which is up in the gigahertz region which is a big area to be worked on at the moment in new interrogation systems, which uses convolvers. Now the next heading is materials and this is an appeal to Howard Glass, but I'm not sure everything we are saying is materials here. We don't really know in these dispersion relations what the real anisotropy is we're talking about and if you're going to build high fidelity devices you are going to have to get a handle on that theory and experiment. Clearly there is a need to get higher $4 \pi M$ materials, to get into higher and higher parts of the microwave spectrum. Now, in this area of temperature compensation, what was in the back of our minds when we wrote that was the oscillators. First, we want to temperature-compensate these oscillators so that they have excellent medium term stability. We've got $4 \pi M$ that varies with temperature, it would be nice if it didn't. Doug Adam described an excellent method, obviously Thomson-CSF has done the same thing, bias magnetic field compensation. There are other techniques you can consider which weren't mentioned, active feedback, and just physically, if they are small enough, ovening the things. So I think we've got a lot of handles on how to approach temperature compensation. I believe Rick Morgenthaler's talk was a most significant talk because there are situations when we only need to produce a uniform bias field over the sample. But synthesizing that field is no pretty problem and Prof. Morgenthaler has shown us techniques for doing that and it is a most original contribution.

We had an excellent talk this morning on waveguiding techniques. They have not really taken off very greatly in SAW technology except for application of the SAW convolver for interrogation systems. It is beginning to take off in SAW, so we better not ignore it and there are lots of waveguiding techniques we can talk about, but the one that Dan Stancil (MIT) put forward, with the permalloy, I think is a very important lesson which we can learn from the bubbles field. Also we pointed out, in relationship to what Douglas Adam (Westinghouse) had said about the transverse 1,2,5 modes that he's running up against in each channel of his channelizer, that we could in fact use profiling for mode control, but Douglas had a very neat technique for dealing with it and congratulations on achieving 45 dB suppression, you've almost arrived. But field profiling is also important to get down the diffraction losses. So I think the presentation of Dr. Morgenthaler's work has been a very major contribution to this meeting. Now if we look to the transducer area I think it jolly needs work. We don't really understand transducers properly because we don't have a scattering matrix of the three port transducer, although my very good friends at Texas say they will soon have it (see if you can get that tomorrow). Indeed to be able to synthesize the transducer to achieve a specification, we are not at the moment able to do it. Maybe we can never do it in which case we better recognize that. That brings us to, really two areas, the control of amplitude and the control of phase. For dispersion control we've heard about intrinsic multi-layers at this meeting; the Larry Adkins paper, the Mike Daniels paper and the Jay Parekh paper. I don't believe this is ever going to give high performance. There you are, provocative. The resonator is a very important device, but if you look at the history of SAW technology it has been built around two techniques. The interdigital transducer, and putting all the design into that, and RACs, reflecting array circuits. But I don't think we have the first option of the inverted IDT open to us in MSW, and therefore you are going to have to play with the RACs.

Now Thomson-CSF is serious about these RACs but America is not serious, and I don't understand why as a Britisher. Thank you again Dick (Damon).

DAMON: I'll assume that you've also represented Charles Smith and John Owens. So now I'll ask if there are any responses or new challenges that Doug Adam, Howard Glass, and Rick Morgenthaler are going to make. How about you first? (Doug Adam)

ADAM: As far as challenges go, I think the only disagreement I have with Jeff (Collins) is on the RACs. I don't think that RACs are a very simple technology. They are extremely complicated, and as John (Owens) has pointed out several times, they will probably have high insertion loss, because they're a transversal filter.

COLLINS: Do you want me to reply?

ADAM: No. I'm just making sure you understand.

COLLINS: Let me say I disagree with him.

ADAM: My professional philosophy is to try and look at things that are as simple as possible. I agree I have misgivings about multi-layer structures, (how reproducible you can make them). On the other hand the possibility of low insertion loss devices is certainly more than you'll get with RACs. I think thats's the main comment I have. There are comments about the oscillators and things like that. It seems to me that there is an established technology for oscillators and when you're competing against an established technology, you've got to do something much better than they can do in order to get someone to use it.

Within our own company, if I were given complete freedom I would work on three devices. I'd work on a multi-channel filter, a signal-to-noise enhancer and a dispersive delay line for a compressive receiver. We are working on two of these very seriously and not on the other. I won't say anything about materials because I think Howard (Glass) is more qualified than I am.

DAMON: Should we now turn to Howard (Glass)?

GLASS: Well actualy, I have completely different concerns about materials. It's

326

very easy to grow a good YIG film if you start with a good substrate, but can we be sure that good substrates will continue to be available? Commercial sources basically have developed to serve the bubble business and the bubble may be bursting. It may be important for us to - I hate to say this - but it may be important for us to do some sort of a market forecast. Of course they did that for bubbles too, to find out whether the whole magnetostatics business is big enough to maintain an interest of the suppliers of GGG, if not, what is that going to do to the cost? I suppose since the Air Force will be the important end user, perhaps it is something they should be taking alead in perhaps even consulting with the suppliers to find out what their longer range plans are, especially what their contingency plans are if bubbles don't make it. The other materials problems are trivial. There are some people here from Allied and Airtron but I don't think they are the people from the right parts of those organizatins to answer these questions for us. Unless, well Michael Cain is here. Will we be able to continue to get GGG if bubbles don't make it?

CAIN: Yes, if MSW can get big enough to carry it.

GLASS: Yes, that's a big if.

DAMON: It does represent a significant concern.

From Audience: I have a quick question in general. I don't know a lot about the electronics involved, I'm mainly a materials person and I see a YIG sphere which Airtron produces and I believe they sell those spheres for 3 or 4 dollars, something like that. Now you take GGG with a YIG film on it and you get a device which is 1 inch long and you're running into 80, 90, 100 dollars to produce that film.

OWENS: I think the point you have to bear in mind is what YIG spheres are sold for per pole. Right now they are in the several hundred dollars per pole range. The expense is not in the YIG, it's in hiring the watchmakers to bring them together,

and praying. Plus the fact that of those spheres that Airtron supplies you, you will throw away two-thirds of them. There are a number of things that push the per pole price on a filter well above that 3 dollar range. Secondly, the problem is that its microphonic, it is tedious, and a number of other things, to assemble and if in principle you can produce a device with better response characteristics that is with higher performance, for military systems in particular, then the arguments rather strong in favor of those that are easier to reproduce and get consistently.

SMITH: Concerning the films, John (Owens) and I buy 1" diameter substrates for 21 dollars a piece in batches of 100. You can produce 5 delay lines about the size he's talking about. So the price is not a hundred dollars because we haven't been selling them for that.

DAMON: Well Rick (Morgenthaler) we haven't given you a chance yet. Mostly what I've heard Jeff (Collins) saying about you was good things.

MORGENTHALER: I'd like to mention just a few points. First of all, there is sort of the _time_, the _dollar_ and the effort curve. We have to look back to SAWs and ask where was that technology when a comparable effort, time dollars, personnel and so on had been invested. I think if you cast your minds back awhile and then project, we're not that terribly bad off right now in MSW. Clearly in my view MSW is a complementary technology - clearly in frequency ranges where there is overlap, SAWs may have tremendous advantage because it's a ready-made technology. But as pressure for higher and higher RF frequencies increases, as in fact the pressure for handling narrower pulses comes along, the ability to cut the time-band width product "pie" into different proportions, the proportions that are sort of natural to the YIG technology where your talking about very large bandwidths, and time delays are more moderate, on the order of a fraction of a microsecond to a microsecond or so, but with bandwidths that are 1, 1.5, 2 gigahertz or maybe more in some situations, then I think that we have perhaps a unique role to fulfill.

Certainly we have to learn to live with and really understand those characteristics of MSW propagation, which at first shot looked deceptively similar to SAWs, but, which are really very different. I think that, for the uninitiated, the biggest shock comes in realizing that when you specify the frequency of an MSW device you have not necessarily specified the wavelength at all. If we include the entire range of wavelengths, down to the short exchange dominated spin waves as well, for a typical microwave frequency let's say 1 to 2 gigahertz, we are talking about a range of wavenumbers of, I calculate, something like seven orders of magnitude. We are certainly not using that entire range in MSW. But we have that ability, and it's a two-edged sword. On the one side we have the ability to make the wavelengths be mm or tens or hundreds of microns instead of the sub micron wavelengths that are obtained in the SAW's if we went into the microwave frequencies. This is an advantage. The fabrication of our electrode structures, whatever they are likely to be, does not seem to me, to require the push to submicron technologies. We are blessed with being able to handle with fairly conventional means, photolithographically derived elements. And that is a good thing which should keep cost lower. But the other blade of the sword is that we can couple to a larger number of modes and we've had to learn, are learning slowly but I think surely, how to arrange things, so that we taper the couplings to those higher modes. In other words, that we do not put our energy in unwanted parts of the spectrum. But it is a very different situation than when you're dealing with most wave propagation where you specify the frequency then you have specified the wavelength to within at least a factor of probably 2 or 3.

I was also very impressed with the adpative antenna paper, and somewhat relieved because I think that there is perhaps a good role to be played by MSW. Since fitting into adaptive systems some of the burdens are reduced from our technology. But we do have to think about that because we're talking about

wide bandwidth systems. We have to, in our minds, break up that bandwidth into
those classes of applications where its instantaneous BW, where we have to deal
with it all at one time, and other situations where the device has to be capable
of handling the entire frequency range, but, only narrower segments at a time.
This makes a difference because if we are dealing with effectively a narrower
band situation within a portion of that overall range then the frequency variations
of some of our MSW parameters could be sorted out by the adaptive technique. But
if the adaptive technique has to essentially handle all frequencies at the same
time then obviously we have trouble unless we had made our devices so that the
systematic errors that we alluded to yesterday are down to tolerable levels.
Finally, I agree with Jeff (Collins) concerning YIG sphere filters, which I agree
is a remarkable product in that it is essentially 20 years old and except for
improvement in packaging, magnet design and so on, has changed virtually not at
all from its genesis. I can't think of hardly a solid state electronic component
that has survived any thing like that time span. We should pay attention to that
vitality, because its obviously telling us something. At the same time, there
is certainly the challenge to come up with planar technologies that would allow
us to integrate several poles of a filter into a reasonable size, to try and get
rid of that hard tweaking, very labor intensive characteristic that we've all
come to know.

DAMON: Are there any instant responses to some of these comments?

COLLINS: I'd like to respond to Douglass Adam. First of all in regard to the
three devices that he would like to work on, two of which he has, the channelizer
and S/N enhancer clearly I totally agree with, but in regard to the microscan
receiver, I really would like Douglass to tell us how he's going to get the
information out and process it.

FROM THE AUDIENCE: Can you tell us first what a microscan receiver is?

COLLINS: Yes. It's basically using a pulse compression filter to actually define frequency in terms of time.

DAMON: Let me put a challenge in on the channelizer. In addition to the Motorola program, we have at Sperry also a program to develop channelizers and we're talking seventy dB out of band rejection all spurious 70 dB. I just wonder if there is anything in the same league that one could even contemplate using this technology.

SMITH: 70 dB dynamic range is probably roughly a limit for this technology. What do you think, John?

OWENS: Yes. By the time you run into saturation, it is what they are talking about 70 dB down spurious and that's a very different thing.

COLLINS: Well I think that illustrates the point I was making.

DAMON: Now there certainly is if you put it in an antenna. That's where you actually operate it at a microwave carrier frequency. So I think you have to identify either systems in which you have to operate at the carrier frequency or else the bandwidth demands are very great.

MORGENTHALER: What about narrow pulse applications? Radar at mm wavelengths?

DAMON: Your'e talking gigahertz bandwidth, correct? (YES) Well then no question about it. There aren't that many systems with such characteristics.

MORGENTHALER: There are potential systems applications. Suppose you wanted to analyze the frequency acquisition of a radar pulse, and you would like to acquire the frequency as rapidly as possible. You would not like to wait over the few microseconds that the pulse may be on, you want to take the first slice of it and essentially process it while the rest of it is going on. In terms of taking that very narrow slice you have now produced a very wideband signal, which you have to lock on to. I believe that some of the MSW or Magnetoelastic wave work, certainly has the potential for doing that kind of thing.

331

DAMON: No question that I can envision systems for it, I'm just saying that ther· aren't that many existing sockets into which you can plug it. So you've got to build a device that the systems' guys believe in enough to build a system.

OWENS: There are design studies going on in optical radars, and if you look at the doppler rates associated in optical radars and ballistic missiles you begin to find numbers which far exceed any bandwidth capability of anything running around today. If you're going to do any signal processing on these things you are talking gigahertz bandwidths for optical frequencies for ballistic missile dopplers.

DAMON: Let's return to Jeff's question for you Douglass (Adam)

ADAM: Okey. Maybe I can answer it this way. When we talk to systems engineers at Westinghouse they don't want to know whether MSW is better than SAW or integrated optics. What they are concerned about is digital technology. In order to do the same type of processing that we can do, digitally they're going to have to increase their bit rates enormously. They're going to have to use nanosecond type pulses and so on. And I am worried about how to read a microscan receiver but if these guys are going to be trying to - if the competition is trying to produce very high speed digital logic, then in the intermediate stage there is going to be a digital processor available that is going to be able to handle the nanosecond data rates. I think it's almost there, I don't think it has too far to go.

COLLINS: It was sort of provoking your answer. I have heard an approach described to do that with a SAW microscan receiver. It didn't have much dynamic range, admittedly. It was presented at the Ultrasonics Symposium. I'm sure you're right, it will come.

We say that MSW oscillators are competing with established technology. It's true the world is full of microwave oscillators. But I don't know of any quartz oscillators that work at microwave frequencies and I think people would use them

if they did. MSW oscillators will never be quartz oscillators at microwave frequency, but they are going to have certain specifications, I'm quite certain, of better performance at microwave frequencies than you can do with certain existing techniques. If one accepts the result of John and Charlie's on the phase noise of the MSW resonator oscillator against the Avantek and the Yigtek devices which are being sold today, sure they will compete with existing technology head on. If this is for real this is a darn sight better and people will buy them.

Next, I believe that temperature compensation should in no way be inferior to the YIG oscillators. Long term stability is another question, but I would think it's going to be a lot better. But we don't know anything about that we haven't been around long enough.

On RAC's I must entirely disagree. Sure they are difficult things to design, but you tell me how you're going to get down to two degree RMS phase error, over 500 MHz, and you're going to do the amplitude weighting. You tell me how you're going to do it with simple devices, it's going to be complex, it's going to be a long haul. I can also pick upon Rick's (Morgenthaler) point, in reference to the effort. If you want hi-fi devices, particularly for your microscan receiver and other communication signals, you will really require very high performance devices. You tell me what other route your going to take, I'd like to hear. There's no guarantee of course that the RAC route will work but it has worked for SAW technology.

ADAM: IDT's work for SAW's also. I agree that RAC's may work for MSW, but as appealing esthetically as it is to compare the two technologies, SAW and MSW, there are two large differences. One is the strength of the coupling and the other is the rate of change of wave number with frequency. And these are two big problems. Personally I think you're better acknowledging the fact that there is very strong coupling; there are very strong interactions and try and use them rather than try and minimize them and do what you feel should be done.

333

MORGENTHALER: I think it's important to focus on the differences as well as the similarities of the technology. Let us remember, it's certainly been vividly portrayed over the last two days, that magnetostatic waves are inherently dispersive whereas the Rayliegh wave, of course, is non-dispersive so the array structures whether it's RAC or others, is where the dispersion comes from. My point of view is we ought to try take maximum advantage of the natural dispersion which the physics gives us and modify it, straighten it out, whatever, to make use of what we already have rather than essentially jettison it and pretending that MSW is a SAW and saying every time there is a SAW device we will build the analog MSW component. Where we can do that, where we can learn from SAW, then the idea is great. But to force a concept into the wrong mold is probably counter-productive. Finally, to a point that Jeff (Collins) raised at the very beginning. In a sense we got bad press in the mid and late 1960's, the YIG technology at the time was, with the exception of probably spheres, over sold. It was sold too rapidly. I think that's something we'd have to acknowledge and put behind us. It would be a pity if any systems designer or potential sponsor were to shoot down a clever concept or good idea, because somebody had a bad idea or oversold one 10-15 years ago.

DAMON: But it is clear Rick, as you said, time, dollars and effort, and were just not going to get the time that SAW people have, were not going to get the dollars they have and we are not going to be allowed to make the total effort before we have to get performance in a systems socket as Jeff said. It is clear from dealing with people that are end users that they have this attitude. They want something to use now. They're impatient. We're not going to have a long lead time in this technology. It's either going to fly or it's not and in some respects it's close to the decision making time.

I have a quick point to make about what Rick said. In the RAC designs I have seen, you certainly live with the dispersion and you work and modify from

334

that position. The point is you can modify from that position because you can use small interactions.

OWENS: Let me make one comment on the RAC's. That one device that is shown up here which may not look beautiful as a flat design, later versions of that thing had 400 MHz BW and 30°RMS phase error. It isn't great, but it is better than anything else I saw here. That's on a crude device, given one year by a master's student. It's not exactly a high effort, but considering that level with a metal RAC with no weighting that's good performance. SMITH: The interesting thing is we weren't trying to make the dispersion linear we were trying to flatten it out, which is even more stubborn. (Question: Then you were making a non-dispersive device?) Yes, a non-dispersive line out of a dispersive one. This is somewhat a worst case and that's why I say it has the promise. I don't see anything that will. COLLINS: You can't get high performance unless you understand every little detail, second or third order effects, then have a technology to fabricate and test the structures.

DAMON: I don't think you want to be too hard on the YIG of 60s either. I think a lot of the people who went into SAWs learned about signal-processing requirements from working with YIG of the 1960's. And those are the device guys who turned out to do it out of SAW work, when that technology became available and was evident. That was the way to go and convince systems engineers to look into that direction and it did fill the sockets much quicker than YIG would have done so. It did a lot of good in priming the pump.

SMITH: Actually on an academic side loop that's justification for supporting programs like that in an academic institution. Very few students learn very much high frequency technology, using modern equipment, unless they have some justifiable program like this to follow.

COLLINS: I entirely agree.

DAMON: Well, have we thoroughly had everyone's view.

SMITH: I believe so. Now we'll take one question from the audience.

DAMON: Why don't we open up the discussion for questions from the audience?

QUESTION: Well we've spent two days on an Air Force Base at an Air Force sponsored workshop, and the Air Force is a major funder of this technology. I think it would be appropriate to get some Air Force words or views.

DAMON: Did you want to say something Paul (Carr), Chief, RF & SAW Components Section, RADC)?

CARR: I was just going to say that you could gather from the way the program was structured, and I think from the response here on the panel, that beam steering components, both the absolute beam steering that Bob Mailloux talked about and the relative adaptive beam steering, has a lot of potential interest. It turns out that my group is the focal point. I came to the meeting looking to see how you (MSW technology) were going to achieve the couple of orders of magnitude improvement that you need to meet the specs that people want. I personally like this RAC idea, particularly the 30° RMS phase error, I feel encouraged. There is one other idea that I'd like to bring up that hasn't come up yet in the meeting. I'd like to direct this to Rick Morgenthaler. He mentioned that when the old Strauss Delay Line was around that with a non-uniform field he came up with maybe an order of magnitude improvement. It seems to me that there is something that hasn't been played out. You've done some preliminary analysis using this non-uniform theory haven't you? I think this is one idea that could be explored and one might find an order of magnitude there, maybe.

MORGENTHALER: Let me pick up on that because it fits in with my earlier comment that we want to try and take the dispersion relations which nature provides us, because of the physics, then, modify them in ways to meet our systems specifications.

336

Although Jeff (Collins) much abused the Strauss magnetoelastic delay line
this afternoon, my group was quite interested in magnetoelastic interactions
and trying to understand fundamental coupling between spin waves, elastic
waves, and electromagnetic waves. We at MIT did not jump onto the magnetoelastic
delay line band wagon in the early days because I didn't know quite what else to
do with it. If you were going to just take the natural field profile that came
from the rod and modify it just slightly, I felt that we were going to have real
difficulties in getting the linear dispersion or the controlled dispersion - the
bandwidth and so on. Although there were some very fine studies, I think Herman
VandeVaart's work at Sperry was a tour de force of what could be done with careful
tweaking of the delay line. That approach did not seem to me to lend itself to a
synthesis of how to change the characteristic slightly and quickly. So, it was
only after we had found out that it was possible to synthesize the DC field profile
relatively easily, that we went and tried that approach on the old Strauss delay
line. Much to my gratification, we found that virtually every characteristic of
the line improved on the first try. The first synthesized pole pieces which came
out of the computer were machined in the shop, we put the thing together and we
got greater bandwidth, particularly second echo free bandwidth, flatter insertion
loss, less ripple and really quite good characteristics. The characteristics were
published three or four years ago by a former doctoral student of mine, including
a paper at the International Systems and Circuits Symposium in 1978 in New York
City. In a nut shell, we were able to obtain easily a gigahertz of bandwidth,
insertion loss including the reflection loss because of the polarization, on the
order of 35-40 dB, ripple was less than 1/2 dB and linearity of the time delay as
a function of frequency that was within, we did not measure the phase error so I
can't tell you that, a percent or so over that wideband. The approach, I think,

lends itself to the possibility of making vernier adjustments to the field, in the synthesis, and therefore corrections. In fact if you are willing to use an active field component, in other words a small supplementary winding to add in a vernier field, you should be able to make the characteristic adaptively change, so that once you have measured its characteristic, if you find the phase error is too great in a certain portion you may be able to tweak it and change it. And, if that approach, synthesizing the field pattern to exacting standards, can be controlled for MSW versions of the linearly dispersive delay lines, then I think there is merit, and that is the sort of approach and the reason my group has been involved with the synthesis for these last several years.

Collins- Through the chair, we said that we thought this is a most original contribution - this field profiling is a most fantastic work described as a result - but, I think that what you've got to look at is these two techniques together, the field profiling and the discontinuity approach.

Morgenthaler- Yes

Collins- And the reason I say that is that, you have got phase characteristics, fine, but you haven't described how you're going to do the necessary amplitude tailoring. So I think both techniques will prove invaluable and should be used in combination, and I repeat that I entirely agree with you. You start with an active characteristic and tweak in ways that are parallel processing the nineteen eighties, and that's why I am a little in doubt, a little bit concerned about what you can do with magnets when you're looking for very, very compact structures. Maybe I'm wrong, maybe it's just a new way of thinking for everybody.

Damon- Well, I think Rick has gone along with much of this. I'd like to make sure that we've gotten all that we can get for questions from the floor, namely whether or not anybody is prepared to say what the Air Force's essential strategic

338

reasons are for being in this business. Do you have any particular sockets you're trying to fill, that you can tell us about.

SETHARES- Well, I think the need has been identified, and it has to do with phased arrays. Designers are looking for time delays in the tens and hundreds of nanoseconds with bandwidths in the hundreds of megahertz, say 200 megahertz. The two biggest problems that came to the forefront right away were what kind of power levels are involved, and the temperature problem. Now we find that in some phased array systems both the power level problem and the temperature problem have been relaxed, one example being the solid state transmit/receive modules that were talked about by Hunter Chilton. Now, he did mention a circulator in that module, however, in that same module there is a phase shifter, and it's a three or four bit phase shifter right now, and that's okay for narrow band antennas. To get the wideband, time delay units will have to go in there, so the Air Force is looking for different ways to get these kind of time delays. They are looking at fiber optics, acoustic waves, coaxial cable and they're also looking at MSW. Each of these different technologies have advantages and disadvantages. One of the characteristics that MSW seems to have is the wide bandwidth. The biggest problem is the dispersion and that's the problem that has to be solved and if it is solved then the applications are enormous. One antenna system for example may use one million time delay units. The way I see it anyway, is that dispersion is the toughest remaining problem and if the technology can handle the dispersion then it will survive, if it can't it won't.

Carr- You mean like the one degree control of phase error.

SETHARES- Well, as far as the phase error is concerned, it's got to get down to a level where adaptive means can be used to bring it down further. I don't think

the technology as it stands can ever hope to get down to one or two degree errors, it may get it down to thirty degrees.

Carr- Well, we're already at thirty degree errors.

SETHARES- Well, it's not good enough. (Laughter)

Adam- You sound like a customer.

Owens- Well, the problem is that the insertion loss for that type of application is totally unacceptable and probably always will be.

SETHARES- Yes, well as for the insertion loss, you can put amplifiers in there to bring it up.

Owens- Yah, but you're paying an awful lot of dollars for amplifiers these days, per dB, and if you've got to pay 20 to 30 dB insertion loss, you've got a problem. The applications you're asking for, particularly there, have to be of the simple variety. I think those are the ones with the low insertion loss. They've got to be low insertion loss, basically, simple modified delay lines. There is very little other choice, because if you're going to achieve the insertion loss and the cheapness you're not going to do it with reflecting array circuits. I don't question that at all.

Smith- I don't know John. Suppose we had a microprocessor in there running the phase shifters. If we can get close and we can either cascade it with a phase shifter that's microprocessor controlled like Hu did, or we just used a microprocessor to control the delay line structure with a tweak in the bias field, and put in memory in that microprocessor to get to the accuracy, we may be all-right.

340

Owens- Yes, but the problem is that it has to be cheap. You've got to limit it

to $50 which means its got to be an exceedingly simple fabrication procedure,

in order to make this viable. You're talking about a million elements. You can't

afford $100 apiece. That's for the whole module, not just the delay line.

Carr: You could probably allow about $20 for the delay line and $80 for the rest

of the module, amplifiers, switches, and so forth.

Damon- Do you have any other interim goals along the way, short of spending 100

million dollars for the phase shifters for the antenna?

Carr- I think the adaptive technique is an interim goal.

Owens- The adaptive technique is almost a natural for an existing MSW device.

Smith- Yes

Carr- The adaptive electronics can take out some of the dispersion.

Owens- You're only asking for a couple of hundred megahertz and you can take out

a few degrees of error on a delay device, a tapped delay device and do the job.

That is a natural. That's the one really bright light in the short tunnel. The

long tunnel, I don't know. But, that one is really a natural, if we got the numbers

right, because the delays are perfect, a few nanoseconds, the tap spacing is right,

and so on. It really is almost perfect.

Morgenthaler- I'd like to throw out a question for Howard or anyone else who would

like to respond. If we project to higher frequencies, higher microwave frequencies,

we obviously worry more about crystal quality. I think in many situations in the

laboratory, Jeff Collins may not know where the 3 dB is going, some reasonable

fraction probably is not going into the loss mechanism, and therefore for up to

some frequency you can tolerate the same material or the same level of quality.

But, what's the forecast, how high a frequency do you really think that we can go

with a viable device. That, of course, is going to bring up the issue of the

natural limits for MSSW versus either forward or backward volume wave. How high a frequency can you go with a conventional surface wave device.

Glass— In YIG? I don't know how high you can go in YIG, but in a conventional MSSW device if you can go to Lithium Ferrite, that will help you out. We just don't know what the eventual losses are going to be in Lithium Ferrite. All we now know how to do is just barely grow it. We don't know how good a crystal we'll be able to get and what it's losses will be. I'm not aware of a calculation of what the intrinsic losses are in Lithium Ferrite. Maybe you are.

Owens— What about the higher frequency sphere filters around 40 GHz.

Morgenthaler— I'm talking now MSW, taking ir   account the dispersion character-istics, and so on, the bandwidth, the natur   ndwidth that occurs.

Smith— The surface wave is going to narrow down to a couple of hundred megahertz bandwidth as you go higher in frequency, as you go up to 10 or 20 gegahertz. For the volume waves the bandwidth saturates out to about 2.2 GHz. The bandwidth is not the problem, the problem is the propagation loss. The true information you get is proportional to frequency.

Owens— Yes, and the probelm is to build a magnet.

Smith— And still be able to carry it around in a wheelbarrow. (Laughter)

Owens— The largest magnets that are presently being built for YIG sphere filters, go to about 40 GHz. Now, we presume if you expand on that technology you might rationally be able to take the technology up to there provided you can accept the loss in the device your talking about.

Adam— If you take something like a phased array delay line, in the limit they're only interested in the differential delay and that can be on the order of ten or twenty nanoseconds. Even if you're dealing with an effective linewidth of one oersted, you're only going to have a propagation loss of a db, so with that line-

width you can probably get to 30 GHz. I think there probably are some circumstances in which you can push pure YIG up pretty high.

Owens- Certainly 20 GHz and perhaps 40 GHz. You may not be able to lift it higher, but certainly 20 GHz would be practical.

Adam- I don't know where Lithium Ferrite helps in high frequency applications because the linewidth is terrible. We would like to use it at lower frequencies because of the increased bandwidth, in the signal to noise enhancer, for example.

Smith- In the surface wave device it helps you a little bit.

Adam- Right.

SETHARES I would like to throw out something to see if we can get some comments on it. We were talking earlier of the natural dispersion of MSW. One question which came to mind was what is meant by the natural dispersion. I know what it is in a YIG sphere. YIG spheres as we have seen have been around for 20 years. We known that the field inside of a sphere is uniform, so we known how to design nice filters. I'm wondering what would happen if we took a different geometry, other than a sphere, and controlled the DC field to high precision. It would have it's own natural frequencies and dispersion. If we were to design it for no dispersion or linear dispersion would this be the natural dispersion?

Morgenthaler- Look at the mode, quasi two dimensional modes, in an oblate spheroid which can model a thin disk, but let the shape be really arbitrary - a sphere, prolate or oblate. Then the dispersion is omega as a function of the mode number, taking $e(-in^{\wedge})$ where n is the mode number. Omega as a function of n is like a dispersion diagram, ω vs k. The natural order of things is that as n increases, $\omega(n)$ saturates at some characteristic value, just the same as with the surface wave. On the slab, the $\omega(k)$ goes in the limit of k $\to\infty$ to Damon Eshbach limit. This is also the characteristic frequency for the uniform

343

precession in infinitely long cylinders because it's really the same mode. How you get there, in other words the particular curvature (slope) will change from one mode family to another as you change the shape. But, as my analysis has shown you can also control things by shaping the magnetic field. It's important to realize that if you once shape the magnetic field, you have some profile, and you let the mode number n still become arbitrarily large, you still come to some asymptote, some characteristic number. So, control of the field allows you to in a sense postpone the inevitable. Suppose you have a dispersion which is rounding of very, very fast. In a sphere for example, the slope of the lowest mode is fairly steep. The energy circulation in a sphere is quite rapid - it's this 5/9 GHz for pure YIG which Jeff considers irrational. But, he has to remember that it's an approximation essentially of the magnetization frequency being approximately 5 GHz - you have to put in the 1780 gauss. Anyway, it's interesting because it's remarkable that the energy frequency in a YIG sphere for the n=1 (uniform precession mode) is independent of the precession frequency. In other words, whether you have tuned a YIG sphere to a frequency of 3 GHz or 5 or 40 GHz the precession frequency is of course changed by that factor, but the frequency at which the energy is circulating around is 5/9 GHz. If you go to the n=2 mode, the next one, it is a vastly smaller number and if you go to n=3 it is vastly small again and monotonically decreasing. If you use field synthesis control you could make the first mode slower, the second mode faster, the third mode maybe still faster and then, eventually you run out of coefficients of your control, the natural order takes over. The more coefficients you have to play with the more control you have, but it's a little bit like lion taming you're trying to keep more lions on the string, and you keep on adding coefficients and they're effecting earlier dispersions. The whole thing has to be put together. You would not like the field that you had to synthesize if you were trying to get for example linear

dispersion over infinite mode number because what it would end up with would be a surface impulse. You've got to remember that these modes are becoming more and more (they're really surface modes) surface bound and are in essence seeing the surface field. Each time you go to a higher mode, it see's the field mostly at the surface and weights the inner volume a small amount. So, if you're trying to raise the frequency of the higher mode numbers you do that by making the field in general an increasing function stronger at the surface than at the center. There are practical limits to the kinds of gradients you can achieve. Nevertheless for reasonable bandwidths and certainly hundreds of megahertz are reasonable bandwidths you should be able to achieve control over the dispersion to straighten it out if necessary, make it so that what is really a forward wave situation the dispersion is negligible over that restricted bandwidth. I think there is hope, but it's going to take work. I agree with Jeff that you cannot ignore the weighting and the coupling structures as far as the microwave part of the circuitry, and the whole job has to be put together.

Damon— We also do some dispersion control through ground plane spacing and so forth, I haven't heard very much discussion of that. (Laughter)

Owens— You haven't been here for the two days.

Damon— I mean by this panel.

Owens— Let me make a provoctive comment. I think that at least one of the lessons of the sixties and seventies has been that planar technologies photo-lithographically defined by simple techniques, where we remove people from the fabrication process, is the way things are going. You can look at a lot of examples, signal processing in either digital or SAW or in the semiconductor business where photolithographic defined technologies are becoming dominant. When we begin to ask to go into three dimensional signal processing technologies we are beginning to ask industry to move in directions which is not a general

345

trend. I think this is at least one possible problem with the field shaping, that we're getting back into the three dimensional technology. If it gets too complex nobody is going to be willing to build. To achieve large quantities, and we're talking literaly in these antenna phase systems about tens and hundreds of thousands of devices, if the process required to fabricate them gets too complex, even though they work, they simply become an unacceptable thing for anyone to put together.

Morgenthaler- Granted, but you have the three dimensional problems for any of the others because you've got to come up with a magnet design. If my computer generates a particular pole piece design which is diffent from yours but it can be manufactured on an automatic milling machine, under computer control, or whatever, why should that cause an uproar any more than providing magnets for yours.

Owens- All I'm saying is if the shaping and here we're talking about shaping literally YIG to an extent where we are asking for complex possible shapes, anything like that I think is an unacceptable type of approach.

MORGENTHALER: I'm glad you raised that point because I did have one slide that did show the energy velocity as a function of shape and that was not intended to be a pitch that we are going to grind the crystals into shapes. It was just to show that you really had only one parameter determining the dispersion if you had a uniform field for an oblate or prolate spheroid, and that was the shape. There was one parameter that would determine what the dispersion was going to be. I think, my own personal view is, that one of the reasons the sphere has been so successful for these twenty years, is because that energy circulation frequency is as large as it is. For the thin disks without any field gradients it's a very small number. I think that this has an effect on the impedance, and as it turns out on the electric fields that are associated with these modes. I shouldn't say the electric fields so much but

RF H-fields are strongly affected by the field gradients and that means the ratio of E to H or impedances.

DAMON: Let me at this point go back to the audience again to see if there are any questions.

ESHBACH: Let me make a comment. Maybe it will be a little bit rambly but maybe it will provoke some response here. We seem to be hoping or relying largely on the phased array application as the hope for a large volume that would allow this technology to get off the ground. We're trying to see ways in which to fit into the trend into phased array technology. I'm a little concerned that the reverse may happen. That is, the things that are happening in phased array technology, they're moving very rapidly, and I'm thinking of things like the Gallium Arsenide FET's and the monolithic circuits and all of that. They will quickly learn to use some of the functions that you're failing to see that MSW might provide. I think there are many lessons (one way of not being able to recall any specific examples is to say there are many obvious lessons) in which technologies that are moving very rapidly and become well entrenched do tend to take over. Look at silicon. Today almost anything you can do with silicon we do with silicon, whereas many other technologies have been by-passed along the way. What I'm trying to say is that I think that, for example in Gallium Arsenide and monolithic circuits, we're learning to make some very good switches which will perform certain functions such as phase shifting. I think we're going to be able to make phase shifters that involve not just a phase shifter but one that has some frequency taper on that phase shifter. I don't see how we're going to provide long delay times if the delay itself is important, but if phase shifting is required I think we're going to very rapidly get more sophisticated than we are now. I just throw that out, that going back to this time, dollars and effort; true it hasn't been invested, but I think if there's

347

sort of an integrated time, dollars and effort that is drawn out too long then it doesn't mean a thing. I think it has to be compact and within a certain time frame. I don't think it can be too short either. Obviously, throwing a lot of money into something in too short a time doesn't have the optimum investment. I think it's true that unless advances are made within the attention span of specific individuals you just re-educate more and more people.

OWENS: I'll make one comment on that. I think the one key, the reason why a lot of people latch on to this phased array business as an area of significant interest is that (at least from anything they can get, and I don't claim to be terribly knowledgeable in the area) they require real time delay in order to get time equalization across the face of the antenna. The problem is that real time delays are not directly available in any Gallium Arsenide circuitry or proposed silicon circuit or anything else. You're asking for tens of nanoseconds of delay across a face. That is somewhat unique, in that it is a delay which is too short for acoustic waves and too long for digital type systems including phase shifters and this type of thing and that technology. It's in a range where right now there is no solution. Now, the other points you make are absolutely valid, I agree.

ESHBACH: Is that entirely true, that actual time delay is that long.

OWENS: For some of these applications, yes.

SMITH: As a metter of fact they want differential delays of 20 to 25 nanoseconds.

OWENS: Real time delays are required in order to get the phase front restored in real time for certain situations. They require real time delays, not merely phase shifts.

DAMON: But, I think John Eshbach has made a very good point. A point that the SAWs have managed to overcome. The SAW's just now are beginning to do some of the very exotic things that were predicted ten years ago; some of the tremendous

time bandwidth product, or fancy coding and decoding. But, along the way they made successful delay lines, filters and a few mundame things that got the engineers to understand them, to know what they could do, to put them in and to test them, and to live with them over all their environmental requirements. I'm just fearful of aiming for the big one way out there, that you will never quite get to and nobody will understand what you've done when you do make it and they won't trust it. So I hope you will be looking, there have got to be some simple sockets to fill along the way.

SMITH: If we could get to a 16,000 G loading capability, we've got a socket.

COLLINS: I think in regards to that, Chairman, putting aside military applications, that certainly the oscillator area should be looked at extremely carefully. It's implications are vast. It will be clear because as Douglas has correctly said it's head on competition because the world is full of oscillators.

SCHROEDER (Dieter): I just wonder about the effort that is being expended in MSW. I think we're looking at the worlds MSW community.

SMITH: Except Japan. There are about five Japanese working MSW, and two or three Russians that are fiddling around there.

SCHROEDER: Our company, Westinghouse, probably has the largest corporate commitment, I would guess. I don't know what these other people have. It's not that huge. There are only a few people working on it. I don't know what the answer is. We probably get as much money as we can get. We have a program with WPAFB. I was just thinking of the bubble aspect. I don't know, but I would guess that Bell or IBM was alone at one time.

MORGENTHALER: Bell had over 150 people working on bubbles at the beginning.

SCHROEDER: Yes, and here our few people are dispersed. They hardly even talk to each other.

SETHARES: That's one of the purposes of the meeting.

DAMON: Are we at a critical mass.

COLLINS: I think that's absolutely true, what has been said, and we said it
in 1978 as Jim Sethares reminded us yesterday morning. But, there are two
thrusts to the business community, or at least there are two ways to come about.
One is to take government R & D dollars and do what the government wants toward
their antennas and so forth, which four companies are apparently doing in this
country. And there, of course, what is happening is entirely being defined by
the government. The other approach is the approach of the Avanteks of the
world, and I could mention one or two more but I won't, who are strictly com-
mercially oriented. They are going to invest their R&D money depending on
the profits they make, and they sell YIG oscillators amongst other things.
So it seems to me that we need to see some enlightened private industry, as
being preached by Ronald Reagan and Margaret Thatcher, and that the scientist
in this room have to communicate to that audience what it's all about. I'm just
saying one thing you can pick on is the oscillator

because that <u>will</u> turn on the microwave industry, if it is for real. There is no
question about it, and you won't have to worry about these funny antennas anymore,
and that crock of gold that Dick says and this gentleman says you're never going to
reach. I'm wondering if Westinghouse has their own promotion dollars in there.

Stancil- I just wanted to raise the question or re-examination of the philosophy
of two dimensions being better than three and the general trend. IBM has just
come out with a new computer which is based on little modules which have a hundred
chips mounted on top of a 30 layer structure where the interconnections are made
in that 30 layer structure with leads hung vertically. The trends in VLSI are also
in multilayers in order to find ways to interconnect with millions of components.
I recently had the opportunity at HP to see first hand how they mount the filters

350

and so forth, and was suprised that it's not at all the idea of a man with tweezers and a magnifying glass. It's really a very highly automated procedure. It takes all of a couple of minutes to spin the sphere around and get it properly oriented and glued in place. H.P. felt that this process saves over going to planar technology when the filters are such a small part of the overall system. What will impress them is if they can improve the performance of the device. So, are we correct in making the assumption that planar is better.

Damon- Maybe Jeff can tell us what performance improvement one can expect out of these oscillators.

Smith- The advantage of VLSI is that they use planar technology to define it, align it, build it and put it together.

Damon- It's multiple planar technology.

Owens- The only reason they're doing that is they can't figure out how to spread it out laterally, they haven't got the design program to do the job. The CAD is so far behind the capability to integrate it they don't know how to do it right.

Stancil- Well of course it's a time delay problem to. You have to get things close together.

Smith- If you put the right chips in the right place then the computer works at high speed.

Owens- It's a software problem. The software is so far behind the ability to lay out a circuit. It's so much larger than what you can figure out how to do anything with.

Damon- Well I think nevertheless the compactness of multilevel technology still gives significant savings in propagation time. Now, again what's the better performance we're going to expect out of MSW oscillators.

Collins- Better phase noise and in a plane. It would appear that the temperature medium term stability can be at least the same maybe better. The long term stability, time will tell, but it is a planar technology. I was remarking to Douglas (Adam) that

351

you don't have the quartz oscillator at microwave frequency, but this could be one step towards that. There can be a dramatic improvement. That's certainly what you could offer H.P. What I'm saying is we should look at it more from a commercial thrust.

Damon- Are there other questions from the audience at this point.

Audience: (Allied Chem.) I want to comment on the materials problem. We mentioned that the entire MSW community is in this room. It brings to mind Prof Collins comment about Margeret Thatcher and the profit motive. We're trying to make a commerical business out of this material, so putting those two thoughts together, don't be surprised if the price you have to pay for these films is rather expensive until the volume gets to a certain level. Obviously, we could supply everyone in this room with ten films of this material and it wouldn't put a strain on our capacity we have for the bubble effort. That also doesn't make us any money. Until this technology develops to the extent that there's some price pressure or price relief, if you will, the price will be higher.

Owens- Since the technology is sufficiently simple don't be surprised if people go out and build their own furnances.

Adams- I'd like to comment on what I'd like in a material. One thing that would be nice is a piece of YIG, apart from zero linewidth, is if we could do what they're doing in bubble materials. They grow high growth induced anisotropy. If we had something that could saturate a film, so that we could take it and just lay it down there and put on a small bias field rather than a big magnetc, and still have a narrow linewidth, then that would be fantastic. You could just stick a piece of YIG there with growth induced anisotropy and it would work. (Laughter)

Glass- Don't laugh because we've seen something like that with epitaxial hexagonal ferrites. They have real high uniaxial anisotropy.

Audience- What do you consider a low linewidth.

Adam- Anything under an oersted I think would be pretty good if you had a high anisotropy field.

Smith- Let's shoot for 2 tenths. No guts, no glory.

Owens- On the other extreme, for the RAC devices we went for zero anisotropy, because it beam steers. That's something you're going to run into as time goes on as you try to increase the phase accuracy.

Audience- What's the specification now for these devices on YIG films in terms of linewidth. I hear everyobdy in the world is making YIG films. They are reasonably hard to make with linewidths of a few tenths of an oersted.

Owens- I'll make a comment here and Adam has a far better system than we do. We believe that we're fairly consistently pulling up to as thick as 50 microns with linewidths of less than one half oersted. For most device applications in terms of the developments we're talking about right now, again this is a University situation but, I don't think we require anything much greater then that. These are more than adequate for most device type work which is now going on, in terms of pure YIG simple type devices. There are specifc requirements that require other things. In many of our own cases we would like lower anisotropy fields because for some of the volume wave studies it creates beam steering. Adam now would like for some of his devices to have a very high anisotropy so as to minimize the amount of field he has to put on it in order to get it to run. So there you have a nice conflicting requirement but the other ones are pretty straight forward, in terms of thickness and basic linewidth, and uniformity within a small fraction of a micron.

Audience- How is the linewidth measured?

Owens- Usually in a cavity or we take it indirectly from our propagation loss measurements. You can put a film in volume waves and given a set of curves for

linewidth, for a certain standard transducer set, versus attenuation you can look at the passband and get a pretty good estimate as to what the linewidth is. That way we don't have to take a crystal and hack it into little bits before we can use it.

Audience- Does the film on the non-epi-side cause a problem?

Owens- We don't grow on the non-epi-side. We grow on one side only. We go face down on the top surface. We're the old style.

Smith- We have grown on the back side, however, in the past and just grind it off.

Damon- Did you have a comment Rick. I'm going to try and terminate this in about 5 minutes.

Morgenthaler- With the exception of the signal to noise enhancer, a very nice device that was described this morning, we haven't talked very much about dynamic range or other nonlinear characteristcs that occur inherently in any YIG device due to parametrically induced spin waves and so on. One of the interesting characteristcs of a conventional YIG filter, sphere, is the frequency selective limiting characteristics that it has. I wondered if any of the people who have been dealing with the MSW resonators and so on want to comment upon either the limitations that they see MSW technology having because of unwanted premature saturation effects or the advantages.

Owens- I'll toss out one in particular in the oscillator area. It's clear that in the resonator the frequencies below 4 GHz, while the surface wave resonators have some strong advantages in terms of Q and in terms of good high isolations, they have some significant disadvantages in terms of power handling capabilities. That is one problem there which may force you into either using one of the volume wave modes or tolerating the relatively low power output coming out of the surface wave device. I think that one of the advantages that can be turned into is simply as a limiter if your going to use a delay device

on the front end of a system which does tend to have problems with being over-loaded particularly on receivers. Then that literally can be turned into an advantage. Using that kind of a device then can have a distinct advantage in things like compressive receivers. There can be some strong advantages to having it limit so it doesn't destroy what's down the line.

Audience- Westinghouse has just recently proposed a non-magnetostatic thin film used as a limiter.

Damon- What do you mean by non-magnetostatic?

Audience- Well, we inentionally avoid magnetostatic modes. We use the film as an extended ferrite sphere.

Morgenthaler- A ferrite sphere resonance is a magnetostatic mode.

Audience- Well, we avoid magnetostatic surface waves.

Damon- O.K. I understand some of the panel members have planes they are concerned about and I don't want to press this too far. I'd like very much to thank our panel members and the Air Force for organizing this. Since I was not here for most of the conference perhaps someone else would like to comment.

Collins- Why don't I. Outside of my good friends at Thompson CSF I think I'm the only one outside of the U.S. here. There are a lot of people here that have come from the U.K. who now live in the U.S. (laughter), and that's why it's not quite such a bad place as it used to be.

On behalf of everyone here I would like to thank our hosts, the arrangements were hospitable and you certainly exercised our minds. I didn't think I would ever be able to sit for a day and a half and just listen again, but I find it very easy to do. It was very enjoyable.

Damon- Do you have a final word Jim.

Sethares- Well O.K., that's it. That concludes the session. Thank you all for coming and I hope you make your planes on time.

Name	Organization	Tel #
J.D. Adam	Westingthouse	412 256-5486
Larry R. Adkins	Rockwell	714 632-3272
David M. Bennett	Westingthouse	617 890-9370
T. Bhattacharje	MIT	253-6902
R.M. Blumgold	AFWAL/AADM-2	513 255-6026
Alan Budreau	RADC/EEA	861-3768
J.W. Carlin	Bell Labs	201 949-3813
Paul H. Carr	RADC/EE	617 861-3686
Jean Paul Castera	Thomnson-CSF	(1)941 82-40
Charles Chandler	Westinghouse	301 765-2123
R.H. Chilton	RADC/OC	315 330-4381
Alejandro Chu	Lincoln Lab	617 862-5500
Randolph Clapp	RADC/EEA	617 861-3764
Ed Cohen	ARCON Corp	890-3330
J. Collins	Univ of Edinburgh	(031) 667-1081 x3260
Mike Daniel	Westinghouse	412 256-3132
John R. Eshbach	GE-CRD	518 385-8254
H.C. Falk	RADC/ET	861-2404
R. Floyd	RADC/EEA	617 861-4663
Peter Franchi	RADC/EEA	617 861-3067
Howard L. Glass	Rockwell	714 632-3691
John Graniero	RADC/DCC	315 330 3171
Devlin M. Gualtieri	Allied Corp	201 455-2370
Dogan Gunes	Sperry Research Ctr	617 369-4000
Pierre Hartemann	Thomson-CSF	(1)941 82-40
Randy Haupt	RADC/EECS	617 861-3581
Larry G. Hegi	MIT	253-4625
Y. Hou	Airtron	201 539-5500
John C. Houver	Electromagnetic Sci	404 448-5770
Leslie Itano	MIT	617 253-4625
Robert L. Kyhl	MIT	617 253-2561
Victor Lander	Airtron	202 559-5500
Philip W. Linke	AFIT	513 255-5533
William Macropoulos	MIT	617 862-5500
H. Mittra	Airtron Litton	205 539 5500
F. Molinet	RADC/EE	617 861-3705
Rick Morgenthaler	MIT	617 253-4623
Philip Noel	Texas Instruments	214 995-5531
M.J. O'Brien	RADC/EECS	617 861-4036
J. Owens	Univ of Texas	817 273-2671
J.P. Parekh	SUNY Stony Brook	516 246-7760
Allan Schell	RADC/EE	861-3700
John K. Schindler	RADC/EEA	617 861-3711
Dieter K. Schroder	Westinghouse	412 256-7592
Jim Sethares	RADC/EEA	861-4663
Michael Shone	Litton Sys	201 539-5500
R. Shore	RADC/EEC	617 861-3684
William J. Skudera	ERADCOM	201 544-2209
A.J. Slobodnik, Jr.	RADC/EEA	861-3716
Bernard Smilowitz	AIL/EATON	516 595-4358
Charles Smith, Jr.	Univ of TX	817 261-6733
Hugh L. Southall	RADC/EEA	617 861-3716
Daniel D. Stancil	MIT/EECS	253-4625
Hans Steyskal	RADC/EEA	861-3683
Martin Stiglitz	RADC/EEA	861-3067

Steven N. Stitzer	Westinghouse	301 765-7348
Donald J. Stukel	RADC/CC	315 330-7701
Thomas L. Szabo	Hewlett Packard	617 687-1501
William J. Tanski	Sperry Research	617 369-4000
Arthur Tauber	USA ET&D Lab	201 544-4407
V.L. Taylor	Westingthouse	301 765-6730
Boris Tomasic	RADC/EEAA	861-3863
Tung-Lin Tsai	Raytheon	617 393-7300
Hang-Sheng Tuan	EE State Univ NY Stony Brook 516 246-5988	
P.F. Tumelty	Allied Corp	201 455-4984
Nickolas P. Vlannes	MIT/EECS	253-4625
Pradeep Wahi	Litton	301 454-9705
Stephen Wanuga	G.E.	315 456-3152
Denis Webb	NRL	202 767-2862
Rick Webster	RADC/EEM	861-3764
Jacob Weinberg	Univ of Lowell	861-4279
Joseph White	Microwave Assoc	617 272-3000
Harry V. Winsor	AFOSR/NE	AV297-4931
Dale Zeskind	MIT	617 253 4625
F.J. Zucker	RADC/EEAA	861-3711

MISSION
of
Rome Air Development Center

RADC plans and executes research, development, test and selected acquisition programs in support of Command, Control Communications and Intelligence (C^3I) activities. Technical and engineering support within areas of technical competence is provided to ESD Program Offices (POs) and other ESD elements. The principal technical mission areas are communications, electromagnetic guidance and control, surveillance of ground and aerospace objects, intelligence data collection and handling, information system technology, ionospheric propagation, solid state sciences, microwave physics and electronic reliability, maintainability and compatibility.

5-83

DTIC